Université de Sherbrooke

Breaking the picosecond barrier in the physics and chemistry of water radiolysis: Applications of Monte-Carlo modeling to high–temperature nuclear reactors and radiobiology

Par
Sunuchakan SANGUANMITH
Programmes de sciences des radiations et imagerie biomédicale

Thèse présentée à la Faculté de médecine et des sciences de la santé
en vue de l'obtention du grade de philosophiae doctor (Ph.D.)
en sciences des radiations et imagerie biomédicale

Sherbrooke, Québec, Canada
May 2021

Membres du jury d'évaluation

Pr Kevin WHITTINGSTALL	Sciences des radiations et imagerie biomédicale
Pr Léon SANCHE	Sciences des radiations et imagerie biomédicale
Pr Armand SOLDERA	Département de chimie, Faculté des sciences
Pr Ghandi KHASHAYAR	Department of Chemistry, Faculty of Science, University of Guelph
Pr Jean-Paul JAY-GERIN	Sciences des radiations et imagerie biomédicale

To my parents, for their support and their unique unconditional great love.
To Naomi, Audrey-Anne, and Georges, they are showing me the best version of myself.

RÉSUMÉ

Breaking the picosecond barrier in the physics and chemistry of water radiolysis: Applications of Monte-Carlo modeling to high–temperature nuclear reactors and radiobiology

Par
Sunuchakan Sanguanmith
Programmes de sciences des radiations et imagerie biomédicale

Thèse présentée à la Faculté de médecine et des sciences de la santé en vue de l'obtention du diplôme de philosophiae doctor (Ph.D.) en sciences des radiations et imagerie biomédicale, Faculté de médecine et des sciences de la santé, Université de Sherbrooke, Sherbrooke, Québec, Canada, J1H 5N4

Comprendre l'interface entre la physique des radiations et la chimie des radiations – à savoir, « briser la barrière de la picoseconde » – est d'une pertinence évidente pour la radiobiologie fondamentale et les sciences connexes, car l'eau sous forme liquide est de loin le constituant le plus abondant des cellules et des tissus biologiques. Ce projet de recherche a utilisé des modèles basés sur l'expérience et la théorie pour produire une description complète et fiable de la nature chimique et de la distribution spatiale hautement non-homogène de toutes les espèces réactives créées à l'échelle des (sous-) picosecondes et impliquées comme précurseurs de dommages radiobiologiques. L'importance du piégeage des précurseurs (électrons « secs ») des électrons hydratés (e^-_{aq}) est démontrée dans le calcul des rendements en H_2 à partir de simulations de solutions aqueuses d'ions azide (N_3^-) irradiées avec des rayons-γ de cobalt-60 (électrons de Compton de ~1 MeV) et des électrons-β du tritium (énergie moyenne des électrons de ~7,8 keV). C'est la première fois que nous introduisons le processus de piégeage des précurseurs des électrons hydratés dans nos simulations Monte-Carlo. Des simulations Monte Carlo de la radiolyse à faible transfert d'énergie linéaire (TEL) de l'eau supercritique (H_2O) à 400 °C ont également été utilisées pour examiner la sensibilité de la dépendance en densité du rendement de e^-_{aq} selon la variation en température de la constante de vitesse d'auto-réaction $k(e^-_{aq} + e^-_{aq})$. Deux valeurs différentes de $k(e^-_{aq} + e^-_{aq})$ à 400 °C ont été utilisées: l'une basée sur la dépendance en température de k au-dessus de 150 °C telle que mesurée dans l'eau alcaline, et l'autre basée sur une extrapolation d'Arrhenius des valeurs de k inférieures à 150 °C. Seul un faible effet de $k(e^-_{aq} + e^-_{aq})$ sur la variation de $G(e^-_{aq})$ en fonction de la densité de l'eau à 60 ps et 1 ns a pu être observé. En conclusion, nos calculs actuels ne nous ont pas permis de confirmer l'applicabilité de la baisse soudaine prédite de $k(e^-_{aq} + e^-_{aq})$ à ~150 °C dans une eau quasi neutre.

Mot Clés : Radiolyse de l'eau, stade physico-chimique, sous-picoseconde, simulations Monte Carlo, électron préhydraté, électron « sec », précurseur, ion azide, capteur, rendement en hydrogène moléculaire, distance de thermalisation de l'électron.

ABSTRACT

Breaking the picosecond barrier in the physics and chemistry of water radiolysis: Applications of Monte-Carlo modeling to high–temperature nuclear reactors and radiobiology

By
Sunuchakan Sanguanmith
Radiation Sciences and Biomedical Imaging Program

The thesis presented at the Faculty of medicine and health sciences to obtain the philosophy doctor (Ph.D.) degree in Radiation Sciences and Biomedical Imaging Program, Faculty of Medicine and Health Sciences, Université de Sherbrooke, Sherbrooke, Québec, Canada, J1H 5N4

Understanding the interface between radiation physics and radiation chemistry (*i.e.*, "breaking the picosecond barrier") is of obvious relevance to fundamental radiobiology and related science as liquid water is by far the most abundant constituent of biological cells and tissue. This research project used experiment-and-theory based models to produce a complete, reliable description of the chemical nature and highly nonhomogeneous spatial distribution of all reactive species created on the (sub-) picosecond time scale and involved as precursors of radiobiological damage. The importance of the scavenging of precursors ("dry" electrons) to hydrated electrons is demonstrated in the calculation of H_2 yields from the simulations of aqueous azide ion (N_3^-) solutions irradiated with ^{60}Co γ-rays (~1 MeV Compton electrons) and tritium β-electrons (mean electron energy of ~7.8 keV). It is the first time that we introduced scavenging of the precursors of hydrated electrons in our Monte-Carlo simulations. Monte Carlo simulations were also used to examine the sensitivity of the density dependence of the yield of e^-_{aq} in the low linear energy transfer (LET) radiolysis of supercritical water (H_2O) at 400 °C on variations in the temperature dependence of $k(e^-_{aq} + e^-_{aq})$. Two different values of the e^-_{aq} self-reaction rate constant at 400 °C were used: one based on the temperature dependence of k above 150 °C as measured in alkaline water, and the other based on an Arrhenius extrapolation of the values of k below 150 °C. Only a small effect of $k(e^-_{aq} + e^-_{aq})$ on the variation of $G(e^-_{aq})$ as a function of water density at 60 ps and 1 ns could be observed. In conclusion, our present calculations did not allow us to unambiguously confirm (or deny) the applicability of the predicted sudden drop of $k(e^-_{aq} + e^-_{aq})$ at ~150 °C in near-neutral water.

Keywords: Water radiolysis, physicochemical stage, sub-picosecond, Monte Carlo simulations, prehydrated electron, "dry" electron, precursor, azide ion, scavenger, molecular hydrogen yield, electron thermalization distance

TABLE OF CONTENTS

LIST OF FIGURES

CHAPTER 1 – INTRODUCTION

CHAPTER 2 – INTERACTION OF IONIZING RADIATION WITH MATTER

CHAPTER 3 – RADIOLYSIS OF LIQUID WATER AND AQUEOUS SOLUTIONS

CHAPTER 4 – INTERACTION OF IONIZING RADIATION WITH MATTER

CHAPTER 6 – EXPERIMENTAL APPROACH

CHAPTER 7 – ARTICLE No.1

CHAPTER 10 – DISCUSSION

LISTE OF TABLES

LIST OF ABBREVIATION

σ	Cross-section
D	Diffusion coefficient
DEA	Dissociative electron attachment
DNA	Deoxyribonucleic acid
$\mathbf{e^-_{aq}}$	Hydrated electron
$\mathbf{e^-_{pre}}$	Pre-hydrated electron
$\mathbf{e^-_{sub}}$	Sub excitation electron
eV	Electronvolts
G_x	Primary yield of radiolytic species X
***G*(X)**	Experimental 100-eV yield of the final product X
Δ*G*	Yields variation
IRT	Independent reaction times
k	Reaction rate constant
keV	Kilo-electronvolts
LET	Linear energy transfer
MC	Monte Carlo
MeV	Mega-electronvolts
molec./100 eV	Molecule/100 eV

1. INTRODUCTION

1.1 Overview of the research project

The absorption of ionizing radiation by living cells can alter atomic structures through *direct* interaction of radiation with target macromolecules, thus producing chemical and biological changes. It can also act *indirectly* through the *radiolysis of water*, thereby generating reactive chemical species that may damage nuclear/mitochondrial DNA, proteins, and lipids (HALL and GIACCIA, 2006). Together, the direct and indirect effects of radiation initiate a series of biochemical and molecular signaling events that may repair the initial DNA damage or culminate in permanent physiological changes or cell death (SPITZ et al., 2004), the damage caused in irradiated cells may spread to neighboring, non-targeted bystander cells through intercellular communication mechanisms. DNA alterations can also be propagated to cells many generations after radiation exposure and bystander cells exhibit genomic instability in ways similar to directly hit cells (BUONANNO et al, 2011; AZZAM et al., 2012). The persistence of such effects in progeny cells has profound implications for long-term health risks, including the emergence of a second malignancy following radiotherapy treatments (TUBIANA, 2009).

The detailed molecular mechanisms of radiation damage to DNA and the biological pathways involved in cell death have received considerable attention from a variety of laboratories. By contrast, the focus of this research project is far less explored, which is the ultrafast primary free radical and molecular events that link chemistry and physics in the first few picoseconds following energy deposition. "*Radiation chemistry comes before radiation biology*" (in the temporal sense) wrote O'Neill and Wardman (O'NEILL and WARDMAN, 2009), adding that: "*The chemical viewpoint helps unite the spatial and temporal insight coming from radiation physics with the diversity of biological responses*". It is increasingly recognized that a full understanding of the physicochemical track structure (*i.e.*, the physical and chemical events that occur in the "native" radiation tracks) and the spatial distribution of these events is essential to unravel the fundamental biochemical mechanisms leading to the biological consequences of ionizing radiation (BECKER et al., 2011).

While fundamental biological processes are numerous and complex, they are triggered in aqueous environments as living cells contain ~70-85% water by weight. It is well known that the biological damage induced by free radicals from water radiolysis ($H_2O^{\bullet+}$, •OH, e^-_{aq}, H•, $O_2^{\bullet-}/HO_2^{\bullet}$,...) far exceeds that caused by direct energy deposition in the target. In the indirect effect the $H_2O^{\bullet+}$, •OH, H•, $O_2^{\bullet-}/HO_2^{\bullet}$, including the pre-hydrated and hydrated electrons can cause cell death, if their attack sites on DNA (and possibly other cell targets) are found inside of 20 base pairs (number of base pair within one or two helical turns of the DNA). Clustered DNA damages are considered as two or more closely spaced damages (strand breaks, abasic sites, or oxidized bases) on opposing strands. The clustered DNA damage can produce lethal and mutagenic effects of ionizing radiation. The efficiency of DNA repair may depend on the complexity of the DNA damage site. Ionizing radiation can also stimulate inducible nitric oxide synthase (NOS) activity in hit cells (MIKKELSEN and WARDMAN, 2003), thereby generating large amounts of •NO. Although •NO is chemically inert toward most cellular constituents (except for heme), it reacts with $O_2^{\bullet-}$ to form the peroxynitrite anion $ONOO^-$. Like •OH radicals, $ONOO^-$ and its conjugate acid ONOOH (pK_a = 6.8 at 37 °C) (PRYOR and SQUADRITO, 1995) are also highly reactive and capable of attacking a wide range of cellular targets. In summary, *the radiolysis of water and early activation of NOS is a major source of ROS/RNS in irradiated cells*.

Monte Carlo (MC) simulations of radiation transport are of increasing importance as researchers strive to understand radiation-induced damage on short-length scales (*i.e.*, interactions with cellular components, particularly DNA). Advanced mathematical-biology and computational models and general-purpose/specialized biophysical MC simulation codes (*e.g.*, EGS, MCNP6, RADACK, PARTRAC, PENELOPE, MCDS, and GEANT4-DNA) have already been developed by several groups for a number of medical and biomedical applications (BARÓ et al., 1995; BĚGUSOVÁ et al., 2001; HIRAYAMA et al., 2005; FRIEDLAND et al., 2011; INCERTI et al., 2011; PELOWITZ, 2013). All of these codes have specific strengths (*e.g.*, for simulations of charged-particle transport) and weaknesses. Notably, none of them has so far offered a detailed/quantitative radiation-chemical description of the transient bioradical processes that take place at early times in "native" tracks. In addition, none of them has taken into account the strong quantum character of primary events, which govern the Spatio-temporal behavior of dependent radical pairs

within a few picoseconds after energy deposition. For example, low-energy electrons in their subexcitation energy range (< 7-10 eV) are delocalized, since their wavelength exceeds atomic dimensions, and have short free-flight segments on the order of 1 nm (FANO and STEPHENS et al., 1986). *The treatment of subexcitation electrons should then be developed in a quantum-mechanical framework rather than by classical models*.

This project will be used state of the art stochastic Monte-Carlo simulations and molecular dynamics calculations in combination with the knowledge gained from current experimental efforts, the research project aims to design experimental and theory-based models to advance our understanding of challenging areas of the radiolysis of aqueous system for which, we feel, an early time, molecular level characterization of the underlying chemistry is essential to produce a complete, accurate picture of this radiolysis. It is without doubt, part of a major challenge in fundamental radiobiology.

This project will benefit from our extensive knowledge of the physical and chemical mechanisms of radiation action on water/aqueous solutions and also from our long-standing experience in Monte Carlo methods applied to the simulation of the radiolysis of aqueous systems (COBUT et al., 1998; FRONGILLO et al., 1998). For applications in radiobiology, we have developed and progressively refined with very fine detail a computationally efficient in-house MC code. It simulates ("event-by-event") the track structure of ionizing particles in water, the production of the various ionized and excited species, and the subsequent reactions of these species in time with one another or with available solutes. The code's ability to give accurate, time-dependent chemical yields under different irradiation conditions has been well validated by comparison with a range of experimental data. *For this project, the current version of this code will be extended and adapted according to the target model considered*.

A wide variety of data are required to simulate the water radiolysis (indirect effect) as well as by direct ionization/excitation processes. Some of the project's key physicochemical considerations are briefly summarized below.

1) Virtually *all* current MC simulations of track structures use a uniform continuum model of the target (water) medium irrespective of the underlying molecular configuration. This continuum approximation is particularly severe for low-energy (< 20 eV) electrons (LEE), whose mean penetration distances are of the order of a few molecular diameters or less (GREEN et al., 1999). As these electrons are thought to contribute to significant genotoxic

effects in cells (ALIZADEH et al., 2015), *a substantial improvement will consist in generating the tracks in a manner that recognizes the molecularity of the medium*.

2) Another critical aspect concerns the *abundant LEE interactions* in the track of a primary energetic (~1 MeV) Compton electron. The majority of these ("dry") electrons have a most probable kinetic energy and mean energy of ~9-10 and ~50-60 eV, respectively, and a mean free path in water of < 10 nm (MEESUNGNOEN and JAY-GERIN, 2002; PIMBLOTTE and LAVERNE, 2007). *Our MC code will require a detailed description of the transport properties of LEE during their slowing-down in the target medium*: until they thermalize, get trapped and hydrated (e^-_{aq}) (COBUT et al., 1998; FRONGILLO et al., 1998; GOULET and JAY-GERIN, 1989) or form a temporary negative ion with water (COBUT et al., 1998; FRONGILLO et al., 1998; GOULET and JAY-GERIN, 1989) ("dissociative electron attachment" or DEA process); or undergo geminate recombination with their parent cation (MEESUNGNOEN and JAY-GERIN, 2001); or are captured by a nearby scavenger (PASTINA and LAVERNE, 1999). While there are large uncertainties in the condensed-phase scattering cross-sections for LEE (below ~10 eV), significant advances have recently been made toward understanding LEE scattering and LEE-driven reaction processes with DNA and its constituents (GREEN et al., 1999; PIMBLOTTE and LAVERNE, 2007; ALIZADEH et al., 2015). These LEE cross-section data, which essentially include direct scattering and "resonant" (DEA) scattering, are used in our track-structure simulations.

3) *The charges (electrons and "holes") generated by the action of ionizing radiation on DNA (in both the solid phase and aqueous solutions) can migrate along the DNA chain before being trapped* (O'NEILL and FIELDEN, 1993; BECKER et al., 2011). Electron migration has been observed over distances up to ~30 nm (*i.e.*, ~100 base pairs). The electrons react preferentially with the pyrimidine bases. In contrast, short-range hole migration processes occur from the initial cation radicals to sites located predominantly at the purine bases, with guanine being where the positive charge is most likely to be localized. The possibility of observing long-range oxidative DNA damage at a distance due to DNA-mediated charge transfer will be incorporated in our simulations.

4) The final stage in the life of a LEE is its trapping and hydration. The exact physical nature of *the short-lived* (sub-picosecond), *weakly bound electron* e^-_{ir} (below zero eV) is still a subject of investigation (WANG et al., 2008). However, *its localized nature may allow it to*

undergo chemical reactions before settling into the fully relaxed e^-_{aq} *state* (LU, 2010). Recently, there has been great interest in studying the role of this fascinating species in radiation biology and the radiotherapy of cancer (ZEWAIL, 2000; MALKA et al., 2010). Current findings challenge the conventional notion that damage to the genome by IR is mainly produced by the •OH radical. This could lead to a new understanding of many aspects of the biological action of radiation. For example, Lu and coworkers (LU, 2010) suggest *the possibility that* e^-_{ir} *scavenging could occur via long-range electron-transfer processes involving quantum-mechanical tunneling of* e^-_{ir} *to the scavenger*. The reactivity of e^-_{ir} has so far been given little attention in Monte Carlo track chemistry. Reactions of e^-_{ir} will be incorporated in our simulations and the role played by this precursor to e^-_{aq} will be addressed. 5) The positive charge (or "hole") on a given $H_2O^{\bullet+}$ produced by ionization may migrate (randomly) before proton transfer occurs (OGARU and HAMILL, 1973). This takes place through a succession of resonant electron transfers (~20 hops on average, over a distance of ~1.5 nm) from neighboring water molecules. During its very short lifetime (~200 fs) (LI et al., 2013), *$H_2O^{\bullet+}$ can act as an extremely strong oxidant and be involved in ultrafast electron transfer reactions* (MA et al., 2014). Thus, when the hydrating water molecules are in direct contact with DNA, the generated $H_2O^{\bullet+}$ radical cations may induce chemistry different from •OH radicals. This possibility has not yet been explored in the formation of initial DNA damage and offers a multitude of hitherto unobserved elementary electron and ion dynamics that are triggered by the ionization of water (LI et al., 2013; MA et al., 2014).

1.2 The important role of the prehydrated electron in DNA damage

It is clear that the complete knowledge of water radiolysis will lead us to a better understanding of fundamental mechanisms of cancer biology and therapy which will finally help us to improve the clinical outcomes. Radiotherapy is the major modality of cancer therapy. Various types of radiation are used to destroy cancer cells. It is well-known that ionizing radiation causes DNA damage mostly through indirect effects rather than the direct effect. In the indirect interaction, ionizing radiation reacts with the cellular environment, which is mainly water, then generates various species of reactive radicals. These reactive radicals from water radiolysis then react with DNA causing DNA damage. It has been

observed that the yields of the single-strand breaks and double-strand breaks of DNA produced by gamma rays radiation are three times higher under the aqueous condition than those in a dry condition on average (ITO et al., 1993). This fact evidently shows the important role of water in enhancing DNA damage by ionizing radiation. The ionizing radiation and low energy electrons (LEE) can ionize or excite water molecules depending on the deposited energy, producing an oxidizing hydroxyl radical, a free electron, hydrogen atom, molecular hydrogen, and hydrogen peroxide. In this part, we focus on the ejected free electron from water radiolysis. The ejected electron quickly get trapped by the surrounding water molecules to become a pre-hydrated electron and finally become a hydrated electron (e^-_{hyd} or e^-_{aq}) (or solvated electron) in a potential well. The discovery of the solvated electron was found in ammonium vapor, potassium metal becomes gold and blue (DYE, 2003). All Alkali metals in liquid ammonia are brightly colored when the solution is dilute, whereas the concentrated solutions (> 3 M) presents copper color. In 1907, Charles Kraus explained the production of bright colors by introducing the concept of the solvated electron (KRAUS, 1907; 1908). He proposed that the alkali metal ionizes in liquid ammonia, forming a cation and a solvated electron. Though the solvated electron is stable in ammonia for many days, but it has a very short lifetime in water. Therefore, owing to its short lifetime in water, the hydrated electron was not confirmed until 1962, when its optical spectrum was successfully measured by E.J. Hart using the pulse radiolysis technique (HART and BOAG, 1962). The hydrated electron has the highest quantum yield, it is deeply trapped in awater cavity at 3.2 eV below vacuum level (TURI and BORGIS, 2002). As a result, these ground-state-like hydrated electrons are ineffective at inducing DNA damage. Therefore, the $^{\bullet}$OH radical has been considered as the sole contributor to radiation-induced indirect DNA damage. However it has been observed that one-third of the DNA damage is not scavengable by a high concentration of $^{\bullet}$OH scavengers cannot completely quench the DNA damage (DELARA et al., 1995). The non-scavengable DNA damage (30% single-strand break, 30-65% double-strand break) was therefore attributed to the direct effect of radiation (LEHNERT, 2007; DELARA et al., 1995). This assignment conflicts with the work of Ito et al. (ITO et al., 1993). Ito and coworkers have shown the dependence of the yield of DNA strand break-induced by gamma rays. The presence of water molecules enhances the yields of single-strand breaks and double-strand breaks more than 10 times in the humid stage, and by more than 1000 times in the aqueous

state. Their experiments showed only 1% of DNA strand breaks were caused by the direct effects. If hydroxyl radicals play a dominant role in the indirect effect, then, high concentration of hydroxyl radical scavenger should be able to scavenge about 99% of DNA strand breaks in an aqueous solution. This is contradictory with the fact that there is about 30-65% of non-scavengable double-strand breaks even when a very high concentration of •OH scavengers is used up to 2M. From this observation, it is confirmed that there may be some important processes missing in the conventional understanding of radiation-induced DNA damage.

With femtosecond time-resolved laser spectroscopy, the existence of the precursor of hydrated electron called e^-_{pre} (pre-hydrated electron) has been found. The first evident observation was made in 1987 by Migus et al using femtosecond laser spectroscopy (MIGUS et al., 1987). The physical and chemical properties of the ultrashort-lived prehydrated electrons have been studied extensively (LONG et al., 1990; PIMBLOTTE and LaVERNE, 1998; PASTINA and LaVERNE, 1999; LAENEN et al., 2000; LU and SANCHE, 2001; LU et al., 2004; HERBERT and JACOBSON, 2001; WANG et al., 2008). The lifetimes of the prehydrated electrons were reported to range from 50 fs to 1 ps (PSCHENICHNIKOVet al.,2004; MIGUS et al., 1987; LONG et al., 1990; LAENEN et al., 2000; LU et al., 2004; SILVA et al., 1998, YOKOYAMA et al., 1998; ASSEL et al., 1998; KAMBHAMPATI et al., 2002). In fact, the prehydrated electron is only weakly bound to the water molecules implies the high reactivity of the prehydrated electron. As a result, the prehydrated electron can attach to the various biomolecules (ex. Amino acid and nucleotide) (ALDRICH et al 1975; GAUDUEL et al., 1988). More recently, it has been observed the dissociative electron transfer (DET) reaction of e^-_{pre} with anticancer drug and DNA. e^-_{pre} can activate chemotherapeutic drug cisplatin (CDDP) (LU, 2007; LU et al., 2007) and potential radiosensitizers –halopyrimidines (CldU, BrdU, and IdU) through the dissociative electron transfer (DET) process (WANG et al., 2006; WANG and LU, 2007; WANG and LU, 2010) had also shown the role of e^-_{pre} in inducing DNA damage. For the case of nucleotide, dXMP (X denotes DNA bases adenine A, Guanine G, Cytosine C, and Thymine T). The transfer of the prehydrated electron to nucleotide leads to bond breaks of T and especially G bases, while results in the stable anions for C and A. In their pump-probe fs-TRLS experiment, excess

electrons produced by two UV photon excitation of water molecules will rapidly be located in pre-existing traps within a few fs to form the e^-_{pre} states that have ultrashort lifetimes of less than 1 ps (~500 fs). A pump wavelength of 318 nm was used to generate excess electrons in water, and a probe wavelength at 330 nm was used to probe the intermediate state ($dXMP^{*-}$) of reaction e^-_{pre} with a dXMP (X denotes DNA bases A, G, C, and T), $dXMP^{*-}$ is a vibrationally-excited intermediate anion. It is well known that the electronic absorption spectrum of dXMP arises solely from the excitation of the ¶–electron system of DNA base X. There is no UV absorption in the phosphate group and sugar moiety. The formation and decay of the $dXMP^{*-}$ can be express in the following reaction:

$$e^-_{pre} + dXMP \rightarrow dXMP^{*-} \rightarrow \text{dissociation}$$
$$\text{or} \quad \rightarrow dXMP^-$$

Among all four mononucleotides, the guanine mononucleotide is the most vulnerable to the DET process, implying that the nucleotide containing guanine ate the weakest link in DNA (WANG et al., 2009). Their results are consistent with the experimental results of Ray et al. which show that dry single-strand DNA oligomers with more G bases have a higher probability to capture low energy electrons (1.0 eV) in the gas phase (RAY et al., 2005). Theoretical works by Schaefer et al. found that the G base is likely to have N-H bond dissociation to induce bond breaks (BERA AND SCHAEFER, 2005). Liu et al. observed that water clusters can protect the collision-induced dissociation of anionic adenosine 5'monophosphate (AMP^-) (LIU et al., 2006). These experimental results are all consistent. The lifetime of e^-_{pre} is much longer than those of free electrons in fs. The e^-_{pre} then becomes the well-bound e^-_{hyd} with a lifetime in µs. If the e^-_{hyd} had a significant contribution to the formation of $dXMP^{*-}$, the rising kinetic of the $dXMP^{*-}$ signal would not be complete within the first ps but would be observed in the timescale of µs corresponding to the lifetime of e^-_{hyd}. It is obviously shown that the formation of $dXMPs^{*-}$ is complete within the ps timescale. Thus it is the ultrashort-lived e^-_{pre} rather than the e^-_{hyd}, that reacts with dXMP and leads to the formation of $dXMP^{*-}$ (WANG, 2012). The main steps of inducing DNA strand break are shown in Figure 1.1. These results have revealed that the DET reaction of the prehydrated

electron is a key step in radiotherapy. It is also shown that the prehydrated electron is an ideal species to study reductive DNA damage.

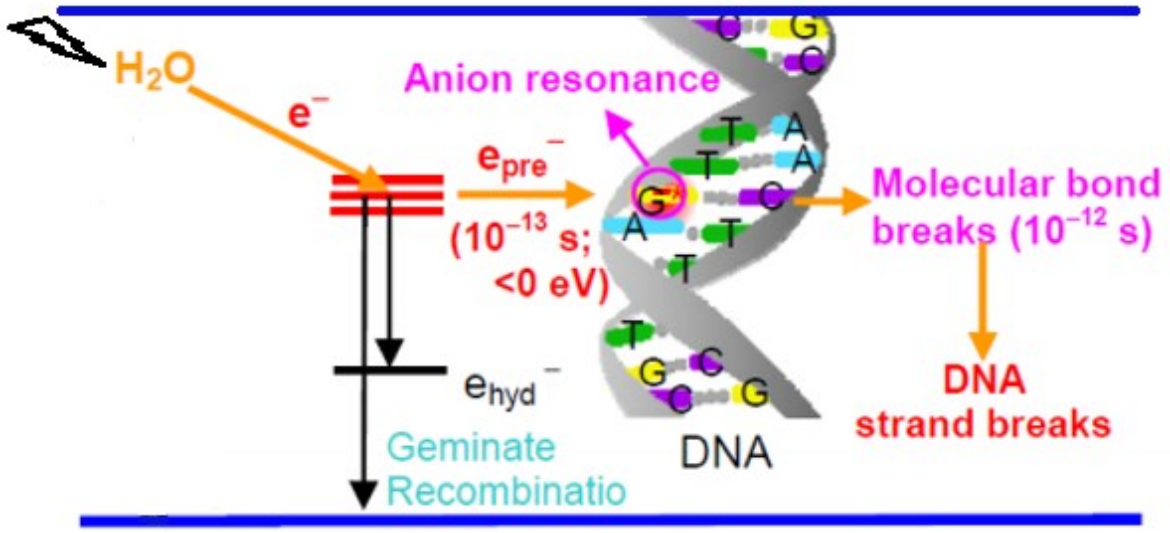

Figure 1.1 The electron (e^-) ejected from water radiolysis get solvates to hydrated state (e^-_{hyd}) or can recombine with a water molecule. When DNA is around the e^-_{pre}, dissociative electron transfer (DET) can occur to form a transient molecular anion resonance which leads to molecular bond breaks in DNA bases, followed by strand breaks of the DNA (Adapted from WANG et al., 2009)

2. INTERACTION OF IONIZING RADIATION WITH MATTER

Ionizing radiations are defined as those types of energetic particles and electromagnetic radiations that, either directly or indirectly, cause ionization of a medium, that is, the removal of a bound orbital electron from an atom or a molecule and, thereby, the production of a residual positive ion. Some molecules, instead of being ionized, may also be excited to upper electronic states (see, for example: EVANS, 1955; ANDERSON, 1984; IAEA-TECDOC-799, 1995; MOZUMDER, 1999; TOBUREN, 2004). Directly ionizing radiations are fast-moving charged particles (e.g., electrons, protons, α-particles, stripped nuclei, or fission fragments) that produce ionizations through direct Coulomb interactions. In this case, note that particle-particle contact is not necessary since the Coulomb force acts at a distance. Indirectly ionizing radiations are energetic electromagnetic radiations (like X- or γ-ray photons) or neutrons that can also liberate bound orbital electrons, but secondarily to a preliminary interaction. For photons, this interaction is predominantly via the production of Compton electrons and photoelectrons (and, if the incident photon energy is greater than 1.02 MeV, the production of electron-positron pairs). Neutrons interact with matter through elastic nuclear scattering resulting in the production of energetic recoil protons or other positively charged nuclei (ions), characteristic of the irradiated medium, which can go on to generate ionized and excited molecules along their paths. Regardless of the type of ionizing radiation, the final common result in all modes of absorption of ionizing radiation is thus the formation of tracks of physical energy-loss events in the form of ionization and excitation processes and in a geometrical pattern that depends on the type of radiation involved.

Generally, the electrons ejected in the ionization events may themselves have sufficient energy to ionize one or more other molecules of the medium. In this way, the primary high-energy electron can produce a large number ($\sim 4 \times 10^4$ by a 1 MeV particle) of secondary or higher-order generation electrons (it is customary to refer to all electrons that are not primary as "secondary") along its track as it gradually slows down (ICRU REPORT 31, 1979). From atomic physics, it is known that most energy-loss events by fast electrons involve small transfers of energy. In fact, the probability of a given energy transfer Q varies inversely with the square of that energy loss (EVANS, 1955). "Distant" or "soft" collisions, in which the

energy loss is small, are therefore strongly favored over "close" or "hard" collisions, in which the energy loss is large (MOZUMDER, 1999). The vast majority of these secondary electrons have low initial kinetic energies with a distribution that lies essentially below 100 eV, and most probable energy below 10 eV (LAVERNE and PIMBLOTT, 1995; SANCHE, 2002; AUTSAVAPROMPORN, 2006). In most cases, they lose all their excess energy by multiple quasi-elastic (i.e., elastic plus phonon excitations) and inelastic interactions with their environment, including ionizations and/or excitations of electronic, intramolecular vibrational or rotational modes of the target molecules (MICHAUD et al., 2003), and quickly reach thermal equilibrium (i.e., they are "thermalized"). Determining exactly which of these competing interaction types will take place is a complex function of the target medium and the energy range of the incident electron. By definition, a measure of the probability that any particular one of these interactions will occur is called the "cross-section" (expressed in units of the area) for that particular interaction type (see, for example JOACHAIN, 1975). The total interaction cross-section σ, summed over all considered individual processes i, is used to determine the distance to the next interaction, and the relative contributions σ_i to σ are used to determine the type of interaction. The mean distance between two consecutive interactions or "mean free path" λ is defined by

$$\lambda = \frac{1}{N\sigma}, \tag{1}$$

where N is the number of atoms or molecules per unit volume, and

$$\sigma = \sum_i \sigma_i \tag{2}$$

In a dilute aqueous environment, thermalized electrons undergo trapping and hydration in quick succession (within ~10^{-12} s) as a result of the water electric dipoles rotating under the influence of the negative charge (BERNAS et al., 1996). Some electrons that have kinetic energies lower than the first electronic excitation threshold of the medium, the so-called "subexcitation" electrons (PLATZMAN, 1955), may also undergo, prior to thermalization, prompt geminate ion recombination (FREEMAN, 1987) or induce the production of energetic (~1-5 eV) anion fragments via formation of dissociative negative ion states

(resonances) (i.e., dissociative electron attachment, or DEA) (CHRISTOPHOROU et al., 1984; BASS and SANCHE, 2003). As a consequence of the energy gained by the medium, a sequence of very fast reactions and molecular rearrangements lead to the formation of new, highly non homogeneously distributed chemical species in the system, such as charged and/or neutral molecular fragments, reactive free radicals, and other excited chemical intermediates. The trail of the initial physical events, along with the chemical species, is generally referred to as the track of a charged particle, and its overall detailed spatial distribution, including contributions from secondary electrons, is commonly known as "track structure" (see, for example PARETZKE, 1987; MAGEE and CHATTERJEE, 1987; KRAFT and KRÄMER, 1993; PARETZKE et al., 1995; MOZUMDER, 1999; LAVERNE, 2000, 2004).

2.1 Track structure in radiation chemistry and radiobiology

Numbers of experimental and theoretical studies have shown that the quantities and proportions of the chemical products formed in the radiolysis of water are highly dependent on the distances separating the primary radiolytic species from each other along the track of the ionization radiation. The distribution of separations referred to as the "track structure" (see above), is determined to a large extent by the distribution of the physical energy deposition events and their geometrical dispositions, or, in other words, by the quality of the radiation. In fact, track-structure effects are also usually called "LET effects" as most of the early studies used this parameter to characterize the different radiation chemical yields (or "*g*-values") for various irradiating ions in liquid water. The radiation track structure is of crucial importance in specifying the precise spatial location and identity of all the radiolytic species and free-radical intermediates generated in the tracks, and their subsequent radiobiological action at the molecular and cellular levels. Track structure, coupled with a reaction scheme and yields of primary species, forms the basis of radiation-chemical theory (MOZUMDER, 1999). It is now well accepted by the scientific community that differences in the biochemical and biological effects (e.g., damage to DNA, changes in cell signaling, etc.) of different qualities of radiation must be analyzed in terms of track structure (CHATTERJEE and HOLLEY, 1993; MUROYA et al., 2006).

2.1.1 Low-LET radiation and track entities

The average LET of a 1-MeV electron in water is ~0.3 keV/μm. The track-averaged mean energy loss per collision event by such a fast electron is in the region ~48–65 eV (LAVERNE and PIMBLOTT, 1995; MOZUMDER, 1999; AUTSAVAPROMPORN, 2006). This means that the energy-loss events are, on average, separated by distances of about 2000 Å. This nonhomogeneous distribution of energy deposition events in space gives rise to the "spur" theory for low-LET track structure (KARA-MICHAILOVA and LEA, 1940; ALLEN, 1948; SAMUEL and MAGEE, 1953; MAGEE, 1953; GANGULY and MAGEE, 1956), according to which the entire track is to be viewed as a random succession of (more or less spherical) spurs (sometimes called the "string-of-beads" model of a track), or *spatially localized* energy-loss events (it is assumed that irradiating particles are isolated from each other, an assumption not necessarily correct at very high dose rates or with very short pulses of intense beams). The few tens of electronvolts deposited in a spur cause a secondary electron to be ejected from a molecule. As the ejected electron moves away, it undergoes collisions with surrounding water molecules, loses its excess energy, and becomes thermalized (~0.025 eV) within about 80–120 Å of its geminate positive ion (GOULET and JAY-GERIN, 1988; MUROYA et al., 2002; MEESUNGNOEN et al., 2002*a*; PIMBLOTT and MOZUMDER, 2004). This electron thermalization distance or "penetration range" can be viewed as an estimate of the average radius of the spurs in the first stages of their development. Thus, the individual spurs produced by a radiation of low LET (so-called "sparsely" ionizing radiation) are so far apart along the track that they are not initially overlapping (but they will overlap somewhat later as they develop in time).

In their pioneering work to model the radiation chemical consequences of the different energy-loss processes, MOZUMDER and MAGEE (1966*a*,*b*) considered, somewhat arbitrarily, a low-LET track as composed of a random sequence of three types of essentially nonoverlapping entities: "spurs, blobs, and short tracks" (Figure. 2.1).

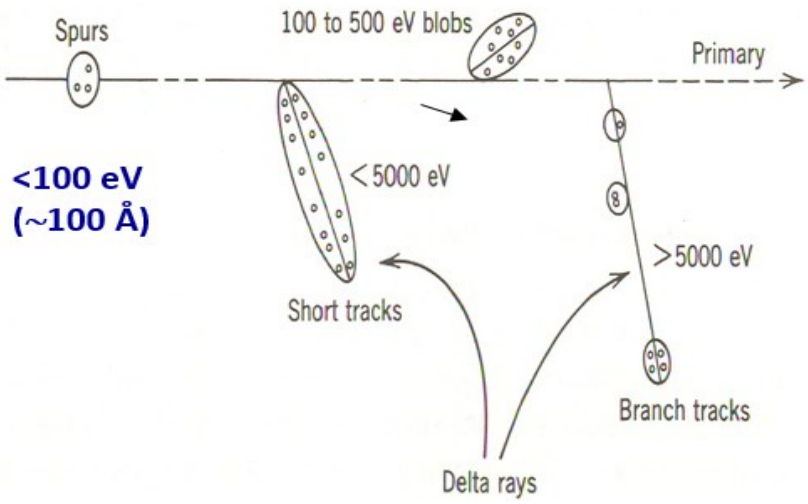

Figure 2.1 Track structure entities classified as spurs (spherical entities, up to 100 eV), blobs (spherical or ellipsoidal, 100-500 eV), and short tracks (cylindrical, 500 eV-5 keV) for a primary high energy electron (not to scale) (Adapted from BURTON, 1969). The energy partition between the three track entities strongly depends on the incident particle energy, dividing approximately as the ratio of 0.75:0.12:0.13 between the spur, blob, and short track fractions for a 1-MeV electron in liquid water (PIMBLOTT et al., 1990).

The spur category contains all track entities created by the energy losses between the lowest excitation energy of water and 100 eV; in most cases, there are one to three ion pairs in such isolated spatial areas and about the same number of excited molecules (PIMBLOTT and MOZUMDER, 1991). Blobs are defined as track entities with energy transfers between 100 and 500 eV, and short tracks as those with energy transfers between 500 eV and 5 keV. Secondary electrons produced in energy transfers above 5 keV are considered as "branch tracks". Short and branch tracks are, collectively, described as δ-rays. This old concept of track entities proved to be very helpful in greatly facilitating the visualization of track processes and in modeling radiation-chemical kinetics. It is still a useful approach for the classification of track structures since it takes into account the spatial arrangements of initial species, which affect their subsequent reactions.

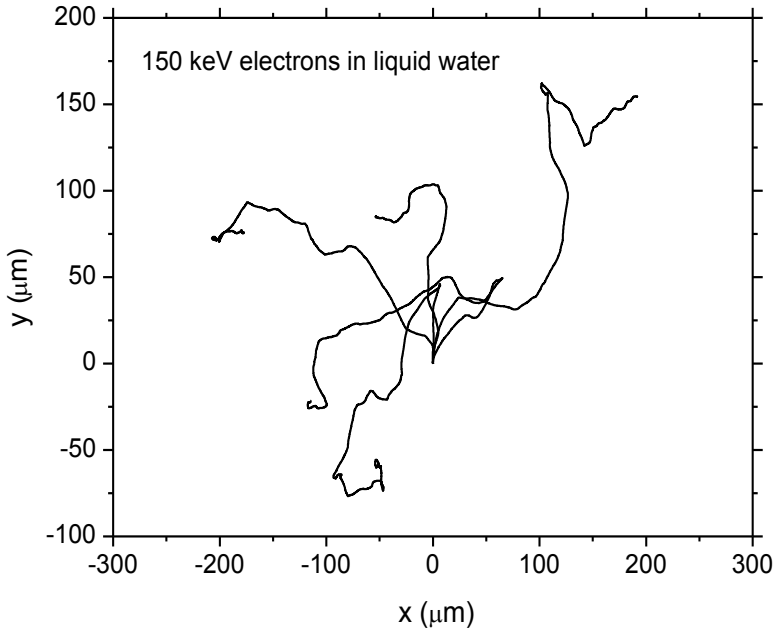

Figure 2.2 Simulated tracks (projected into the *XY* plane of the figure) of five 150-keV electrons in water, showing the stochastic nature of paths. Each electron is generated at the origin and starts moving vertically upwards.

To illustrate the low-LET tracks, Figure. 2.2 shows an example of the complete tracks of five 150-keV electrons and the secondary electrons they produce in water, calculated by our Monte-Carlo simulation program.

2.1.2 High-LET radiation and track structure

High-LET tracks produced by the heavy particles consist initially of a cylindrical "core" (see Figure 2.3) and a surrounding region traversed by the emergent, comparatively low-LET secondary electrons, called the "penumbra" (MOZUMDER et al., 1968; CHATTERJEE and SCHAEFER, 1976; FERRADINI, 1979; MAGEE and CHATTERJEE, 1980, 1987; MOZUMDER, 1999; LAVERNE, 2000, 2004).

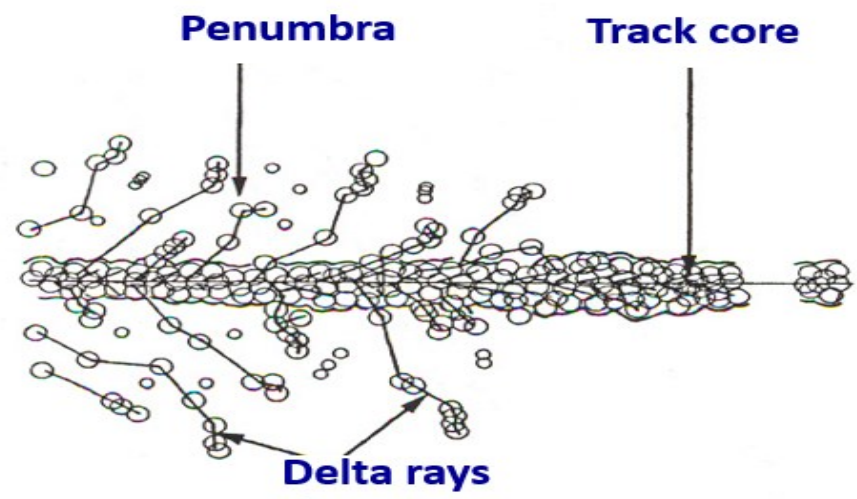

Figure 2.3 Primary energy-loss events in high-LET radiation tracks (Adapted from FERRADINI, 1979).

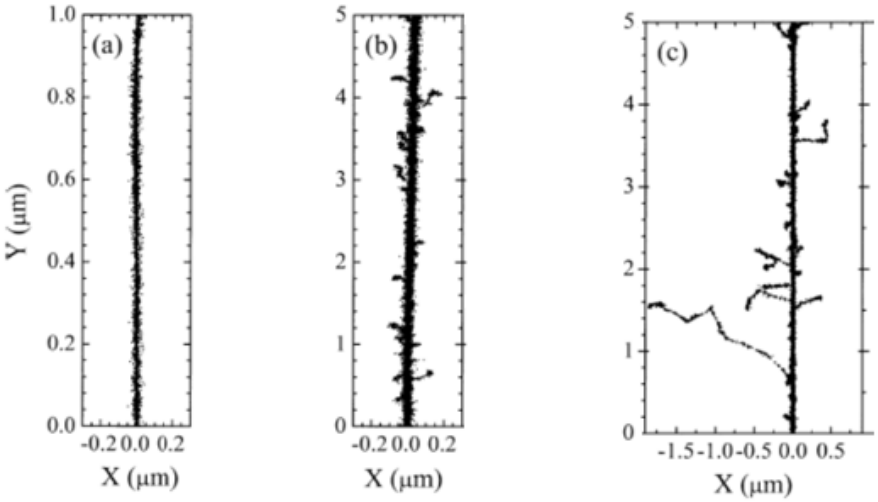

Figure 2.4 Projections over the XY-plane of track segments calculated (at ~10^{-13} s) for (a) H^+ (0.15 MeV), (b) $^4He^{2+}$ (1.75 MeV/nucleon), and (c) $^{12}C^{6+}$ (25.5 MeV/nucleon) impacting ions. Ions are generated at the origin and along the Y-axis in liquid water under identical LET conditions (~70 keV/μm). Dots represent the energy deposited at points where an interaction occurred. Figure adapted fromMUROYA et al. (2006).

Figure 2.4 illustrates typical two-dimensional representations of short (1-5 μm) track segments of H^+ , $^4He^{2+}$, and $^{12}C^{6+}$ ions. The Monte Carlo simulation code IONLYS developed in our laboratory was used to calculate the track segment under the same LET conditions (~70 keV/μm). We can observe that these tracks can be considered as straight lines with the ejected high-energy secondary electrons traveling to a greater average distance away from the track core as the velocity of the incident ion increases, from protons to carbon ions. In other words, even though all those particles are depositing the same amount of energy per unit path length, that energy is lost in a volume that increases in the order $H^+ < {}^4He^{2+} < {}^{12}C^{6+}$, indicating that the higher-Z particle (where Z is the carbon charge number) has the lower mean density of reactive species (MUROYA et al., 2006; MEESUNGNOEN and JAY-GERIN, 2011). The fact that tracks of different ions with the same LET have different radial distributions of energy deposited by δ-rays is in accord with Bethe's theory of stopping power (BETHE, 1930; BETHE and ASHKIN, 1953) indicates that LET is not a unique descriptor of the radiation chemical effects within heavy charged particle tracks (SCHULER and ALLEN, 1957; SAUER et al., 1977; LAVERNE and SCHULER, 1987; KAPLAN and MITEREV, 1987; FERRADINI, 1990; FERRADINI and JAY-GERIN, 1999; LAVERNE, 2000, 2004).

3. RADIOLYSIS OF LIQUID WATER AND AQUEOUS SOLUTIONS

Radiolysis of water is defined as the chemical decomposition of the water molecules due to the action of ionizing radiation. This complex sequence of events that occur between ionizing radiation with water can be divided into three stages (PLATZMAN, 1958):

The overall process of producing chemical changes by ionizing radiation can be usually divided into three stages (PLATZMAN, 1958; KUPPERMANN, 1959) as described below.

3.1 Physical stage

The "*physical stage*" consists of the phenomena by which energy is transferred from the incident ionizing radiation (energetic photons, for example, γ-rays from ^{60}Co or X-ray photons, or charged particles, such as fast electrons, protons, or heavy ions generated by a particle accelerator, or neutron radiation, or high-energy α-particles from suitable radioactive nuclides) to the system. It lasts not more than ~10^{-16} s. The result of this energy absorption is the production, along the path of the radiation, of a large number of ionized and electronically excited water molecules (denoted $H_2O^{\bullet+}$ and $H_2O^*_{elec}$, respectively; note that $H_2O^*_{elec}$ represents here the many excited states, including the so-called superexcitation states (PLATZMAN, 1962*a*) and the collective electronic oscillations of the "plasmon" type (HELLER et al., 1974; KAPLAN and MITEREV, 1987; WILSON et al., 2001). The earliest processes in the radiolysis of water are:

$$H_2O \rightsquigarrow H_2O^{\bullet+} + e^- \qquad (3)$$

$$H_2O \rightsquigarrow H_2O^*_{elec} \qquad (4)$$

Generally, the electron ejected in the ionization event has sufficient energy to ionize or excite one or more other water molecules in the vicinity, and this leads, as mentioned above, to the formation of track entities, or "spurs", that contain the products of the events. For low-LET radiation, the spurs are separated by large distances relative to their diameter and the track can be viewed, at this stage, as a random succession of isolated spherical spurs.

3.2 Physicochemical stage

The Physicochemical stage consists of the processes that lead to the establishment of thermal equilibrium in the system with reactions and reorganization of initial products to give stable molecules and chemically reactive species such as free atoms and radicals. Its duration is about 10^{-12} s for aqueous solutions. During this stage, the ions and excited-state water molecules dissipate their excess energy by bond rupture, luminescence, energy transfer to neighboring molecules, etc.

The ionized water molecules are unstable. They are allowed to undergo a random walk during their very short lifetime (~10^{-14} s) (MOZUMDER and MAGEE, 1975) via a sequence of electron transfers (about 20, one the average, over a few molecular diameters; COBUT et al., 1998) from neighboring water molecules to the $H_2O^{\bullet+}$ hole (i.e., electron-loss center) (OGURA and HAMILL, 1973). These short-lived $H_2O^{\bullet+}$ radical cations subsequently decompose to form $^{\bullet}OH$ radicals by transferring a proton to an adjacent H_2O molecule:

$$H_2O^{\bullet+} + H_2O \rightarrow H_3O^{+} + {}^{\bullet}OH\,, \qquad (5)$$

where H_3O^+ (or equivalently, H^+_{aq}) represents the hydrated hydrogen ion.

The energetic (or "dry") secondary electrons lose their kinetic energy via a sequence of interactions with the medium until they attain thermal energies (~0.025 eV at 25 ºC) after about 4×10^{-14} s (MEESUNGNOEN et al., 2002*a*). In the course of their thermalization, "dry" electrons can be recaptured by their parent ions due to the Coulomb attraction of the latter which tends to draw them back together to undergo electron-cation "geminate" recombination:

$$e^- + H_2O^{\bullet+} \rightarrow H_2O^*_{vib} \qquad (6)$$

As the electron is recaptured, the parent ion is transformed into a (vibrationally) excited neutral molecule.

The electron released in the ionization event can cause further ionization and excitation to occur if it has sufficient kinetic energy. Eventually, its energy falls below the first electronic

excitation threshold of water (~7.3 eV; see: MICHAUD et al., 1991), forming the so-called "subexcitation electron" (PLATZMAN, 1955). This latter loses the rest of its energy relatively slowly by exciting vibrational and rotational modes of water molecules. Once thermalized (e^-_{th}), it can be localized or "trapped" (then forming the so-called "wet" electron whose exact physical nature is still the subject of investigation) (e^-_{tr}) in a pre-existing potential energy well of appropriate depth in the liquid before it reaches a fully relaxed, hydrated state (e^-_{aq}) as the dipoles of the surrounding molecules orient under the influence of the negative charge of the electron. In liquid water at 25 ºC, thermalization, trapping, and hydration can then follow in quick succession in less than ~10^{-12} s (for example, see: JAY-GERIN et al., 2008, and references therein):

$$e^- \rightarrow e^-_{th} \rightarrow e^-_{tr} \rightarrow e^-_{aq} \qquad (7)$$

In the course of its thermalization, the ejected electron can also temporarily be captured by a water molecule to form a transient anion

$$e^- + H_2O \rightarrow H_2O^- \qquad (8)$$

This anion then undergoes dissociation mainly into H^- and $^\bullet OH$ according to

$$H_2O^- \rightarrow H^- + {}^\bullet OH\,, \qquad (9)$$

followed by the reaction of the hydride anion with another water molecule through a fast proton transfer reaction:

$$H^- + H_2O \rightarrow H_2 + OH^-. \qquad (10)$$

Reactions (8) and (9) correspond to the so-called "dissociative electron attachment" (or DEA) process, which has been observed in amorphous solid water at ~20 K for electron energies

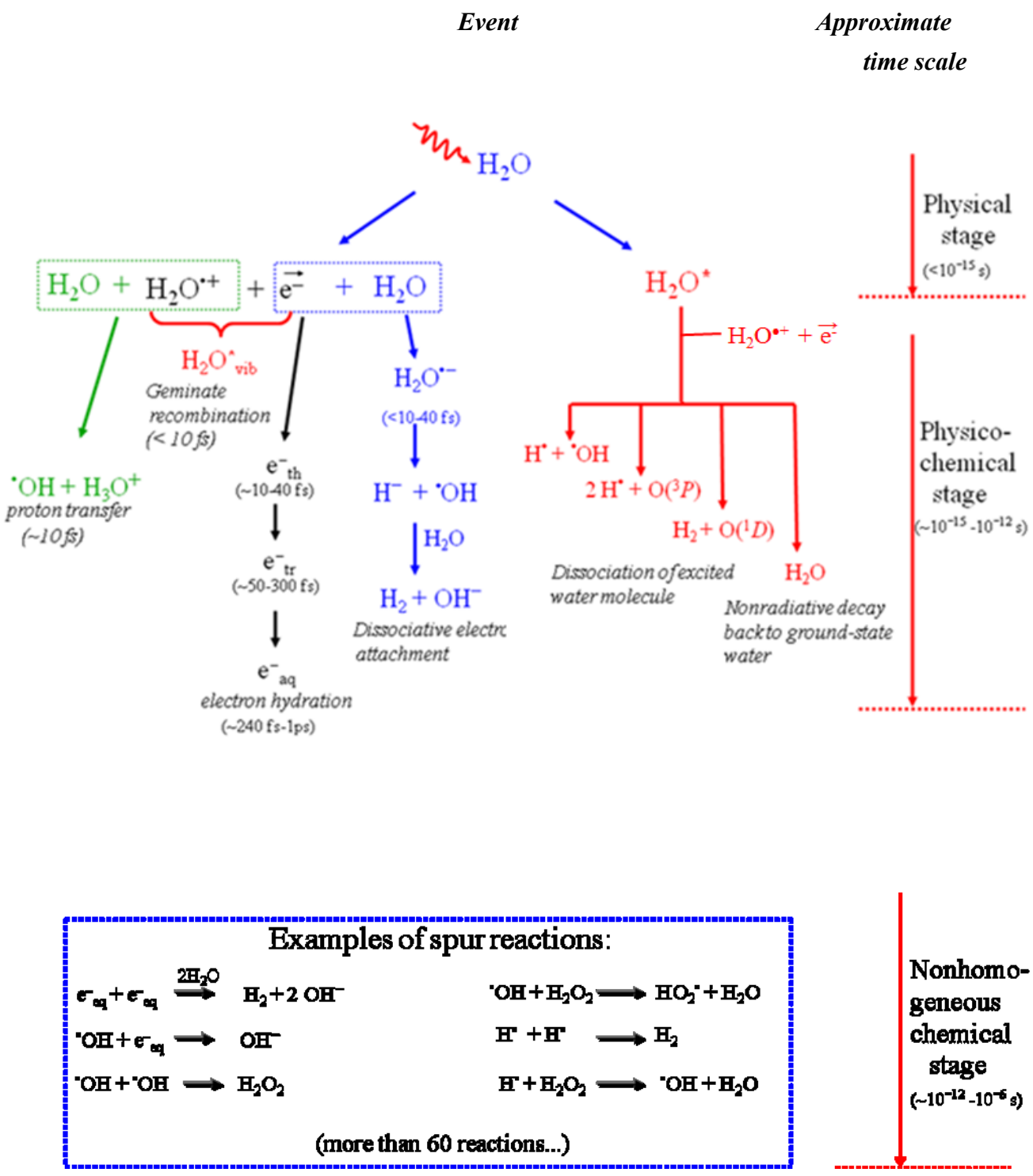

Figure 3.1 Time scale of events that occur in the low-LET radiolysis of neutral, deaerated water (Adapted from MEESUNGNOEN, 2007).

between about 5 and 12 eV (ROWNTREE et al., 1991). DEA to water was suggested to be responsible, at least in part, for the yield of "nonscavengeable" molecular hydrogen in the radiolysis of liquid water at early times (PLATZMAN, 1962*b*; FARAGGI and DÉSALOS, 1969; GOULET and JAY-GERIN, 1989; KIMMEL et al., 1994; COBUT et al., 1996). This proposed mechanism for the production of H_2 has received strong support from recent experiments that have shown that the previously accepted nonscavengeable yield of H_2 is due to precursors of e^-_{aq} and it can be lowered with appropriate (dry electron) scavengers at high concentration (PASTINA et al., 1999).

Excited molecules may be produced directly in an initial act [reaction (2)] or by neutralization of an ion [reaction (6)]. We have little knowledge about the channels through which the excited water molecules in the liquid phase decay and the branching ratios associated with each of them. Fortunately, the contribution of the water excited states to the primary radical and molecular products in the water radiolysis is of relatively minor importance in comparison with that of the ionization processes, so that the lack of information about their decomposition has only limited consequences. Consequently, the competing deexcitation mechanisms of H_2O^* are generally assumed to be essentially the same as those reported for an isolated water molecule (it should be noted here that the same decay processes have been reported to occur for the electronically and vibrationally excited H_2O molecules in the gas phase), namely (see, for example: SWIATLA-WOJCIK and BUXTON, 1995; COBUT et al., 1998; MEESUNGNOEN and JAY-GERIN, 2005*a*):

$$H_2O^* \rightarrow H^\bullet + {}^\bullet OH \qquad (11a)$$

$$H_2O^* \rightarrow H_2 + O(^1D) \qquad (11b)$$

$$H_2O^* \rightarrow 2\,H^\bullet + O(^3P) \qquad (11c)$$

$$H_2O^* \rightarrow H_2O + \text{release of thermal energy} \qquad (11d)$$

where O(^1D) and O(^3P) represent oxygen atoms produced in their singlet ^1D excited state and triplet ^3P ground state, respectively (see Figure. 4.1). Note that the dissociation of H_2O^* via reaction (11*a*) is the main source of the "initial" (at ~10^{-12} s, i.e., at the end of the physicochemical stage, prior to spur or track expansion) yield of hydrogen atoms. As for the different branching ratios (or decay probabilities) associated with reactions (11*a-d*), they are chosen in order to consistently match the observed picosecond *G*-values of the various spur species (MUROYA et al., 2002; MEESUNGNOEN and JAY-GERIN, 2005*a*). It should also be noted here that the O(^1D) atoms produced in reaction (11*b*) react very efficiently with water to form H_2O_2 or possibly also 2$^\bullet$OH (TAUBE, 1957; BIEDENKAPP et al., 1970). By contrast, ground-state oxygen atoms O(^3P) in an aqueous solution are rather inert to water but react with most additives (AMICHAI and TEININ, 1969).

3.3 nonhomogeneous chemical stage

The nonhomogeneous chemical stage consists of the period after ~10^{-12} s, during which the radiolytic species generated previously in a nonhomogeneous track structure (e^-_{aq}, $^\bullet$OH, H$^\bullet$, H_3O^+, H_2, H_2O_2, OH^-, $^\bullet O^\bullet$,...) undergo chemical reactions as they diffuse away from the site where they were originally produced. These species react together to form molecular or secondary radical products, or with dissolved solutes (if any) present at the time of irradiation, until all spur/track reactions are complete. Table 1 gives the principal reactions that are likely to occur while the spurs expand. The time for completion of spur processes is generally taken to be ~10^{-7}-10^{-6} s. By this time, the spatially nonhomogeneous distribution of reactive species has relaxed. Beyond a few microseconds, the reactions which occur in the bulk solution at room temperature can usually be described with conventional homogeneous chemistry methods (for example, see: PASTINA and LAVERNE, 2001).

Briefly, the radiolysis of pure deaerated liquid water by low-LET radiation (such as ^{60}Co γ-rays, hard X-rays, fast electrons, or high-energy protons) principally leads to the formation of the radicals and molecular products e^-_{aq} (hydrated electron), H$^\bullet$ (hydrogen atom), H_2 (molecular hydrogen), $^\bullet$OH (hydroxyl radical), H_2O_2 (hydrogen peroxide), $HO_2^\bullet/O_2^{\bullet-}$ (hydroperoxyl/superoxide anion radicals, pK_a = 4.8), H^+, OH^-, etc. (for a review, see: SPINKS and WOODS, 1990). Under ordinary irradiation conditions, these species are

generated nonhomogeneously on subpicosecond time scales in small, spatially isolated regions of dense ionization and excitation events, referred to as "spurs" (MAGEE, 1953), along the track of the radiation. Owing to diffusion from their initial positions, the radiolytic products then either react within the spurs as they expand or escape into the bulk solution. At ambient temperature, this spur expansion is essentially complete by about 10^{-6}-10^{-7} s after the initial energy deposition. The so-called "primary" radical and molecular yields ("long-time" or "escape" yields) $g(e^-_{aq})$, $g(H^\bullet)$, $g(H_2)$, $g(^\bullet OH)$, $g(H_2O_2)$, etc., represent the numbers of species of each kind formed or destroyed per 100 eV of absorbed energy that remain after

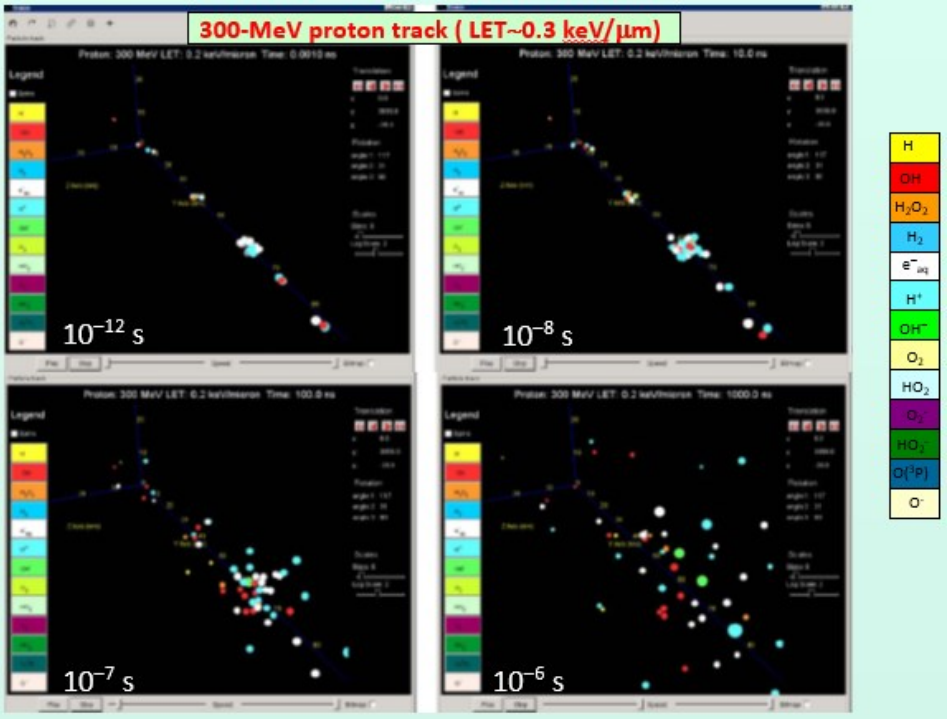

Figure 3.2 Track development from non homogeneous to homogeneous chemical stage (Adapted from PLANTE et al., 2005).

Table 1 Main spur/track reactions and rate constants (k) for the radiolysis of pure liquid water at 25 ºC (from MEESUNGNOEN, 2007). Some values of k have been updated by using the most recently available data of ELLIOT and BARTELS (2009).

Reaction	k (M^{-1} s^{-1})	Reaction	k (M^{-1} s^{-1})
$H^{\bullet} + H^{\bullet} \rightarrow H_2$	5.2×10^9	$e^-_{aq} + e^-_{aq} \rightarrow H_2 + 2\ OH^-$	7.3×10^9
$H^{\bullet} + {}^{\bullet}OH \rightarrow H_2O$	1.6×10^{10}	$e^-_{aq} + H^+ \rightarrow H^{\bullet}$	2.1×10^{10}
$H^{\bullet} + H_2O_2 \rightarrow H_2O + {}^{\bullet}OH$	3.6×10^7	$e^-_{aq} + O_2^{\bullet-} \rightarrow H_2O_2 + 2\ OH^-$	1.3×10^{10}
$H^{\bullet} + e^-_{aq} \rightarrow H_2 + OH^-$	2.8×10^{10}	$e^-_{aq} + HO_2^- \rightarrow O^{\bullet-} + OH^-$	3.51×10^9
$H^{\bullet} + OH^- \rightarrow H_2O + e^-_{aq}$	2.4×10^7	$e^-_{aq} + O^{\bullet-} \rightarrow 2\ OH^-$	2.31×10^{10}
$H^{\bullet} + O_2 \rightarrow HO_2^{\bullet}$	1.3×10^{10}	$e^-_{aq} + H_2O \rightarrow H^{\bullet} + OH^-$	15.8
$H^{\bullet} + HO_2^{\bullet} \rightarrow H_2O_2$	1.1×10^{10}	$e^-_{aq} + O_2 \rightarrow O_2^{\bullet-}$	2.3×10^{10}
$H^{\bullet} + O_2^{\bullet-} \rightarrow HO_2^-$	1.1×10^{10}	$e^-_{aq} + HO_2^{\bullet} \rightarrow HO_2^-$	1.3×10^{10}
$H^{\bullet} + HO_2^- \rightarrow {}^{\bullet}OH + OH^-$	1.5×10^9	$e^-_{aq} + O(^3P) \rightarrow O^{\bullet-}$	2.0×10^{10}
$H^{\bullet} + O(^3P) \rightarrow {}^{\bullet}OH$	2.0×10^{10}	$e^-_{aq} + O_3 \rightarrow O_3^{\bullet-}$	3.6×10^{10}
$H^{\bullet} + O^{\bullet-} \rightarrow OH^-$	2.0×10^{10}	$H^+ + O^{\bullet-} \rightarrow {}^{\bullet}OH$	5.0×10^{10}
$H^{\bullet} + O_3 \rightarrow O_2 + {}^{\bullet}OH$	3.7×10^{10}	$H^+ + O_2^{\bullet-} \rightarrow HO_2^{\bullet}$	5.0×10^{10}
$H^{\bullet} + O_3^{\bullet-} \rightarrow OH^- + O_2$	1.0×10^{10}	$H^+ + OH^- \rightarrow H_2O$	1.2×10^{11}
${}^{\bullet}OH + {}^{\bullet}OH \rightarrow H_2O_2$	6.3×10^9	$H^+ + O_3^{\bullet-} \rightarrow {}^{\bullet}OH + O_2$	9.0×10^{10}
${}^{\bullet}OH + H_2O_2 \rightarrow HO_2^{\bullet} + H_2O$	2.9×10^7	$H^+ + HO_2^- \rightarrow H_2O_2$	5.0×10^{10}
${}^{\bullet}OH + H_2 \rightarrow H^{\bullet} + H_2O$	4.0×10^7	$OH^- + O(^3P) \rightarrow HO_2^-$	4.2×10^8
${}^{\bullet}OH + e^-_{aq} \rightarrow OH^-$	3.6×10^{10}	$OH^- + HO_2^{\bullet} \rightarrow O_2^{\bullet-} + H_2O$	1.3×10^{10}
${}^{\bullet}OH + OH^- \rightarrow O^{\bullet-} + H_2O$	1.3×10^{10}	$O_2 + O^{\bullet-} \rightarrow O_3^{\bullet-}$	3.7×10^9
${}^{\bullet}OH + HO_2^{\bullet} \rightarrow O_2 + H_2O$	9.0×10^9	$O_2 + O(^3P) \rightarrow O_3$	4.0×10^9
${}^{\bullet}OH + O_2^{\bullet-} \rightarrow O_2 + OH^-$	1.1×10^{10}	$HO_2^{\bullet} + O_2^{\bullet-} \rightarrow HO_2^- + O_2$	9.7×10^7
${}^{\bullet}OH + HO_2^- \rightarrow HO_2^{\bullet} + OH^-$	8.3×10^9	$HO_2^{\bullet} + HO_2^{\bullet} \rightarrow H_2O_2 + O_2$	1.94×10^8
${}^{\bullet}OH + O(^3P) \rightarrow HO_2^{\bullet}$	2.02×10^{10}	$HO_2^{\bullet} + O(^3P) \rightarrow O_2 + {}^{\bullet}OH$	2.02×10^{10}
${}^{\bullet}OH + O^{\bullet-} \rightarrow HO_2^-$	1.0×10^9	$HO_2^{\bullet} + H_2O \rightarrow H^+ + O_2^{\bullet-}$	1.4×10^4
${}^{\bullet}OH + O_3^{\bullet-} \rightarrow O_2^{\bullet-} + HO_2^{\bullet}$	8.5×10^9	$O_2^{\bullet-} + O^{\bullet-} \rightarrow O_2 + 2\ OH^-$	6.0×10^8
${}^{\bullet}OH + O_3 \rightarrow O_2 + HO_2^{\bullet}$	1.11×10^8	$O_2^{\bullet-} + H_2O \rightarrow HO_2^{\bullet} + OH^-$	0.155
$H_2O_2 + e^-_{aq} \rightarrow OH^- + {}^{\bullet}OH$	1.1×10^{10}	$O_2^{\bullet-} + O_3 \rightarrow O_3^{\bullet-} + O_2$	1.5×10^9
$H_2O_2 + OH^- \rightarrow HO_2^- + H_2O$	1.33×10^{10}	$HO_2^- + H_2O \rightarrow H_2O_2 + OH^-$	1.27×10^6
$H_2O_2 + O(^3P) \rightarrow HO_2^{\bullet} + {}^{\bullet}OH$	1.6×10^9	$HO_2^- + O^{\bullet-} \rightarrow O_2^{\bullet-} + OH^-$	8.02×10^8
$H_2O_2 + O^{\bullet-} \rightarrow HO_2^{\bullet} + OH^-$	5.55×10^8	$HO_2^- + O(^3P) \rightarrow O_2^{\bullet-} + {}^{\bullet}OH$	5.3×10^9
$H_2 + O(^3P) \rightarrow H^{\bullet} + {}^{\bullet}OH$	4.77×10^3	$O^{\bullet-} + O^{\bullet-} \rightarrow H_2O_2 + 2\ OH^-$	1.0×10^8
$H_2 + O^{\bullet-} \rightarrow H^{\bullet} + OH^-$	1.3×10^8	$O^{\bullet-} + O_3^{\bullet-} \rightarrow 2\ O_2^{\bullet-}$	7.0×10^8
$O(^3P) + O(^3P) \rightarrow O_2$	2.2×10^{10}	$O^{\bullet-} + H_2O \rightarrow {}^{\bullet}OH + OH^-$	1.3×10^6
$O(^3P) + H_2O \rightarrow 2\ {}^{\bullet}OH$	1.9×10^3	$O_3^{\bullet-} + H_2O \rightarrow O^{\bullet-} + O_2$	46.5

spur expansion and become available to react with added solutes (treated as spatially homogeneous) at moderate concentrations.

The radiolysis of pure deaerated (air-free) liquid water for low-LET radiation can be described by the following *global* equation, written for absorbed energy of 100 eV (FERRADINI and JAY-GERIN, 1999) (the symbol $\sim\!\!\rightarrow$ is used to distinguish reactions brought about by the absorption of ionizing radiation):

$$G_{-H_2O}\ H_2O \sim\!\!\rightarrow G_{e^-_{aq}}\ e^-_{aq} + G_{H^\bullet}\ H^\bullet + G_{H_2}\ H_2 + G_{H^+}\ H^+ + G_{OH^-}\ OH^- + G_{^\bullet OH}\ {}^\bullet OH + G_{H_2O_2}\ H_2O_2 + G_{HO_2^\bullet/O_2^{\bullet-}}\ HO_2^\bullet/O_2^{\bullet-} + \ldots, \qquad (12)$$

where the coefficients G_X – also written as $g(X)$ – are the "primary" radical and molecular yields of the various radiolytic species X, and G_{-H_2O} denotes the corresponding yield for net water decomposition. For ^{60}Co γ-rays (photon energies of 1.17 and 1.33 MeV), hard X-rays or fast electrons of the same energies, at neutral pH and 25 °C (average LET ~ 0.3 keV/μm), the most recently reported values of the primary yields are (LAVERNE, 2004) (in units of molecules per 100 eV):[1]

$$G_{e^-_{aq}} = 2.50 \qquad G_{H^\bullet} = 0.56 \qquad G_{H_2} = 0.45$$
$$G_{^\bullet OH} = 2.50 \qquad G_{H_2O_2} = 0.70 \qquad (13)$$

These primary yield values, including the contribution of $HO_2^\bullet/O_2^{\bullet-}$ [note that, for low-LET radiolysis, $HO_2^\bullet/O_2^{\bullet-}$ is a minor radiolytic product because its very small yield of ~0.02 molec./100 eV (HART, 1955; BJERGBAKKE and HART, 1971) accounts for less than 1% of the other primary radiolytic species], are linked by the following equations:

$$G_{e^-_{aq}} + G_{OH^-} = G_{H^+}$$

[1] These units (abbreviated as "molec./100 eV") for *g*-values are used throughout in this work. For conversion into SI units (mol J^{-1}): 1 molec./100 eV ≈ 1.0364 × 10^{-7} mol J^{-1}.

$$G(e^-_{aq}) + G(H\bullet) + 2\,G(H_2) = G(\bullet OH) + 2\,G(H_2O_2) + 3\,G(HO_2\bullet/O_2\bullet^-)\,, \quad (14)$$

expressing the charge conservation and material balance of Eq. (12).

The yields of the radical and molecular species produced by the irradiation within the lifetime of a spur vary with time and also depend on the radiation type (or LET) and the added solute (scavenger) concentration. One of the main goals in the study of the radiation chemistry of water is the determination of those yields and their dependences as a function of those different parameters.

4. RADIOLYSIS OF TRITIUM (^{3}H) β– PARTICLES

Tritium (^{3}H or T) is a radioactive isotope of hydrogen (see Figure 4.1). Its nucleus consists of a proton and two neutrons. Tritium can replace hydrogen atoms and present in the environment in form of tritiated water (HTO), Gaseous tritium (HT), Organically bound tritium (OBT). As a form of hydrogen, it readily forms water molecules, which explains why natural background levels of tritium can be found everywhere in the environment where water is present. Tritium is highly mobile and will become incorporated into key components of the environment — including precipitation, surface water, groundwater, ice, soil moisture, animals and plants. The most common chemical form of tritium is tritium oxide, also called "tritiated water" (usually represented as "^{3}HOH"). In tritiated water, a tritium atom replaces one of the stable hydrogen atoms in the water molecule. The physical, chemical and pharmacological properties of tritium are essentially the same as those of ordinary hydrogen.

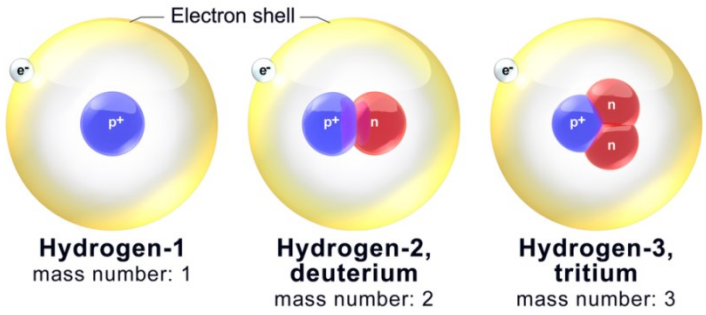

Figure 4.1 Hydrogen Isotopes

The tritium atom is unstable with a half-life of 12.3 years. It fully disintegrates into a nonradioactive, positively charged helium-3 by β decay (FRIEDLANDER et al., 1981):1

$$^3\mathrm{H} \rightarrow {}^3\mathrm{He}^+ + \beta - + \bar{\nu}_e \qquad (15)$$

where $\bar{\nu}_e$ is an antineutrino (which is of no significance because it does not interact with matter and is essentially undetectable) and the β^- particle is the electron from the decay of

one of the neutrons in the nucleus. As it decays, ^{3}H emits ionizing radiation in the form of low-energy β-electrons whose characteristics are: maximum kinetic energy E_{max} ~ 18.6 keV, frequency-weighted mean kinetic energy E_{av} ~ 5.7 keV (this energy is the lowest for the known beta-emitting radioactive elements), mean (averaged over the whole track) "linear energy transfer" (LET) in water ~/μm, the maximum range in the water at 25 °C ~ 5.5 μm (~6 mm in the air). Figure 4.2 shows the ^{3}H β^- energy spectrum.

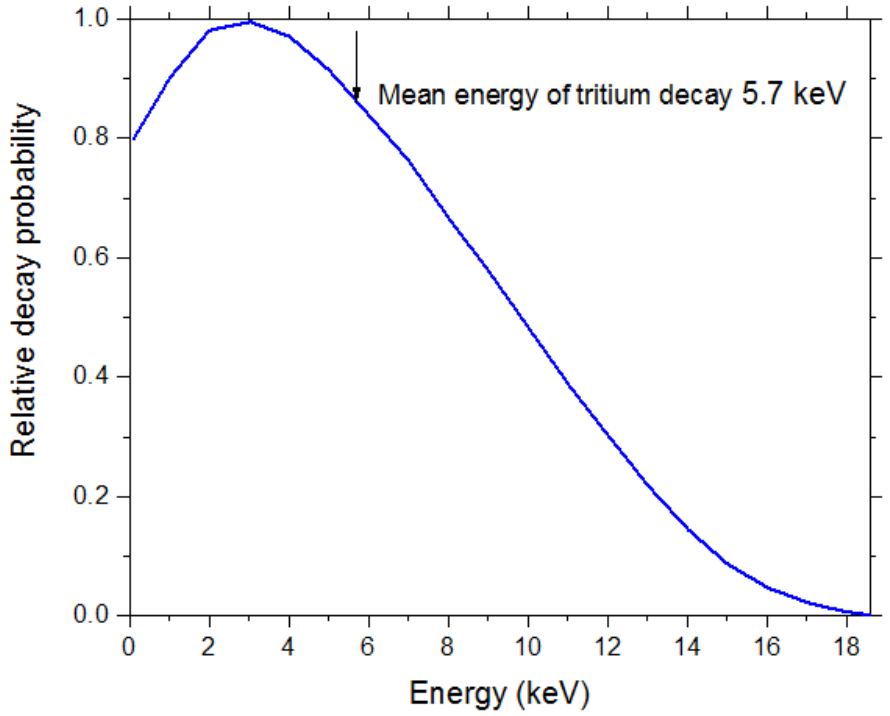

Figure 4.2 The ^{3}H β – decay energy spectrum (Source: T.J. BOWLES and R.G.H. ROBERTSON, Los Alamos Science 1997, No. 25, 86).

While the choice of 5.7 keV is obvious (average kinetic energy released by tritium decay), that of ~7.8 keV requires further explanation. The various electron energies released by the decay of ^{3}H contribute differently to the absorbed dose in the solution. Appropriate weighting according to energy deposition (or "energy fluence rate") by the β-electrons should thus logically be applied in determining accurate G-values. In this context, the distribution of energies deposited by the β-particles appears to be more appropriate to use than the commonly used distribution of tritium beta-decay energies. This energy deposition

distribution, defined as the product $f(E) = E\,h(E)$, where $h(E)$ is the distribution of Figure 4.2, is given in Figure 4.3. The single "mean" or "equivalent" electron energy to properly mimic the radiation chemical action of the ^{3}H β-particles and produce representative *G*-values can then be derived from this $f(E)$ distribution (assuming that the β radiation is totally absorbed in the solution), according to (LAW, 1969; ICRU REPORT, 1970)[76]

$$\int_0^{Emax} Ef(E)dE \,/\, \int_0^{Emax} f(E)dE \quad , \tag{16}$$

where E_{max} = 18.6 keV. This mean energy of energy deposition is 7.8 keV.

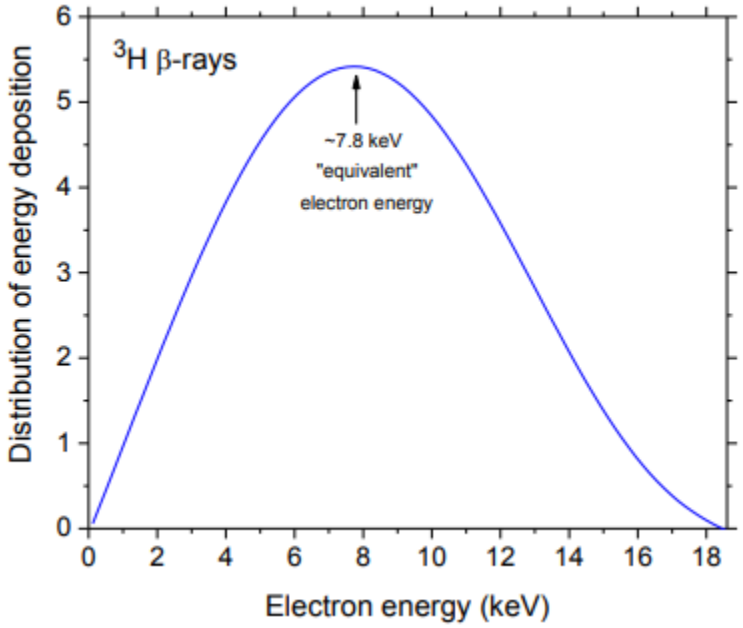

Figure 4.3 Distribution of energy deposition (or "energy fluence rate") by the tritium β-electrons with respect to energy, $f(E)$. The "equivalent" electron energy of ~7.8 keV corresponds to the mean energy derived from this distribution.

Distribution of energy deposition (or "energy fluence rate") by the tritium β- electrons with respect to energy, f(E) (see text). The "equivalent" electron energy of ~7.8 keV corresponds to the mean energy derived from this distribution.

Presently, the utilization of tritium is widely spread in many areas. For example, it is used commercially as the production of self-luminescent lights and paints (ex. exit signs, airport runway lights, watch dials). Tritium gas is combined with phosphor to create luminescence. In biomedical and academic research, tritium is used as a tracer for the development of new drugs (pharmacokinetic properties, absorption, distribution, metabolism, and elimination characteristics). It is also used as radioactive tracers to determine the location of fractures created by hydraulic fracturing in natural gas production. In groundwater research, it is therefore important to know and understand how regularly groundwater gets recharged. Tritium is used to determine whether groundwater is a renewable resource or not. In the future, tritium may also be used to generate electricity in fusion reactors which are currently under development.

Tritium forms naturally in the Earth's upper atmosphere, due to the interaction of gases and cosmic rays. The interaction of cosmic ray neutrons with ^{14}N in the upper atmosphere (cosmogenic tritium)

$$^{14}N(n,^{3}H)^{12}C$$

Tritium produced artificially from (i) fission process of heavy atomic nuclei as ^{235}U in a nuclear reactor, (ii) by-product nuclear power reactor

The capture of a neutron by a deuteron (^{2}H) occurs in heavy water moderated reactors (CANDU). The deuterium nucleus has a small absorption cross-section which in turn makes heavy water a good neutron moderator) and is chemically bound as tritiated heavy water ($^{3}HO_2H$)

$$^{2}H\ (n)^{3}H$$

-Tritium can produce mainly through neutron reactions with boron and lithium that are generally added to the primary cooling water for reactivity control and pH adjustment.

$$^{6}Li(n,\ \alpha)^{3}H$$

$$^{10}B(n,2\alpha)^{3}H$$

(iii) By-product in particle accelerator which occur when bombarding ^{3}He with neutrons

$$^{3}He(n,^{1}H)^{3}H$$

Tritium's long half-life results in a long-term build-up within the plant system. As radiolytically produced chemical species (such as $^{\bullet}OH$, H_2O_2, O_2, and $HO_2^{\bullet}$ or $O_2^{\bullet-}$ depending on the pH) modify the oxidizing character of the medium, an increase in the rate of some corrosion processes can occur in critically important parts of the plant, potentially leading to efficiency and safety problems (BELLANGER, 2004). Considering its radiolytic properties and its corrosion effects on materials, tritiated water is routinely processed after removing it from the reactor vessel. The fraction of the cooling water which is not returned to the reactor vessel is stored in holding tanks. It is periodically released to the environment after further treatment and dilution to bring the tritium concentration to a level that meets regulatory requirements.

Tritiated water can be readily taken in and distributed throughout living cells and organisms. Compounds (other than water) containing hydrogen can also be labeled with tritium (by exchange with other H• atoms) and inhaled, ingested, or absorbed through the skin. Although the maximum range of the emitted electron in a tritium nuclear disintegration is ~5.5 μm in water, tritium is taken into the body and incorporated into cellular structures within or near biologically important molecular sites such as the DNA, might do considerable damage either directly or indirectly through a chemical attack by radiolytic products (STRAUME & CARSTEN, 1993; CHAO et al., 2012).

Generally, the energy of β – particles formed through ^3H radioactive decay is sufficient to both ionize (Eion ~ 6.5 ± 0.5 eV for liquid water at 25 °C) (GOULET et al., 1990) and excite water. This interaction between β-electrons and water molecules initiate the decomposition of water through the phenomenon called "self-radiolysis". Primary radical and molecular products are formed by (neutral) water radiolysis (BUXTON, 1987; SPRINKS & WOOD, 1990; FERRADINI & JAY-GERIN, 1999; MEESUNGNOEN & JAY-GERIN, 2011) along the path of the emitted electron. These include the hydrated electron (e^-_{aq}), H^+ , $H^{\bullet}$, $^{\bullet}OH$, H_2, H_2O_2, OH^- , $O_2^{\bullet-}$ [or its protonated form $HO_2^{\bullet}$, depending on the pH; pKa ($HO_2^{\bullet}/O_2^{\bullet-}$) = 4.8 in water at 25 °C], etc. Molecular oxygen, which is not a direct radiolysis product, is produced through secondary reactions involving the decomposition of H_2O_2. Compared to the chemical effects of ^{60}Co γ-radiolysis, which is mainly due to Compton electrons with an initial energy of about 1 MeV, the chemistry of water and aqueous solutions is very different

after irradiation with ^{3}H β-rays. This difference reflects the influence of the electron energy on the initial spatial distribution of all the radiolytic species and free radical intermediates (i.e., the structure of the electron tracks) created in the two cases (APPLEBY and GAGNON, 1971; LEMAIRE et al., 1972; HARRIS and PIMBLOTTE, 2002)17-19 primary events are more well-separated in the tracks of higher-energy electrons. This is well illustrated in Figure 4.4, which shows typical two-dimensional representations of the complete track of a ~7.8-keV β-electron (mean LET ~ 5.9 keV/μm) and the track segment of a 300-MeV proton (which mimics irradiation with ^{60}Co γ-rays, with an average, LET value of ~0.3 keV/μm), calculated with our IONLYS Monte Carlo simulation code (see below). More precisely, using the terminology of the Mozumder-Magee model of energy deposition, (MOZUMDER and MAGEE, 1966; MOZUMDER, 1999) while the Compton electrons generated by the cobalt-60 γ-rays predominantly form "spurs" (spherical in shape), the low-energy β-electrons of tritium predominantly deposit energy in "short tracks" (short cylinder shapes); this leads to an increased local concentration of reactants and therefore an increased amount of intra-track chemistry. The effects of higher LET of tritium β-rays as compared with ^{60}Co γ-rays are clear in several consequences of ^{3}H β^- particle irradiation (HARDWICK, 1952; HART, 1954; COLLISON et al., 1962; FREGENE, 1967; APPLEBY and GAGNON, 1971; LEMAIRE et al., 1972; GAGNON and APPLEBY, 1973; CHRISTMAN, 1977; HARRIS and PIMBLOTTE, 2002).

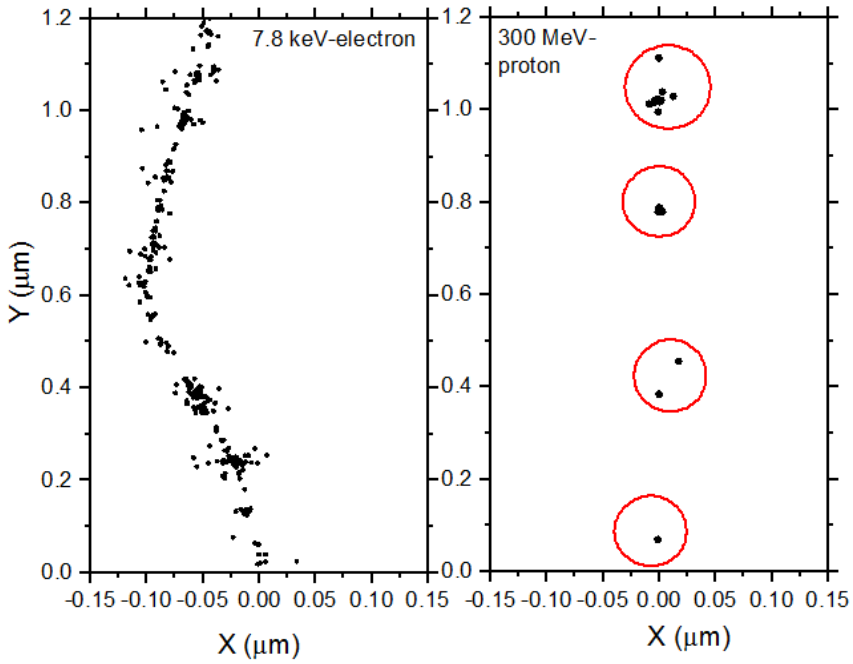

Figure 4.4 Simulated track histories (at ~10^{-13} s, projected into the XY plane of figure) of a 7.8-keV β-electron (mean LET ~ 5.9 keV/μm) and a 300-MeV proton (LET ~ 0.3 keV/μm) incident on liquid water at 25 °C. The two irradiating particles are generated at the origin and start traveling along the Y-axis. Dots represent the energy deposited at points where an interaction occurred.

Table 2 presents estimated the fraction of the total absorbed energy deposited in short tracks, blobs, and spurs for different types of radiation: low-LET ^{60}Co γ radiation and moderately high LET ^{3}H β radiation.

Table 2 Fraction of the total absorbed energy deposited in short tracks, blobs, and spurs for different types of radiation: low-LET ^{60}Co γ radiation and moderately high-LET ^{3}H β radiation (SPINKS and WOODS, 1990).

Energy deposited in:	^{60}Co γ radiation	^{3}H β^- radiation
Short tracks	25%	74.4%
Blobs	11%	7.6%
Spurs	64%	18%

Lower radical and higher molecular yields were observed for ^{3}H β-rays. These differences in yields are completely consistent with differences in the nonhomogeneous distribution of primary transient species (i.e., the structure of electron tracks) in the two cases. In the "short-track" (columnar) geometry of tritium β-electron radiolysis, radicals were formed in much closer initial proximity than in the "spur" (spherical) geometry of γ radiolysis. The "short-track" geometry favors radical-radical reactions in the diffusing tracks, which increases the proportion of molecular products at the expense of the radical products.

5. RESEARCH OBJECTIVE

An understanding of radiation-induced processes in aqueous systems is vital to many areas of basic and applied chemistry, biology, medicine, and in a variety of technological and industrial applications. If nowadays, a general understanding of the phenomena that underlie the radiation chemistry of water and aqueous solutions has been obtained in many cases, it appears that certain quantitative aspects of this radiolysis are not yet fully resolved. This is especially true for *ultrafast processes that link chemistry and physics in the first few picoseconds* following energy deposition. Understanding this interface between radiation physics and radiation chemistry (*i.e.*, "breaking the picosecond barrier") is of obvious relevance to fundamental radiobiology and related science as liquid water is by far the most abundant constituent of biological cells and tissue. Detail knowledge of the early physical and chemical stage of radiation action is central to a reliable description of the chemical nature and highly nonhomogeneous spatial distribution of all reactive species created on the (sub-) picosecond time scale and involved as precursors of radiobiological damage. In the present work, Monte-Carlo simulations have been performed in an attempt

To better understand the interface between radiation physics and radiation chemistry of water. By using Monte-Carlo simulations, we want to produce a complete, reliable description of the chemical nature and highly nonhomogeneous spatial distribution of all reactive species created at very short time and involved as *precursors* of radiobiological damage or corrosion in nuclear reactors.

To get a better understand of the impact of parameters from early time supercritical water, we also see the effect of the $e^-_{aq} + e^-_{aq}$ reaction rate constant on the hydrated electron yield in the low-linear energy transfer (LET) radiolysis of SCW (H_2O) at 400 °C as a function of water density in the range of 0.15 - 0.6 g/cm^3 were also studied

6. EXPERIMENTAL APPROACH

This project will be used state of the art stochastic Monte-Carlo simulations and molecular dynamics calculations in combination with the knowledge gained from currents experimental effort, the proposed research program aims to design experimental and theory based models to advance our understanding of challenging areas of the radiolysis of aqueous system for which, we feel, an early time, molecular level characterization of the underlying chemistry is essential to produce a complete, accurate picture of this radiolysis. It is without doubt, part of a major challenge in fundamental radiobiology.

This project will benefit from our extensive knowledge of the physical and chemical mechanisms of radiation action on water/aqueous solutions and also from our long-standing experience in Monte Carlo methods applied to the simulation of the radiolysis of aqueous systems (COBUT et al., 1998; FRONGILLO et al., 1998). For applications in radiobiology, we have developed and progressively refined with very fine detail a computationally efficient in-house MC code. It simulates ("event-by-event") the track structure of ionizing particles in water, the production of the various ionized and excited species, and the subsequent reactions of these species in time with one another or with available solutes. The code's ability to give accurate, time-dependent chemical yields under different irradiation conditions has been well validated by comparison with a range of experimental data. *For this project, the current version of this code will be extended and adapted according to the target model considered*.

Monte-Carlo simulation

Monte-Carlo simulation techniques were used to model the complex sequence of events that are generated in liquid water and aqueous solutions after the absorption of ionizing radiation. Such a procedure is well adapted to account for the *stochastic* nature of the phenomena, provided that realistic probabilities and cross sections for all possible events are adequately known. The simulation then allows one to reconstruct the intricate action of the radiation. It also offers a powerful tool for appraising the validity of different assumptions, for making a critical examination of proposed reaction mechanisms, and for estimating some unknown parameters. The accuracy of these calculations is best determined by comparing

their predictions with experimental data on well-characterized chemical systems that have been examined with a wide variety of incident radiation particles and energies.

TURNER and his coworkers (1981, 1983, 1988) at the Oak Ridge National Laboratory (Oak Ridge, Tennessee, U.S.A.) jointly with MAGEE and CHATTERJEE at Lawrence Berkeley Laboratory (Berkeley, California, U.S.A.) were the first to use Monte-Carlo simulations to derive computer-plot representations of the chemical evolution of a few keV electron tracks in liquid water at times between ~10^{-12} and 10^{-7} s. Following this pioneering work, stochastic simulation codes employing Monte Carlo procedures were used with success by several investigators to study the relationship between the initial track structure and the ensuing chemical processes that occur in the radiolysis of both pure water and water containing solutes (for a comprehensive list and reviews, see, for example: BALLARINI et al., 2000; UEHARA and NIKJOO, 2006). Two main approaches have been widely used: (1) the "step-by-step" (or random flights Monte Carlo simulation) method, in which the trajectories of the diffusing species of the system are modeled by time-discretized random flights and in which reaction occurs when reactants undergo pairwise encounters, and (2) the "independent reaction times" (IRT) method (CLIFFORD et al., 1986; PIMBLOTT et al., 1991; PIMBLOTT and GREEN, 1995), which allows the calculation of reaction times without having to follow the trajectories of the diffusing species. Among the stochastic approaches, the most reliable is certainly the full random flights simulation, which is generally considered as a measure of reality. However, this method can be exceedingly consuming in computer time when large systems (such as complete radiation tracks or track segments) are studied. The IRT method, a computer efficient stochastic simulation technique, has been devised to achieve much faster realisation than is possible with the full Monte-Carlo model. In essence, it relies on the approximation that the distances between pairs of reactants evolve independently of each other, and therefore the reaction times of the various potentially reactive pairs are independent of the presence of other reactants in the system.

In a program begun in the early 1990s, the Sherbrooke group has also developed and progressively refined with very high levels of detail several Monte Carlo codes that simulate the track structure of ionizing particles in water, the production of the various ionized and

excited species, and the subsequent reactions of these species in time with one another or with available solutes (COBUT et al., 1994, 1998; FRONGILLO et al., 1996, 1998; HERVÉ DU PENHOAT et al., 2000; MEESUNGNOEN et al., 2001, 2003; MEESUNGNOEN and JAY-GERIN, 2005*a*,*b*; MUROYA et al., 2002, 2006; PLANTE et al., 2005; AUTSAVAPROMPORN et al., 2007). A most recent version of the Sherbrooke codes, called IONLYS-IRT (MEESUNGNOEN and JAY-GERIN, 2005*a*,*b*), has been used in the present work. Briefly, the IONLYS step-by-step simulation program models all the events of the physical and physicochemical stages in the track development. The third and final nonhomogeneous chemical stage is covered by the program IRT, which employs the "independent reaction times" (IRT) method (CLIFFORD et al., 1986; GREEN et al., 1990; PIMBLOTT et al., 1991) to model the chemical development that occurs during this stage and to simulate the formation of measurable yields of chemical products. The detailed description and implementation of the IONLYS-IRT had already been given (MEESUNGNOEN and JAY-GERIN, 2005*a*,*b*, and references therein), and will not be reproduced here, only a brief overview of the most essential features of the simulation methodology and reaction scheme, pertinent to the current calculations, is given below.

6.1.1 The IONLYS code

The IONLYS simulation code is used to simulate the early "physical" and "physicochemical" stages of radiation action up to ~10^{-12} s. It is actually composed of two components, one (either TRACEPR for an impacting primary electron or TRACPRO for an incident proton) for transporting the investigated incident charged particle (proton or any other heavy ion projectile) and another (called TRACELE) for transporting all of the energetic electrons (collectively named "secondary electrons") that result from the ionization of the water molecules. The code models, event by event, *all* the basic physical interactions (energy deposition) and the subsequent establishment of thermal equilibrium in the system (conversion of the physical products created locally after completion of the physical stage into the various "initial" chemical species of the radiolysis).

In particular, IONLYS provides the detailed distribution of coordinates of *all* physical events that occur locally during the slowing-down of the irradiating charged particle and of all the secondary electrons that it has generated. The particle will interact with water based

on the probability per unit distance of each particle's energy or cross-section. The code begins by selecting a particular distance to the first interaction site for the incident particle. The calculation continues with the random choice of the type of interaction (ionization, excitation of electronic, vibrational and rotational levels of single water molecules, excitation of plasmon-type collective modes, and elastic scattering) that occurs. If an inelastic collision is an ionization, the particle's energy is reduced by the energy loss selected. The secondary electron produced is given kinetic energy equal to this energy loss minus the binding energy (or ionization energy) of the target electron. Delta rays are produced at sites of high energy loss. Each time a secondary electron is produced, the code proceeds by transporting it until its energy falls below the threshold for electronic excitations, equal to ~7.3 eV for liquid water (MICHAUD et al., 1991) (these electrons we denote as "subexcitation" electrons). If a collision is elastic, an angle of scattering is selected and the flight distance for the next collision site is chosen. The probabilities or cross-sections for all of the individual molecular processes and their alternatives are entered as input data in Monte-Carlo code, based on direct measurements (where available, as cross-section data in the case of liquid water are scarce) or on the theoretical estimations (COBUT et al., 1998; MEESUNGNOEN and JAY-GERIN, 2005*a*). These collision cross sections are needed to follow the history of an energetic charged particle and its products, covering all ranges of energy transferred in individual collisions. Most importantly, they provide the mean free path used to determine the distance to the next interaction, the type of interaction at each event, energy loss, and the angle of emission of the scattered particle (for example, see: DINGFELDER and FRIEDLAND, 2001; NIKJOO et al., 2006; DINGFELDER et al., 2008). The computer simulation thus provides complete information on the spatial distribution of ionized and excited water, $H_2O^{\bullet+}$ and H_2O^*, and subexcitation electrons, e^-_{sub} (energy < 7.3 eV), produced along the incident charged particle trajectory during the physical stage of the radiation action. This stage is concluded in ~10^{-15} s. Full details of the *cross-section database* used in the IONLYS code can be found in the references cited (COBUT, 1993; COBUT et al., 1998; MEESUNGNOEN and JAY-GERIN, 2005*a*).

The simulations performed with IONLYS consist of the generation of short high-energy proton (ion) *track segments* in water. The primary particle is simulated until it has penetrated the chosen length of the track segment into the medium. Note that, due to its large mass, the

proton (or the impacting heavy ion) is almost not deflected by collisions with the target electrons. In the present simulations, these deflections are simply neglected. The use of small path segments is particularly useful as the instantaneous LET of the incident particle is nearly constant over such segments and can be varied simply by changing its energy. All of the produced energetic (dry) secondary electrons are explicitly transported spatially from their initial energies until they reach the subexcitation energy region below ~7.3 eV, the threshold assumed for electronic excitation in liquid water.[2] The location, type of collision, specific quantum transition, and energy transferred are determined by the IONLYS code, event by event. All physical details about the various elastic and energy-loss processes involved and the corresponding scattering cross-sections employed by IONLYS for the simulation can be found in COBUT (1993), COBUT et al. (1998), and MEESUNGNOEN and JAY-GERIN (2005*a*). The time that it takes a secondary electron to reach a subexcitation energy is $<10^{-15}$ s.

The thermalization of subexcitation electrons is treated by IONLYS using the distribution of thermalization distances obtained from Monte-Carlo track-structure calculations (GOULET and JAY-GERIN, 1989; GOULET et al., 1990, 1996; MEESUNGNOEN et al., 2002*b*) based on experimental scattering cross-sections of slow (~1-100 eV) electrons in amorphous ice films at 14 K (MICHAUD et al., 2003) with corrections to account for the liquid phase. Given the initial position of the subexcitation electron, its position is simply displaced in a randomly selected, isotropic direction by the corresponding, energy-dependent mean penetration distance. At this new position, the

[2] Recall here that most energy-loss events by the fast primary charged particle involve small transfers of energy. In fact, Monte-Carlo simulations have shown that the most probable energy loss for liquid water is 15-20 eV, while the track-averaged mean energy loss is around 50-60 eV, depending on the authors (LAVERNE and PIMBLOTT, 1995; COBUT et al., 1998; AUTSAVAPROMPORN, 2006). COBUT et al. (1998) also calculated that, if we sum all the electrons ejected directly by the primary particle and by the successive generations of secondary electrons, 88% of them have kinetic energies less than 20 eV.

electron is regarded as thermalized (e^-_{th}) and subsequently trapped (e^-_{tr}) and hydrated (e^-_{aq}) *where it is*, an approximation likely to be valid in a highly polar medium such as liquid water in which very-low energy (e.g., "subvibrational") electrons have a strong tendency – due to the presence of a large density of possible electron trapping sites – to get instantly trapped prior to thermalization (MOZUMDER, 1999). As mentioned earlier, the time scale of thermalization, trapping, and hydration of a subexcitation electron in liquid water at 25 ºC is less than ~10^{-12} s. Finally, it is worth recalling here that a certain proportion of subexcitation electrons will actually never get thermalized, but will instead undergo prompt recombination[3] with their positive parent ion $H_2O^{\bullet+}$ or dissociative attachment onto a surrounding H_2O molecule. All details about the various parameters intervening in the IONLYS code to describe this competition between thermalization, geminate recombination, and dissociative attachment, as well as the values of the branching ratios used in the code for the different dissociative decay channels of the electronically and vibrationally excited H_2O molecules, will be explained in the article No. 1 (SANGUANMITH et al., 2011*a*). Obviously, the TRACEPR module of IONLYS, which is entirely dedicated to the description of electron track structures, was used in this study to simulate the radiolysis of water by the tritium-

[3] About 25.5% of the subexcitation electrons are found to initially recombine with $H_2O^{\bullet+}$ (MEESUNGNOEN and JAY-GERIN, 2005*a*), with an average recombination time as short as a few femtoseconds (GOULET et al., 1990). This average recombination time shows that the recombination process mainly occurs on the water cation and *not* on H_3O^+, that is, before the proton transfer reaction $H_2O^{\bullet+} + H_2O \rightarrow H_3O^+ + {}^\bullet OH$ takes place (~10 fs) (which would change the nature of the cation and therefore affect the values of the recombination cross section). In other words, the subexcitation electron recombines quickly (in the first steps of its random walk) on $H_2O^{\bullet+}$. If it does not recombine quickly, it will never recombine, and will thus become thermalized (unless, of course, it makes a dissociative attachment on a water molecule) (~56 fs), trapped (~50-300 fs), and hydrated (~240 fs-1 ps) (MEESUNGNOEN and JAY-GERIN, 2005*a*; JAY-GERIN et al., 2008 and references therein).

decay β-electrons. As for the TRACPRO module, it was used here to simulate track segments of 300-MeV incident protons (LET ~ 0.3 keV/μm), which mimic irradiation with ^{60}Co γ-rays

6.1.2 The IRT code

This code begins at 10^{-12} s in the calculations, after the end of the physicochemical stage (~10^{-12} s; we assume that this time also marks the beginning of diffusion), which is provided as an output of the IONLYS program, is then used directly as the starting point for the subsequent nonhomogeneous chemical stage. This third and final stage, during which the individual reactive species diffuse randomly at rates determined by their diffusion coefficients and react with one another (or with any added solutes present at the time of irradiation) until all spur or track processes are complete, is covered by the IRT program.

This program employs a Monte-Carlo simulation technique, the so-called "*independent reaction times*" (IRT) method (CLIFFORD et al., 1986; GREEN et al., 1990; PIMBLOTT et al., 1991). This method is based on the approximation that the distances between pairs of reactants evolve independently of each other, and therefore the reaction times of the various potentially reactive pairs are independent of the presence of other reactants in the system. In essence, the simulation begins by considering the initial, or "zero-time", the spatial distribution of the reactants (given by the IONLYS program). The separations between all the pairs of reactants are first calculated. Overlapping pairs (i.e., pairs formed in a reactive configuration) are assumed to combine immediately. For each remaining pair, a reaction time is stochastically sampled according to the reaction time probability distribution function (GREEN et al., 1990; GOULET and JAY-GERIN, 1992; FRONGILLO et al., 1998) that is appropriate for the type of reaction considered. This function depends upon the initial distance separating the species, their diffusion coefficients, their Coulomb interaction (for reactions between ionic species), their encounter distance,[4] and the probability of reaction during one of their encounters. The competition between the various reactions is taken into account by realizing them in the ascending order of sampled reaction times. When a reaction occurs, the reactants become unavailable for the competing reactions that are sampled to occur at longer times but one must then consider the possible

[4] The "encounter distance" ($a_{A,B}$) for each pair of interacting species A and B can be derived from the Smoluchowski equation.

reactions of the newly formed products with the species that have survived up to that point. Since the IRT method is solely based on a comparison of reaction times, it does not follow the trajectories of the diffusing species. Therefore, a special procedure must be devised to sample the positions of the reaction products and of the species with which newly formed species can in turn react (CLIFFORD et al., 1986). The inclusion of a scavenger in the system does not affect the general simulation technique. In fact, the IRT program allows one to incorporate in a simple way pseudo-first-order reactions of the radiolytic products with various scavengers that are homogeneously distributed in the solution, such as H^+, OH^-, and H_2O itself, or more generally any solutes for which the relevant reaction rates are known. Similarly, the truly first-order fragmentations of the species are easily simulated. Finally, the IRT method is very well suited for the description of reactions that are only partially diffusion-controlled (most reactions that occur in irradiated water are not diffusion-controlled even at room temperature), an adequate description of the activation processes that are involved in those reactions is a prerequisite for the modeling of the effects of high temperature on water radiolysis), in which the species do not react instantaneously on encounter but experience, on the average, many encounters and separations before they actually react with each other. The ability of the IRT method to give accurate time-dependent chemical yields under different irradiation conditions has been well validated by comparison with full random flights (or "step-by-step") Monte-Carlo simulation, which does follow the particle trajectories in detail (PIMBLOTT et al., 1991 and references cited therein; GOULET et al., 1998; PLANTE, 2009).

6.2 Simulation of azide aqueous solution

To simulate the radiolysis of the N_3^- solutions, we have supplemented the pure-water reaction scheme to include the primary e^-_{aq} and $H^\bullet$ atom scavenging reactions that occur in the system. The reaction scheme of azide with reaction rate constants is shown in Table 4. Under normal irradiation conditions, the concentrations of radiolytic products are low compared with the background concentrations of N_3^- ions considered, and their reactions could be modeled in the IRT program as pseudo-first-order reactions. In the computer simulations reported here, the diffusion coefficient used for N_3^- in liquid water at 25 °C was

1.84×10^{-5} cm^2/s.[54] This same value was also used for the diffusion coefficient of the azide radical $N_3^{\bullet}$.

In addition, we have introduced in the IRT program the effect of the ionic strength of the solutions on all reactions between ions. To relate the rate constant and ionic strength of the solution over the 25-350 °C temperature range, we used the following equation, obtained from the Brönsted-Bjerrum model of ionic reactions and the extended Debye-Hückel theory of ionic solutions (GUGGENHEIM, 1935; DAVIES, 1938; ROBINSON and STOKES, 1959; CZAPSKI and SCHWARZ, 1962; WESTON and SCHWARZ, 1972; JONAH et al., 1977; ELLIOT et al., 1990):

$$\log\left(\frac{k}{k_0}\right) = 3.64 \times 10^6 \frac{Z_a Z_b}{(\varepsilon T)^{3/2}} \left(\frac{I^{1/2}}{1 + I^{1/2}}\right) \qquad (17)$$

where k is the rate constant at ionic strength I, k_0 is the rate constant at infinite dilution of ions (i.e., in the limit of zero ionic strength), Z_a and Z_b are the algebraic numbers of charges on the reactants (positive for cations and negative for anions), T is the absolute temperature (in K), ε is the dielectric constant of the medium (for water, ε = 78.5 at 25 °C and 13.0 at 350 °C). The ionic strength I (in M) of the solution is defined as (SOLOMON, 2001):

$$I = \frac{1}{2} \sum_i Z_i^2 C_i \qquad (18)$$

where Z_i is the charge number of the i_{th} ion and C_i is its molar concentration. The sum extends over all ionic species present in the solution. According to Eq. (17), the rate constant will increase, decrease, or remain the same with increasing ionic strength, depending on whether the reactants have the same sign, opposite signs, or whether one reactant is neutral. Finally, even though some experimental results are available for highly concentrated N_3^- solutions (up to 5 M), we generally restricted ourselves here to solute concentrations not exceeding ~1 M to avoid any complications due to the "direct" action of ionizing radiation on the solute (which our Monte Carlo code does not take into account).

Table 3 Reactions added to the pure water reaction scheme to simulate the radiolysis of azide aqueous solutions, at 25 ºC (from SANGUANMITH et al., 2018).[(a)]

	Reaction	k (M^{-1} s^{-1})
19	$N_3^- + H^\bullet \rightarrow HN_3^{\bullet -}$,	3.15×10^9 $M^{-1}s^{-1}$
20	$N_3^- + e^-_{aq} \rightarrow$ products	$\leq 1.5 \times 10^6$ $M^{-1}s^{-1}$
21	$N_3^- + H^+ \leftrightarrow HN_3$	pKa= HN_3/N_3^- = 4.7, $k_{forward} = 10^9$-10^{10}
22	$HN_3 + e^-_{aq} \rightarrow HN_3^{\bullet -}$	1.2×10^{10}
23	$HN_3 + H^\bullet \rightarrow$ products	6.31×10^7
24	$N_3^- + {}^\bullet OH \rightarrow N_3^\bullet + OH^-$	1.2×10^{10}
25	$HN_3 + {}^\bullet OH \rightarrow N_3^\bullet + H_2O$	$k_9 < 10^7$
26	$N_3^\bullet + e^-_{aq} \rightarrow N_3^-$	2.34×10^{10}
27	$N_3^\bullet + H^\bullet \rightarrow HN_3$	$>10^{10}$
28	$N_3^\bullet + {}^\bullet OH \rightarrow$ products	$< 10^6$
29	$N_3^\bullet + H_2O_2 \rightarrow$ products	$< 5 \times 10^6$
30	$N_3^\bullet + N_3^\bullet \rightarrow 3N_2$	3.95×10^9
31	$N_3^\bullet + N_3^- \rightarrow (N_3)_2$	2.4×10^5

[(a)] Note that the rate constants given here for the reactions between ions are at ionic strength equal to zero.

6.3 Simulation of the effect of temperature

In the "physical" stage, *the scattering cross sections used in the simulations are independent of the medium's temperature* because the energy of the ionizing particles is much larger than the thermal energies and because the motion of the target (water molecules) can be neglected. However, the density (ρ) of pressurized water varies with temperature (from ρ = 1 g/cm^3 at room temperature to ρ = 0.575 g/cm^3 at 350 ºC),

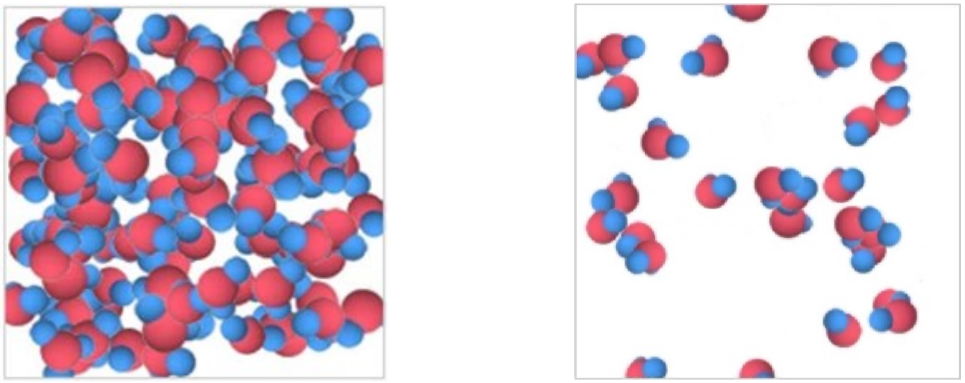

ρ = 1 g/cm^3 at 25 °C ρ = 0.7125 g/cm^3 at 300 ºC

Figure 6.1 The configuration of water molecules with density (ρ) of pressurized water varies with temperature from ρ = 1 g/cm^3 at 25 °C (on the left) and ρ = 0.7125 g/cm^3 at 300 ºC (MATATLA et al., 2016).

and this influences the particles scattering mean free paths (MFP) which are related to the scattering cross cross-sections through the simple relation MFP = 1/(σ*N*), where σ is the total cross-section and *N* is the number of scatterers per unit volume. The 42.5% decrease in *N* that takes place when the temperature is increased from 25-350 ºC thus causes the energy depositions to become significantly further apart. As a result of the invariance of the scattering cross-sections, this dilatation is proportional to the inverse of the density..

In the "physicochemical" stage, the influence of the temperature is not well understood. It seems that many parameters intervening in this stage (such as the dissociative decay channels for H_2O^*, the migration of the ions H_2O^+ and of the subexcitation electrons) are likely to be sensitive to temperature. It should be mentioned that many authors, such as SWIATLA-WOJCIK and BUXTON (1995), have suggested that the temperature – through a diminution of hydrogen bonding in liquid water – could possibly change the relative contributions of the dissociative decay channels for H_2O^*. First of all, the variations of density would act as they did in the physical stage, increasing (on average) each step of the random walk. But any number of other phenomena could come into play. For example, when a "hot" (subvibrational) electron is slowing down before eventually getting trapped, it goes

through a stage during which its energy is nearly thermal, so that it can not only lose energy but also gain some from the surrounding medium. If the duration of this quasi-equilibrium stage depends on temperature, it could affect the electron thermalization distances.

Another temperature effect that could turn out to be the most important one in the physicochemical stage, is its influence on the scattering cross-section of the low-energy electrons. In fact, electrons in the subexcitation energy range are known to be sensitive to the structural order of the surrounding medium, owing to their nonnegligible delocalized character. In various media, their scattering cross-sections have been shown to increase rapidly when the degree of order diminishes (HERVÉ DU PENHOAT et al., 2000 and references cited therein). This also seems to be the case for water, since the electron cross sections found in amorphous ice at low incident energy (MICHAUD and SANCHE, 1987) appear to be somewhat smaller (by a factor of ~2) than those that apply to liquid water (COBUT et al., 1998; GOULET et al.,1996) and much smaller (by at least an order of magnitude) than those reported for the gas phase (MICHAUD and SANCHE, 1987). On this basis, one could expect the scattering cross-sections of subexcitation electrons to increase with temperature in the range 25-350 ^{o}C, since the breaking of the hydrogen bonds gives rise to a decrease of the structural order. It is difficult to estimate to what extent this could affect thermalization distances, but one cannot exclude the possibility that this effect could overcome the 42.5% decrease in the density as temperature increases from 25-350 ^{o}C and in turn reduce those distances significantly. A similar conclusion was obtained previously by HOCHANADEL and GHORMLEY (1962), who suggested that, at the higher temperature, "subexcitation electrons are thermalized more rapidly". And it seems that our simulations are better to reproduce the experimental yields if the electron thermalization distances decrease with increasing temperature.

In the "nonhomogeneous chemical" stage, during which the radiolytic species diffuse and react with one another with a kinetic dictated by their initial nonhomogeneous spatial distribution. At room temperature, this stage is essentially completed at the time of the end of spur expansion after which homogeneous chemistry takes over. It should be noted that the time at the end of the spur depends on temperature. The nonhomogeneous spur/track

expansion is complete by ~ 4.2 × 10^{-7} s at 25 °C and decreases to ~ 5.7 × 10^{-8} s at 350 °C (SANGUANMITH et al., 2011*b*).

Some chemical reactions can take place before any diffusion of species occurs because the latter are formed already "in contact" at the end of the physicochemical stage (COBUT et al., 1998; FRONGILLO et al., 1998). For simplicity, we consider that those "contact reactions" occur at ~10^{-12} s (i.e., the starting point of the nonhomogeneous kinetics). The occurrence of all the other reactions depends on the ability of reactants to meet and on the probability that their encounter gives rise to a reaction (most reactions are not diffusion-controlled). The physical parameters that will determine the time-dependent reaction probability of a pair of reactants will therefore be (i) their initial separation, (ii) their diffusion coefficient, (iii) their electrostatic interaction (i.e., their charge and the dielectric constant of the medium), (iv) their reaction radius, and (v) their probability of reaction per encounter. The temperature of the medium has an influence on many of those parameters. The effect of temperature on the initial position of the species comes from the temperature dependence of the scattering mean free paths mentioned in the first two stages. Its influence on the diffusion coefficient depends on the actual species considered, but this parameter always increases with temperature. In the simulation, the temperature dependences of the diffusion coefficients of H_3O^+, OH^-, e^-_{aq}, and H_2O are represented by polynomial fits to the experimental data (ELLIOT and BARTELS, 2009). For the other species, whose diffusion coefficients are unknown at elevated temperatures, the following scaling procedure has been adopted:

$$D_I(t) = D_I(25\,^\circ\mathrm{C}) + \frac{D_{H_2O}}{D_{H_2O}(25\,^\circ\mathrm{C})} \qquad (32)$$

where t denotes the temperature in degrees Celsius.

Compared to the original version of our IRT program some diffusion coefficients (D) of reactive species and temperature dependence of reaction rate constants have been updated. Figure 6.2 shows the diffusion coefficients of various species as a function of temperature which has been updated in our Monte-Carlo simulations.

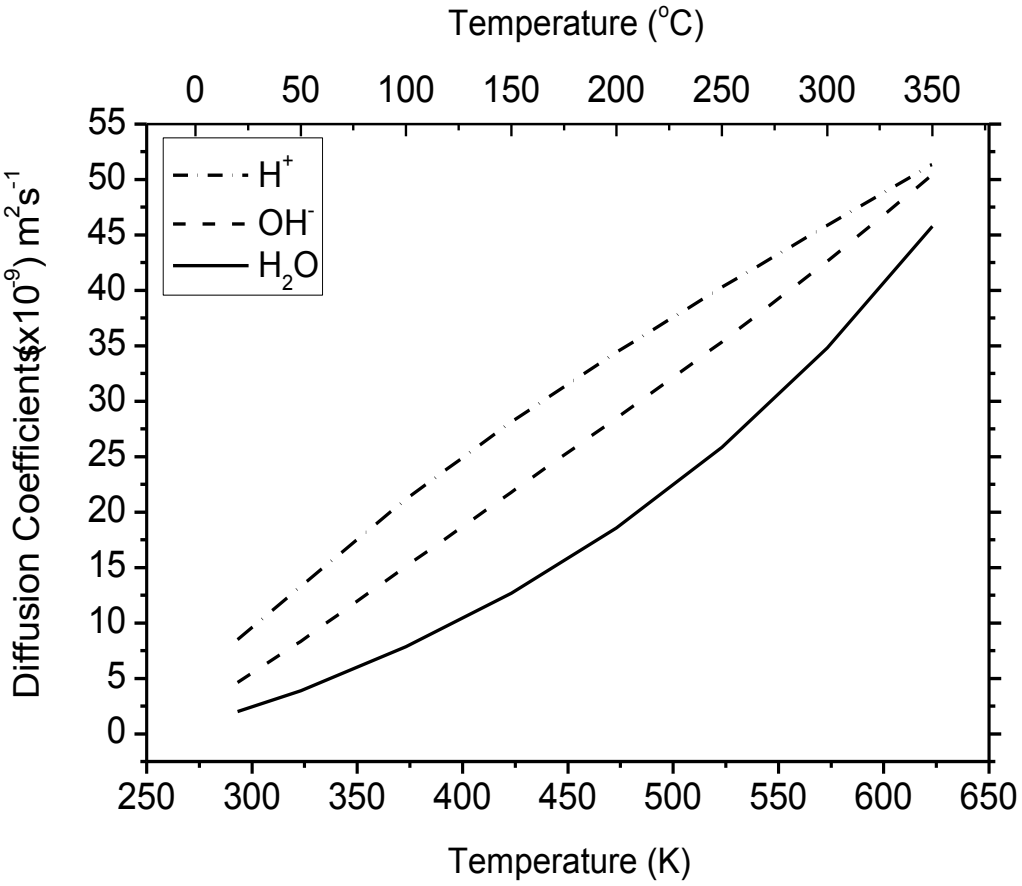

Figure 6.2 Diffusion coefficients (D) for the various track species involved in our simulations (ELLIOT and BARTELS, 2009).

Rate constants are sensitive functions of temperature and for this reason, are important parameters in predictive modeling of high-temperature water chemistry. What is generally known is the temperature dependence of the "observed" reaction rate constant (k_{obs}), from which it is possible to extract information on the temperature dependences of the "activation" and "diffusion" processes that are involved in the reaction. For reactions whose rates are nearly diffusion-controlled at room temperature, k_{obs} are best described by the Noyes equation:

$$\frac{1}{k_{obs}} = \frac{1}{k_{diff}} + \frac{1}{k_{act}} , \qquad (33)$$

where k_{diff} is the rate constant for a truly diffusion-controlled reaction and k_{act} is the rate constant that would be measured if diffusion had no influence on the reaction rate (NOYES, 1961). A number of reactions pertinent to the radiation chemistry of water have been found to be best described by Eq. (33) (see, for example: ELLIOT, 1994). The Arrhenius equation is used to evaluate k_{act} empirically:

$$k_{act} = A \exp(E_{act}/RT) , \tag{34}$$

where E_{act} is the activation energy of the process, A is referred to as the pre-exponential factor, R is the gas constant and T is the absolute temperature. k_{diff} is given by the Smoluchowski equation (see, for example: ELLIOT et al., 1990; ELLIOT, 1994; SWIATLA-WOJCIK and BUXTON, 1995; HERVÉ DU PENHOAT et al., 2000):

$$k_{diff} = 4\pi\beta N_{Av} (D_A + D_B) a_{A,B} \tag{35}$$

where N_{Av} is Avogadro's number, $(D_A + D_B)$ is the sum of diffusion coefficients for both reacting species, β is a spin statistical factor for radical-radical reactions, and $a_{A,B}$ is the encounter (or reaction) distance. When the reactants are ions, Eq. (34) is multiplied by the Debye factor (DEBYE, 1942):

$$f_D = \frac{\delta}{e^{\delta} - 1} \tag{36}$$

where δ is given by

$$\delta = \frac{Z_A Z_B e^2}{4\pi\varepsilon_o \varepsilon(T) a_{A,B} k_B T} , \tag{37}$$

where Z_A and Z_B are the charges on the ions, e is the electron charge, ε_o is the permittivity of free space, $\varepsilon(T)$ is the dielectric constant of the medium, and k_B is Boltzmann's constant.

The list of the main spur/track chemical reactions and values of reaction rate constants considered in our pure liquid water radiolysis simulations as a function of temperature (ELLIOT and BARTELS., 2009) has been illustrated in Appendix 2.

To reproduce the effect of temperature on the low-LET (~0.3 keV/μm at 25 °C) radiolysis of water from ambient up to 350 °C, we used an extended version of our IONLYS-IRT code which was developed previously (HERVÉ DU PENHOAT et al., 2000; TIPPAYAMONTRI et al., 2009; SANGUANMITH et al., 2011*a*). In this version, we used the self-consistent radiolysis database, including rate constants, diffusion coefficients, reaction mechanisms, and *g*-values, compiled by ELLIOT and BARTELS (2009). This new database provides a recommendation for the best values to use in high-temperature modeling of water radiolysis up to 350 °C. In addition, to counterbalance the strong influence of the rapid drop observed in the rate of the self reaction of e^-_{aq} above 150 °C (CHRISTENSEN and SEHESTED, 1986; ELLIOT, 1994; MARIN et al., 2007) and thus obtain a good agreement between model and experiment for the temperature dependence of H_2 yield, we were led to adjust the temperature dependence of some parameters involved in the early physicochemical stage of the radiolysis, namely, the electron thermalization distance (r_{th}), the dissociative electron attachment (DEA), and the branching ratios of the different excited water molecule decomposition channels. The details of this adjustment are published elsewhere (SANGUANMITH et al., 2011*a*) but we briefly summarize them here. In essence, the values of r_{th} were obtained by comparing our simulated time-dependent e^-_{aq} yield data to recent picosecond (~60 ps to 6 ns) and conventional nanosecond (using e^-_{aq} scavenging by methyl viologen MV^{2+}) pulse radiolysis measurements of the decay kinetics of e^-_{aq} at several different temperatures between 25 and 350 °C (MUROYA et al., 2010; MUROYA, unpublished data). Using this best fitting procedure, r_{th} was found to remain relatively unchanged below ~100-150 °C (and equal to its value at 25 °C), but to decrease sharply at higher temperatures with $r_{th}/r_{th}(25\ °C) \approx 0.4$ at 300 °C. This decrease in r_{th} above 100-150 °C was interpreted as indicating an increase in the scattering cross-sections of subexcitation electrons (e^-_{sub}) (GOULET and JAY-GERIN, 1989; MOZUMDER, 1999) that accounts for a decrease in the degree of structural order of water molecules due to an increasing breaking of hydrogen bonds with temperature (HERVÉ DU PENHOAT et al., 2000). Building on these findings on r_{th}, we incorporated in our modeling calculations a temperature dependence of the DEA and of the branching ratios of the different decay channels for excited water molecules (as r_{th}, these parameters are sensitive to the local structural order of water) in a form similar to that of r_{th}, that is, unchanged below 100-150 °C and then followed by a

marked discontinuity around these temperatures. In the absence of any other detailed experimental information, we assumed that the values of these latter parameters at 350 °C were equal to those observed in water vapor (SWIATLA-WOJCIK and BUXTON, 1995; SANGUANMITH et al., 2011*a*).

All Monte-Carlo simulations reported here were performed along the liquid-vapor coexistence curve, the density of the pressurized water decreasing from 1 g/cm^3 (1 bar or 0.1 MPa) at 25 °C to 0.575 g/cm^3 (16.5 MPa) at 350 °C (LINSTROM and MALLARD, 2005). For this range of temperature, calculations show that *g*-values vary only a little with the applied pressure. Finally, to reproduce the effects of ^{60}Co γ-rays or fast electrons, we used short segments (~150 μm) of ~300-MeV proton tracks, over which the average LET value obtained in the simulations was nearly constant and equal to ~0.3 keV/μm at 25 °C (McCRACKEN et al., 1998; COBUT et al., 1998; FRONGILLO et al., 1998). The number of proton histories (~150) Tritium-β primary electron track structures were simulated using ~6000 different whole track histories. This number was chosen to ensure only small statistical fluctuations in the computed averages of chemical yields, while keeping acceptable computer time limits.

7. ARTICLE 1

Radiolysis of Supercritical Water at 400 °C: A Sensitivity Study of the Density Dependence of the Yield of Hydrated Electrons on the (e^-_{aq} + e^-_{aq}) Reaction Rate Constant

Authors: Sunuchakan Sanguanmith, Jintana Meesungnoen, David A. Guzonas, Craig R. Stuart, and Jean-Paul Jay-Gerin

Status: published in Journal of Nuclear Engineering and Radiation Science 2 (2), 0210141-5 (2016).

Forewords: In this work, I did all the calculations of the yield of hydrated electrons in the low LET radiolysis of supercritical water over the density range 0.15-0.6 g/cm^3 by using the two different values of the e^-_{aq} self-reaction rate constant at 400 °C. I have used all reaction rate constants which correspond to the best recommended values reported by Elliot and Bartels (2009). I also wrote the first draft of the manuscript of this work.

Résumé : Des simulations Monte Carlo ont été utilisées dans cette étude pour examiner la sensibilité de la dépendance de la densité du rendement de l'électron hydraté (e^-_{aq}) dans la radiolyse à faible « transfert d'énergie linéaire » (LET) de l'eau supercritique (H_2O) à 400 °C aux variations de la dépendance en température de la constante de vitesse d'auto-réaction k(e^-_{aq} + e^-_{aq}). Deux valeurs différentes de k(e^-_{aq} + e^-_{aq}) à 400 °C ont été utilisées: l'une basée sur la dépendance en température de k au-dessus de 150 °C telle que mesurée dans l'eau alcaline ($4{,}2 \times 10^8$ M^{-1} s^{-1}) et l'autre basée sur une extrapolation d'Arrhenius des valeurs de k inférieures à 150 °C ($2{,}5 \times 10^{11}$ M^{-1} s^{-1}). Dans les deux cas, les dépendances en densité de nos rendements de e^-_{aq} calculés à ~60 ps et 1 ns comparent assez bien avec les données expérimentales de radiolyse à impulsions picosecondes disponibles (pour le D_2O) sur toute la plage de densité de l'eau étudiée (~0,15-0,6 g/cm^3). Seul un faible effet de k sur la variation de G(e^-_{aq}) en fonction de la densité de l'eau à 60 ps et 1 ns a pu être observé. En conclusion, nos calculs actuels ne nous ont pas permis de confirmer (ou de nier) sans ambiguïté l'applicabilité de la baisse soudaine prévue de k(e^-_{aq} + e^-_{aq}) à ~150 °C dans une eau quasi neutre.

Radiolysis of Supercritical Water at 400 °C: A Sensitivity Study of the Density Dependence of the Yield of Hydrated Electrons on the (e^-_{aq} + e^-_{aq}) Reaction Rate Constant

Sunuchakan Sanguanmith
Université de Sherbrooke
Department of Nuclear Medicine and Radiobiology
3001, 12e Avenue Nord
Sherbrooke (Québec) J1H 5N4
Canada
sunuchakan.sanguanmith@USherbrooke.ca

Jintana Meesungnoen
Université de Sherbrooke
Department of Nuclear Medicine and Radiobiology
3001, 12e Avenue Nord
Sherbrooke (Québec) J1H 5N4
Canada
jintana.meesungnoen@USherbrooke.ca

David A. Guzonas
Canadian Nuclear Laboratories
Reactor Chemistry and Corrosion
20 Forest Avenue
Deep River (Ontario) K0J 1P0
Canada
david.guzonas@cnl.ca

Craig R. Stuart
Canadian Nuclear Laboratories
Reactor Chemistry and Corrosion
20 Forest Avenue
Deep River (Ontario) K0J 1P0
Canada
craig.stuart@cnl.ca

Jean-Paul Jay-Gerin[5]
Université de Sherbrooke
Department of Nuclear Medicine and Radiobiology

[5] Corresponding author. Tel: +1-819-821-8000 ext. 74682/74773; E-mail: jean-paul.jay-gerin@USherbrooke.ca

3001, 12e Avenue Nord
Sherbrooke (Québec) J1H 5N4
Canada
jean-paul.jay-gerin@USherbrooke.ca

ABSTRACT

The temperature dependence of the rate constant (k) of the bimolecular reaction of two hydrated electrons (e^-_{aq}) measured in alkaline water exhibits an abrupt drop between 150 and 200 °C; above 250 °C, it is too small to be measured reliably. Although this result is well established, the applicability of this sudden drop in k(e^-_{aq} + e^-_{aq}) above ~150 °C to neutral or slightly acidic solution, as recommended by some authors, still remains uncertain. In fact, recent work suggested that in near-neutral water the abrupt change in k above ~150 °C does not occur and that k should increase, rather than decrease, at temperatures greater than 150 °C with roughly the same Arrhenius dependence of the data below 150 °C. In view of this uncertainty of k, Monte Carlo simulations were used in this study to examine the sensitivity of the density dependence of the yield of e^-_{aq} in the low linear energy transfer (LET) radiolysis of supercritical water (H_2O) at 400 °C on variations in the temperature dependence of k. Two different values of the e^-_{aq} self-reaction rate constant at 400 °C were used: one based on the temperature dependence of k above 150 °C as measured in alkaline water (4.2×10^8 M^{-1} s^{-1}) and the other based on an Arrhenius extrapolation of the values below 150 °C (2.5×10^{11} M^{-1} s^{-1}). In both cases, the density dependences of our calculated e^-_{aq} yields at ~60 ps and 1 ns were found to compare fairly well with the available picosecond pulse radiolysis experimental data (for

D_2O) for the entire water density range studied (~0.15-0.6 g/cm^3). Only a small effect of k on the variation of G(e^-_{aq}) as a function of density at 60 ps and 1 ns could be observed. In conclusion, our present calculations did not allow us to unambiguously confirm (or deny) the applicability of the predicted sudden drop of k(e^-_{aq} + e^-_{aq}) at ~150 °C in near-neutral water.

Keywords: radiolysis, linear energy transfer, near neutral water, high temperature, self-reaction of two hydrated electrons, rate constant, radiation chemical yield, dependence on water density at 400 °C, Monte Carlo simulations.

1 INTRODUCTION

The Generation IV supercritical water-cooled reactor (SCWR) is an advanced reactor, which would operate with core inlet and outlet temperatures of ~350 and 625 °C, respectively, at a pressure of 25 MPa. It is an extremely energy-efficient system; its thermodynamic cycle efficiency is greater than ~45% vs. 28-32% for current conventional pressurized water reactors. By generating lower-cost electricity, SCWRs offer considerable economic advantages [1-7].

Supercritical water (SCW) refers to water above its thermodynamic critical point: for H_2O, t_c = 373.95 °C and P_c = 22.06 MPa or 217.7 atm; and for D_2O, t_c = 370.74 °C and P_c = 21.67 MPa or 213.9 atm [8]. A quantitative understanding of the radiation chemistry of SCW is required in the design and operation of Generation IV SCWRs, particularly to specify chemical control strategies. It is important to minimize the corrosion and degradation of reactor components resulting from the radiolytic formation of oxidizing

species at high concentrations, such as $^{\bullet}OH$, H_2O_2, O_2, and $O_2^{\bullet-}$ (or its protonated form $HO_2^{\bullet}$, depending on the pH) [4, 5, 7, 9, 10]. They are the main source of oxidizing products, but radiolysis is difficult to determine experimentally.

The water in reactor cores is subject not only to extreme conditions of high temperature and pressure but also to the action of intense fluxes of ionizing radiation: fast neutrons, γ-rays, recoil protons and heavy ions. As a result, direct observations or measurements at very high temperatures and pressures and in mixed radiation fields are difficult to perform. In addition, Generation IV SCWRs are still at the conceptual design stage. For these two reasons, chemical models and computer simulations are an important route of investigation for predicting the detailed radiation chemistry in SCWRs and the consequences for materials [5, 7, 11-14]. A key parameter to assess the chemical effects of ionizing radiation is the radiation-chemical yield or *G* value of each radiolytic species. The *G* value is defined as the number of species formed or consumed per 100 eV of absorbed energy. Another key parameter is the rate constant for each of the chemical reactions involving these species (and any other chemicals present in the system).

Experimental data on the radiation chemistry and reaction kinetics of transients under proposed SCWR operating conditions are very limited, and there are significant gaps [15]. Some data are still controversial. Certain preliminary studies suggest markedly different behavior for the effects of radiation under supercritical conditions compared to what would be predicted from simplistic extrapolations of values originally measured at lower temperatures. Here we examine one of these controversies regarding the

temperature dependence of the rate constant (*k*) for the bimolecular reaction of two hydrated electrons (e^-_{aq}) [16]:

$$e^-_{aq} + e^-_{aq} (+ 2H_2O) \rightarrow H_2 + 2OH^- . \quad (1)$$

In *alkaline* water, *k* exhibits a "catastrophic" drop between 150 and 200 °C; above 250 °C, it is too small to be measured reliably (Fig. 1) [17-20]. The mechanism behind this non-Arrhenius behavior above 150 °C is not well understood, but it is generally thought to involve the formation of some transient intermediate, such as a hydrated electron dimer (or "dielectron", $e_2^{2-}{}_{aq}$) sharing the same solvent cavity, a hydride ion (H^-), or yet an "incompletely relaxed" localized electron (e^-_{ir}) [17, 20-22]. The controversy here concerns the applicability of this drop in *k* above 150 °C to *neutral* or *slightly acidic* (as the pH of water at 150-200 °C is about 5.7-6) solution, as recommended by Bartels and coworkers [20]. In fact, this matter has long been a subject of discussion because the observed drop could be a function of the pH of the solution [18]. Up to now, an Arrhenius extrapolation procedure of the values below 150 °C, previously proposed by Elliot [18] and Stuart et al. [19], has been used in most computer models of the radiolysis of water at high temperatures in neutral solution (Fig. 1). This procedure assumes that such an abrupt change in *k* does *not* occur and that reaction (1) is diffusion controlled at temperatures greater than 150 °C. This assumption was justified by the good agreement obtained between the model and experiments [23-25].

Recently, Hatomoto et al. [26] directly measured the time dependence of $G(e^-_{aq})$ in pure deaerated neutral water by using picosecond and nanosecond pulse radiolysis in the temperature range from room temperature to 250 °C. The results were analyzed using a

spur diffusion kinetic simulation model. Their findings suggest that $k(e^-_{aq} + e^-_{aq})$ under neutral conditions increases monotonically at high temperature; no abrupt drop was observed at temperatures higher than 150 °C.

The present work aims to examine the impact of the $(e^-_{aq} + e^-_{aq})$ reaction rate constant on the hydrated electron yield at 400 °C as a function of water density in the range of ~0.15-0.6 g/cm^3. To show the sensitivity of $G(e^-_{aq})$ to $k(e^-_{aq} + e^-_{aq})$ in our simulations, we used two distinct temperature dependences for k above 150 °C (Fig. 1): one extrapolated from the values below 150 °C following an Arrhenius procedure [18, 19] (k_a) and the other extrapolated from the last three data points measured between 250 and 300 °C by Bartels and coworkers [20, 27] in alkaline solution (k_b). In the results and discussion section, we compare our calculated density dependence for $G(e^-_{aq})$ in irradiated SCW (H_2O) at 400 °C with the available experimental data obtained from time-resolved picosecond pulse radiolysis measurements in supercritical D_2O [28, 29].

2 MONTE CARLO SIMULATIONS

Supercritical water conditions have several specific features; we have developed an extended version of our Monte Carlo track chemistry simulation code, called IONLYS-IRT, for liquid water at ambient and elevated temperatures and which simulates irradiation by high-energy protons or heavier ions.

This IONLYS-IRT program simulates, in a three-dimensional geometrical environment, the initial production of various radiolytic species and the subsequent track expansion during which these species diffuse randomly and react with one another or

with dissolved solutes (if any) present at the time of irradiation. A detailed description of the code has been given previously [13, 24, 30, 31]. Briefly, the IONLYS step-by-step simulation program is used to cover the early *physical* and *physicochemical* stages [32] of track development. It models all the physical interactions (energy deposition) and the subsequent establishment of thermal equilibrium in the system (conversion of the physical products created locally after completion of the physical stage into the various "initial" free radicals and molecular products of the radiolysis). The complex, highly nonhomogeneous spatial distribution of reactants at the end of the physicochemical stage ($\sim 10^{-12}$ s; we assume that this time also marks the beginning of diffusion), which is provided as an output of the IONLYS program, is then used directly as the starting point for the subsequent *nonhomogeneous chemical* stage [32]. This third stage, which consists of diffusion and reactions of the reactive species during track expansion until all track processes are complete, is modeled by our IRT program. This program employs the "independent reaction times" (IRT) method [33-35], a computer-efficient stochastic simulation technique used to simulate reaction times without having to follow the trajectories of the diffusing species. The IRT method relies on the approximation that the reaction time of each pair of reactants is independent of the presence of other reactants in the system. Within the framework of this approach, the competition between the reactions is simply described via a sorting out of the stochastically sampled reaction times of each potentially reactive pair. The implementation of this program has been previously described in detail [35, 36]; its ability to give accurate, time-dependent chemical yields has been well validated by comparison with full random flight (or step-by-step) Monte Carlo

simulations, which do follow the reactant trajectories in detail [37, 38]. This IRT program can also be used to efficiently describe the reactions that occur in the bulk solution during the *homogeneous chemical* stage [32], *i.e.*, in the time domain typically beyond a few microseconds.

In the current version of IONLYS-IRT, several updates and modifications have been made, as fully described elsewhere [13, 28, 31]. In particular, we used the self-consistent radiolysis database, including rate constants, diffusion coefficients, reaction mechanisms and *G* values, recently compiled by Elliot and Bartels [27]. This new database provides recommendations for the best values to use in high-temperature modeling of light water radiolysis over the range of 20-350 °C. These data were simply extrapolated above their experimentally studied temperature range to obtain the rate constants of the various reactions involved in the radiolysis of SCW at 400 °C, as well as the diffusion coefficients of the intervening reactive species. In some cases, we also used the kinetic data of Ghandi and Percival [39] and of Alcorn et al. [40] inferred from muon spin spectroscopy measurements in SCW (up to 450 °C). In the absence of any other information, we chose to neglect any dependence of the reaction rate constants on water density for the 400 °C isotherm of interest [13, 14]. In the ~0.15-0.6 g/cm^3 density range studied here, this approximation seems reasonable, judging from the relatively slowly varying reaction rate values for the few reactions whose rates have been measured as a function of water density [40-42]. The recent re-evaluation of the temperature dependence of certain key parameters involved in the early physicochemical stage of radiolysis (*e.g.*, the thermalization distance of subexcitation electrons, the dissociative electron attachment,

and the branching ratios of the different excited water molecule decay channels) has also been incorporated in the simulations [28, 31]. Finally, we included in the simulations a prompt geminate electron-cation ($H_2O^{\bullet+}$) recombination (*i.e.*, prior thermalization of the electron) that decreased in irradiated SCW at 400 °C as the water density decreased from ~0.6 to 0.15 g/cm^3 [13].

The density (pressure) dependence of the self-diffusion coefficient of compressed SCW at 400 °C was taken from the measurements of Lamb et al. [43] in the region from 0.1 to 0.7 g/cm^3. For the diffusion coefficients of the radiolytic species $^{\bullet}OH$, $H^{\bullet}$, H_2O_2, and H_2, which have been explicitly determined only at 25 °C but are essentially unknown at 400 °C, we have assumed here that they scale proportionally to the self-diffusion of water above room temperature [24, 30, 43]. The diffusion coefficients of e^-_{aq}, H^+, and OH^- were estimated as previously described [30]. For the hydrated electron, we extrapolated the data of Schmidt et al. [44] (up to 90 °C) and of Marin et al. [20] (at 300 °C). For the proton and the hydroxide ion, we extrapolated the data reported by Elliot and Bartels [27] over the 20-350 °C temperature range. The density dependences of the viscosity, static dielectric constant and molar concentration of SCW at 400 °C used in this work were taken from the NIST Chemistry WebBook [8]. The values for the ionic product of water (K_w) were obtained from Bandura and Lvov [45].

We have ignored the heterogeneous molecular structure of SCW originating from the existence of large local density fluctuations (or water "clustering") that are fundamentally connected to the high compressibility of water in the vicinity of the critical point [46-49]. In our simulations, we assumed that the overall instantaneous picture of

SCW could simply be viewed as a *homogeneous* medium with a *mean* density equal to the density of bulk water. This approximation was shown to be reasonable in determining the radiation chemistry of SCW at 400 °C at the water densities considered in this study [12, 30, 50].

To mimic ^{60}Co γ-ray or fast electron irradiation, we used short (typically ~100 μm) track segments of ~300-MeV incident protons for which the average linear energy transfer (LET) obtained in the simulations was essentially constant and equal to ~0.3 keV/μm at 25 °C. Such model calculations thus gave "track segment" yields at a well-defined LET [51]. The number of proton histories (usually ~500) was chosen so as to ensure only small statistical fluctuations when calculating average yields, while keeping acceptable computer time limits.

3 RESULTS AND DISCUSSION

Figure 2 displays our calculated e^-_{aq} yields at 60 ps and 1 ns after the ionizing event, for the low-LET radiolysis of pure, deaerated SCW (H_2O) at 400 °C as a function of water density over the range of ~0.15 to 0.6 g/cm^3, using 300-MeV incident protons. To show the sensitivity of $G(e^-_{aq})$ to $k(e^-_{aq} + e^-_{aq})$, our simulations were carried out for two different values of k at 400 °C, namely, 2.5×10^{11} M^{-1} s^{-1} (based on the Arrhenius extrapolation of the values below 150 °C; represented by the solid line k_a in Fig. 1) [18, 19, 26] and 4.2×10^8 M^{-1} s^{-1} (based on the temperature dependence of k above 150 °C observed in alkaline water; represented by the dashed line k_b in Fig. 1) [20, 27]. Available e^-_{aq} yields obtained from time-resolved picosecond pulse radiolysis experiments in

supercritical D_2O at 400 °C, for both times considered (*i.e.*, ~60 ps, the rise time of the signal of e^-_{aq}, and 1 ns) [28, 29], are also included in the figure for comparison.

A very good agreement is found between our calculations and the experimental data at 1 ns for the entire density range studied. At ~60 ps, there is also a good agreement between experiment and theory at the highest densities plotted, but at low density our calculated yields slightly deviate from the experimental data. It can be seen that, at the water density of ~0.18 g/cm^3, our calculated e^-_{aq} yield is about 1 *G*-unit lower than the experimental value. The origin of these deviations at short times has been previously discussed [13]. One reason that could explain this difference is that we compare our calculated yields of e^-_{aq} for H_2O with values obtained experimentally for D_2O. As for the radiolysis of D_2O, it is worth pointing out that Bartels et al. [52] predicted that the ”initial” yield of e^-_{aq} in D_2O should be ~7% larger than in H_2O (due to the greater distance of secondary electron travel in heavy water). Based on this result, our e^-_{aq} yields calculated at ~60 ps would agree very well with the experimental data [53]. Another reason that could explain the deviations observed at ~60 ps in the low-density region near ~0.2 g/cm^3 is a possible increase in the electron thermalization distance (r_{th}) (recall here that r_{th} was kept constant in the present calculations and equal to ~3 nm, a value that we determined at 350 °C from an analysis of the spur decay kinetics of e^-_{aq} at elevated temperatures) [28]. Such an increase would slightly augment the yields of e^-_{aq} at ~60 ps and thus our simulated values would be closer to the experimental data.

Figure 2 also shows that $G(e^-_{aq})$ is relatively little affected by the choice of $k(e^-_{aq} + e^-_{aq})$ at 400 °C at both times considered (~60 ps and 1 ns). The calculated e^-_{aq} yields are only *slightly* lower when the value of 2.5×10^{11} M^{-1} s^{-1} (k_a) is used in the simulations. Indeed, decreasing the value of k to 4.2×10^8 M^{-1} s^{-1} (k_b), *i.e.*, by roughly three orders of magnitude, leads to an increase of $G(e^-_{aq})$ of at most ~7% at the water density of ~0.18 g/cm^3, at both ~60 ps and 1 ns. Given the relative insensitivity of $G(e^-_{aq})$ to the value of the $(e^-_{aq} + e^-_{aq})$ reaction rate constant, we cannot favor either of the k values used over the other. Based on the present results, we are therefore unable to unambiguously confirm or deny the applicability of the sudden drop of $k(e^-_{aq} + e^-_{aq})$ at 150 °C in *near-neutral water*, as suggested by Bartels and coworkers [20].

4 CONCLUSION

Monte Carlo simulations have been used to study the effect of the temperature dependence of $k(e^-_{aq} + e^-_{aq})$ up to 400 °C on the hydrated electron yield in the low-LET radiolysis of supercritical water (H_2O) at 400 °C over the density range of ~0.15 to 0.6 g/cm^3. Two different values of k were used: one (2.5×10^{11} M^{-1} s^{-1}) was based on an Arrhenius extrapolation procedure of the values below 150 °C (k_a) and the other (4.2×10^8 M^{-1} s^{-1}) was based on the temperature dependence of k observed above 150 °C in alkaline water (k_b). In both cases, the density dependences of our calculated e^-_{aq} yields at ~60 ps and 1 ns compared well with the available picosecond pulse radiolysis experimental data in supercritical D_2O for the entire water density range studied.

Decreasing k by about three orders of magnitude increased $G(e^-_{aq})$ by a factor of at most ~7% at low water densities, at both ~60 ps and 1 ns. Such a small effect of $k(e^-_{aq} + e^-_{aq})$ on the variation of $G(e^-_{aq})$ as a function of density prevented us from *unambiguously* confirming or denying the applicability of the predicted sudden drop of k at ~150 °C in near-neutral water.

Considering the importance of the self-reaction of e^-_{aq} as a source of molecular hydrogen in high-temperature water radiolysis, further measurements of its rate constant in pure water are obviously highly desirable. These measurements, which would be *extremely beneficial to the aqueous radiation chemistry modeling community*, would generate valuable insight for better understanding and predicting reactor coolant water chemistry in SCWRs.

ACKNOWLEDGMENT

The authors are grateful to Professor Yusa Muroya of Osaka University (Japan) for his close collaboration, constant encouragement, and important experimental input for the re-evaluation of our Monte Carlo simulation code for the radiolysis of water at high temperatures.

FUNDING

This work received financial assistance from the Generation IV Energy Technologies Program of the Natural Sciences and Engineering Research Council of Canada, Natural Resources Canada, and Atomic Energy of Canada Limited (Grant No. NNAPJ/424113-11).

NOMENCLATURE

D_2O	heavy water (or deuterium oxide)
e^-_{aq}	hydrated electron
eV	electron volt (1.602×10^{-19} J)
G value	radiation chemical yield
H_2O	light (ordinary) water
IRT	independent reaction times
k	reaction rate constant
keV/MeV	kilo/megaelectron volt
K_w	ionic product of water
LET	linear energy transfer
M	molarity (measure of concentration equal to the number of moles of solute per liter of solution)
Monte Carlo	general term used to describe any algorithm or computational method that employs random numbers.
MPa	megapascal
NIST	National Institute of Standards and Technology
ns/ps	nano/picosecond
pH	measure of the acidity or alkalinity of a solution, defined (in most common applications) as the negative logarithm (base 10) of the molar concentration of hydrogen ions (H+) in the solution: pH = - log $[H^+]$

r_{th}	electron thermalization distance
SCW	supercritical water
SCWR	supercritical water-cooled reactor

REFERENCES

[1] Viswanathan, R., Armor, A. F., and Booras, G., 2004, "A Critical Look at Supercritical Power Plants," Power, **148**(3), pp. 42-49.

[2] Oka, Y., and Koshizuka, S., 1998, "Conceptual Design Study of Advanced Power Reactors," Prog. Nucl. Energy, **32**(1/2), pp. 163-177.

[3] Khartabil, H. F., Duffey, R. B., Spinks, N., and Diamond, W., May 15-19, 2005, "The Pressure-Tube Concept of Generation IV Supercritical Water-Cooled Reactor (SCWR): Overview and Status," *Proc. International Congress on Advances in Nuclear Power Plants*, Seoul, Korea, Paper 5564.

[4] Katsumura, Y., 2004, "Application of Radiation Chemistry to Nuclear Technology," *Charged Particle and Photon Interactions with Matter: Chemical, Physical, and Biological Consequences with Applications*, A. Mozumder and Y. Hatano, eds., Marcel Dekker, New York, pp. 697-727. ISBN: 0-8247-4623-6

[5] Bartels, D. M., Anderson, M., Wilson, P., Allen, T., and Sridharan, K., 2006, *Supercritical Water Radiolysis Chemistry. Supercritical Water Corrosion*. Available from the Idaho National Laboratory Web site:
http://nuclear.inl.gov/deliverables/docs/uwnd_scw_level_ii_sep_2006_v3.pdf

[6] Růžičková, M., Hájek, P., Šmida, Š., Všolák, R., Petr, J., and Kysela, J., 2008, "Supercritical Water Loop Design for Corrosion and Water Chemistry Tests under Irradiation," Nucl. Eng. Technol., **40**(2), pp. 127-132.

[7] Guzonas, D., Brosseau, F., Tremaine, P., Meesungnoen, J., and Jay-Gerin, J.-P., 2012, "Water Chemistry in a Supercritical Water-Cooled Pressure Tube Reactor," Nucl. Technol., **179**(2), pp. 205-219.

[8] Linstrom, P. J., and Mallard, W. G., eds., 2005, *NIST Chemistry WebBook*, NIST Standard Reference Database No. 69, National Institute of Standards and Technology, Gaithersburg, MD. Available at:
http://www.webbook.nist.gov

[9] Guzonas, D. A., and Cook, W. G., Dec. 2012, "Cycle Chemistry and its Effect on Materials in a Supercritical Water-Cooled Reactor: A Synthesis of Current Understanding," Corrosion Sci., **65**, pp. 48-66. DOI: 10.1016/j.corsci.2012.08.006

[10] Was, G. S., Ampornrat, P., Gupta, G., Teysseyre, S., West, E. A., Allen, T. R., Sridharan, K., Tan, L., Chen, Y., Ren, X., and Pister, C., 2007, "Corrosion and Stress Corrosion Cracking in Supercritical Water," J. Nucl. Mater., **371**(1-3), pp. 176-201. DOI: 10.1016/j.jnucmat.2007.05.017

[11] Kanjana, K., Haygarth, K. S., Wu, W., and Bartels, D. M., Jan. 2013, "Laboratory Studies in Search of the Critical Hydrogen Concentration," Radiat. Phys. Chem., **82**, pp. 25-34. DOI: 10.1016/j.radphyschem.2012.09.011

[12] Sanguanmith, S., Meesungnoen, J., and Jay-Gerin, J.-P., 2012, "Density Dependence of the “Escape” Yield of Hydrated Electrons in the Low-LET Radiolysis of Supercritical Water at 400 °C," Phys. Chem. Chem. Phys., **14**(32), pp. 11277-11280. DOI: 10.1039/c2cp41399j

[13] Meesungnoen, J., Sanguanmith, S., and Jay-Gerin, J.-P., 2013, "Density Dependence of the Yield of Hydrated Electrons in the Low-LET Radiolysis of Supercritical Water at 400 °C: Influence of the Geminate Recombination of Subexcitation-Energy Electrons Prior to Thermalization," Phys. Chem. Chem. Phys., **15**(39), pp. 16450-16455. DOI: 10.1039/c3cp52630e

[14] Butarbutar, S. L., Meesungnoen, J., Guzonas, D. A., Stuart, C. R., and Jay-Gerin, J.-P., 2014, "Modeling the Radiolysis of Supercritical Water by Fast Neutrons: Density Dependence of the Yields of Primary Species at 400 °C," Radiat. Res., **182**(6), pp. 695-704. DOI: 10.1667/RR13715.1

[15] Guzonas, D. A., Stuart, C. R., Jay-Gerin, J.-P., and Meesungnoen, J., Jan. 2010, "Testing Requirements for SCWR Radiolysis," Report AECL No. 153-127160-REPT-001, Atomic Energy of Canada Limited, Mississauga, Ontario, Canada.

[16] Butarbutar, S. L., Muroya, Y., Mirsaleh Kohan, L., Sanguanmith, S., Meesungnoen, J., and Jay-Gerin, J.-P., 2013, "On the Temperature Dependence of the Rate Constant of the Bimolecular Reaction of Two Hydrated Electrons," Atom Indonesia, **39**(2), pp. 51-56. ISSN 0126-1568

[17] Christensen, H., and Sehested, K., 1986, "The Hydrated Electron and its Reactions at High Temperatures," J. Phys. Chem., **90**(1), pp. 186-190. DOI: 10.1021/j100273a042

[18] Elliot, A. J., Oct. 1994, "Rate Constants and *g*-Values for the Simulation of the Radiolysis of Light Water over the Range 0-300 °C," Report AECL-11073, Atomic Energy of Canada Limited, Chalk River, Ontario, Canada.

[19] Stuart, C. R., Ouellette, D. C., and Elliot, A. J., Sept. 2002, "Pulse Radiolysis Studies of Liquid Heavy Water at Temperatures up to 250 °C," Report AECL-12107, Atomic Energy of Canada Limited, Chalk River, Ontario, Canada.

[20] Marin, T. W., Takahashi, K., Jonah, C. D., Chemerisov, S. D., and Bartels, D. M., 2007, "Recombination of the Hydrated Electron at High Temperature and Pressure in Hydrogenated Alkaline Water," J. Phys. Chem. A, **111**(45), pp. 11540-11551. DOI: 10.1021/jp074581r

[21] Ferradini, C., and Jay-Gerin, J.-P., 1993, "A Conjecture on the Fate of the Hydrated Electron during its Disproportionation Reaction," Radiat. Phys. Chem., **41**(3), pp. 487-490. DOI: 10.1016/0969-806X(93)90009-J

[22] Schmidt, K. H., and Bartels, D. M., 1995, "Lack of Ionic Strength Effect in the Recombination of Hydrated Electrons: $(e^-)_{aq} + (e^-)_{aq} \rightarrow 2(OH^-) + H_2$," Chem. Phys., **190**(1), pp. 145-152. DOI: 10.1016/0301-0104(94)00332-5

[23] Swiatla-Wojcik, D., and Buxton, G. V., 1995, "Modeling of Radiation Spur Processes in Water at Temperatures up to 300 °C," J. Phys. Chem., **99**(29), pp. 11464-11471. DOI: 10.1021/j100029a026

[24] Hervé du Penhoat, M.-A., Goulet, T., Frongillo, Y., Fraser, M.-J., Bernat, Ph., and Jay-Gerin, J.-P., 2000, "Radiolysis of Liquid Water at Temperatures up to 300 °C: A Monte Carlo Simulation Study," J. Phys. Chem. A, **104**(50), pp. 11757-11770. DOI: 10.1021/jp001662d

[25] Tippayamontri, T., Sanguanmith, S., Meesungnoen, J., Sunaryo, G. R., and Jay-Gerin, J.-P., 2009, "Fast Neutron Radiolysis of the Ferrous Sulfate (Fricke) Dosimeter: Monte Carlo Simulations," Recent Res. Devel. Physical Chem., **10**, pp. 143-211. ISBN: 978-81-7895-431-8

[26] Hatomoto, D., Muroya, Y., Katsumura, Y., Yamashita, S., and Kozawa, T., Sept. 8-11, 2014, "Reactivity of Hydrated Electron Formed by Radiolysis of Water at High Temperature," *Book of Abstracts, 5th Asia-Pacific Symposium on Radiation Chemistry*, The University of Tokyo, Tokyo, Japan, Paper P08, p. 140.

[27] Elliot, A. J., and Bartels, D. M., July 2009, "The Reaction Set, Rate Constants and *g*-Values for the Simulation of the Radiolysis of Light Water over the Range 20 to 350 °C Based on Information Available in 2008," Report AECL No. 153-127160-450-001, Atomic Energy of Canada Limited, Mississauga, Ontario, Canada.

[28] Muroya, Y., Sanguanmith, S., Meesungnoen, J., Lin, M., Yan, Y., Katsumura, Y., and Jay-Gerin, J.-P., 2012, "Time-Dependent Yield of the Hydrated Electron in Subcritical and Supercritical Water Studied by Ultrafast Pulse Radiolysis and Monte Carlo Simulation," Phys. Chem. Chem. Phys., **14**(41), pp. 14325-14333. DOI: 10.1039/c2cp42260c

[29] Muroya, Y., Lin, M., de Waele, V., Hatano, Y., Katsumura, Y., and Mostafavi, M., 2010, "First Observation of Picosecond Kinetics of Hydrated Electrons in Supercritical Water," J. Phys. Chem. Lett., **1**(1), pp. 331-335. DOI: 10.1021/jz900225a

[30] Meesungnoen, J., Guzonas, D., and Jay-Gerin, J.-P., 2010, "Radiolysis of Supercritical Water at 400 °C and Liquid-Like Densities near 0.5 g/cm^3. A Monte Carlo Calculation," Can. J. Chem., **88**(7), pp. 646-653. DOI: 10.1139/V10-055

[31] Sanguanmith, S., Muroya, Y., Meesungnoen, J., Lin, M., Katsumura, Y., Mirsaleh Kohan, L., Guzonas, D. A., Stuart, C. R., and Jay-Gerin, J.-P., 2011, "Low-Linear Energy Transfer Radiolysis of Liquid Water at Elevated Temperatures up to 350 °C: Monte Carlo Simulations," Chem. Phys. Lett., **508**(4-6), pp. 224-230. DOI: 10.1016/j.cplett.2011.04.059

[32] Platzman, R. L., 1958, "The Physical and Chemical Basis of Mechanisms in Radiation Biology," *Radiation Biology and Medicine. Selected Reviews in the Life Sciences*, W. D. Claus, ed., Addison-Wesley Publishing, Reading, MA, pp. 15-72.

[33] Pimblott, S. M., Pilling, M. J., and Green, N. J. B., 1991, "Stochastic Models of Spur Kinetics in Water," Radiat. Phys. Chem., **37**(3), pp. 377-388. DOI: 10.1016/1359-0197(91)90006-N

[34] Tachiya, M., 1983, "Theory of Diffusion-Controlled Reactions: Formulation of the Bulk Reaction Rate in Terms of the Pair Probability," Radiat. Phys. Chem., **21**(1-2), pp. 167-175. DOI: 10.1016/0146-5724(83)90143-7

[35] Frongillo, Y., Goulet, T., Fraser, M.-J., Cobut, V., Patau, J. P., and Jay-Gerin, J.-P., 1998, "Monte Carlo Simulation of Fast Electron and Proton Tracks in Liquid Water. II. Nonhomogeneous Chemistry," Radiat. Phys. Chem., **51**(3), pp. 245-254. DOI: 10.1016/S0969-806X(97)00097-2

[36] Meesungnoen, J., and Jay-Gerin, J.-P., 2011, "Radiation Chemistry of Liquid Water with Heavy Ions: Monte Carlo Simulation Studies," *Charged Particle and Photon Interactions with Matter. Recent Advances, Applications, and Interfaces*, Y. Hatano, Y. Katsumura, and A. Mozumder, eds., Taylor & Francis Group, Boca Raton, FL, pp. 355-400. ISBN: 978-1-4398-1177-1

[37] Goulet, T., Fraser, M.-J., Frongillo, Y., and Jay-Gerin, J.-P., 1998, "On the Validity of the Independent Reaction Times Approximation for the Description of the Nonhomogeneous

Kinetics of Liquid Water Radiolysis," Radiat. Phys. Chem., **51**(1), pp. 85-91. DOI: 10.1016/S0969-806X(97)00060-1

[38] Plante, I., 2009, "Développement de Codes de Simulation Monte-Carlo de la Radiolyse de l'Eau par des Électrons, Ions Lourds, Photons et Neutrons. Applications à Divers Sujets d'Intérêt Expérimental," Ph.D. thesis, Université de Sherbrooke, Sherbrooke, Québec, Canada.

[39] Ghandi, K., and Percival, P. W., 2003, "Prediction of Rate Constants for Reactions of the Hydroxyl Radical in Water at High Temperatures and Pressures," J. Phys. Chem. A, **107**(17), pp. 3005-3008. DOI: 10.1021/jp027858q

[40] Alcorn, C. D., Brodovitch, J.-Cl., Percival, P. W., Smith, M., and Ghandi, K., May 2014, "Kinetics of the Reaction between $H^{\bullet}$ and Superheated Water Probed with Muonium," Chem. Phys., **435**, pp. 29-39. DOI: 10.1016/j.chemphys.2014.02.016

[41] Lin, M., and Katsumura, Y., 2011, "Radiation Chemistry of High Temperature and Supercritical Water and Alcohols," *Charged Particle and Photon Interactions with Matter. Recent Advances, Applications, and Interfaces*, Y. Hatano, Y. Katsumura, and A. Mozumder, eds., Taylor & Francis Group, Boca Raton, FL, pp. 401-424. ISBN: 978-1-4398-1177-1

[42] Cline, J., Takahashi, K., Marin, T. W., Jonah, C. D., and Bartels, D. M., 2002, "Pulse Radiolysis of Supercritical Water. 1. Reactions between Hydrophobic and Anionic Species," J. Phys. Chem. A, **106**(51), pp. 12260-12269. DOI: 10.1021/jp0270250

[43] Lamb, W. J., Hoffman, G. A., and Jonas, J., 1981, "Self-Diffusion in Compressed Supercritical Water," J. Chem. Phys., **74**(12), pp. 6875-6880. DOI: 10.1063/1.441097

[44] Schmidt, K. H., Han, P., and Bartels, D.M., 1995, "Radiolytic Yields of the Hydrated Electron from Transient Conductivity: Improved Calculation of the Hydrated Electron Diffusion Coefficient and Analysis of Some Diffusion-Limited $(e^{-})_{aq}$ Reaction Rates," J. Phys. Chem., **99**(26), pp. 10530-10539. DOI: 10.1021/j100026a016

[45] Bandura, A. V., and Lvov, S. N., 2006, "The Ionization Constant of Water over Wide Ranges of Temperature and Density," J. Phys. Chem. Ref. Data, **35**(1), pp. 15-30. DOI: 10.1063/1.1928231

[46] Akiya, A., and Savage, P. E., 2002, "Roles of Water for Chemical Reactions in High-Temperature Water," Chem. Rev., **102**(8), pp. 2725-2750. DOI: 10.1021/cr000668w

[47] Ohtaki, H., Radnai, T., and Yamaguchi, T., 1997, "Structure of Water under Subcritical and Supercritical Conditions Studied by Solution X-Ray Diffraction," Chem. Soc. Rev., **26**(1), pp. 41-51. DOI: 10.1039/CS9972600041

[48] Metatla, N., Jay-Gerin, J.-P., and Soldera, A., March 13-16, 2011, "Molecular Dynamics Simulation of Subcritical and Supercritical Water at Different Densities," *Proc. 5th International Symposium on Supercritical-Water-Cooled Reactors*, Vancouver, British Columbia, Canada, Paper 101. ISBN: 978-1-926773-02-5

[49] Jay-Gerin, J.-P., Lin, M., Katsumura, Y., He, H., Muroya, Y., and Meesungnoen, J., 2008, "Effect of Water Density on the Absorption Maximum of Hydrated Electrons in Sub- and Supercritical Water up to 400 °C," J. Chem. Phys., **129**(11), 114511. DOI: 10.1063/1.2978955

[50] Sanguanmith, S., Meesungnoen, J., Guzonas, D. A., Stuart, C. R., and Jay-Gerin, J.-P., 2014, "Low-LET Radiation Chemistry of Supercritical Water at 400 °C: A Re-Analysis of the Water Density Dependence of the Spur Lifetime and the "Escape" e^-_{aq} Yield," Recent Res. Devel. Physical Chem., **11**, pp. 1-14. ISBN: 978-81-7895-608-4

[51] LaVerne, J. A., 2000, "Track Effects of Heavy Ions in Liquid Water," Radiat. Res., **153**(5), pp. 487-496. DOI: 10.1667/0033-7587(2000)153[0487:TEOHII]2.0.CO;2

[52] Bartels, D. M., Gosztola, D., and Jonah, C. D., 2001, "Spur Decay Kinetics of the Solvated Electron in Heavy Water Radiolysis," J. Phys. Chem. A, **105**(34), pp. 8069-8072. DOI: 10.1021/jp012153u

[53] Measurements of $G(e^-_{aq})$ using time-resolved picosecond pulse radiolysis of supercritical H_2O conducted at 400 °C at diverse water densities are currently being undertaken at Osaka University and the University of Tokyo in Japan (Y. Muroya, personal communication).

Figure Captions List

Fig. 1 Rate constant for the self-reaction of two hydrated electrons as a function of temperature. The solid line (denoted k_a) shows the ($e^-_{aq} + e^-_{aq}$) reaction rate constant that was obtained by using an Arrhenius extrapolation procedure above 150 °C as proposed by Elliot [18], Stuart et al. [19] and Hatomoto et al. [26]. The dashed line (denoted k_b) shows the ($e^-_{aq} + e^-_{aq}$) reaction rate constant that was measured by Bartels and coworkers [20, 27] (■) under alkaline conditions. Note that k_b was assumed to remain constant between 275 and 400 °C.

Fig. 2 Density dependence of $G(e^-_{aq})$ (in molecule per 100 eV) in SCW at 400 °C measured directly by picosecond pulse radiolysis experiments (in D_2O) [28, 29] at ~60 ps (○) and 1 ns (■) (estimated uncertainty of ±10%). The solid and dashed lines show our Monte Carlo simulated results in supercritical H_2O when $k(e^-_{aq} + e^-_{aq}) = 2.5 \times 10^{11}$ M^{-1} s^{-1} was used at ~60 ps and 1 ns, respectively. The dash-dot and dash-dot-dot lines show our corresponding calculated e^-_{aq} yields when $k(e^-_{aq} + e^-_{aq}) = 4.2 \times 10^8$ M^{-1} s^{-1} was used at ~60 ps and 1 ns, respectively. For conversion into SI units (mol/J), 1 molecule per 100 eV ≈ 0.10364 μmol/J.

Information Regarding Figures and Tables

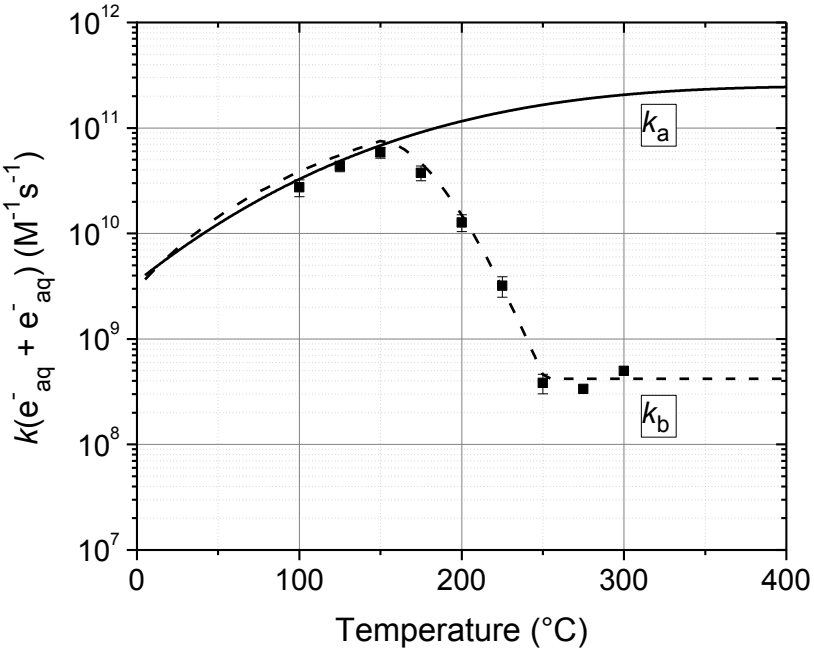

Fig. 1

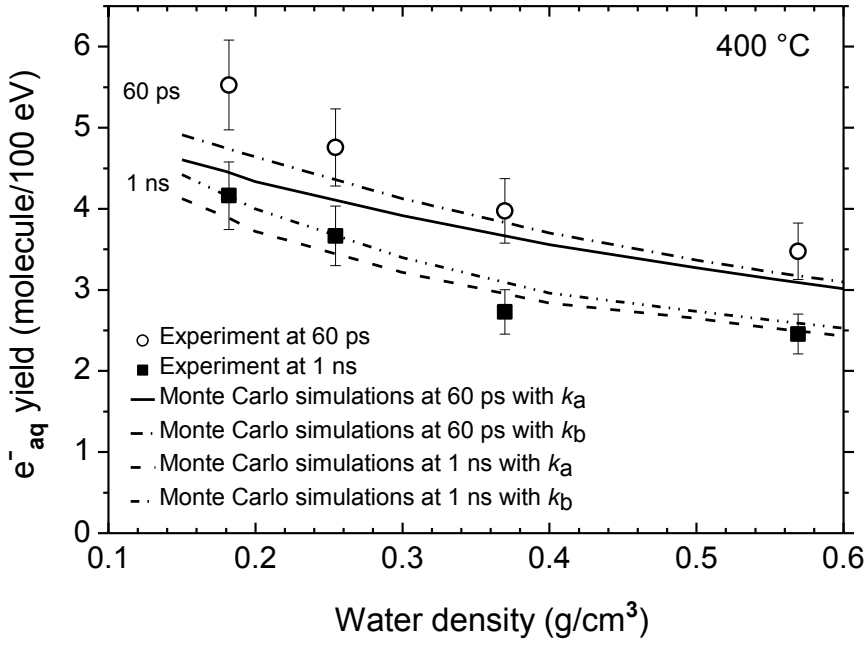
400 °C
60 ps
1 ns
Experiment at 60 ps
Experiment at 1 ns
Monte Carlo simulations at 60 ps with k_a
Monte Carlo simulations at 60 ps with k_b
Monte Carlo simulations at 1 ns with k_a
Monte Carlo simulations at 1 ns with k_b
e^-_{aq} yield (molecule/100 eV)
Water density (g/cm^3)
0
1
2
3
4
5
6
0.1
0.2
0.3
0.4
0.5
0.6

Fig. 2

8. ARTICLE 2

Self-radiolysis of tritiated water. 4. The scavenging effect of azide ions (N_3^-) on the molecular hydrogen yield in the radiolysis of water by ^{60}Co γ-rays and tritium β-particles at room temperature

Authors: Sunuchakan Sanguanmith, Jintana Meesungnoen, Craig R. Stuart, Patrick Causey, and Jean-Paul Jay-Gerin

Status: published in Royal Society of Chemistry Advances Vol. **8**, (2018) 2449-2458.

Foreword: In this work, I built the complete reaction set of azide ions to our IRT programs. I also calculated the ionic strength of the solutions and incorporated this effect into our programs. I performed all the calculations of the hydrogen yields in the presence of azide by using ^{60}Co γ-rays (~1 MeV Compton electrons) and tritium β-electrons (mean electron energy of ~7.8 keV). Finally, I had a significant contribution to the idea of this work and to all the preparation process for the first version of this article.

Résumé : L'effet de l'ion azide N_3^- sur le rendement en hydrogène moléculaire dans l'eau irradiée avec les rayons γ de ^{60}Co (électrons de Compton de ~1 MeV) et des électrons-β du tritium (énergie moyenne des électrons de ~7,8 keV) à 25 °C est étudié à l'aide de simulations de Monte Carlo. Il est démontré que N_3^- interfère avec la formation de H_2 grâce à sa forte réactivité vis-à-vis des atomes d'hydrogène et des électrons hydratés, qui sont les deux principaux précurseurs radiolytiques du rendement en H_2 dans les trajectoires du rayonnement. Des changements chimiques sont observés dans la capacité de piégeage de H_2 en fonction du type particulier de la radiation considérée. Dans la géométrie des « trajectoires courtes » des électrons β du tritium à plus grand « transfert d'énergie linéaire » (TEL) (TEL moyen de ~5,9 eV/nm), les radicaux se forment localement à une concentration initiale beaucoup plus élevée que dans les « grappes » isolées des électrons énergétiques de Compton (LET ~ 0,3 eV/nm) générés par les rayons γ de cobalt 60. En conséquence, la géométrie à trajectoires courtes favorise les réactions radical-radical impliquant des électrons hydratés et des atomes d'hydrogène, conduisant à une nette augmentation du rendement de H_2 pour les électrons β de tritium par rapport aux rayons-γ ^{60}Co.

Self-radiolysis of tritiated water. 4. The scavenging effect of azide ions (N_3^-) on the molecular hydrogen yield in the radiolysis of water by ^{60}Co γ-rays and tritium β-particles at room temperature

by

Sunuchakan Sanguanmith,[a] Jintana Meesungnoen,[a] Craig R. Stuart,[b] Patrick Causey[c] and Jean-Paul Jay-Gerin[a,*]

[a]*Département de médecine nucléaire et de radiobiologie, Faculté de médecine et des sciences de la santé, Université de Sherbrooke, 3001, 12e Avenue Nord, Sherbrooke (Québec) J1H 5N4, Canada.*

[b]*Reactor Chemistry and Corrosion Branch, Canadian Nuclear Laboratories, Chalk River (Ontario) K0J 1J0, Canada.*

[c]*Radiological Protection Research and Instrumentation Branch, Canadian Nuclear Laboratories, Chalk River, Ontario, K0J 1J0, Canada*

* Corresponding author. Tel.: +1 819 346 1110, ext. 74682/74773; fax: +1 819 564 5442.
E-mail address: jean-paul.jay-gerin@USherbrooke.ca (Jean-Paul Jay-Gerin).

RSC Adv. **508** (2011) 224-230

Abstract

The effect of the azide ion N_3^- on the yield of molecular hydrogen in water irradiated with ^{60}Co γ-rays (~1 MeV Compton electrons) and tritium β-electrons (mean electron energy of ~7.8 keV) at 25 °C is investigated using Monte Carlo track chemistry simulations in conjunction with available experimental data. N_3^- is shown to interfere with the formation of H_2 through its high reactivity towards hydrogen atoms and, but to a lesser extent, hydrated electrons, the two major radiolytic precursors of the H_2 yield in the diffusing radiation tracks. Chemical changes are observed in the H_2 scavengeability depending on the particular type of radiation considered. These changes can readily be explained on the basis of differences in the initial spatial distribution of primary radiolytic species (*i.e.*, the structure of the electron tracks). In the "short-track" geometry of the higher "linear energy transfer" (LET) tritium β-electrons (mean LET ~ 5.9 eV/nm), radicals are formed locally in much higher initial concentration than in the isolated "spurs" of the energetic Compton electrons (LET ~ 0.3 eV/nm) generated by the cobalt-60 γ-rays. As a result, the short-track geometry favors radical-radical reactions involving hydrated electrons and hydrogen atoms, leading to a clear increase in the yield of H_2 for tritium β-electrons compared to ^{60}Co γ-rays. These changes in the scavengeability of H_2 in passing from tritium β-radiolysis to γ-radiolysis are in good agreement with experimental data, lending strong support to the picture of tritium β-radiolysis mainly driven by the chemical action of short tracks of high local LET. At high N_3^- concentrations (>1 M), our H_2 yield results for ^{60}Co γ-radiolysis are also consistent with previous Monte Carlo simulations that suggested the necessity of including the capture of the precursors to the hydrated electrons (*i.e.*, the short-lived "dry" electrons prior to hydration) by N_3^-. These processes tend to reduce significantly the yields of H_2, as is observed experimentally. However, this dry electron scavenging at high azide concentrations is not seen in the higher-LET ^{3}H β-radiolysis, leading us to conclude that the increased amount of intra-track chemistry intervening at early time under these conditions favors the recombination of these electrons with their parent water cations at the expense of their scavenging by N_3^-.

1. Introduction

A detailed understanding of the radiolysis of water and aqueous solutions is important both from a fundamental science point of view and for a variety of practical applications,[1-4] in particular, in the nuclear power industry and in radiation biology where living cells and tissues consist mainly of water (~70-85% by weight). Exposed to ionizing radiation, water is the site of ionizations and excitations:

$$H_2O \xrightarrow{\sim} H_2O^{\bullet+} + e^- \text{ (ionization)}$$

$$H_2O \xrightarrow{\sim} H_2O^* \text{ (excitation),}$$

which result, within a few picoseconds, in a cascade of events leading to the formation of free radicals and molecular products along the track of the incident radiation. Ejected secondary electrons (also called "dry" electrons) have generally sufficient kinetic energy to cause further ionizations and excitations in close proximity to the original water positive ion. After slowing down to sub-

excitation energies and thermalization, these electrons become trapped and hydrated. Under ordinary irradiation conditions (*i.e.*, at modest dose rates so that no track overlap occurs), the initial products of radiolysis are generated in a highly nonhomogeneous "track structure" geometry.[5-11] They include[12,13] the hydrated electron (e^-_{aq}), H_3O^+, OH^-, $H^\bullet$, H_2, $^\bullet OH$, H_2O_2, $O_2^{\bullet-}$ (or its protonated form $HO_2^\bullet$; pK_a = 4.8 at 25 °C), $O(^1D)$, $^\bullet O^\bullet(^3P)$, $O^{\bullet-}$, *etc*. This early nonhomogeneous spatial distribution of radiolytic species is strongly dependent on the radiation quality, a measure of which is given by the "linear energy transfer" (LET) (also called "stopping power" by physicists and denoted by -dE/dx). For low-LET, sparsely ionizing radiation (such as γ-rays from ^{60}Co or fast electrons; LET ~ 0.3 eV/nm), tracks are formed initially by widely spaced clusters of reactive species, commonly known as "spurs" (spherical in shape).[14,15] In this case, the predominant effect of radiolysis is radical production. In fact, when diffusion has brought about homogeneity in the system (*i.e.*, within a few microseconds after the initial energy deposition), relatively few radicals have combined in the spurs, resulting in an excess of radicals over molecular products. However, with increasing LET, the isolated spur structure changes to a situation in which the spurs eventually overlap and form (initially) a dense continuous column of species. This is actually the case for the low-energy β-electrons of tritium, which are involved in the "self-radiolysis" of tritiated water (^{3}HOH),[16-18] the subject matter of the present study. In the terminology of the Mozumder-Magee model of energy deposition,[6,19] while the Compton electrons (~1 MeV) produced by ^{60}Co γ-radiolysis predominantly form spurs, these soft, higher-LET tritium β-electrons predominantly deposit their energy as "short tracks". This leads to an increased local concentration of reactants and therefore an increased amount of intra-track chemistry that favors radical-radical reactions. Under these conditions, the radiation chemical yields (or G-values)[20] of the molecular products increase at the expense of the individual radicals. For the sake of illustration, Fig. 1 shows typical 2-D representations of the complete track of a 7.8-keV ^{3}H β-electron and the track segment of a 300-MeV proton (which mimics irradiation with ^{60}Co γ-rays), calculated with our IONLYS Monte Carlo track structure simulation code (see below).

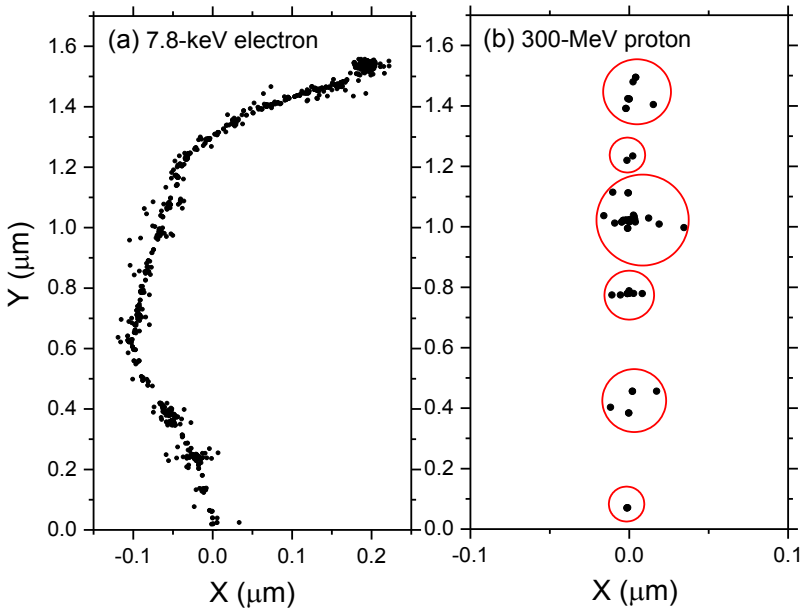

Fig. 1 Simulated track histories (projected into the *XY* plane of figure) of a 7.8-keV tritium β-electron (complete track; mean LET ~ 5.9 eV/nm) (panel a) and a 300-MeV proton (track segment; LET ~ 0.3 eV/nm) (panel b) incident in liquid water at 25 °C. The two irradiating particles are generated at the origin and start traveling along the *Y* axis. Dots represent the energy deposited at points where an interaction occurred.

In close connection with the LET and the relationship between track structure and chemistry, one critical area of research focuses on elucidating the basic radiation chemical mechanisms that operate in the "self-radiolysis" of tritiated water as compared with ^{60}Co γ-radiolysis.[21-26] The present paper is the fourth in a series[18,27,28] dedicated to this subject. The Monte Carlo track-chemistry simulation work we reported previously revealed significant differences between the chemical properties of short tracks and spurs using either γ-rays/fast electrons or tritium β-particles. Overall, the results of our simulations provided strong support for the picture of tritium β-radiolysis mainly driven by the chemical action of short tracks of high local LET. In the present study, we now attempt to distinguish further the chemical properties of spur and short track geometries by examining the differences in the scavengeability of molecular H_2 – whose yields are relatively well-documented experimentally[21,22,25,26,29-32] – when passing from γ- to tritium β-electron radiolysis.

Molecular hydrogen is one of the most interesting radiolytic species, in part because of the questions it raises about the source of its formation. At very short times (<50-300 fs) after the passage of the ionizing radiation,[33] H_2 can be formed by the following reactions:[34,35]

(1) geminate recombination of the sub-excitation electron (e^-_{sub})[36] with its parent cation $H_2O^{\bullet+}$

$$H_2O^{\bullet+} + e^-_{sub} \rightarrow H_2O^*$$

(2) "dissociative electron attachment" (or DEA) involving the resonant capture of e^-_{sub} by a water molecule

$$H_2O + e^-_{sub} \rightarrow (H_2O^{\bullet-*}) \rightarrow H^- + {}^\bullet OH,$$

followed by

$$H^- + H_2O \rightarrow H_2 + OH^-$$

(3) dissociation of excited water molecules

$$H_2O^* \rightarrow H_2 + O(^1D),$$

where $O(^1D)$ is the oxygen atom in its singlet ^1D first excited state.

In the low-LET γ-irradiation case, this "initial" – then described as "unscavengeable" (*i.e.*, not removable by scavenger experiments) – H_2 yield was first estimated by Schwarz[37] in 1969 to be ~30% of the total "escape" yield[20] for molecular hydrogen [$g(H_2)$ = 0.45 molecule/100 eV].[5,7,11,12] Recent scavenger studies[38] have shown, however, that Schwarz's initial estimate was undervalued. In fact, it was found that a major fraction (~75%, *i.e.*, ~0.34 molecule/100 eV) of the total H_2 produced was due to reactions of the dry/subexcitation electrons in the subpicosecond physicochemical stage of the radiolysis. In other words, these results suggest that only ~0.11 molecule of H_2 per 100 eV remains to be formed during the subsequent nonhomogeneous chemical stage (*i.e.*, in the radiation tracks as they expand by diffusion) on the picosecond-microsecond time scale. At this stage, three radical-radical combination reactions of the hydrated electron and $H^\bullet$ atom intervene in hydrogen formation. They are[18,34,39,40]

$$e^-_{aq} + H^\bullet (+H_2O) \rightarrow H_2 + OH^-,\ k_1 = 2.5 \times 10^{10}\ M^{-1}\ s^{-1} \quad (1)$$

$$e^-_{aq} + e^-_{aq} (+2H_2O) \rightarrow H_2 + 2OH^-,\ k_2 = 6.2 \times 10^{9}\ M^{-1}\ s^{-1} \quad (2)$$

and, but to a much lesser extent,

$$H^\bullet + H^\bullet \rightarrow H_2,\ k_3 = 4.6 \times 10^{9}\ M^{-1}\ s^{-1} \quad (3)$$

with the corresponding rate constants (k) taken from the compilation of Elliot and Bartels.[12]

Besides the mechanism of its formation, a better knowledge of the radiolytic production of molecular hydrogen is crucial in the "water chemistry" management of current water-cooled nuclear reactors to optimize plant performance and lifetime. As we know,[2] H_2 is currently added to the primary coolant water to suppress the formation of stable oxidizing products (H_2O_2 and eventually its decomposition product O_2) from water radiolysis by a short chain reaction, thereby preventing corrosion and activity transport. The *in situ* radiolytic formation of H_2 in these reactors could, therefore, affect the minimum concentration of excess H_2, referred to as the "critical hydrogen

concentration",[41,42] required to suppress net radiolysis (no stable products formed) in the cores. Knowledge of this optimum H_2 level, which would minimize the damaging consequences of corrosion, is still a subject of debate in the chemical literature.

The anomalous increase in the escape yield of H_2 at high temperature is another key motivation for this study. In fact, although H_2 is a molecular product, $g(H_2)$ increases with temperature under γ/fast electron irradiation,[12,34,35] from ~0.45 molecule/100 eV at 25 °C to ~0.76 molecule/100 eV at 350 °C. This behavior is an exception to the generally accepted diffusion-kinetic model,[6,43] which predicts that, when the temperature increases, diffusion of free radicals out of spurs or tracks becomes more important than recombination, resulting in less molecular recombination products. At present, no definitive mechanism has yet been established to account for this anomalous radiolytic production of H_2 at high temperature.[34]

For these different reasons, the escape yield of H_2 has attracted much attention from experimentalists and modelers in order to explore in more detail its formation under various irradiation conditions. In this work, we use Monte Carlo track chemistry simulations to examine further the chemical differences underlying the production of molecular hydrogen in tritium β-radiolysis as compared with cobalt γ-radiolysis. No real-time studies on H_2 formation have been performed; its temporal dependence is usually probed by varying the concentration of appropriate scavengers for the hydrated electron and the hydrogen atom, which are the dominant free radical precursors of H_2 within the diffusing spurs or tracks. We here report data on the scavengeability by azide ions (N_3^-) of the molecular H_2 yield produced by γ- and tritium β-radiolysis. This particular scavenger was chosen as it presents very different reactivities towards e^-_{aq} and $H^\bullet$ atoms, being highly unreactive towards the former but reacting very rapidly with the latter. Our aim is to study the different H_2 scavengeabilities found for the two types of irradiation considered and to examine how these differences reflect the structure of the radiation track (*i.e.*, spurs *vs.* short tracks) in both cases.

2. Monte-Carlo track chemistry simulations

Monte Carlo simulation methods are well suited to take into account the stochastic nature of the complex sequence of events that are generated in irradiated aqueous solutions containing reactive scavengers. In the case of interest here, the experimentally observed yield value for molecular hydrogen is a composite one to which each of the processes producing H_2 contributes. The addition of a scavenger that competes with these processes to different extents will change the relative amount that each process contributes to the total yield. The simulation allows the reconstruction of the intricate action of the radiation, thus providing a powerful tool for studying the relationship between the initial radiation track structure, the ensuing chemical processes, and the stable final products formed. In this work, a full Monte Carlo track-chemistry computer code, called IONLYS-IRT,[11] has been used to simulate the radiolysis of water and

aqueous solutions containing various concentrations of scavengers. This code first models, in a 3D geometrical environment, the initial, highly nonhomogeneous radiation track structure ("IONLYS" program), and then the diffusion and chemical reactions of the various radical and molecular products formed by radiolysis with themselves or with solutes if present ("IRT" program). A detailed description of this code has been given previously.[11,18,28,34,44-46] Only a brief overview of its most essential features is given below.

The IONLYS code is a step-by-step simulation program that covers the early physical and physicochemical stages[47] of radiation action up to ~1 ps in the track development. It is composed of two modules. One is for transporting the investigated incident charged particle (called either TRACEPR for an impacting primary electron or TRACPRO/TRACION for an incident proton/ion). The other (called TRACELE) is for transporting all of the energetic (or dry) electrons (collectively named "secondary electrons") resulting from the ionization of the water molecules until they become hydrated. In this study, we used the TRACEPR module of IONLYS to simulate the track structures of low-energy (~7.8 keV) tritium β-electrons. As for the TRACPRO module, it was used here to simulate track segments of 300-MeV incident protons (which, as mentioned before, mimic ^{60}Co γ/fast electron irradiation) (see Fig. 1).

The complex, highly nonhomogeneous spatial distribution of reactants at the end of the physicochemical stage is provided as an output of the IONLYS (TRACELE) program. It is then used directly as the starting point for the subsequent nonhomogeneous chemical stage[47] (from ~1 ps to ~0.1-1 μs at 25 °C,[48] *i.e.*, until all tracks/spurs have dissipated). This stage, during which all different species diffuse (we assume ~1 ps also marks the beginning of diffusion) randomly at rates determined by their diffusion coefficients and react with one another or with any added solutes present at the time of irradiation, is covered by our "independent reaction times" (IRT) program. This program employs the IRT method,[49,50] a computer-efficient stochastic simulation technique used to simulate reaction times without having to follow the trajectories of the diffusing species. Its implementation has been previously described in detail[45] and its ability to give accurate, time-dependent chemical yields has been well validated[51,52] by comparison with full random flight (or step-by-step) Monte Carlo simulations, which do follow the reactant trajectories in detail. Finally, this IRT program has also been used successfully to describe the evolution of radiation-induced yields in the homogeneous chemical stage[47] after spur/track expansion is complete (*i.e.*, when the radiolytic products are homogeneously distributed in the bulk solution), in the time domain typically beyond a few microseconds.

The reaction scheme and rate constants for the radiolysis of pure liquid water at 25 °C employed in the current version of IONLYS-IRT are the same as used previously (see Table 1 of ref. 18). The values of the diffusion coefficients of the various intervening track species are listed in Table 6 of ref. 53. In order to simulate the radiolysis of the N_3^- solutions, we have supplemented the pure-water reaction scheme to include the primary e^-_{aq} and $H^\bullet$ atom scavenging

reactions that occur in the system (*vide infra*). The corresponding reaction rate constants were taken from the literature. Under normal irradiation conditions, the concentrations of radiolytic products are low compared with the background concentrations of N_3^- ions considered, and their reactions could be modeled in the IRT program as pseudo first-order reactions. In the computer simulations reported here, the diffusion coefficient used for N_3^- in liquid water at 25 °C was 1.84×10^{-5} cm^2/s.[54] This same value was also used for the diffusion coefficient of the azide radical $N_3^{\bullet}$.

In addition, we have introduced in the IRT program the effect of the ionic strength of the solutions on all reactions between ions.[55] The correction to the reaction rate constants was made as described in ref. 56 and 57. Finally, even though some experimental results are available for highly concentrated N_3^- solutions (up to 5 M), we generally restricted ourselves here to solute concentrations not exceeding ~1 M to avoid any complications due to the "direct" action of ionizing radiation on the solute (which our Monte Carlo code does not take into account).

To mimic the effects of ^{60}Co γ/fast electron-radiolysis, we used short segments (typically, ~150 μm) of ~300-MeV irradiating proton tracks, over which the average LET of the proton remains nearly constant and equal to ~0.3 eV/nm at 25 °C.[2,45] Such model calculations thus gave "track segment" yields[8,45] at a well-defined LET. Briefly, the simulations, performed with the TRACPRO module of IONLYS, consisted of following the transport and energy loss of an incident proton until it penetrated the chosen length of the track segment into the solution. As shown in Fig. 1, due to its large mass, the impacting proton is almost not deflected by collisions with the target electrons. The number of individual proton "histories" (usually ~150) was chosen to ensure only small statistical fluctuations in the computed averages of chemical yields, while keeping acceptable computer time limits.

As indicated above, tritium-β primary electron track structures were simulated using the TRACEPR module of IONLYS. Each simulation typically involved 6000 different whole track histories. This number was chosen to permit averaging of results with acceptable statistical confidence. In all the simulations, a single "effective" initial electron energy of ~7.8 keV (mean LET in water: ~5.9 eV/nm)[16] was used to mimic the radiation chemical action of the tritium β-particles at 25 °C (Fig. 1). This energy was found previously to be better suited to produce representative *G*-values when using tritium β-rays than the commonly used mean kinetic energy of ~5.7 keV released by tritium decay.[18,58]

Throughout this study, we assumed that tritiated water could simply be described as a "dilute" solution of ^3HOH in light water, with concentrations of low volumic activity (typically, less than ~1 Ci per mL) so that dose-rate effects could be ignored.[25,59]

3. Results and discussion

The azide ion N_3^- reacts very fast with H• atoms and very slowly with the hydrated electron, according to[22,25,60-63]

$$N_3^- + H^\bullet \rightarrow HN_3^{\bullet-},\ k_4 = 3.15 \times 10^9\ M^{-1}s^{-1} \quad (4)$$

$$N_3^- + e^-_{aq} \rightarrow \text{products},\ k_5 \leq 1.5 \times 10^6\ M^{-1}s^{-1}, \quad (5)$$

where the decay of $HN_3^{\bullet-}$ by proton addition has been shown not to involve H_2 as a final product[63] and where it is assumed here that the products of reaction (5) do not influence the H_2 chemistry. In contrast, its protonated form, hydrazoic acid (or hydrogen azide) HN_3,[22,54,63]

$$N_3^- + H^+ \leftrightarrow HN_3,\ pK_a(HN_3/N_3^-) = 4.7 \text{ in water at } 25\ °C,$$
$$k_6(\text{forward}) \approx 10^9\text{-}10^{10}\ M^{-1}\ s^{-1}, \quad (6)$$

is highly reactive towards e^-_{aq} but it reacts slower with H• atoms:[60,62-64]

$$HN_3 + e^-_{aq} \rightarrow HN_3^{\bullet-},\ k_7 = 1.2 \times 10^{10}\ M^{-1}s^{-1} \quad (7)$$

$$HN_3 + H^\bullet \rightarrow \text{products} (\neq H_2),\ k_8 = 6.3 \times 10^7\ M^{-1}s^{-1} \quad (8)$$

However, even if a fraction of the azide ions may react with H^+ ions in the spurs/tracks[13,22] to yield HN_3, especially at high N_3^- concentration (which is equivalent to short times), the Henderson-Hasselbalch equation indicates that, under the neutral pH conditions of this work, this compound will exist almost entirely in anion form. Hence, HN_3 should not significantly affect the radiolytic H_2 yield.

The azide ion can also react with the •OH radical to produce the one-electron oxidant azide radical, $N_3^\bullet$:[64,65]

$$N_3^- + {}^\bullet OH \rightarrow N_3^\bullet + OH^-,\ k_9 = 1.2 \times 10^{10}\ M^{-1}s^{-1}, \quad (9)$$

or, for its protonated form,[64]

$$HN_3 + {}^\bullet OH \rightarrow N_3^\bullet + H_2O,\ k_{10} < 10^7\ M^{-1}s^{-1}. \quad (10)$$

In this case, the •OH radicals (or at least part of them) are replaced by the $N_3^\bullet$ radicals and we need to consider the following reactions:[60,62,64,66-71]

$$N_3^\bullet + e^-_{aq} \rightarrow N_3^-,\ k_{11} = 2.4 \times 10^{10}\ M^{-1}\ s^{-1} \quad (11)$$

$$N_3^\bullet + H^\bullet \rightarrow HN_3,\ k_{12} \approx 10^{10}\ M^{-1}\ s^{-1} \quad (12)$$

$$N_3^\bullet + H_2O_2 \rightarrow \text{products},\ k_{13} < 5 \times 10^6\ M^{-1}\ s^{-1} \quad (13)$$

$$N_3^\bullet + N_3^\bullet \rightarrow 3N_2,\ k_{14} = 3.9 \times 10^9\ M^{-1}\ s^{-1} \quad (14)$$

$$N_3^\bullet + N_3^- \rightarrow (N_3)_2^{\bullet-},\ k_{15} = 2.4 \times 10^5\ M^{-1}\ s^{-1} \quad (15)$$

The rather slow reaction of azide with e^-_{aq} virtually excludes any effect of N_3^- on reactions involving e^-_{aq} in the spurs/tracks,[60] particularly in solutions with

low N_3^- concentration. Indeed, even in a 5 M N_3^- solution, the scavenging time[72] of e^-_{aq} by N_3^- is about the same order of magnitude as the lifetime of a spur (~0.2 μs)[48] in the ^{60}Co γ-radiolysis of water at 25 °C. Under these conditions, the molecular hydrogen yield was measured in irradiated *aerated* azide solutions.[22,25,60] Oxygen between ~2.5×10^{-4} M (air-saturated conditions) and ~$3\text{-}5 \times 10^{-5}$ M was used as e^-_{aq} scavenger on the ~0.1-1 μs time scale. Noteworthy, the azide radical is inert towards molecular oxygen,[66] but may react with the superoxide anion radical[62,66]

$$N_3^\bullet + O_2^{\bullet-} \rightarrow O_2 + N_3^-,\ k_{16} = 1.2 \times 10^{10}\ M^{-1}\ s^{-1}. \quad (16)$$

While these low O_2 concentrations hardly affect $g(H_2)$, they do prevent, at long times, the reactions of e^-_{aq} with itself and with water[62]

$$e^-_{aq} + H_2O \rightarrow H^\bullet + OH^-,\ k_{17} = 19\ M^{-1}\ s^{-1} \quad (17)$$

in the bulk of the solutions.

Fig. 2 (panels a and b) shows the effect of azide concentration on the kinetics of H_2 formation over the interval ~1 ps to 10 μs, as obtained from our Monte Carlo simulations of the radiolysis of aerated neutral pH aqueous solutions of NaN_3 by ~300-MeV incident protons and ~7.8-keV tritium β-electrons at 25 °C. Results are shown for six different concentrations of azide anions, ranging from 10^{-4} to 5 M. As can be seen, for both types of radiation, the time profiles of the H_2 yields are essentially similar although the magnitude of the $G(H_2)$ values differs. In fact, the simulations show a clear increase in the absolute value of $G(H_2)$ for ^3H β-electrons compared to ^{60}Co γ-rays. As mentioned earlier, this increase in H_2 yields, when comparing the effects of higher-LET tritium β-radiolysis with the γ/fast electron-radiolysis, is consistent with differences in the initial structure of electron tracks in the two cases. In the short-track geometry of the β-electrons (in contrast with spur geometry), the reactive intermediates are formed in much closer initial proximity, which is favorable to the additional formation of H_2 through the inter-radical combination reactions (1)-(3).

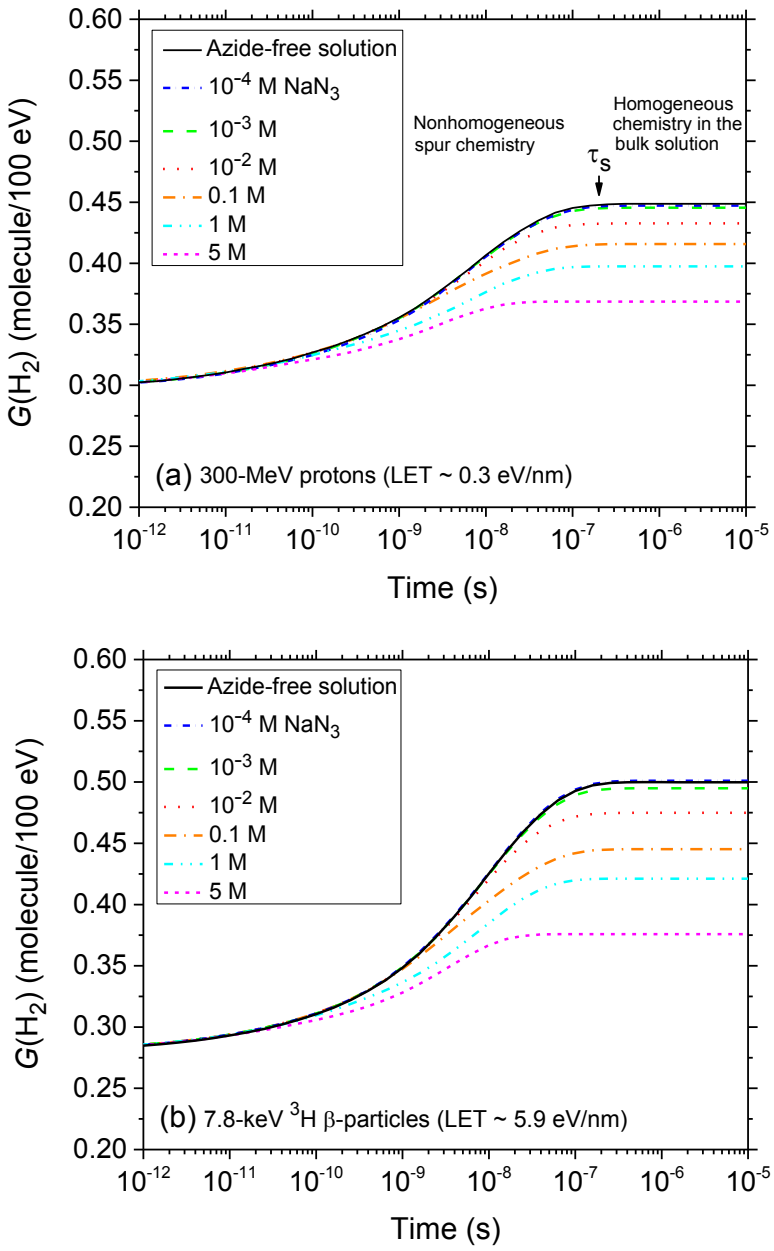

Fig. 2 Time evolution of the H_2 yield (in molecule per 100 eV) for the radiolysis of air-saturated aqueous sodium azide (NaN_3) solutions by 300-MeV incident protons (which mimic irradiation with ^{60}Co γ-rays or fast electrons, LET ~ 0.3 eV/nm) (panel a) and by 7.8-keV ^{3}H β-particles (LET ~ 5.9 eV/nm) (panel b) at neutral pH and 25 °C. Calculations were carried out using our Monte-Carlo track chemistry simulations over the time interval 1 ps-10 μs. The blue, green, red, orange, cyan, and magenta lines correspond to six different concentrations of N_3^- anions: 10^{-4}, 10^{-3}, 10^{-2}, 0.1, 1 and 5 M, respectively. For both types of radiation, the limiting plateau values of $G(H_2)$ continuously decrease with increasing the concentration of N_3^- ions. For ^{60}Co γ/fast electron irradiation, the arrow pointing downwards indicates the time τ_s ~ 0.2 μs required for the changeover from

nonhomogeneous spur kinetics to homogeneous kinetics in the bulk solutions, at 25 °C. The black solid line in panels a and b show the kinetics of H_2 formation in azide-free aerated solutions (shown here for the sake of reference). Finally, the concentration of dissolved oxygen used in the simulations was 2.5×10^{-4} M.

The decrease in the yield of H_2 with concentration of N_3^- ions for 300-MeV incident protons and 7.8-keV ^3H β-electrons in the radiolysis of aerated azide solutions is further illustrated in Fig. 3. The H_2 yields shown in this figure are the $G(H_2)$ limiting plateau values corresponding to each considered N_3^- concentration, taken from Fig. 2. As can be seen, our simulated yields compare well with the experimental escape yields of Gagnon and Appleby,[22] Christman,[25] and Peled *et al.*[60] obtained for ^{60}Co γ and tritium β-particle irradiations. In the case of γ-radiolysis, this agreement is particularly good at low and moderated N_3^- concentrations. However, at concentrations higher than ~0.5 M, there are significant differences, the experimentally observed H_2 yields showing a very sharp decrease[73] compared to the simulation results. This efficiency in reducing the molecular hydrogen produced strongly suggests that the concentration of azide ions is now high enough to allow their reaction with the dry electron (e^-_{dry}) prior to trapping and hydration (*i.e.*, with the precursor to e^-_{aq}), in the subpicosecond physicochemical stage.[33]

Similar findings about the N_3^- scavenging of the short-lived hydrated electron precursor were obtained by Harris and Pimblott[26] in recent Monte Carlo studies of the ^{60}Co γ-radiolysis of azide solutions of concentration greater than 1 M. The present study clearly corroborates their results. Assuming the validity of this hypothesis would imply a ($e^-_{dry} + N_3^-$) reaction rate constant of ~10^{12}-10^{13} M^{-1} s^{-1} at 25 °C, in agreement with Harris and Pimblott[26,74] results.

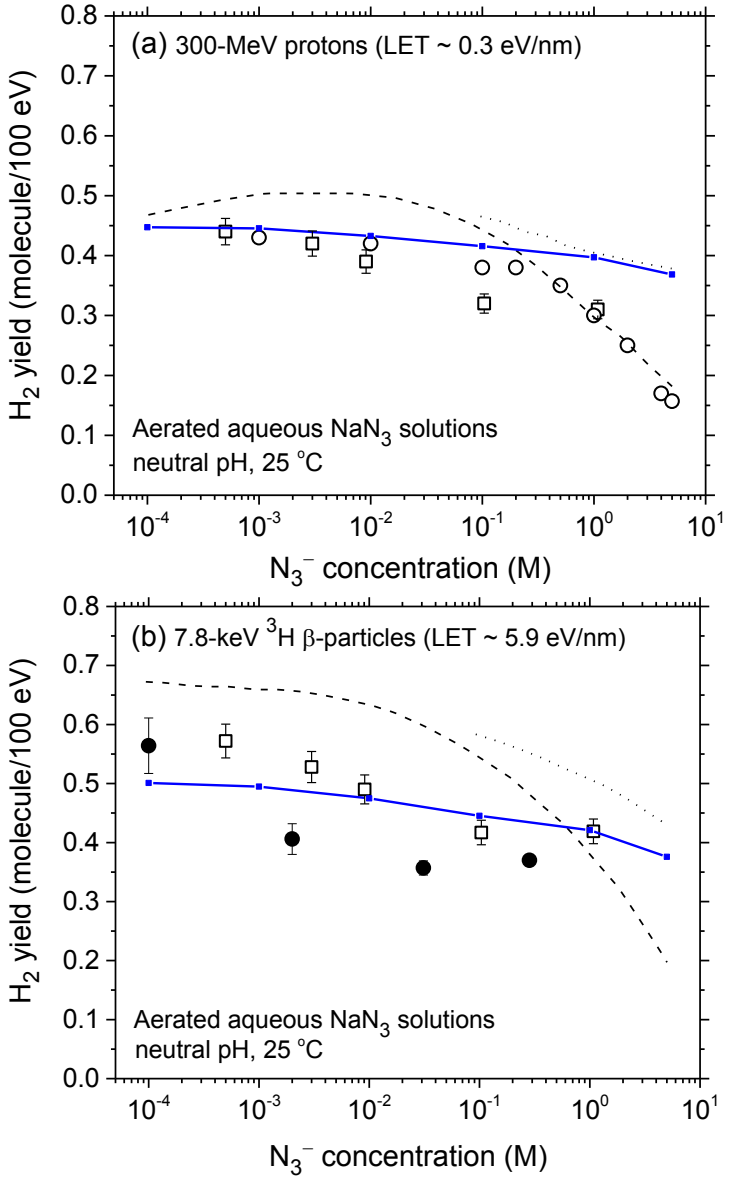

Fig. 3 Decrease in the molecular hydrogen yield (in molecule per 100 eV) with concentration of N_3^- ions for 300 MeV incident protons (LET ~ 0.3 eV/nm) (panel a) and for 7.8 keV ^3H β-particles (LET ~ 5.9 eV/nm) (panel b) in the radiolysis of air-saturated aqueous azide (NaN_3) solutions (neutral pH, 25 °C), calculated from our Monte Carlo simulations over the range of 10^{-4} to 5 M. The blue solid lines show our simulated results (see text). Experimental data for γ and tritium β-particle irradiations: (●), ref. 22; (□), ref. 25; (○), ref. 60. For the sake of comparison, the H_2 yields calculated from ref. 26 for both types of radiation, assuming that N_3^- scavenges the short-lived precursor to H_2 with a rate constant of 10^{12} M^{-1} s^{-1} (dashed line) and does not scavenge the short-lived precursor to H_2 (dotted line), are also shown in the figure.

For the case of ^{3}H β-particle radiolysis, the effectiveness in lowering $g(H_2)$ at high azide concentration differs considerably from the case of γ-radiolysis. Despite a relatively large dispersion of experimental data,[75] we do not observe any sharp decrease at concentrations higher than ~0.1-1 M as we do for γ irradiation. There is only a slight continuous decrease of the yield of H_2 without any clear supporting evidence that, in this case, N_3^- ions scavenge the short-lived dry electrons. This is consistent with the enhanced contribution of short tracks for the higher LET tritium β-radiolysis as compared to γ radiolysis. Indeed, in this case, the short-track geometry would be competitively more favorable to the subpicosecond recombination reaction of e^-_{dry} with its nearby parent water cation ($H_2O^{\bullet+}$) than to its scavenging by the homogeneously distributed N_3^- ions.

A final remark should be made here regarding the origin of the small reduction that is observed, for both types of radiation, in the yields of H_2 with increasing azide concentration from 10^{-4} up to ~0.1-1 M. In fact, as shown in Fig. 4, our calculations indicate that the H_2 production originating from the ($H^\bullet$ + e^-_{aq}) reaction (1) quickly decreases as the N_3^- concentration increases. This result is of course a clear signature that N_3^- ions readily scavenge $H^\bullet$ atoms, thus preventing them from contributing to this reaction. By contrast, the formation of H_2 through the (e^-_{aq} + e^-_{aq}) reaction (2) should in principle be rather unaffected by the presence of N_3^-, N_3^- being highly unreactive towards e^-_{aq}. Actually, it is indirectly because the hydrated electrons that have not reacted with $H^\bullet$ through reaction (1) become now available to participate to reaction (2). Overall, there is a kind of compensation between the two contributions involved in the H_2 production, the contribution from reaction (1) dominating slightly.

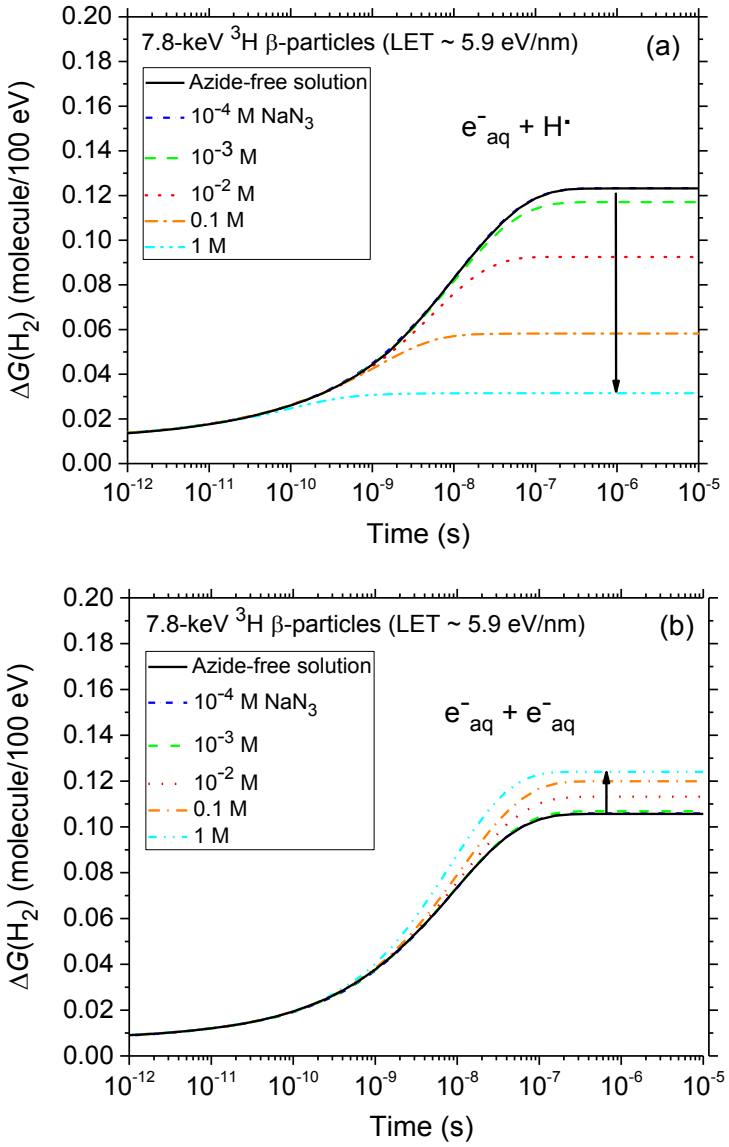

Fig. 4 Time dependence of the extents $\Delta G(H_2)$ (in molecule/100 eV) of the reactions (e^-_{aq} + H•) (panel a) and (e^-_{aq} + e^-_{aq}) (panel b) that contribute to the formation of molecular hydrogen, calculated from our Monte Carlo simulations of the radiolysis of air-saturated aqueous azide (NaN_3) solutions (pH neutral, 25 °C) by 7.8-keV ^{3}H β-particles (LET ~ 5.9 eV/nm) in the time interval 1 ps-10 μs. The blue, green, red, orange, and cyan lines correspond to the five different concentrations of azide anions studied: 10^{-4}, 10^{-3}, 10^{-2}, 0.1, and 1 M, respectively (see text). For the sake of reference, the black lines in panels a and b show the cumulative yield variations $\Delta G(H_2)$ of the two reactions (e^-_{aq} + H•) and (e^-_{aq} + e^-_{aq}) that contribute to the formation of H_2. Finally, the concentration of dissolved oxygen used in the simulations was 2.5×10^{-4} M.

4. Conclusions

Monte Carlo track chemistry simulations have been employed to investigate the scavengeability by azide ions (N_3^-) of the molecular hydrogen yield produced in water irradiated with 300-MeV protons (which mimic irradiation with ^{60}Co γ rays or fast electrons) and tritium β-electrons at 25 °C. From this study, we clearly show that the formation of H_2 from ^3H β-particles is higher than in the case of ^{60}Co γ rays, a result that is easily explained by the difference of the structure of radiation tracks. The track structure in the case of ^{60}Co γ irradiation is composed of well-separated (spherical) spurs, which contrasts with the short (roughly cylindrical) tracks observed in the case of higher-LET tritium β-electrons. The greater linear energy transfer of ^3H β-electrons leads to an increased local concentration of reactants. The distance between the primary events is thus much smaller than in the tracks of ^{60}Co γ rays. Consequently, we find more molecular products (H_2 in the case considered in this work) in tritium radiolysis than in γ radiolysis.

Our calculations of the H_2 yields from γ- and ^3H β-radiolysis of NaN_3 solutions show a very good agreement with experiment over a large range of N_3^- concentrations. For ^{60}Co γ-radiolysis, however, our H_2 yields fail to reproduce the sharp decrease that is observed experimentally at high (>1 M) azide concentrations. These results are consistent with previous Monte Carlo simulations that suggested that such a decrease reflected the possibility that low-energy (or "dry") secondary electrons could be scavenged by N_3^- prior to trapping and hydration in the subpicosecond physicochemical stage. Most interestingly, for ^3H β-radiolysis, we do not observe any marked decrease in the molecular hydrogen yields at high N_3^- concentrations as we do for γ irradiation. In other words, there is no clear evidence that, in this case, N_3^- ions scavenge the short-lived dry electrons. This is consistent with the enhanced contribution of short tracks for the higher LET ^3H β-radiolysis as compared to γ radiolysis. Indeed, the short-track geometry is competitively more favorable to the geminate recombination of e^-_{dry} with their nearby parent water cations than their scavenging by the homogeneously distributed N_3^- ions. In order to further examine these results, we are currently working to introduce this ultra-fast (<1 ps) capture of the dry electron into our simulation models.

In summary, this work, like our previous ones on the subject, provides a strong support for a picture of tritium β-radiolysis in terms of short tracks of high local LET.

Conflicts of interest

There are no conflicts of interest to declare.

Acknowledgements

S. S. is the recipient of a doctoral scholarship from the Natural Sciences and Engineering Research Council of Canada (NSERC). This work received financial

assistance from Atomic Energy of Canada Limited (Contract no. RD-1.3.5.1-4511). The research of J.-P. J.-G. is supported by the NSERC Discovery Grant No. RGPIN-2015-06100.

Notes and references

1 C. von Sonntag, *Free-Radical-Induced DNA Damage and Its Repair*, Springer-Verlag, Berlin, 2006.
2 D. R. McCracken, K. T. Tsang and P. J. Laughton, *Aspects of the physics and chemistry of water radiolysis by fast neutrons and fast electrons in nuclear reactors*, Report AECL No. 11895, Atomic Energy of Canada Limited, Chalk River, Ontario, Canada, 2009.
3 P. O'Neill and P. Wardman, *Int. J. Radiat. Biol.*, 2009, **85**, 9; P. Wardman, *Br. J. Radiol.*, 2009, **82**, 89.
4 E. I. Azzam, J.-P. Jay-Gerin and D. Pain, *Cancer Lett.*, 2012, **327**, 48.
5 J. W. T. Spinks and R. J. Woods, *An Introduction to Radiation Chemistry*, Wiley, New York, 3rd edn, 1990.
6 A. Mozumder, *Fundamentals of Radiation Chemistry*, Academic Press, San Diego, California, 1999.
7 C. Ferradini and J.-P. Jay-Gerin, *Can. J. Chem.*, 1999, **77**, 1542. See also J.-P. Jay-Gerin and C. Ferradini, in *Excess Electrons in Dielectric Media*, ed. C. Ferradini and J.-P. Jay-Gerin, CRC Press, Boca Raton, Florida, 1991, p. 259.
8 J. A. LaVerne, *Radiat. Res.*, 2000, **153**, 487.
9 G. V. Buxton, in *Charged Particle and Photon Interactions with Matter: Chemical, Physicochemical, and Biological Consequences with Applications*, ed. A. Mozumder and Y. Hatano, Marcel Dekker, New York, 2004, p. 331.
10 Y. Muroya, I. Plante, E. I. Azzam, J. Meesungnoen, Y. Katsumura and J.-P. Jay-Gerin, *Radiat. Res.*, 2006, **165**, 485.
11 J. Meesungnoen and J.-P. Jay-Gerin, in *Charged Particle and Photon Interactions with Matter. Recent Advances, Applications, and Interfaces*, ed. Y. Hatano, Y. Katsumura and A. Mozumder, Taylor & Francis Group, Boca Raton, Florida, 2011, p. 355. See also J. Meesungnoen, *Ph.D. thesis*, Université de Sherbrooke, Sherbrooke, Québec, Canada, 2007.
12 A. J. Elliot and D. M. Bartels, *The reaction set, rate constants and g-values for the simulation of the radiolysis of light water over the range 20 to 350 °C based on information available in 2008*, Report AECL No. 153-127160-450-001, Atomic Energy of Canada Limited, Chalk River, Ontario, Canada, 2009.
13 V. Kanike, J. Meesungnoen and J.-P. Jay-Gerin, *RSC Adv.*, 2015, **5**, 43361.
14 J. L. Magee, *Annu. Rev. Nucl. Sci.*, 1953, **3**, 171.
15 G. R. Freeman, in *Proceedings of the Workshop on the Interface between Radiation Chemistry and Radiation Physics*, Report ANL-82-88, ed. M. A. Dillon, R. J. Hanrahan, R. Holroyd, Y.-K. Kim, M. C. Sauer Jr and L. H. Toburen, Argonne National Laboratory, Argonne, Illinois, 1983, p. 9.
16 Hydrogen-3 or tritium (^{3}H) is a radioactive isotope of hydrogen. Its nucleus consists of a proton and two neutrons. The most common chemical form of tritium is tritium oxide, also called "tritiated water" (usually represented as

^{3}HOH). As it decays, ^{3}H emits ionizing radiation in the form of β-electrons with the following characteristics: maximum kinetic energy: ~18.6 keV, mean kinetic energy released: ~5.7 keV, "mean energy of energy deposition" in water: ~7.8 keV, maximum range in water at 25 °C: ~5.5 μm (~6 mm in air). The mean (averaged over whole track) LET of ^{3}H β-electrons in water (~5.9 eV/nm) is ~20 times greater than that of the Compton electrons (~1 MeV) generated by ^{60}Co γ-rays (~0.3 eV/nm).

17 D. E. Watt, *Quantities for Dosimetry of Ionizing Radiations in Liquid Water*, Taylor & Francis, London, 1996.

18 L. Mirsaleh Kohan, S. Sanguanmith, J. Meesungnoen, P. Causey, C. R. Stuart and J.-P. Jay-Gerin, *RSC Adv.*, 2013, **3**, 19282.

19 A. Mozumder and J. L. Magee, *J. Chem. Phys.*, 1966, **45**, 3332; A. Mozumder and J. L. Magee, *Radiat. Res.*, 1966, **28**, 203.

20 Throughout this paper, radiation chemical yields are quoted in units of molecules per 100 eV, as g(X) for primary (or "escape") yields and G(X) for experimentally measured yields. Recall here briefly that the so-called "primary" radical and molecular yields are defined as the numbers of species formed or destroyed per 100 eV of absorbed energy that remain after spurs/tracks have dissipated and become available to react with added solutes (if any) at moderate concentrations. For conversion into SI units (mol/J), 1 molecule per 100 eV ≈ 0.10364 μmol/J.

21 A. Appleby and W. F. Gagnon, *J. Phys. Chem.*, 1971, **75**, 601.

22 W. F. Gagnon and A. Appleby, *Scavenger studies in tritiated water*, Paper of the Journal Series, New Jersey Agricultural Experimental Station, Rutgers University, Department of Environmental Sciences, New Brunswick, New Jersey, 1971.

23 G. Lemaire, C. Ferradini and J. Pucheault, *J. Phys. Chem.*, 1972, **76**, 1542. See also G. Lemaire and C. Ferradini, *Radiochem. Radioanal. Lett.*, 1970, **5**, 175; G. Lemaire and C. Ferradini, in *Proceedings of the Third Tihany Symposium on Radiation Chemistry*, ed. J. Dobó and P. Hedvig, Akadémiai Kiadó, Budapest, 1972, vol. 2, p. 1213.

24 W. F. Gagnon and A. Appleby, in *Tritium*, ed. A. A. Moghissi and M. W. Carter, Messenger Graphics, Phoenix, Arizona, 1973, p. 192.

25 E. A. Christman, *Ph.D. thesis*, Rutgers University, New Brunswick, New Jersey, 1977.

26 R. E. Harris and S. M. Pimblott, *Radiat. Res.*, 2002, **158**, 493.

27 S. L. Butarbutar, S. Sanguanmith, J. Meesungnoen, P. Causey, C. R. Stuart and J.-P. Jay-Gerin, *RSC Adv.*, 2014, **4**, 22980.

28 S. Mustaree, J. Meesungnoen, S. L. Butarbutar, P. Causey, C. R. Stuart and J.-P. Jay-Gerin, *RSC Adv.*, 2014, **4**, 43572.

29 T. J. Hardwick, *Discuss. Faraday Soc.*, 1952(12), 203. See also A. O. Allen, *Radiat. Res.*, 1954, **1**, 85.

30 E. J. Hart, *Radiat. Res.*, 1954, **1**, 53. See also W. R. McDonell and E. J. Hart, *J. Am. Chem. Soc.*, 1954, **76**, 2121.

31 E. Collinson, F. S. Dainton and J. Kroh, *Proc. R. Soc. London*, 1962, **A265**, 422. See also E. Collinson, F. S. Dainton and J. Kroh, *Nature*, 1960, **187**, 475. These same authors (E. Collinson, F. S. Dainton and J. Kroh, *Proc. R. Soc. London*, 1962, **A265**, 430) also described and discussed the isotope effects observed for irradiations of 0.05 M sulfuric acid solutions with 1.6 and 3 MeV α-particles and tritium β-particles.
32 R. Bensasson, A. Bernas, M. Bodard, L. Bouby, M. Cottin, M. Duflo, F. Kieffer, A. Koulkès, N. Leray, J. Pucheault and C. Vermeil, in *Tables of Constants and Numerical Data*, ed. M. Haïssinsky and M. Magat, Pergamon, Oxford, 1963, vol. 13, p. 15.
33 In liquid water at 25 °C, time-resolved femtosecond laser spectroscopic experiments have revealed that electron "localization" and "hydration" occur in quick succession on time scales of ~50-300 fs and ~240 fs-1 ps, respectively (see, for example, C.-R. Wang, T. Luo and Q.-B. Lu, *Phys. Chem. Chem. Phys.*, 2008, **10**, 4463). Monte Carlo simulations of the thermalization of e^-_{sub} in solid water have shown that thermalization times vary from ~3 to 182 fs when the initial electron energy changes from 0.35 to 7.2 eV, respectively, with an estimated average value of ~60 fs (see T. Goulet, J. P. Patau and J.-P. Jay-Gerin, *J. Phys. Chem.*, 1990, **94**, 7312).
34 J. Meesungnoen, S. Sanguanmith and J.-P. Jay-Gerin, *RSC Adv.*, 2015, **5**, 76813.
35 M. Sterniczuk and D. M. Bartels, *J. Phys. Chem. A*, 2016, **120**, 200.
36 The secondary (or "dry") electron released in the ionization event can cause further ionization and excitation to occur if it has sufficient kinetic energy. Eventually, its energy falls below the first electronic excitation threshold of water (~7.3 eV in amorphous ice at 14 K, see: M. Michaud, P. Cloutier and L. Sanche, *Phys. Rev. A*, 1991, **44**, 5624), forming the so-called "sub-excitation electron" (R. L. Platzman, *Radiat. Res.*, 1955, **2**, 1). The latter loses the rest of its energy relatively slowly by exciting vibrational and rotational modes of water molecules. Once it is thermalized (e^-_{th}), it can get localized or "trapped" (e^-_{tr}) in a pre-existing potential energy well of appropriate depth in the liquid before it reaches a fully relaxed, hydrated state (e^-_{aq}) as the dipoles of the surrounding molecules orient under the influence of the negative charge of the electron. The trapped (or "wet") electron has sometimes been called "incompletely relaxed" or "prehydrated" electron in the literature (G. R. Freeman, in *Kinetics of Nonhomogeneous Processes*, ed. G. R. Freeman, Wiley, New York, 1987, p. 19).
37 H. Schwarz, *J. Phys. Chem.*, 1969, **73**, 1928.
38 B. Pastina, J. A. LaVerne and S. M. Pimblott, *J. Phys. Chem. A*, 1999, **103**, 5841.
39 V. Cobut, J.-P. Jay-Gerin, Y. Frongillo and J. P. Patau, *Radiat. Phys. Chem.*, 1996, **47**, 247.
40 M.-A. Hervé du Penhoat, T. Goulet, Y. Frongillo, M.-J. Fraser, P. Bernat and J.-P. Jay-Gerin, *J. Phys. Chem. A*, 2000, **104**, 11757.
41 D. M. Bartels, J. Henshaw and H. E. Sims, *Radiat. Phys. Chem.*, 2013, **82**, 16; K. Kanjana, K. S. Haygarth, W. Wu and D. M. Bartels, *Radiat. Phys. Chem.*, 2013, **82**, 25.

42 C. D. Alcorn, J.-C. Brodovitch, P. W. Percival, M. Smith and K. Ghandi, *Chem. Phys.*, 2014, **435**, 29.
43 A. Kuppermann, in *Actions Chimiques et Biologiques des Radiations*, ed. M. Haïssinsky, Tome 5, Masson, Paris, 1961, p. 85.
44 V. Cobut, Y. Frongillo, J. P. Patau, T. Goulet, M.-J. Fraser and J.-P. Jay-Gerin, *Radiat. Phys. Chem.*, 1998, **51**, 229.
45 Y. Frongillo, T. Goulet, M.-J. Fraser, V. Cobut, J. P. Patau and J.-P. Jay-Gerin, *Radiat. Phys. Chem.*, 1998, **51**, 245.
46 R. Meesat, S. Sanguanmith, J. Meesungnoen, M. Lepage, A. Khalil and J.-P. Jay-Gerin, *Radiat. Res.*, 2012**, 177**, 813.
47 R. L. Platzman, in *Radiation Biology and Medicine. Selected Reviews in the Life Sciences*, ed. W. D. Claus, Addison-Wesley, Reading, Massachusetts, 1958, p. 15. See also A. Kuppermann, *J. Chem. Educ.*, 1959, **36**, 279.
48 S. Sanguanmith, J. Meesungnoen, Y. Muroya, M. Lin, Y. Katsumura and J.-P. Jay-Gerin, *Phys. Chem. Chem. Phys.*, 2012, **14**, 16731.
49 M. Tachiya, *Radiat. Phys. Chem.*, 1983, **21**, 167.
50 S. M. Pimblott, M. J. Pilling and N. J. B. Green, *Radiat. Phys. Chem.*, 1991, **37**, 377. See also S. M. Pimblott and N. J. B. Green, in *Research in Chemical Kinetics*, ed. R. G. Compton and G. Hancock, Elsevier, Amsterdam, 1995, vol. 3, p. 117.
51 T. Goulet, M.-J. Fraser, Y. Frongillo and J.-P. Jay-Gerin, *Radiat. Phys. Chem.*, 1998, **51**, 85.
52 I. Plante, Ph.D. thesis, Université de Sherbrooke, Sherbrooke, Québec, Canada, 2009.
53 T. Tippayamontri, S. Sanguanmith, J. Meesungnoen, G. R. Sunaryo and J.-P. Jay-Gerin, in *Recent Research Developments in Physical Chemistry*, ed. S. G. Pandalai, Transworld Research Network, Trivandrum, Kerala, India, 2009, vol. 10, p. 143.
54 *CRC Handbook of Chemistry and Physics*, ed. D. R. Lide, CRC Press, Boca Raton, Florida, 84th edn, 2003.
55 Except for the peculiar bimolecular self-recombination of e^-_{aq} for which there is no experimental evidence of any ionic strength effect (see K. H. Schmidt and D. M. Bartels, *Chem. Phys.*, 1995, **190**, 145).
56 S. Sanguanmith, Y. Muroya, T. Tippayamontri, J. Meesungnoen, M. Lin, Y. Katsumura and J.-P. Jay-Gerin, *Phys. Chem. Chem. Phys.*, 2011, **13**, 10690.
57 R. E. Weston, Jr. and H. A. Schwarz, *Chemical Kinetics*, Prentice-Hall, Englewood Cliffs, New Jersey, 1972.
58 ICRU Report 17, *Radiation Dosimetry: X Rays Generated at Potentials of 5 to 150 kV*, International Commission on Radiation Units and Measurements, Washington, D.C., 1970. See also J. Law, *Phys. Med. Biol.*, 1969, **14**, 607.
59 S. Heinze, T. Stolz, D. Ducret and J.-C. Colson, *Fusion Sci. Technol.*, 2005, **48**, 673.
60 E. Peled, U. Mirski and G. Czapski, *J. Phys. Chem.*, 1971, **75**, 31. Note that these authors used a ^{137}Cs γ source for their irradiations.
61 M. Ye, K. P. Madden, R. W. Fessenden and R. H. Schuler, *J. Phys. Chem.*, 1986, **90**, 5397.

62 G. V. Buxton, C. L. Greenstock, W. P.Helman and A. B. Ross, *J. Phys. Chem. Ref. Data*, 1988, **17**, 513.
63 S. P. Mezyk and D. M. Bartels, *J. Phys. Chem. A*, 2005, **109**, 11823.
64 Z. B. Alfassi and R. H. Schuler, *J. Phys. Chem.*, 1985, **89**, 3359; Z. B. Alfassi, W. A. Prütz and R. H. Schuler, *J. Phys. Chem.*, 1986, **90**, 1198.
65 E. Hayon and M. Simic, *J. Am. Chem. Soc.*, 1970, **92**, 7486.
66 T. E. Eriksen, J. Lind and G. Merényi, *Radiochem. Radioanal. Lett.*, 1981, **48**, 405.
67 T. Ichino and R. W. Fessenden, *J. Phys. Chem. A*, 2007, **111**, 2527.
68 A. Singh, G. W. Koroll and R. B. Cundall, *Radiat. Phys. Chem.*, 1982, **19**, 137.
69 G. R. Dey, *Res. Chem. Intermed.*, 2007, **33**, 599.
70 P. Neta, R. E. Huie and A. B. Ross, *J. Phys. Chem. Ref. Data*, 1988, **17**, 1027.
71 X. Liu, M. A. MacDonald and R. D. Coombe, *J. Phys. Chem.*, 1992, **96**, 4907.
72 The product of a solute's (or scavenger's) concentration and its rate constant for reaction with one of the primary radical species is called its "scavenging power", with units of s^{-1}. The inverse of the scavenging power gives a measure of the time scale over which the scavenging is occurring or, in other words, the lifetime of the radical with respect to that reaction (see ref. 2).
73 For example, in the presence of 5 M N_3^-, the measured yield of H_2 is decreased to almost one-third of its value in the absence of azide (see ref. 60).
74 See also S. M. Pimblott and J. A. LaVerne, *J. Phys. Chem.*, 1998, **102**, 2967.
75 This relatively large dispersion of experimental data is probably explained by the fact that experiments are difficult to perform with ^3H as the source of β-particle radiation. Contrary to γ-irradiation studies, the irradiation cannot be stopped and hence estimation of the dose given to the sample is susceptible to significant error (see ref. 26).

9. ARTICLE 3

Scavenging of "dry" electrons prior to hydration by azide ions: Effect on the formation of H_2 in the radiolysis of water by ^{60}Co γ-rays and tritium β-electrons

Authors: Sunuchakan Sanguanmith, Jintana Meesungnoen, Yusa Muroya, and Jean-Paul Jay-Gerin

Status: submitted to ***Canadian Journal of Chemistry,*** December 2020

Forwords: From our previous work (article no. 2) it is shown that at high N_3^- concentrations (>1 M), our H_2 yield results for ^{60}Co γ-radiolysis do not agree well with the experimental data. This suggests the necessity of including the capture of the precursors to the hydrated electrons (*i.e.*, the short-lived "dry" electrons prior to hydration) by N_3^-. In this work, we have introduced in our program the possibility that the electron prior to hydration can react with N_3^-. We built a new program for introducing the possibility that scavengers can react with prehydrated electrons. I performed all the calculations, incorporating and adjusting parameters intervening in all processes of the radiolysis of azide solutions. Finally, I had a significant contribution to the idea of this work and all the preparation process for the first version of this article.

Résumé : À des concentrations élevées de N_3^- (>1 M), nos résultats du rendement en H_2 pour les rayons γ de ^{60}Co sont également cohérents avec des simulations Monte Carlo précédentes qui suggéraient la nécessité d'inclure la capture des précurseurs des électrons hydratés (à savoir, les électrons « secs » avant hydratation) par N_3^-. Ces processus ont tendance à réduire considérablement les rendements en H_2, comme observé expérimentalement. Cependant, cette capture d'électrons secs à des concentrations élevées d'azide n'est pas observée dans la radiolyse-β du tritium à TEL plus élevée, ce qui nous amène à conclure que l'augmentation de la quantité de chimie intra-trajectoire intervenant à un moment précoce dans ces conditions favorise la recombinaison de ces électrons avec leurs cations parents de l'eau aux dépens de leur capture par N_3^-.

Scavenging of "dry" electrons prior to hydration by azide ions: Effect on the formation of H_2 in the radiolysis of water by ^{60}Co γ-rays and tritium β-electrons

By

Sunuchakan Sanguanmith,[1] Jintana Meesungnoen,[1] Yusa Muroya,[2] and Jean-Paul Jay-Gerin[1,*]

[1] Département de Médecine Nucléaire et de Radiobiologie, Faculté de Médecine et des Sciences de la Santé, Université de Sherbrooke, 3001, 12e Avenue Nord, Sherbrooke (Québec) J1H 5N4, Canada. *E-mail: jean-paul.jay-gerin@USherbrooke.ca*

[2] Department of Beam Materials Science, Institute of Scientific and Industrial Research, Osaka University, 8-1 Mihogaoka, Ibaraki, Osaka 567-0047, Japan.

[*] Corresponding author.

Canadian Journal of Chemistry
Manuscript No. cjc-2020-0504 (revised)
May 8, 2021

Abstract:

In this study, we use Monte Carlo track chemistry simulations to show that “dry” secondary electrons, precursors of the “hydrated” electron (e^-_{aq}), can be scavenged on the sub-picosecond time scale prior to hydration, by a high concentration (>0.1–1 M) of azide ions (N_3^-) in water irradiated with ^{60}Co γ-rays and tritium β-electrons at 25 °C. This is a striking result, as N_3^- is known to react very slowly with e^-_{aq}. These processes tend to significantly reduce the yields of H_2 as observed experimentally. For both energetic Compton electrons (“linear energy transfer”, LET ~ 0.3 keV/μm), which are generated by the cobalt-60 γ-rays, and ^{3}H β-electrons (LET ~ 6 keV/μm), our H_2 yield results confirm previous Monte Carlo simulations, which indicated the necessity of including the capture of the precursors to e^-_{aq}. Interestingly, our calculations show no significant changes in the scavenging of “dry” electrons at high azide concentrations in passing from γ-radiolysis to tritium β-radiolysis (*i.e.*, with LET). This led us to the conclusion that the higher H_2 yield observed experimentally for ^{3}H β-electrons compared to ^{60}Co γ-rays is mainly explained by the difference in the radiation track structures during the chemical stage (>1 ps). The higher LET of tritium β-electrons leads to more molecular products (H_2 in this case) in tritium radiolysis than in γ-radiolysis. Finally, a value of ~0.5 nm was derived for the reaction distance between N_3^- and the “dry” electron from the H_2 yields observed in ^{60}Co γ-radiolysis at high N_3^- concentrations.

Keywords: Liquid water, azide ion (N_3^-) solutions, radiolysis, linear energy transfer (LET), cobalt γ-rays, tritium β-electrons, secondary electrons, “dry” electron scavenger, mobility, H_2 yield, Monte Carlo track chemistry simulations.

1. Introduction

The radiation chemistry of liquid water[1-3] is of fundamental importance for a variety of practical applications, particularly in the nuclear power industry, where radiolysis products cause corrosion and activity transport,[4,5] and in radiation biology,[6-9] where living cells and tissues consist mainly of water (~70%–85% by weight). Exposed to ionizing radiation, water is the site of ionizations and direct excitations:

(1) $H_2O \rightsquigarrow H_2O^{\bullet+} + e^-$ (ionization)

(2) $H_2O \rightsquigarrow H_2O^*$ (direct excitation),

which result, on the picosecond time scale, in a cascade of events leading to the formation of free radicals and molecular products along the track of the incident radiation. In pure water radiolysis, they essentially comprise the "hydrated" electron (e^-_{aq}), $H^\bullet$, $^\bullet OH$, H_2, H_2O_2, and $HO_2^\bullet/O_2^{\bullet-}$ ($pK_a \approx 4.8$ at 25 °C). Among these radiolysis products, one of the most interesting is molecular hydrogen, largely due to the questions it raises about the mechanism(s) by which it is formed or the nature of its precursor(s). Studies of a variety of scavenger systems at high concentrations using computer simulations in conjunction with available experimental data[10-12] have suggested that the majority of the total H_2 "primary" yield[13] in ^{60}Co γ-radiolysis involves reactions of the short-lived, low-energy ("dry") secondary electrons prior to trapping and hydration,[14] *during the sub-picosecond physicochemical stage*. These reactions include[15,16]

- *The geminate recombination of the "dry" electron with its short-lived $H_2O^{\bullet+}$ parent cation (or "hole")* due to their Coulomb attraction, which tends to draw them back together:

(3) $H_2O^{\bullet+} + e^- \rightarrow H_2O^*$,

followed by the *dissociation of the excited water molecule*[17,18]

(4) $H_2O^* \rightarrow H_2 + O(^1D)$,

where $O(^1D)$ is the oxygen atom in its singlet ^1D (non-radical) first excited state. Note that reaction (3) *must* take place before the $H_2O^{\bullet+}$ cation (whose lifetime has recently been estimated at 46 ± 10 fs)[19] undergoes proton transfer to a neighboring water molecule

(5) $H_2O^{\bullet+} + H_2O \rightarrow H_3O^+ + {}^\bullet OH$

to give the hydronium cation H_3O^+ and the hydroxyl radical $^\bullet OH$. In fact, this recombination affects only the "dry" electrons which are formed *in the vicinity of the parent water cation* and occurs in the first steps of their random walk, *i.e.*, in times as short as a few femtoseconds.[20]

- *The "dissociative electron attachment" (or DEA) involving the resonant capture of a low-energy, "dry" electron by a water molecule*[21-25]

(6) $H_2O + e^- \rightarrow (H_2O^{\bullet-})^* \rightarrow H^- + {}^\bullet OH$

followed by the reaction of the hydride anion with a second water molecule via instant proton transfer

(7) $H^- + H_2O \rightarrow H_2 + OH^-$.

The remainder of the radiolytic formation of H_2 is due to the following three radical-radical combination reactions of the hydrated electron and $H^\bullet$ atom in the tracks as they expand by diffusion during the nonhomogeneous chemical stage on the ps-μs time scale:[15,16,26]

(8) $e^-_{aq} + H^\bullet (+ H_2O) \rightarrow H_2 + OH^-$, $k_8 = 2.5 \times 10^{10}$ M^{-1} s^{-1}

(9) $e^-_{aq} + e^-_{aq} (+ 2H_2O) \rightarrow H_2 + 2OH^-$, $k_9 = 6.2 \times 10^9$ M^{-1} s^{-1}

and, but to a much lesser extent,

(10) $H^\bullet + H^\bullet \rightarrow H_2$, $k_{10} = 4.6 \times 10^9$ M^{-1} s^{-1}

with the corresponding rate constants (*k*) taken from the compilation of Elliot and Bartels.[27]

Since no real-time studies on H_2 formation have been performed, the temporal dependence of the radiolytic H_2 yield is usually investigated by varying the concentration of appropriate scavengers for e^-_{aq} and the $H^\bullet$ atom, which are the two main free radical precursors of H_2 *within the diffusing radiation tracks*. In a previous paper[12] that explored the basic radiation chemical mechanisms underlying the "self-radiolysis" of tritiated water, we used Monte Carlo track chemistry simulations to investigate the scavengeability of the molecular H_2 yield produced in water irradiated by cobalt γ-rays and tritium β-electrons (maximum kinetic energy of 18.6 keV) by azide anions (N_3^-). This particular scavenger was chosen because it has very different reactivities towards e^-_{aq} and $H^\bullet$ atoms, reacting very slowly with the hydrated electron and very quickly with the hydrogen atom. Our work revealed significant chemical changes in the H_2 scavengeability by N_3^- when passing from γ- to tritium β-electron radiolysis, which can be explained by *differences in the electron track structures*, namely:

- In the case of the energetic (~1 MeV) Compton electrons generated by low-LET ^{60}Co γ irradiation, the track structure is initially formed by well-separated clusters of radiolytic species (or "spurs")[28,29] that are approximately spherical in shape.

- The low-energy, higher-LET β-electrons of tritium, on the other hand, deposit their energy mainly as dense, continuous (roughly cylindrical) columns of species (referred to as "short tracks" in the terminology of the Mozumder-Magee model[30] of energy deposition). In contrast to the spur geometry, this short-track geometry favors radical-radical combination reactions involving e^-_{aq} and $H^\bullet$ atoms, which leads to a clear increase in the

H_2 yield for tritium β-electrons compared to ^{60}Co γ-rays. This agrees very well with the experimental data[31-33] over a large range of N_3^- concentrations.[12]

However, at azide concentrations higher than ~0.1–1 M, our calculations[12] of the H_2 yields from ^{60}Co γ-radiolysis failed to reproduce the sharp decrease observed experimentally (*e.g.*, for 5 M N_3^-, the H_2 yield is decreased to about one-third of its original value[31]). For the ^3H β-radiolysis, there was no clear evidence of such a sharp decrease in $G(H_2)$ in solutions with high N_3^- concentrations due to a relatively large dispersion in the experimental data.[32-34] Nevertheless, based on recent work[10,11] on the influence of scavengers of the precursors to e^-_{aq} on the yield of "non-scavengeable" H_2 formation,[35] we decided to include *the ultra-fast capture of these precursors* (thereafter referred to as e^-_{pre}) *by* N_3^- (Fig. 1) in our simulation model for the two types of radiation considered.

2. Simulation model

A) Monte Carlo track-chemistry simulations: The IONLYS-IRT code

The experimentally observed yield value for molecular hydrogen is a composite value to which each of the H_2 production processes contributes. Adding a scavenger that competes with these processes to varying degrees changes the relative amount that each process contributes to the total yield. In this work, we use our Monte Carlo track-chemistry computer code, called IONLYS-IRT,[36] to simulate the radiolysis of water containing various concentrations of N_3^- scavengers. This code is described in detail elsewhere.[12,15,36,37] Only a brief overview of its most essential features is given below.

Our code first models *the early physical and physicochemical stages of the radiation action up to ~1 ps in the track development* in a 3D geometric environment *("IONLYS" program)*. In the case considered here, we have modified this program to take into account the interaction of azide anions in concentrated N_3^- solutions with the initially formed "dry" electrons (*vide infra*). In the absence of dose-rate effects, the chemical effects of irradiation can be represented as the sum of the separate effects of individual (non-overlapping) tracks. Therefore, the history of only a single track needs to be considered. Note that the IONLYS program consists of two modules. One is used to transport the incident charged particle under consideration (called either TRACEPR for an impacting primary electron or TRACPRO/TRACION for an incident energetic proton/ion). The other (called TRACELE) is for transporting all of the "dry" secondary electrons resulting from the ionization of the water molecules until they are hydrated. To mimic the effects of ^{60}Co γ/fast electron-radiolysis, we simulated short segments of ~300 MeV (LET ~ 0.3 keV/μm) irradiating proton tracks, using the TRACPRO module of IONLYS. Tritium-β primary electron ("effective" initial energy of ~7.8 keV; mean LET in water: ~6 keV/μm)[37] track structures were simulated using the TRACEPR module of IONLYS. However, as explained below, we found it advantageous to use the TRACPRO module to mimic tritium β-radiolysis by simulating short track segments of ~7 MeV incident protons that have a similar track structure and LET (~6 keV/μm)[38] to those of the ^{3}H β-electrons (Fig. 2A). In addition, we neglected the "direct" action of ionizing radiation on the solute. This is a good approximation for N_3^- concentrations up to ~1–2 M (in the latter case, approximately 2–4% of the total energy is absorbed directly by the azide anions). In the presence of 3 M N_3^- (the highest N_3^- concentration

considered in this work given the limitations of our computing capacities), the proportion of direct effects is relatively greater (~7%) but can reasonably be ignored.

The complex spatial distribution of the reactants of the considered track system at the end of the physicochemical stage is provided as an output of the IONLYS program. It is then used directly as *the starting point for the subsequent chemical stage, which is covered by the "IRT" component of the code (>1 ps).* This program describes the resulting diffusion and chemical reactions of the various radical and molecular products of radiolysis with each other or in competition with dissolved solutes (N_3^- in the case studied here) present in the solution at the time of irradiation. It uses the "independent reaction times" or IRT method,[39-41] a computationally efficient stochastic simulation technique that can simulate reaction times without having to follow the trajectories of the diffusing species. Its implementation has previously been described elsewhere.[41] The ability of this method to give accurate time-dependent chemical yields over a wide range of irradiation conditions has been well validated by comparison with full random flights Monte Carlo simulations[42,43] that follow the reactant trajectories in detail.

B) The physicochemical stage: Modeling "dry" electron scavenging by Azide ions

As mentioned above, we modified the step-by-step IONLYS program to include the possibility of azide anions scavenging the short-lived precursors (e^-_{pre}) to the hydrated electron, which are involved in the ultrafast formation of H_2. *We used a simulation model consisting of a right circular cylindrical volume of water containing the studied azide concentration* (Fig. 2B). Protons of either 300 MeV (LET ~ 0.3 keV/μm) or 7 MeV (LET ~ 6 keV/μm) (mimicking irradiation by ^{60}Co γ

or ^{3}H β rays, respectively), or by 7.8-keV (LET ~ 6 keV/μm) tritium β-electrons, are generated at the center of the front circle of the cylinder and penetrate perpendicular to this surface. In this cylindrical geometry, the proton tracks, which are essentially rectilinear trajectories, run along the cylinder axis and consist mainly of aligned, well-separated "spurs".[12,37] For the ^{3}H β-electron irradiation, the "short-track" trajectories are not linear, but rather have a more or less tortuous shape due to the successive angular deflections experienced by the primary electrons (Fig. 2). Compared to proton irradiations, this non-linearity of electron trajectories has two main disadvantages: 1) from a computational point of view, it significantly increases computer times, and 2) the simulated electron trajectories have a non-negligible probability of crossing the limits of the model cylinder used, resulting in irregularities in the yield calculations. To avoid this, *we used 7-MeV incident protons here to simulate the tritium β-radiolysis of azide solutions*.

In preliminary simulations we varied the secondary electron energy above which we could neglect the capture of the "dry" electron by N_3^-, and showed that *only the electrons in the region of subexcitation energy* (*i.e.*, those with kinetic energies lower than ~7.3 eV, the first electronic excitation threshold of water)[20,30,44,45] *could most efficiently be captured by N_3^- scavengers*. Taking into account the track structures and the previously calculated low-energy secondary electron penetration ranges in water[46] enabled us to set appropriate values for the parameters of the cylinder. The length of the cylinder (*i.e.*, the track length of the incident protons) was chosen to vary between 100 μm (for 10^{-4}–0.1 M N_3^-), 60 μm (for 1 M N_3^-), and 40 μm (for 2 and 3 M N_3^-). The energy and LET of the protons were well defined over these simulated track segments. With regard to the radius of the circular base of the cylinder, we chose a value of 15 nm in accordance with our electron thermalization distance results reported in ref. 46.[47]

Note that, in the computer simulations reported here, the number of individual proton "histories" (~100) was chosen to ensure only minor statistical fluctuations in the computed average H_2 yields while maintaining acceptable computer time limits.

Since there are no experimental data on the reactivity of N_3^- towards e^-_{pre}, *we considered the (N_3^- + e^-_{pre}) reaction distance (R_{react}) as an adjustable parameter*. Using the ^{60}Co γ-radiolysis case of 1 M N_3^- solutions as a reference, we varied R_{react} using a trial-and-error approach until a good fit was obtained between our calculated $G(H_2)$ value and the corresponding experimental value[31,32] of ~0.3 molecule/100 eV (Fig. 3A). This was achieved for R_{react} ~ 0.5 nm, a value that can simply be viewed as the sum of the reaction radius of the azide anion (~0.26 nm)[48] and the spatial extent of the "dry" electron if we assume it has the same value as that for the hydrated electron (~0.245 nm).[49-52]

An estimate of the scavenging rate constant (k) of e^-_{pre} can be obtained from the Smoluchowski equation:[53,54]

$$(11)\quad k = 4\pi N_A \left\lfloor D\left(N_3^-\right) + D\left(e^-_{pre}\right) \right\rfloor R_{react},$$

where N_A is Avogadro's constant, $D(N_3^-)$ and $D(e^-_{pre})$ are diffusion coefficients, and R_{react} is the reaction distance. Of course, eq. (11) – which is often used to evaluate diffusion-controlled rate constants – can only be given approximately here, since the low-energy "dry" electron scavenging by N_3^- is presumably not controlled by diffusion. An additional factor is the Coulomb repulsion between N_3^- and e^-_{pre},[55] which makes it somewhat more difficult for these two reactive species to approach each other closely. Using R_{react} = 0.5 nm obtained in this work and the (N_3^- + e^-_{pre}) rate constant proposed by Harris and Pimblott[11] (k ~ 10^{12} M^{-1} s^{-1}) in their studies on the effect of azide-ion concentration on the yield of H_2 in ^{3}H β-particle and ^{60}Co γ radiolysis readily yields $D(N_3^-) + D(e^-_{pre}) = 2.64 \times 10^{-7}$ m^2 s^{-1}. Since

$D(N_3^-)$ = 1.84 × 10^{-9} m^2 s^{-1},[12] we then deduce that *$D(e^-_{pre})$ ~ 2.62 × 10^{-7} m^2 s^{-1}, i.e., a value 54 times greater than the diffusion coefficient of the hydrated electron at 25 °C $D(e^-_{aq})$ = 4.9 × 10^{-9} m^2 s^{-1}.*[56]

An estimate of the mobility of e^-_{pre}, $\mu(e^-_{pre})$, can be derived from the Einstein formula, which relates the diffusion coefficient and mobility: $\mu(e^-_{pre})$ = e $D(e^-_{pre})$ / k_B T, where e = 1.6 × 10^{-19} C, k_B is Boltzmann's constant (1.38 × 10^{-23} J/K) and T = 298 K. Using $D(e^-_{pre})$ ~ 2.62 × 10^{-7} m^2 s^{-1}, one finds $\mu(e^-_{pre})$ ~ 0.1 cm^2/V s, a value that is approximately 8 to 10 times higher than the highest mobilities reported for solvated electrons in weakly polar liquids, such as n-propylamine (1.3 × 10^{-2} cm^2/V s), dimethylsulfide (1.36 × 10^{-2} cm^2/V s) or dimethyl ether (10^{-2} cm^2/V s).[57]

C) The chemical stage: The reaction mechanism

The reaction scheme and rate constants for the radiolysis of pure liquid water at 25 °C are the same as used previously (see Table 1 of ref. 37). This series of reactions, initially compiled in refs. 36 and 41, now includes some newly measured or recently re-assessed reaction rates.[27] The complete reaction scheme describing the radiolysis of aerated aqueous solutions containing azide anions has been reported elsewhere.[12] Below we briefly give *the reactions of N_3^- with the radiolytic species formed in the water of the irradiated solutions that we added to the IRT program*. These reactions compete with the reactions of pure water radiolysis.

The azide ion reacts very fast with $H^•$ atoms and very slowly with e^-_{aq}

(12) $N_3^- + H^• \rightarrow HN_3^{•-}$, k_{12} = 3.15 × 10^9 M^{-1} s^{-1}

(13) $N_3^- + e^-_{aq} \rightarrow$ products, $k_{13} \leq 1.5 \times 10^6$ M^{-1} s^{-1}.

In contrast, its protonated form, HN_3,

(14) $N_3^- + H^+ \leftrightarrow HN_3$, $pK_a(HN_3/N_3^-) = 4.7$ in water at 25 °C,

k_{14} (forward) ≈ 10^9–10^{10} M^{-1} s^{-1},

is highly reactive towards e^-_{aq} but it reacts more slowly with $H^\bullet$

(15) $HN_3 + e^-_{aq} \rightarrow HN_3^{\bullet-}$, $k_{15} = 1.2 \times 10^{10}$ M^{-1} s^{-1}

(16) $HN_3 + H^\bullet \rightarrow$ products ($\neq H_2$), $k_{16} = 6.3 \times 10^7$ M^{-1} s^{-1}.

Note, however, that under the neutral pH conditions in this work, HN_3 occurs almost entirely as an anion and should therefore not significantly affect the H_2 yield.

The azide ion can also react with $^\bullet OH$ to produce the azide radical $N_3^\bullet$

(17) $N_3^- + {}^\bullet OH \rightarrow N_3^\bullet + OH^-$, $k_{17} = 1.2 \times 10^{10}$ M^{-1} s^{-1}.

In this case, we need to consider the following reactions:

(18) $N_3^\bullet + e^-_{aq} \rightarrow N_3^-$, $k_{18} = 2.4 \times 10^{10}$ M^{-1} s^{-1}

(19) $N_3^\bullet + H^\bullet \rightarrow HN_3$, $k_{19} \approx 10^{10}$ M^{-1} s^{-1}

(20) $N_3^\bullet + H_2O_2 \rightarrow$ products, $k_{20} < 5 \times 10^6$ M^{-1} s^{-1}

(21) $N_3^\bullet + N_3^\bullet \rightarrow 3N_2$, $k_{21} = 3.9 \times 10^9$ M^{-1} s^{-1}

(22) $N_3^\bullet + N_3^- \rightarrow (N_3)_2^{\bullet-}$, $k_{22} = 2.4 \times 10^5$ M^{-1} s^{-1}.

The rather slow reaction of azide with e^-_{aq} practically excludes any effect of N_3^- on reactions involving e^-_{aq} in the spurs or tracks. In fact, since the H_2 yield is measured in irradiated *aerated* (2.5×10^{-4} M O_2) azide solutions, oxygen will scavenge e^-_{aq}

(23) $O_2 + e^-_{aq} \rightarrow O_2^{\bullet-}$, $k_{23} = 2.3 \times 10^{10}$ M^{-1} s^{-1}

on the ~0.1 μs time scale, *i.e.*, before reaction (13) can occur (even in a 3 M N_3^- solution where the scavenging time[58] of e^-_{aq} by N_3^- is ≥ 0.2 μs). Experimentally, the presence of oxygen prevents, at long times, the reactions of e^-_{aq} with itself

and with water in the bulk of the solutions. Interestingly, $N_3^{\bullet}$ is inert to O_2, but may react with the superoxide anion radical

(24) $N_3^{\bullet} + O_2^{\bullet -} \rightarrow O_2 + N_3^{-}$, $k_{24} = 1.2 \times 10^{10}$ M^{-1} s^{-1}

to reform N_3^{-}.

We also introduced the effect of ionic strength of the solutions on all reactions between ions (with the exception of the peculiar bimolecular self-recombination of e^{-}_{aq} for which there is no evidence of an ionic strength effect[59]) in the IRT program. The correction of the reaction rate constants was carried out as described in refs. 60 and 61. Finally, the values of the diffusion coefficients at room temperature used for the various reactive species involved in our IRT simulations of the radiolysis of water are given in Table 6 of ref. 56. The diffusion coefficient for the azide radical $N_3^{\bullet}$ in water at 25 °C was assumed to be the same as that of N_3^{-} (1.84×10^{-9} m^2 s^{-1}).[12]

3. Results and discussion

The effect of azide-ion concentration on the yield of H_2 for 300- and 7-MeV incident protons (mimicking ^{60}Co γ-rays or fast electrons, and 7.8-keV ^{3}H β-electrons, respectively) in the radiolysis of aerated aqueous N_3^{-} solutions is illustrated in Figs. 3 and 4. The H_2 yields shown in these figures are the limit plateau values of the time profiles of $G(H_2)$[12] corresponding to each considered N_3^{-} concentration between 10^{-4} and 3 M. As can be seen, our simulated $G(H_2)$ values, assuming that N_3^{-} scavenges the low-energy "dry" electrons before they are hydrated (solid lines), agree better with experimental data[31-33] than our previously reported results (dashed lines),[12] which did not consider the scavenging of the short-lived precursor to H_2. This applies in particular to γ-radiolysis at high N_3^{-} concentrations, in which our calculated H_2 yields reproduce

the experimentally observed sharp decrease in $G(H_2)$ well (Fig. 3A). These results confirm previous studies by Harris and Pimblott[11] who obtained similar findings in the case of ^{60}Co γ radiolysis on N_3^- scavenging of the short-lived precursor to e^-_{aq} and H_2 on the subpicosecond time scale. In the case of ^3H β-electron radiolysis (Fig. 3B), at high (>0.1 M) azide concentrations, there is a relatively large dispersion/variability of the experimental data[32,33] which prevents us from observing any clear, continuous lowering of $G(H_2)$ as with γ irradiation. This experimental error is readily explained by the difficulty to perform experiments with ^3H as a source of β-electrons.[11,34]

Figure 4 shows a *direct* comparison of our calculated $G(H_2)$ values as obtained from the radiolysis of aerated azide solutions by 300-MeV (LET ~ 0.3 keV/μm) and 7-MeV (LET ~ 6 keV/μm) irradiating protons as a function of N_3^- concentration. As we can see, our calculations indicate that, over the entire N_3^- concentration range studied, the production of H_2 originating from the higher LET (*i.e.*, ^3H β-electron) radiolysis is always greater than that in the case of 300-MeV protons (*i.e.*, ^{60}Co γ-rays or fast electrons). This result is consistent with the *difference in the structure of radiation tracks*, the "short-track" geometry of ^3H β-electrons (in contrast to spur geometry) favoring radical-radical reactions (8–10) involving hydrated electrons and $H^\bullet$ atoms[12] and, therefore, leading to more molecular products (H_2 in this case) in tritium β-radiolysis than in γ-radiolysis. It is however interesting to note that this influence of the radiation track structure, which is largest in solutions with low N_3^- concentrations (typically, $<10^{-2}$–0.1 M),[62] decreases continuously as the concentration of N_3^- increases up to 3 M. This is illustrated in Fig. 5, where we show the effect of azide concentration on the fate of e^-_{pre} *during the first picosecond* in the radiolysis of aerated solutions of N_3^- by 300- and 7-MeV irradiating protons, as

obtained from our Monte Carlo simulations. As can be seen, at low N_3^- concentrations, the possibility that azide affects $G(H_2)$ *via* the scavenging of "dry" electrons is highly improbable, if not practically zero, for both types of radiation. At concentrations of N_3^- above ~10^{-2}–0.1 M, the effect of azide anions on $G(H_2)$ comes mainly from their increasing ability to scavenge e^-_{pre}, thereby reducing considerably the production of hydrated electrons. This continuous decrease in e^-_{aq} indicates that as the N_3^- concentration increases, the influence of the radiation track structure gradually decreases. This explains why the two $G(H_2)$ vs. N_3^- concentration curves shown in Fig. 4 approach each other more and more at the highest N_3^- concentrations considered.

Finally, for the sake of completeness, we compare in Fig. 6 the extents $\Delta G(H_2)$ of the various components that contribute to the formation of H_2 in azide solutions irradiated by low-LET 300 MeV and high-LET 7 MeV protons, calculated from our Monte Carlo simulations. As can be seen, the contribution of early time (sub-picosecond) processes (including the prompt DEA, geminate recombination of subexcitation electrons with $H_2O^{\bullet+}$, and dissociation of directly excited water molecules) is nearly the same for both radiation types, regardless of the azide concentration. Remarkably, this result agrees well with recent experimental data[16] showing relatively small changes in the sub-picosecond presolvated electron scavenging efficiency *versus* LET. In contrast, at N_3^- concentrations lower than ~0.2–0.1 M, we observe a clear increase in the contribution of track reactions (8)–(10) (in the ps–μs time scale) that produce H_2 in the 7-MeV proton (or 7.8-keV β-electron) radiolysis compared to 300-MeV proton (or ^{60}Co γ-) radiolysis. As discussed above, this result is consistent with the picture of tritium β-radiolysis mainly driven by the chemical action of short tracks of high local LET.[12]

Figure 6 also shows that the production of H_2 from the ($H^\bullet + e^-_{aq}$) reaction (8) decreases rapidly with increasing N_3^- concentration.[12] This is a clear indicator that N_3^- ions readily scavenge $H^\bullet$ atoms in the track development on the ps–μs time scale, thus preventing them from contributing to reaction (8). Since azide anions only react very slowly with e^-_{aq}, the formation of H_2 by the ($e^-_{aq} + e^-_{aq}$) reaction (9) should be rather unaffected by the presence of N_3^-, at least at low enough N_3^- concentrations. However, the hydrated electrons that have not reacted with $H^\bullet$ through reaction (8) become now available to participate in reaction (9). Overall, as Fig. 6 clearly shows, there is some compensation between the two contributions involved in the production of H_2, the contribution from reaction (8) being slightly dominant. It should be remembered that the ($H^\bullet + H^\bullet$) reaction (10) plays a relatively negligible role in the production of H_2.[41]

4. Conclusion

The scavengeability by azide anions of the molecular hydrogen yield, which is generated in the radiolysis of water by cobalt γ-rays and tritium β-electrons, was studied using Monte Carlo track chemistry simulations. Confirming previous work, we demonstrate that low-energy ("dry") secondary electrons (e^-_{pre}) can be scavenged by a high N_3^- concentration (> 1 M) on a timescale of less than one picosecond before hydration. This is a remarkable result, as azide is known to be highly unreactive towards the "hydrated" electron. Our calculations of $G(H_2)$, which include the ultra-fast capture of e^-_{pre} by N_3^- agree very well with experimental data for both γ- and tritium β-radiolysis over the entire range of N_3^- concentrations studied in this work, from 10^{-4} to 3 M.

Interestingly, we do not observe any clear changes in the scavenging of "dry" electrons by N_3^- in passing from γ-radiolysis to tritium β-radiolysis. We concluded, therefore, that the higher H_2 yield observed experimentally for ^3H β-electrons compared to ^{60}Co γ-rays is mainly due to the difference in the radiation track structures during the ps-μs time scale. This is consistent with the short-track geometry of the higher LET tritium β-electrons, which favors radical-radical combination reactions to form more molecular products (H_2 in this case) in tritium radiolysis than in γ radiolysis. However, as the N_3^- concentration increases, the influence of the track structure gradually decreases. This explains why the two curves of $G(H_2)$ *vs.* N_3^- concentration come closer and closer at the highest N_3^- concentrations studied.

Moreover, a value of R_{react} ~ 0.5 nm was derived for the (N_3^- + e^-_{pre}) reaction distance from the H_2 yields observed in ^{60}Co γ radiolysis at high N_3^- concentrations. Using this value of R_{react} and the (N_3^- + e^-_{pre}) reaction rate constant of 10^{12} M^{-1} s^{-1} proposed in the literature, we estimated a mobility of e^-_{pre} of about 0.1 cm^2/V s at 25 °C, a value that is 8 to 10 times higher than the highest mobilities reported for solvated electrons in weakly polar liquids.

Acknowledgements

S.S. was the recipient of a doctoral scholarship from the Natural Sciences and Engineering Research Council of Canada (NSERC). She wishes to thank Professor Yusa Muroya for the wonderful opportunity he gave her to learn more about picosecond electron pulse radiolysis techniques during her internship in Professor Takahiro Kozawa's Laboratory at the Institute of Scientific and Industrial Research (ISIR), Osaka University, Japan (October–December 2015).

The research of J.-P.J-G. is supported by the NSERC Discovery Grant No. RGPIN-2015-06100.

References

(1) Spinks, J. W. T.; Woods, R. J. *An Introduction to Radiation Chemistry*, 3rd ed.; Wiley: New York, NY, 1990.

(2) Ferradini, C.; Jay-Gerin, J.-P. *Can. J. Chem.* **1999**, *77*, 1542.

(3) Garrett, B. C.; Dixon, D. A.; Camaioni, D. M.; Chipman, D. M.; Johnson, M. A.; Jonah, C. D., et al. *Chem. Rev.* **2005**, *105*, 355.

(4) McCracken, D. R.; Tsang, K. T.; Laughton, P. J. *Aspects of the Physics and Chemistry of Water Radiolysis by Fast Neutrons and Fast Electrons in Nuclear Reactors*; Report AECL-11895; Atomic Energy of Canada Limited: Chalk River, ON, 1998.

(5) Guzonas, D.; Novotny, R.; Penttilä, S.; Toivonen, A.; Zheng, W. *Materials and Water Chemistry for Supercritical Water-cooled Reactors*; Woodhead Publishing (Elsevier): Duxford, UK, 2018.

(6) von Sonntag, C. *Free-Radical-Induced DNA Damage and its Repair: A Chemical Perspective*; Springer-Verlag: Berlin, 2006.

(7) O'Neill, P.; Wardman, P. *Int. J. Radiat. Biol.* **2009**, *85*, 9.

(8) Azzam, E. I.; Jay-Gerin, J.-P.; Pain, D. *Cancer Lett.* **2012**, *327*, 48.

(9) Hall, E. J.; Giaccia, A. J. *Radiobiology for the Radiologist*, 8th ed.; Wolters Kluwer: Philadelphia, PA, 2019.

(10) Pastina, B.; LaVerne, J. A.; Pimblott, S. M. *J. Phys. Chem. A* **1999**, 103, 5841.

(11) Harris, R. E.; Pimblott, S. M. *Radiat. Res.* **2002**, *158*, 493.

(12) Sanguanmith, S.; Meesungnoen, J.; Stuart, C. R.; Causey, P.; Jay-Gerin, J.-P. *RSC Adv.* **2018**, *8*, 2449.

(13) Due to the random diffusion from their initial positions, the radiolytic species either react within the tracks as they develop over time or escape into the "bulk" solution. The so-called "primary" radical and molecular yields (or "escape" yields), quoted as *g*(X), are defined as the numbers of species that are formed (or destroyed) per 100 eV of energy absorbed that remain after tracks have dissipated and become available to react with added solutes (if any) at moderate concentrations. For conversion into SI units (mol J^{-1}), 1 molecule per 100 eV ≈ 0.10364 μmol J^{-1}. For low linear energy transfer (LET) ^{60}Co γ-rays, fast electrons or 300-MeV protons, the escape yield value for H_2, *g*(H_2), is ~0.45 molecule per 100 eV at 25 °C.[1,2]

(14) A very recent determination of the formation time of the hydrated electron is 1.3 ± 0.5 ps. See: LaForge, A. C.; Michiels, R.; Bohlen, M.; Callegari, C.; Clark, A.; von Conta, A., et al. *Phys. Rev. Lett.* **2019**, 122, 133001.

(15) Meesungnoen, J.; Sanguanmith, S.; Jay-Gerin, J.-P. *RSC Adv.* **2015**, *5*, 76813.

(16) Sterniczuk, M.; Bartels, D. M. *J. Phys. Chem. A* **2016**, *120*, 200.

(17) Buxton, G. V. In *Charged Particle and Photon Interactions with Matter: Chemical, Physicochemical, and Biological Consequences with Applications*; Mozumder, A., Hatano, Y., Eds.; Marcel Dekker: New York, NY, 2004; pp. 331–363.

(18) Horne, G. P.; Pimblott, S. M.; LaVerne, J. A. *J. Phys. Chem. B* **2017**, *121*, 5385.

(19) Loh, Z.-H.; Doumy, G.; Arnold, C.; Kjellsson, L.; Southworth, S. H.; Al Haddad, A., et al. *Science* **2020**, *367*, 179.

(20) Goulet, T.; Patau, J. P.; Jay-Gerin, J.-P. *J. Phys. Chem.* **1990**, *94*, 7312.

(21) Platzman, R. L. In *Abstracts of Papers*, Second International Congress of Radiation Research (ICRR), Harrogate, England, August 5-11, 1962; p. 128.

(22) Faraggi, M. *Int. J. Radiat. Phys. Chem.* **1973**, *5*, 197.

(23) Goulet, T.; Jay-Gerin, J.-P. *Radiat. Res.* **1989**, *118*, 46.

(24) Rowntree, P.; Parenteau, L.; Sanche, L. *J. Chem. Phys.* **1991**, *94*, 8570.

(25) Cobut, V.; Jay-Gerin, J.-P.; Frongillo, Y.; Patau, J. P. *Radiat. Phys. Chem.* **1996**, *47*, 247.

(26) Draganić, I. G.; Draganić, Z. D. *The Radiation Chemistry of Water*; Academic Press: New York, 1971.

(27) Elliot, A. J.; Bartels, D. M. *The Reaction Set, Rate Constants and g-Values for the Simulation of the Radiolysis of Light Water over the Range 20° to 350 °C Based on Information Available in 2008*; Report AECL No. 153-127160-450-001; Atomic Energy of Canada Ltd.: Chalk River, ON, 2009.

(28) Magee, J. L. *Annu. Rev. Nucl. Sci.* **1953**, *3*, 171.

(29) Freeman, G. R. In *The Study of Fast Processes and Transient Species by Electron Pulse Radiolysis: Proceedings of the NATO Advanced Study Institute held at Capri, Italy, 7-18 September, 1981*; Baxendale, J. H., Busi, F., Eds.; D. Reidel Publishing: Dordrecht, Netherlands, 1982; pp. 19–34.

(30) Mozumder, A. *Fundamentals of Radiation Chemistry*; Academic Press: San Diego, CA, 1999.

(31) Peled, E.; Mirski, U.; Czapski, G. *J. Phys. Chem.* **1971**, *75*, 31.

(32) Christman, E. A. Ph.D. Thesis, Rutgers University, New Brunswick, NJ, 1977.

(33) Gagnon, W. F.; Appleby, A. *Scavenger Studies in Tritiated Water*; Paper of the Journal Series, New Jersey Agricultural Experimental Station, Rutgers University, Department of Environmental Sciences, New Brunswick, NJ, 1971.

(34) In fact, the ^{3}H β-electron irradiation cannot be stopped as in ^{60}Co γ-ray experiments. It follows that the dose given to the sample is difficult to estimate with precision, which can thus lead to significant errors in the measured yields (ref. 11).

(35) Schwarz, H. A. *J. Phys. Chem.* **1955**, *77*, 4960; **1969**, *73*, 1928.

(36) Meesungnoen, J.; Jay-Gerin, J.-P. In *Charged Particle and Photon Interactions with Matter: Recent Advances, Applications, and Interfaces*; Hatano, Y., Katsumura, Y., Mozumder, A., Eds.; Taylor & Francis: Boca Raton, FL, 2011; pp. 355–400.

(37) Mirsaleh Kohan, L.; Sanguanmith, S.; Meesungnoen, J.; Causey, P.; Stuart, C. R.; Jay-Gerin, J.-P. *RSC Adv.* **2013**, *3*, 19282.

(38) Watt, D. E. *Quantities for Dosimetry of Ionizing Radiations in Liquid Water*; Taylor & Francis: London, UK, 1996.

(39) Tachiya, M. *Radiat. Phys. Chem.* **1983**, *21*, 167.

(40) Pimblott, S. M.; Pilling, M. J.; Green, N. J. B. *Radiat. Phys. Chem.* **1991**, *37*, 377.

(41) Frongillo, Y.; Goulet, T.; Fraser, M.-J.; Cobut, V.; Patau, J. P.; Jay-Gerin, J.-P. *Radiat. Phys. Chem.* **1998**, *51*, 245.

(42) Goulet, T.; Fraser, M.-J.; Frongillo, Y.; Jay-Gerin, J.-P. *Radiat. Phys. Chem.* **1998**, *51*, 85.

(43) Plante, I. Ph.D. Thesis, Université de Sherbrooke, Sherbrooke, QC, 2009.

(44) Platzman, R. L. *Radiat. Res.* **1955**, *2*, 1.

(45) Michaud, M.; Cloutier, P.; Sanche, L. *Phys. Rev. A* **1991**, *44*, 5624.

(46) Meesungnoen, J.; Jay-Gerin, J.-P.; Filali-Mouhim, A.; Mankhetkorn, S. *Radiat. Res.* **2002**, *158*, 657.

(47) Even if a large majority of the ejected, low-energy secondary electrons have their complete path inside the scavenging cylinder, some of them, more energetic (the so-called δ-rays), could get out of the volume of the cylinder. We considered those electrons in our simulations by adding scavengers (with the appropriate studied concentration) around them after each free path to check whether they could be scavenged or not. The process was repeated until they were scavenged or else thermalized and hydrated. Of course, these electrons could also undergo, competitively with N_3^- scavenging, a DEA process before their hydration (refs. 21-25).

(48) Dean, J. A. *Handbook of Organic Chemistry*; McGraw-Hill: New York, NY, 1987.

(49) Hart, E. J.; Anbar, M. The Hydrated Electron; Wiley: New York, NY. 1970.

(50) Kee, T. W.; Son, D. H.; Kambhampati, P.; Barbara, P. F. *J. Phys. Chem. A* **2001**, *105*, 8434.

(51) Herbert, J. M.; Coons, M. P. *Annu. Rev. Phys. Chem.* **2017**, *68*, 447.

(52) This assumption is obviously very approximate. In fact, it would be more accurate to consider the "dry" subexcitation energy secondary electron *quantum mechanically*, described either by an electronic wave function whose extent would depend on its energy, or even better as a "*polaron*", *i.e.*, an electron dressed with the induced polarization of the surrounding water molecules. The "hydrated" electron is the limiting case where the electron is completely localized in the potential well of nearby strongly polarized water molecules.

(53) Smoluchowski, M. v. *Z. Phys. Chem.* **1917**, *92U*, 129.

(54) Hervé du Penhoat, M.-A.; Goulet, T.; Frongillo, Y.; Fraser, M.-J.; Bernat, P.; Jay-Gerin, J.-P. *J. Phys. Chem. A* **2000**, *104*, 11757.

(55) Debye, P. *Trans. Electrochem. Soc.* **1942**, *82*, 265.

(56) Tippayamontri, T.; Sunuchakan, S.; Meesungnoen, J.; Sunaryo, G. R.; Jay-Gerin, J.-P. In *Recent Research Developments in Physical Chemistry*; Pandalai, S. G., Ed.; Transworld Research Network: Trivandrum, Kerala, India, 2009; vol. 10, pp. 143–211.

(57) Jay-Gerin, J.-P.; Ferradini, C. In *Excess Electrons in Dielectric Media*; Ferradini, C., Jay-Gerin, J.-P., Eds; CRC Press: Boca Raton, FL, 1991; pp. 259–285.

(58) The product of a scavenger's concentration and its rate constant for the reaction with one of the primary radical species is called its "scavenging power", with units of s^{-1}. *The inverse of the scavenging power gives a measure of the time scale over which the scavenging occurs* (ref. 4).

(59) Schmidt, K. H.; Bartels, D. M. *Chem. Phys.* **1995**, *190*, 145.

(60) Weston, R. E., Jr.; Schwarz, H. A. *Chemical Kinetics*; Prentice-Hall: Englewood Cliffs, NJ, 1972.

(61) Sanguanmith, S.; Muroya, Y.; Tippayamontri, T.; Meesungnoen, J.; Lin, M.; Katsumura, Y.; Jay-Gerin, J.-P. *Phys. Chem. Chem. Phys.* **2011**, *13*, 10690.

(62) At these low N_3^- concentrations, the possibility that azide affects $G(H_2)$ *via* the scavenging of “dry” electrons is highly improbable, if not practically zero, for both types of radiation (see Fig. 5).

Figure captions

Figure 1:

(A) The low-energy ("dry") secondary electron (e^-_{pre}) travels through the N_3^- solution following a tortuous path until it is successively thermalized, trapped, and hydrated (e^-_{aq}).[30,36]

(B) e^-_{pre} is scavenged by the azide anion (scavenger "S" in the figure) prior to hydration.

Figure 2:

(A) Simulated track histories (projected over the *XY* plane of the figure) for the following impacting particles: panel a: 7.8-keV β-electron (mean LET ~ 6 keV/μm), panel b: 7-MeV proton (LET ~ 6 keV/μm), and panel c: 300-MeV proton (LET ~ 0.3 keV/μm). The three particles are generated at the origin and start traveling along the *Y* axis in liquid water at 25 °C. Dots represent the positions of all radiolytic species (e^-_{aq}, $H^\bullet$, H_2, $^\bullet OH$, H_2O_2, *etc.*) present at ~1 ps. Panels a and b show the similarity of the "short track" structure of a 7.8-keV electron and the track structure of a 7-MeV proton (under identical LET conditions). The track segment of a 300-MeV proton in panel c mimics the irradiation with ^{60}Co γ-rays where Compton electrons predominantly form "spurs" (more or less spherical in shape).

(B) Illustration of the simulation model used in this work, which consists of a right circular cylindrical volume of water containing the studied azide concentration. The front surface of the cylinder is irradiated by protons of either 300 or 7 MeV (mimicking irradiation by ^{60}Co γ or ^3H β rays, respectively), or by 7.8-keV tritium β-electrons that penetrate perpendicular to this surface at its center. In this cylindrical geometry, the proton tracks, which are essentially

rectilinear trajectories, run along the cylinder's axis. The path of a 7.8-keV non-linear, and has a more or less tortuous shape due to the successive angular deflections it undergoes. The length of the cylinder (*i.e.*, the track length of the incident particle) was chosen to vary between 100 μm (for 10^{-4}–1 M N_3^-) and 50 μm (for 2 and 3 M N_3^-). The radius of the circular base of the cylinder was set to 15 nm.[47]

Figure 3:

Decrease in the yield of H_2 (in molecule per 100 eV) with the concentration of N_3^- for 300- and 7-MeV incident protons in the radiolysis of air-saturated aqueous azide solutions (neutral pH, 25 °C), calculated from our Monte Carlo simulations over the range of 10^{-4} to 3 M (panels A and B, respectively). Recall that here 300-MeV protons (LET ~ 0.3 keV/μm) mimic ^{60}Co γ-radiolysis while 7-MeV protons (LET ~ 6 keV/μm) mimic ^{3}H β-electron radiolysis (see text). The solid lines show our simulated results under the assumption that N_3^- scavenges the prehydrated ("dry") secondary electrons (e^-_{pre}) with a scavenging reaction distance R_{react} = 0.5 nm. The dashed lines show our results, assuming that N_3^- does not scavenge e^-_{pre}. Experimental data for γ and tritium β-electron irradiations: ○, Peled et al.[31]; □, Christman[32]; ●, Gagnon and Appleby.[33] For comparison, the $G(H_2)$ values calculated by Harris and Pimblott[11] for both types of radiation, with e^-_{pre} scavenging by N_3^- using a (N_3^- + e^-_{pre}) rate constant of 10^{12} M^{-1} s^{-1} (dash-dotted lines) and without "dry" electron scavenging (dotted lines). The concentration of dissolved oxygen used in the simulations was 2.5×10^{-4} M.

Figure 4:

Direct comparison of $G(H_2)$ (in molecule per 100 eV) as a function of the concentration of N_3^- ions for 300- and 7-MeV incident protons (mimicking ^{60}Co γ-

radiolysis and ^{3}H β-electron radiolysis, respectively), calculated from our Monte Carlo simulations of the radiolysis of aerated aqueous azide solutions (neutral pH, 25 °C) over the range of 10^{-4} to 3 M. The solid and dashed lines are for 300- and 7-MeV irradiating protons, respectively (they correspond to the solid lines shown in Fig. 3A and B, respectively).

Figure 5:

Fate (in percentage) of e^{-}_{pre}, the short-lived, low-energy ("dry") precursor to e^{-}_{aq}, during the first picosecond following irradiation as a function of azide concentration from 10^{-4} to 3 M, as obtained from our Monte Carlo simulations of the radiolysis of aerated aqueous N_3^- solutions by 300-MeV (^{60}Co γ radiolysis, LET ~ 0.3 keV/μm) and 7-MeV (7.8-keV ^{3}H β-electron radiolysis, LET ~ 6 keV/μm) irradiating protons, at 25 °C. Recall here that the DEA, or "dissociative electron attachment" process corresponds to the resonant capture of e^{-}_{pre} by a water molecule [reaction (6)]. As can be seen, the recombination of e^{-}_{pre} with its geminate cation $H_2O^{\bullet+}$ [reaction (3)] is more probable than the DEA process, a result in agreement with recent experimental data.[16]

Figure 6:

Variation of the extents $\Delta G(H_2)$ (in molecule per 100 eV) with concentration of N_3^- ions of the different "early-time" and "track" processes that contribute to the yield of H_2, calculated from our Monte Carlo simulations of the radiolysis of air-satured aqueous N_3^- solutions, using 300-MeV (LET ~ 0.3 keV/μm, panel A) and 7-MeV (LET ~ 6 keV/μm, panel B) incident protons over the range of 10^{-4} to 3 M (pH neutral, 25 °C). The solid lines represent the *total* yield of H_2 produced by these two types of processes. H_2 formation from early-time (sub-picosecond) processes include the very fast DEA, geminate recombination of e^{-}_{pre} with $H_2O^{\bullet+}$,

and dissociation of directly excited water molecules. Comparison of panels A and B shows only very small changes in the H_2 yield contribution from these early-time processes (*i.e.*, in the scavenging efficiency of N_3^- on the subpicosecond time scale) as a funtion of LET. As for the production of H_2 from track reactions (in the ps–μs time interval), they include the three radical-radical combination reactions, namely, reaction (8) $e^-_{aq} + H^\bullet$ (dash-dot-dot line), reaction (9) $e^-_{aq} + e^-_{aq}$ (dash-dot line), and reaction (10) $H^\bullet + H^\bullet$ (dotted line). The dashed lines show our simulated results assuming that N_3^- does not scavenge the short-lived e^-_{pre}. The concentration of dissolved oxygen used in the simulations was 2.5×10^{-4} M.

FIGURE 1

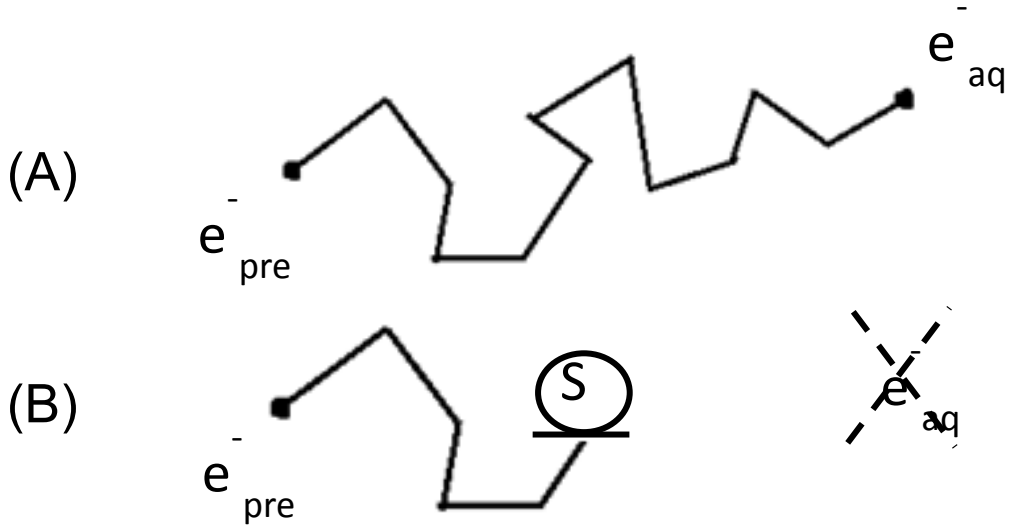

FIGURE 2

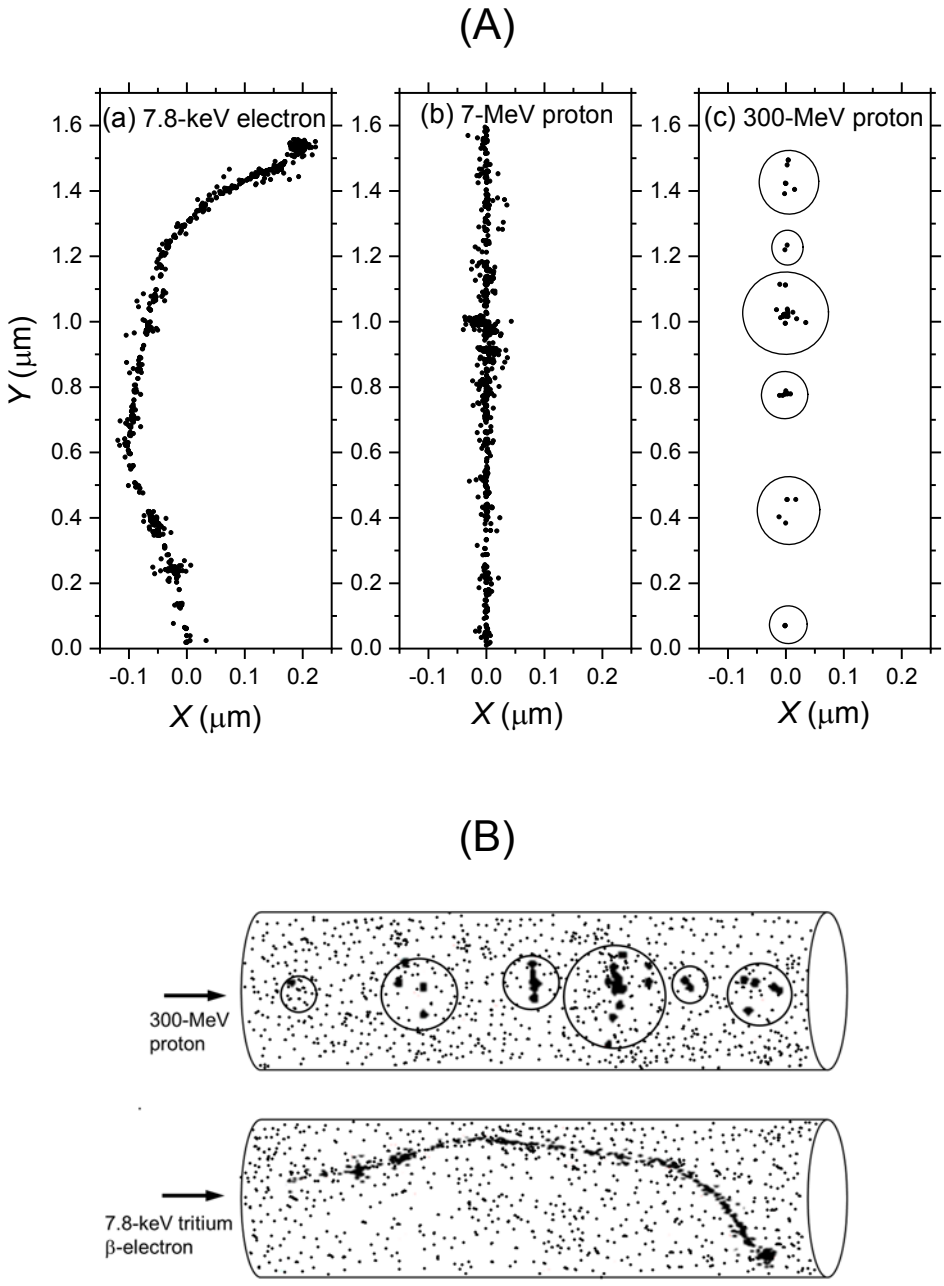
(A)
(a) 7.8-keV electron
(b) 7-MeV proton
(c) 300-MeV proton
Y (μm)
X (μm)
X (μm)
X (μm)
(B)
300-MeV
proton
7.8-keV tritium
β-electron

FIGURE 3

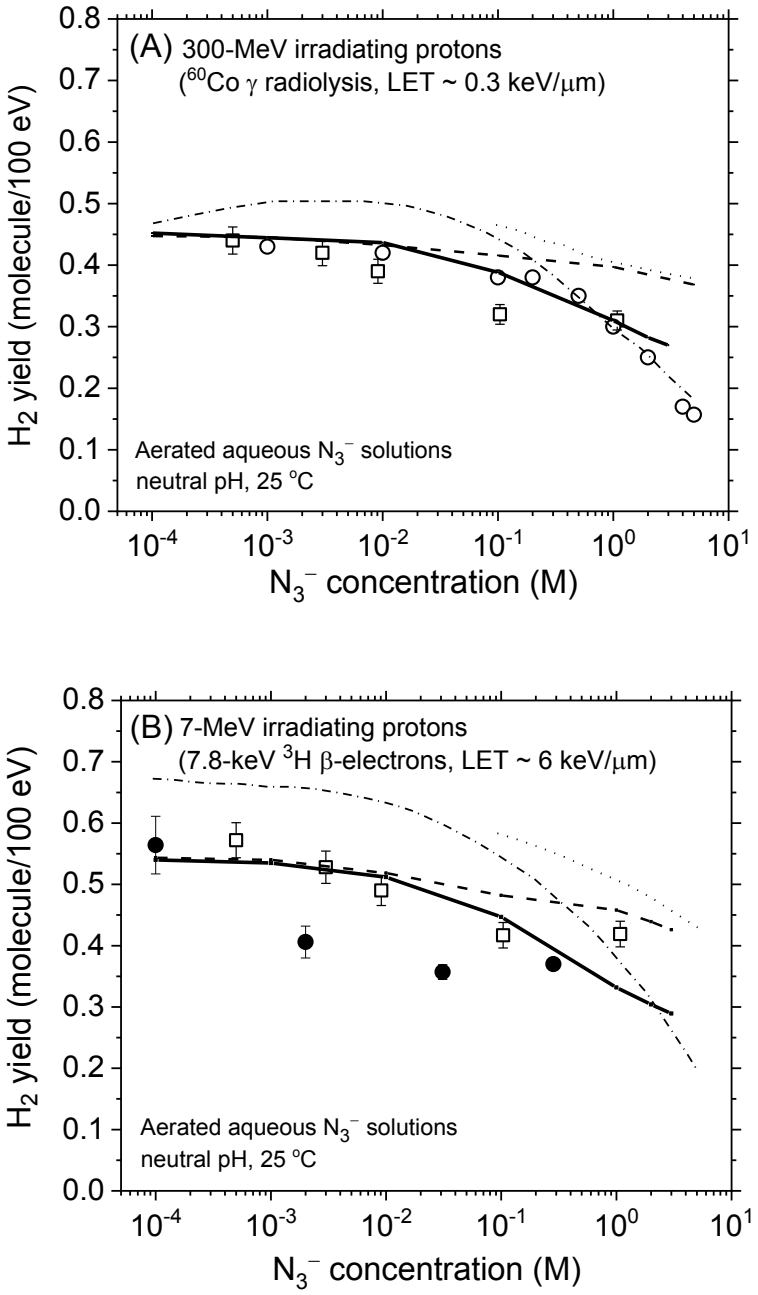
(A) 300-MeV irradiating protons
(60Co γ radiolysis, LET ~ 0.3 keV/μm)
Aerated aqueous N3− solutions
neutral pH, 25 °C
H2 yield (molecule/100 eV)
N3− concentration (M)
(B) 7-MeV irradiating protons
(7.8-keV 3H β-electrons, LET ~ 6 keV/μm)
Aerated aqueous N3− solutions
neutral pH, 25 °C
H2 yield (molecule/100 eV)
N3− concentration (M)

FIGURE 4

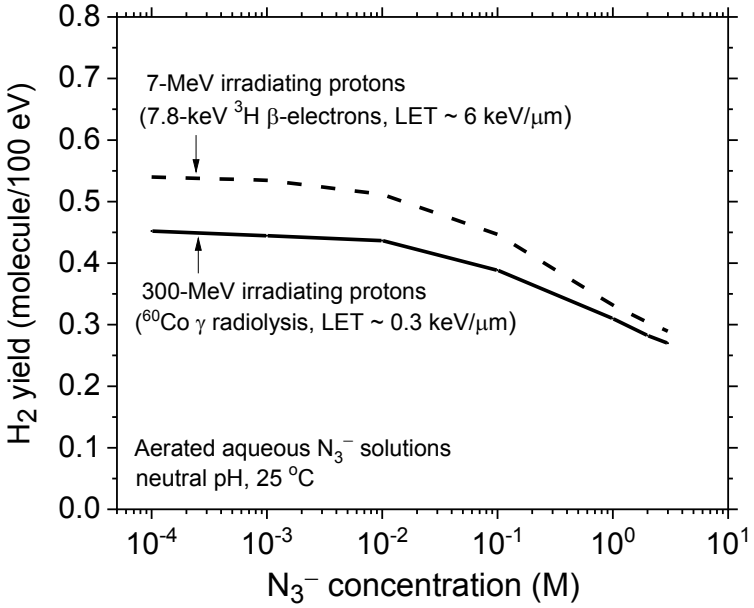
0.8
0.7
0.6
0.5
0.4
0.3
0.2
0.1
0.0
H2 yield (molecule/100 eV)
7-MeV irradiating protons
(7.8-keV 3H β-electrons, LET ~ 6 keV/μm)
300-MeV irradiating protons
(60Co γ radiolysis, LET ~ 0.3 keV/μm)
Aerated aqueous N3− solutions
neutral pH, 25 °C
10-4
10-3
10-2
10-1
100
101
N3− concentration (M)

FIGURE 5

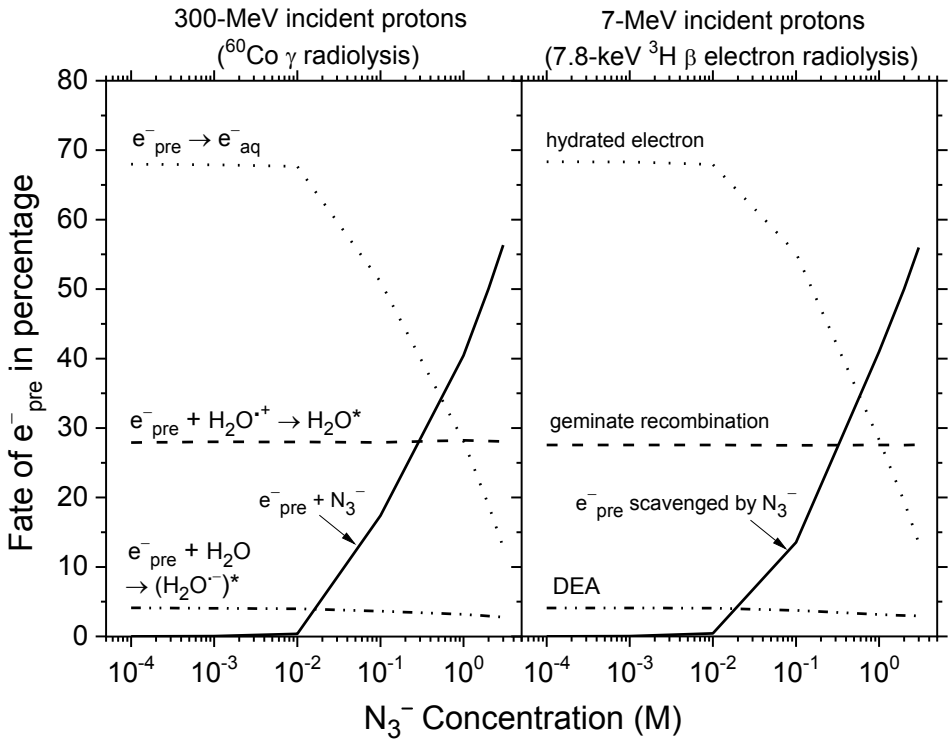
300-MeV incident protons
(^{60}Co γ radiolysis)
7-MeV incident protons
(7.8-keV ^{3}H β electron radiolysis)
Fate of e^-_{pre} in percentage
$e^-_{pre} \rightarrow e^-_{aq}$
hydrated electron
$e^-_{pre} + H_2O^{\bullet+} \rightarrow H_2O^*$
geminate recombination
$e^-_{pre} + N_3^-$
e^-_{pre} scavenged by N_3^-
$e^-_{pre} + H_2O$
$\rightarrow (H_2O^{\bullet-})^*$
DEA
N_3^- Concentration (M)

FIGURE 6

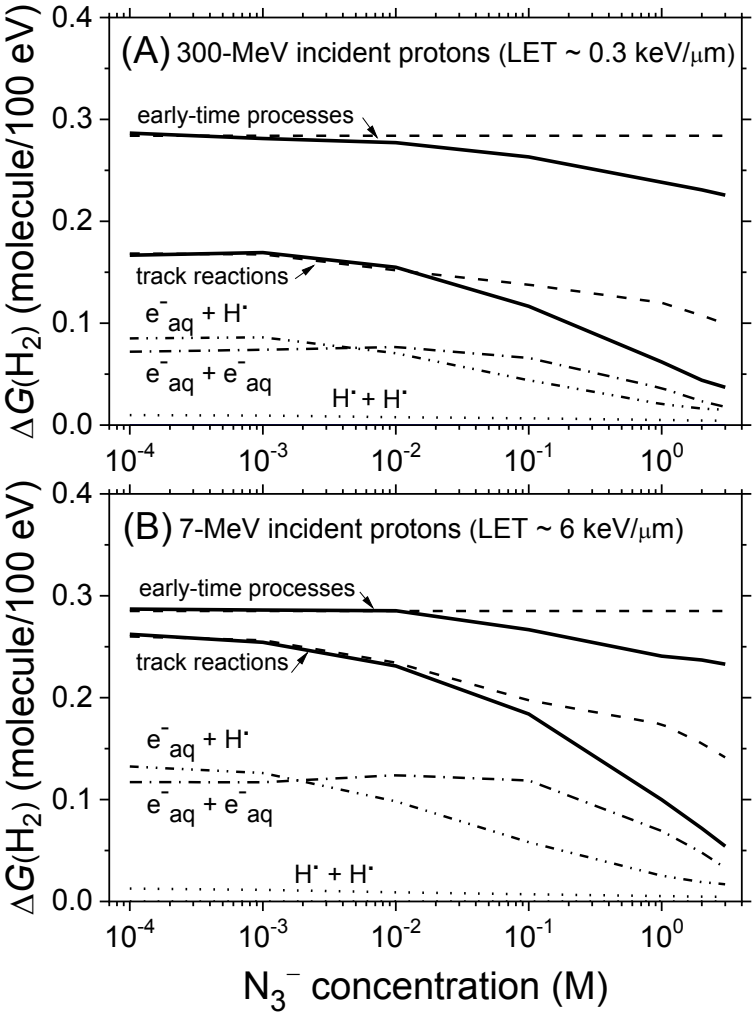
(A) 300-MeV incident protons (LET ~ 0.3 keV/μm)
early-time processes
track reactions
e⁻aq + H•
e⁻aq + e⁻aq
H• + H•
(B) 7-MeV incident protons (LET ~ 6 keV/μm)
early-time processes
track reactions
e⁻aq + H•
e⁻aq + e⁻aq
H• + H•
ΔG(H2) (molecule/100 eV)
0.0
0.1
0.2
0.3
0.4
10⁻⁴
10⁻³
10⁻²
10⁻¹
10⁰
N3⁻ concentration (M)

10. DISCUSSION

10.1 The importance of molecular hydrogen in the radiolysis of water

Molecular hydrogen is one of the most interesting species since it has raised the interesting question concerning the origin of its formation. H_2 yield has been found to be important for reducing the oxidizing species in the primary coolant in the nuclear core. A key challenge in controlling the water chemistry of water-moderated nuclear reactors is the ability to understand and mitigate the effects of water radiolysis (see, for example: LIN, 1996; McCRACKEN et al., 1998; KATSUMURA, 2004; GUZONAS et al., 2009). In fact, under the operating conditions (high temperature and pressure) of existing reactors, the radiolytic formation of oxidizing species, both radical and stable species such as $^{\bullet}OH$, $O_2^{\bullet-}$ (or $HO_2^{\bullet}$ depending on the pH), H_2O_2, and O_2 (the latter two beings of greatest concern), may lead, unless mitigating steps are taken, to corrosion and degradation of components in the reactor circuits, as well as to the release and transport of corrosion products (radioactive and inactive) with the development of deposits on in-core and piping surfaces. In current reactor designs, one commonly used remedial measure is to add excess molecular hydrogen to the coolant in sufficient concentrations to chemically suppress the net radiolytic decomposition of the water. In the presence of a surplus of dissolved H_2 in the system, the corrosive H_2O_2 and O_2 gas production can be efficiently reduced through a short chain reaction, whereby H_2 initially reacts with $^{\bullet}OH$ radicals to produce $H^{\bullet}$ atoms, the latter then reacting with H_2O_2 to reproduce $^{\bullet}OH$ radicals and water. The decrease in H_2O_2 concentration occurs finally because the overall rate of reactions that destroy H_2O_2 is faster than that of reactions that produce H_2O_2 including its radiolytic formation. Note that in the absence of added H_2, H_2O_2 normally reacts with $^{\bullet}OH$ radicals to give $HO_2^{\bullet}$ (or $O_2^{\bullet-}$), a precursor of O_2.

In such a context of industrial applicability, it is of prime importance to clearly identify and quantify all sources of in situ radiolytic H_2 production (or consumption). This information is obviously essential to the development of comprehensive simulation models of the coolant's radiation chemistry capable of predicting as realistically as possible the true value of the so-called "critical hydrogen concentration", defined as the minimum

concentration of added H_2 required in the reactor coolant to suppress the production of oxidants by water radiolysis. In close connection with these remarks, it has been experimentally reported that, although H_2 is a molecular product, the primary molecular hydrogen yield, $g(H_2)$, in deaerated neutral water irradiated by low-LET radiation (X- or γ-rays, fast electrons) increases with increasing temperature, particularly above 200 °C. It is worth noting that, with the exception of $g(H_2)$, all g-values are consistent with the general (and expected) observation that when the temperature is increased, the yields of free radicals $g(e^-_{aq})$, $g(^\bullet OH)$, and $g(H^\bullet)$ continuously increase while the yield of the other molecular recombination product, hydrogen peroxide $g(H_2O_2)$, decreases (ELLIOT and BARTELS, 2009; SANGUANMITH et al., 2011*a*). The exact mechanism responsible for this anomalous increase in $g(H_2)$ is still unknown. However, SWIATLA-WOJCIK and BUXTON (2005, 2010) (henceforth referred to as SWB) suggested that the reaction of hydrogen atoms with water

$$H^\bullet + H_2O \rightarrow H_2 + {}^\bullet OH, \qquad (38)$$

which can normally be neglected at room temperature, could *quantitatively* explain the temperature dependence of H_2 yield at high temperatures. Quite remarkably, several other authors, including ISHIGURE et al. (1987), SHIRAISHI et al. (1995), and especially SUNARYO et al. (1995*a*), had already discussed in the past the possible importance of this reaction in the high temperature γ-radiolysis of water, although no measurement of its rate constant had been reported. Using deterministic diffusion-kinetic modeling calculations, SWB calculated activation energy of ~66.3 kJ/mol over the range 20-300 °C and inferred that a rate constant $k_{55} \approx 3.18 \times 10^4\ M^{-1}\ s^{-1}$ was required to account for the additional yield of H_2 observed at 300 °C. Given its potential applications in a better understanding of the reactions occurring in water-cooled nuclear reactors (SIMS, 2006; SIMS et al., 2010), this reaction has received a great deal of attention recently. In particular, the rate constant proposed by SWB was disputed by BARTELS (2009) on the basis of thermodynamic considerations. The latter pointed out that this reaction could not be as fast as required by SWB and suggested that the best estimate for its rate constant was $2.2 \times 10^3\ M^{-1}\ s^{-1}$ at 300 °C. In reply to these comments, SWIATLA-WOJCIK and BUXTON (2010) re-analyzed Bartels' thermodynamic estimate and showed that an upper limit for k_{38} at 300 °C was

actually 1.79×10^4 M^{-1} s^{-1}, thereby confirming the high value they had previously predicted. In 2014, GHANDI et al. (2014) have investigated the reaction of $H^{\bullet}$ atoms with superheated water (H_2O and D_2O) at temperatures up to 450 °C using muon spin spectroscopy experiments with muonium as an analog of a hydrogen atom. From these experiments, these authors were able to infer a rate constant of ~$9.4x10^3$ M^{-1} s^{-1} at 300 °C (±35%) for reaction (38), a value that actually lies between those suggested by SWB and Bartels. Finally, this reaction rate constant has been studied by the group of Muroya. The reaction rate constant of $k_{(H+H2O)}$ was reported 3.2 (±0.4) $\times$ 10^3 M^{-1} s^{-1} at 300 °C Notwithstanding these recent developments, the values for k_{38} reported thus far, which span a range of more than one order of magnitude (8.14×10^2 to 3.2×10^4 M^{-1} s^{-1} at ~300°C) (BURNS and MARSH, 1981; ISHIGURE et al., 1987, 1995; SWIATLA-WOJCIK and BUXTON, 2005, 2010; BARTELS, 2009; ELLIOT and BARTELS, 2009; ALCORN et al., 2014; MUROYA et al., 2017), remain largely uncertain, thereby making it difficult to obtain a clear conclusion as to the real contribution of reaction (38). For all these reasons, H_2 yield pulls a lot of attention from various experimentalists and modelers to explore in more detail about its formation at different conditions.

10.2 H_2 formation in the radiolysis of water

Molecular hydrogen is one of the most interesting species since it has raised the interesting question concerning the origin of its formation. H_2 yield has been found to be important for reducing the oxidizing species in the primary coolant in the nuclear core. Another reason which brings the H_2 yield to come to our interest is that H_2 yield has an unusual trend with its temperature effect. The competition between recombination and diffusive escape of the primary radical species depends on temperature. With increasing temperature, radicals escape the recombination. Radical yield tends to increase and molecular yield tends to decrease. Unfortunately, the escape H_2 yield increase with temperature.

A variety of precursors and mechanisms, both physicochemical and chemical, have been proposed for the formation of the observed yield of H_2 in the γ-radiolysis of water (see, for example: SWIATLA-WOJCIK and BUXTON, 1995; COBUT et al., 1996; PASTINA et al., 1999*b*; HERVÉ DU PENHOAT et al., 2000). The primary yield of molecular hydrogen is reported to be 0.45 molecule per 100 eV (SPRINKS and WOOD, 1990; FERRADINI and JAY-GERIN, 1999; ELLIOT and BARTELS, 2009). The early time yield of H_2 is reported

to be ~0.34 molecule/100 eV, and only 0.15 molec./100 eV comes from the chemical reaction. It is shown that most of the increase of H_2 yield originates from *prehydrated electrons* (PASTINA AND LAVERNE, 1999; STERNICZUK AND BARTELS, 2016). The source of H_2 can be demonstrated with the following reactions (see Figure 10.1):

***At* early time (physicochemical stage)**,

- Geminate recombination

  $e^-_{sub} + H_2O^{\bullet+} \rightarrow H_2O^*$ (7)

  DEA (dissociative electron attachment) process

  $e^-_{sub} + H_2O \rightarrow H_2O^- \rightarrow H^- + \bullet OH$ (8)

  This anion then undergoes dissociation mainly into H- and •OH according to

  $H_2O^- \rightarrow H^- + \bullet OH$, (9)

  followed by

  $H^- + H_2O \rightarrow H_2 + OH^-$ (10)

- The dissociation of excited water molecules

  H_2O^* → $H^{\bullet} + {}^{\bullet}OH$ (79%) (dissociation deexcitation) (11a)

  → $H_2 + O(^1D)$ (13%) (11b)

  → $2H^{\bullet} + O(^3P)$ (8%) (11c)

  →H_2O + thermal energy (nondissociation deexcitation) (11d)

  → $H_2O^{+\cdot} + e^-$ (auto ionization) (11e)

where $O(^1D)$ is atomic oxygen in its singlet ^1D state] formed directly in an initial act or by geminate recombination of a subexcitation electron with the water cation (MEESUNGNOEN and JAY-GERIN, 2010), and

DEA process clearly appears to be the most important source of H_2 formation. According to our calculations, at 25 °C, the contribution from DEA to the total formation of H_2 at ~10^{-12} s amounts to ~68%, while that of the dissociative electron cation geminate recombination is ~28%. The contribution from directly excited water molecules is less than 4% (see Figure 10.1).

During the time of spur expansion (i.e., in the nonhomogeneous chemical stage) the four following chemical reactions can contribute to the formation of H_2 yield:

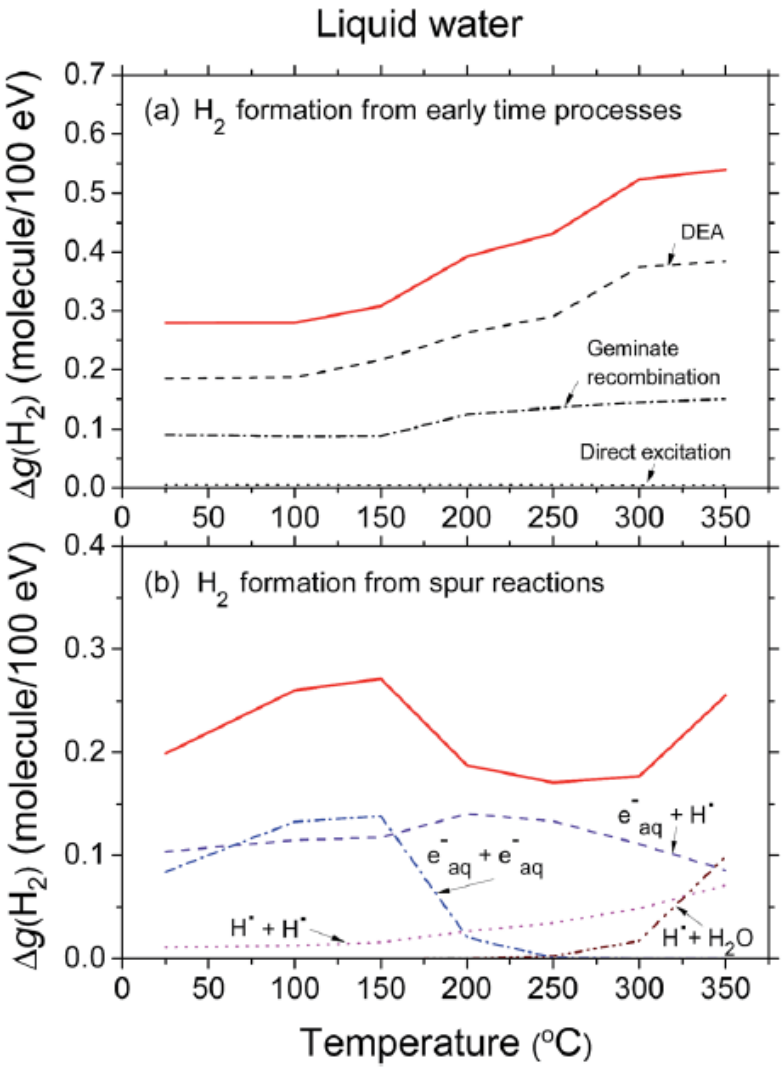

Figure 10.1 Temperature dependence of the extents $\Delta g(H_2)$ (in molecule per 100 eV) of the different processes/reactions that contribute to the primary yield of H_2, calculated from our Monte Carlo simulations of the radiolysis of pure liquid water, using 300 MeV incident protons up to350 °C. Panel (a): H_2 formation from early time processes, including the very fast DEA (dashed line), geminate recombination of e^-_{sub} with $H_2O^{\bullet+}$ (dash-dot line), and dissociation of directly excited water molecules, (dotted line). The red solid line represents the total yield of H_2 produced on a sub-picosecond time scale by these three processes. Panel (b): H_2 formation from spur reactions, including $e^-_{aq} + H^\bullet$, (dashed line) $e^-_{aq} + e^-_{aq}$, (dash-dot line), $H^\bullet + H^\bullet$, (dotted line), and $H^\bullet + H_2O$, (dash-dot-dot line). The red solid line represents the sum of the contributions of all these four reactions to $g(H_2)$ (adapted from MEESUNGNOEN, 2015)

$$e^-_{aq} + H^\bullet \ (+ \ H_2O) \rightarrow H_2 + {}^\bullet OH^- \quad (39)$$

$$e^-_{aq} + e^-_{aq} + (2\ H_2O) \rightarrow H_2 + 2OH^- \quad (40)$$

$$H^\bullet + H^\bullet \rightarrow H_2 \quad (41)$$

$$H^\bullet + H_2O \rightarrow H_2 + {}^\bullet OH \quad (38)$$

The first two reactions (reaction 39 and reaction 40) are the two main reactions to produce the H_2 yields from water radiolysis. The reaction $H^\bullet + H^\bullet$ (reaction 41) shows a very small contribution to the formation of H_2. The reaction of the oxidizing of water with a hydrogen atom (reaction 38) gives no effect to H_2 yield at room temperature. One should note that reaction 38 cannot quantitatively explain, by itself, the increase in $g(H_2)$ with temperature observed experimentally above 200 °C (MEESUNGNOEN et al., 2015). There should be some reaction at early time that is responsible for the increase of H_2 yield at high-temperature radiolysis. Increasing the probability the dissociation of excited water molecules to give H_2 from the recombination process should be considered.

10.3 Excited water molecule (H_2O^*) another short-life transient to the formation of H_2

From our result of the H_2 yields as a function of NaN_3 concentration, it is shown that the H_2 yield is still a bit higher than the experimental data at azide concentration higher than 3 M for both radiation types (gamma rays and tritium beta ray). These results are suggested that there should be more than one short-lived transient that can play a role in the formation of H_2 yield in water radiolysis. This mechanism has been proposed by Horne, G.P. et al. in 2007. Horne, G.P., and co-workers used their Monte-Carlo simulation to demonstrate that the nitrate anion scavenging of the hydrated electron, its precursor, and hydrogen atom cannot account for the observed decrease in the molecular hydrogen yield at high nitrate anion concentrations in the gamma radiolysis of water and aqueous nitrate solution. But there is the necessity to include the quenching of the excited state of water by the nitrate anion to reproduce well the experimental data. The excited water molecule form either by direct excitation or the recombination of water radical cation with the precursor to the hydrated electron. Here all the pathways of H_2 production from water radiolysis. H_2 can be produced from the dissociation of the direct excited water molecule

$$H_2O^* \rightarrow H_2 + O\ (^1D/^3P) \quad (11b)$$

Or from the dissociation of excited water molecule which comes from the recombination of the water radical cation with the prehydrated electron.

$$H_2O^{\bullet+} + e^-_{pre} \rightarrow H_2O^* \text{ (vibrational excited water molecule)} \quad (7)$$

$$H_2O^* \rightarrow H_2 + O\ (^1D/^3P)$$

Or by the auto detachment of an energetic electron (E > 6 eV) from water molecule,

$$H_2O + e^- (\Delta E) \rightarrow H_2O^{*-} \rightarrow H_2O^* + e^- (\Delta E') \quad (8)$$

Follow by $H_2O^{*-} \rightarrow H^- + {}^\bullet OH\ (+H_2O) \rightarrow H_2 + OH^-$ (9, 10)

This process is called DEA (dissociative electron attachment) process.

The decrease of H_2 yield with increasing the concentration of scavenger was originally explained in terms of increased reaction between the scavenger with the precursors to H_2 involving these species (hydrated electron, prehydrated electron, and a hydrogen atom), However, it has been shown long ago that the scavenging of the precursors to H_2 (e^-_{pre}, e^-_{hyd}, $H^\cdot$) could not account for all of the H_2 production in gamma water radiolysis (SCHWARZ, 1969).

It has been demonstrated by LAVERNE and PIMBLOTT (2002) the radiolytic yield of H_2 is strongly dependent on the linear energy transfer (LET) of the radiation, but the time scale of formation was independent of LET. Their results indicate that the dominant mechanism for H_2 formation must involve more than one short-lived transient. It was postulated to be the dissociative electron recombination:

$$H_2O^{\bullet+} + e^-_{pre} \rightarrow H_2O^* \text{ (vibrational excited water molecule)} \quad (7)$$

$$H_2O^* \rightarrow H_2 + O\ (^1D/^3P) \quad (11b)$$

This proposed mechanism is in agreement with our work (see Figure 10.2) and the work of Sterniczuk and Bartels from their studies in high-temperature water radiolysis. They suggested that the radiolytic H_2 production is dominated reactions involving e^-_{pre} and that the dissociative electron attachment reactions have a negligible role (STERNICZUK and BARTELS, 2016). They used the correlation between e^-_{pre} scavenging and the inhibition of H_2 formation in positronium (Ps) lifetime studies. Since the prehydrated electron is the precursor to positronium formation.

$$\beta^+ + e^-_{pre} \rightarrow Ps$$

By scavenging e-pre positronium formation can be completely inhibited (BYAKOV, 1976; BYAKOV et al., 1977; DUPLÂTRE et al., 1984). The inhibition of positronium by the scavenging of the prehydrated electrons conclude that the formation of H_2 occurs primarily from the hydrated electron, but it does not disprove the contribution of the H_2 yield from excited water molecule though the DEA process. The decreasing yield of positronium with increasing concentration of e^-_{pre} scavengers is not directly comparable to the effect on the yield of molecular hydrogen. Positronium is solely formed by the reaction of e^-_{pre} with β^+. Since the scavenging of e^-_{pre} leads to complete inhibition of positronium formation, however for complete inhibition of H_2, all H_2O^* would have to be produced by the reaction of e^-_{pre} with $H_2O^{\bullet+}$.

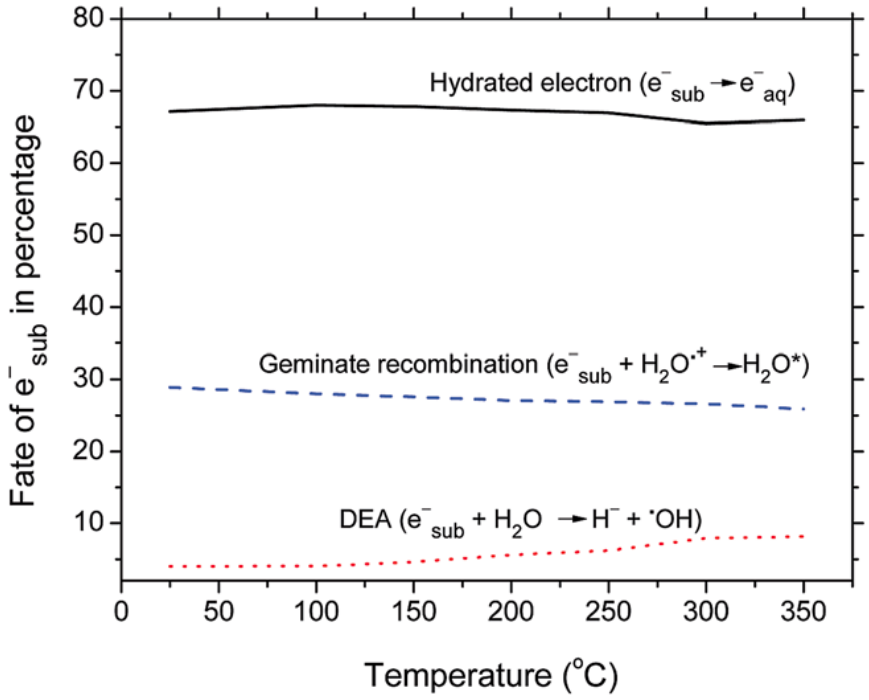

Figure 10.2 The fate of a subexcitation electron (in percentage) during the first picosecond following irradiation as a function of temperature up to 350 °C, as obtained from our Monte Carlo simulations) (adapted from MEESUNGNOEN et al., 2015).

Figure 10.2, it is shown – in percentage – the fate of a subexcitation electron during the first picosecond following irradiation as a function of temperature up to 350 °C, as obtained from our Monte Carlo simulations. Most of the subexcitation electrons pass through the slowing

down process from subexcitation energies (< 7.3 eV), to be thermalization, trapping, and hydration.

$$e^- \rightarrow e^-_{sub} \rightarrow e^-_{th} \rightarrow e^-_{tr} \rightarrow e^-_{aq} \text{ (~240 fs – 1.1 ps)} \quad (6)$$

It is also useful to note here why the recombination of e^-_{sub} with its geminate cation $H_2O^{\bullet+}$, which is more probable than its resonant capture by a water molecule contributes less to the formation of H_2 than the DEA process does. This can be explained as follows: (1) H_2O^* has more or less an equal chance to de-excited nondissociatively or dissociatively, and (2) if the de-excitation of H_2O^* is dissociative, it only has ~15-20% chance of forming H_2 (MEESUNGNOEN et al., 2005a, SANGUANMITH et al., 2011a).

This "nonscavengeable" yield of H_2 estimated to be about ~0.34 (or ~75% of the total molecular hydrogen formed), indicating that the maximum contribution of the chemical reactions (38-41) to H_2 production is only $\Delta g(H_2) \sim 0.11$. A prompt initial H_2 yield of ~0.34 could readily be reproduced in our numerical simulations, by adjusting the value of the DEA cross-section for the capture of precursors to e^-_{aq} by a water molecule ($H_2O + e^- \rightarrow H_2O^- \rightarrow H^- + OH$) to ~$4.0 \times 10^{-18}$ cm^2 (MEESUNGNOEN et al., 2015). DEA cross sections used in our Monte-Carlo simulation were obtained by fitting our simulated yields of H_2 to the experimental $G(H_2)$ data from Janik et al. (JANIK et al., 2007) in phenol/N_2O solutions at each temperature in the range of 25–350 °C. This value compares very well with that determined in amorphous ice (~2.7×10^{-18} cm^2) (MICHAU et al., 2003) and with the corresponding gas-phase value (6.6×10^{-18} cm^2) (MELTON, 1972). Under these conditions, our simulation shows the contribution of the DEA to H_2 formation amounts to $\Delta g(H_2) \sim 0.18$ (see Figure 10.1) and thus appears to be the most important physicochemical process for producing H_2 at early times, in contrary to Pimblott and LaVerne (PIMBLOTT and LAVERNE, 2002; STERNICZUK and BARTELS, 2016) which show that the dominant mechanism for H_2 formation mostly forms by dissociative electron recombination. To increase our H_2 yield from the dissociative electron recombination in our program, we need to revisit the branching ratio of excited water molecules. Our present value of the dissociation electron recombination which gives H_2 may be too small. This could be easily done shortly to help to clarify the formation of H_2 yield at a very early time.

10.4 The formation of molecular hydrogen by scavenging systems (Copper (Cu^{2+}), nitrate (NO_3^-), nitrite (NO_2^-), and acetone (CH_3COCH_3))

In this work, we used our Monte-Carlo simulation to explore the formation of molecular hydrogen by employing many other scavenging systems rather than (azide (N_3^-). Copper (Cu^{2+}), nitrate (NO_3^-), nitrite (NO_2^-), and acetone (CH_3COCH_3) had been used to study the formation of H_2 yield. All scavenging systems were studied to compare the formation of molecular hydrogen for ^{60}Co γ-radiation against tritium β-particle. The important mechanism of each scavenging system, the time-dependent of H_2 yield at various concentrations of each scavenger will be shown below. One should be noted that to study the effect of ^{60}Co γ–radiolysis we used a short (typically, ~ 150 μm) track segment of 300 MeV incident proton tracks, over which the average LET value obtained in the simulations was nearly constant and equal to 0.3 keV/μm. For self-radiolysis of tritiated water (^3HOH), one of the stable hydrogen atoms in the water molecule is replaced by a tritium atom (^3H). This tritium atom emits ionizing radiation in the form of low energy β-electrons with the mean energy of energy deposition by the β-particles ~ 7.8 keV (mean LET in water ~ 5.9 keV/μm). To mimic the radiation chemical action of ^3H β-particles and produce representative G-values, the mean energy of energy deposition by the β-particles ~ 7.8 keV is better suited than the frequency-weighted mean kinetic energy ~5.7 keV.

From this study, we restrict all solute concentrations not exceeding 5 mol/dm^3 to avoid the complications introduced by the direct effect of the radiation on the solute. In addition, we assumed tritiated water concentration to be low enough to avoid the dose rate effects.

10.4.1 Copper sulfate ($CuSO_4$) solutions.

$$CuSO_4 \rightarrow Cu^{2+} + SO_4^- \qquad (42)$$

In this work, we used various concentrations of copper sulfate ($CuSO_4$) to demonstrate the reduction of molecular hydrogen H_2 in ^3H- β-particles and ^{60}CO γ-radiolysis. 10^{-4} M NaBr is used to prevent the reaction between hydroxyl radical and molecular hydrogen. The concentration of NaBr at 10^{-4} M was tested with our Monte-Carlo simulation. The result shows that 10^{-4} M can completely prevent the reaction of hydroxyl radical with molecular hydrogen. Copper sulfate is a good scavenger of the hydrated electron but it is not the ideal

scavenger for probing the ultrafast formation of molecular hydrogen (H_2) because $CuSO_4$ is not completely dissociated to Cu^{2+} in even reasonably concentrated solutions ($K \sim 4.3x10^{-3}$) (OWEN and CURRY, 1938).

Reactions 43 and 44 show that Cu^{2+} can scavenge hydrated electrons much faster than hydrogen atoms (BUXTON et al., 1988; HARRIS and PIMBLOTT, 2002). Reactions 43 and 44 lead to the reduction of molecular hydrogen H_2. Remarkably, both reactions 43 and 44 produce Cu^+. Subsequently, this Cu^+ can have a further mechanism that can reform Cu^{2+} back to the system through the reactions of CuH^+ as shown below. Reaction rate constants of these reaction were taken from *a* (HARRIS and PIMBLOTT, 2002), *b* (BUXTON et al., 1988), *c* (JOHNSON and NAZHAT, 1984), *d* (GOLDSTEIN et al., 1992)

Table 4 Reactions added to the pure water reaction scheme to simulate the radiolysis of $CuSO_4$ aqueous solutions, at 25 ºC.

Reactions	k ($M^{-1}s^{-1}$)	reaction number
$Cu^{2+} + e^-_{aq} \rightarrow Cu^+$	3.9×10^{10}	(43)[a,b]
$Cu^{2+} + {}^\bullet H \rightarrow Cu^+ + H_3O^+$	9.1×10^{7}	(44)[a,b]
$Cu^{+} + {}^\bullet H \rightarrow CuH^+$	5.0×10^{9}	(45)[a]
$Cu^{+} + {}^\bullet OH \rightarrow Cu^{2+} + OH^-$	3.0×10^{9}	(46)[c,d]
$CuH^+ + H_3O^+ \rightarrow Cu^{2+} + H_2$	1.0×10^{6}	(47)[a,c]
$CuH^+ (+H_2O) \rightarrow Cu^{2+} + H_2 + OH^-$	4.0×10^{3} s^{-1}	(48)[a,c]
$CuH^+ + Cu^{2+} \rightarrow 2Cu^+ + H_3O^+$	7.0×10^{6}	(49)[a,c]
$Cu^{2+} + {}^\bullet OH \rightarrow Cu^{3+} + OH^-$	8.0×10^{8}	(50)[c]
$Cu^{3+} + Cu^{+} \rightarrow 2Cu^{2+}$	4.0×10^{9}	(51)[c]

Figure 10.3 presents the time evolution of molecular hydrogen yield obtained from our Monte-Carlo simulation over the Cu(II) concentration range from 10^{-4} M to 5 M in the absence of oxygen for both types of radiations (300 MeV protons irradiation (LET ~ 0.3 keV/µm) and 7.8 keV electrons (LET ~ 5.9 keV/µm)). For both types of radiations, the formation of H_2 decreases as the concentration of Cu(II) increases. In the case of ^{60}Co, the $G(H_2)$ decreasing from 0.5 to 0.33 molecule/100 eV and $G(H_2)$from tritium beta radiolysis

decreases from 0.6 to 0.3 molecule/100 eV over the concentration range 10^{-4} to 5 M. The amount of H_2 yield formed from tritium beta radiolysis is higher than gamma radiolysis can

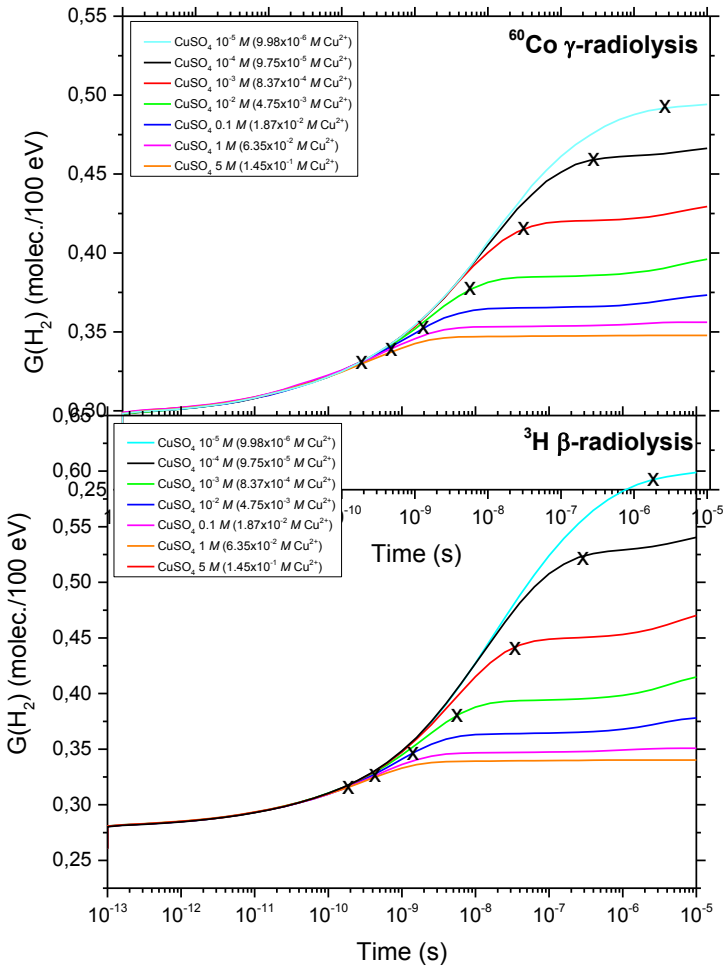

Figure 10.3 Time evolution of molecular hydrogen yield $G(H_2)$ (in molecule/100 eV) for the radiolysis of copper sulfate solution (from 10^{-5} to 5 M) by 300 MeV incident protons (which mimic irradiation with ^{60}Co γ-rays or fast electrons) (LET ~ 0.3 keV/μm) is shown in upper panel and 7.8 keV electrons (mean energy of energy deposition by the β-particle) (LET ~ 5.9 keV/μm) is shown in the lower panel, calculated from our Monte-Carlo simulations over the interval 10^{-12} to 10^{-5} s in the presence of 10^{-4} M NaBr, at 25 °C.

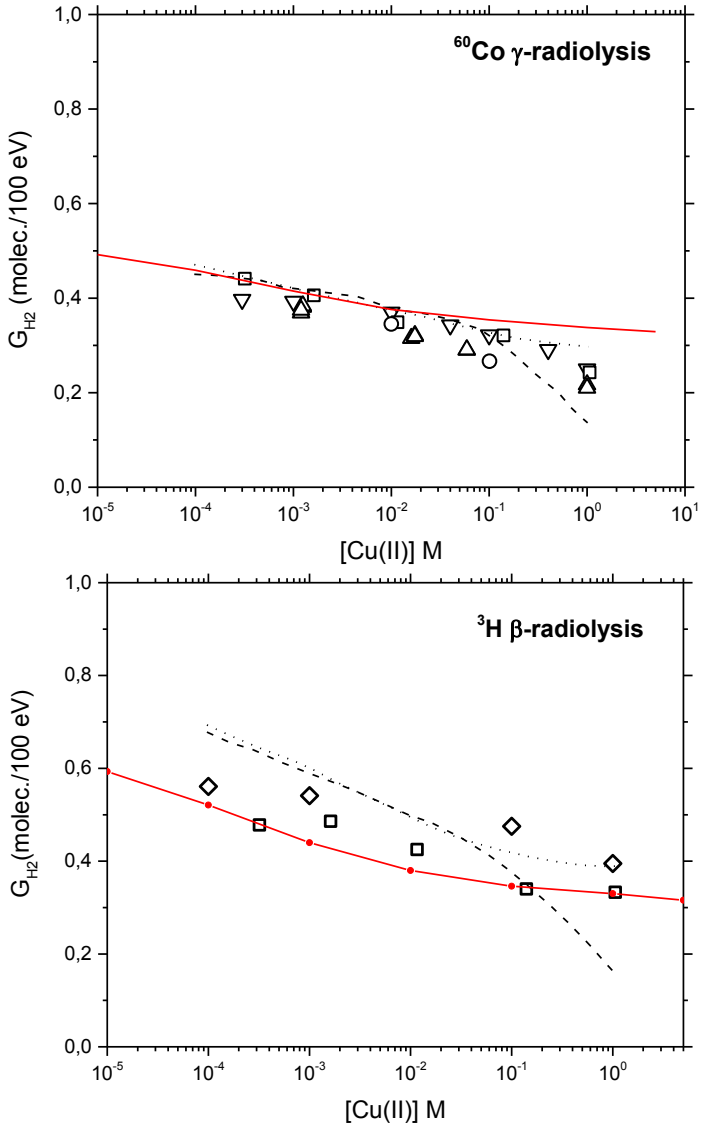

Figure 10.4 The variation of molecular hydrogen yield $G(H_2)$ as a function of Copper concentration (from 10^{-5} to 5 M of Cu^{2+}) in the presence of 10^{-4} M NaBr at 25ºC by 300 MeV incident protons (which mimic irradiation with ^{60}Co ϒ-rays or fast electrons) (LET ~ 0.3 keV/µm) and ^{3}H β-particles with an initial energy of ~ 5.7 keV (average energy of tritium decay) and ~ 7.8 keV (mean energy of energy deposition by the β-particle) (LET ~ 5.9 keV/µm). The solid line shows our calculate $G(H_2)$ as a function of Copper ion. (·····) shows the calculate $G(H_2)$ from Harris and Pimblott[16] where it is assumed that short-lived precursor is scavenged only by hydrated Cu(II) ions; (– – –) represents the calculated H_2 yield where it is assumed that the short-lived precursor is scavenged by all Cu(II) species (HARRIS and PIMBLOTT, 2002). Experimental data are represented in symbols: (□) (CHRISMAN, 1977), (◊)

(APPLEBY and GAGNON, 1971), (o) (PELED et al., 1971), (Δ) (SCHWARZ, 1955), (∇) (FARAGGI and DESALOS, 1969).

be explained by the track structure terminology. The track structure form in the case of ^{60}Co showed as the isolated spurs. The cylinder tracks were observed in the case of tritium. The greater the linear energy transfer of tritium leads to an increased local concentration of reactants. As a consequence, we found more H_2 in tritium radiolysis rather than in gamma radiolysis over the time range 10^{-12} to 10^{-5} s.

Figure 10.4 shows the effect of Copper(II) concentration (10^{-4} M to 5 M) on the production of molecular hydrogen yield. The upper panel represents the result of molecular hydrogen obtained by using ^{60}Co ϒ-radiolysis and the lower panel represents the molecular hydrogen (H_2) yield obtained from ^{3}H β -particle radiolysis. At low concentration of Cu (II), the calculated H_2 reproduce very well the experimental data. At high concentration of Cu (II), our calculated H_2 is a bit higher than experimental data observed. This difference may come from the fact that our simulations have not yet included the possibility that
the scavenger can scavenge the precursor of hydrated electron and the direct effect.

Despite the incomplete dissociation of $CuSO_4$ in aqueous solution, it shows less capacity to scavenge the short live precursors to the hydrated electrons and molecular hydrogen than other scavengers such as NO_3^-.

10.4.2 Nitrate (NO_3^-) solutions.

The nitrate ion NO_3^- is known as a good scavenger of the hydrated electron, forming a relatively stable product NO_3^{2-} as shown in reaction 52. It is used mainly to probe the significance of e^-_{aq} in the formation of H_2 in the radiation track. The nitrate ion can also react with hydrogen atom but with a much lower reaction rate constant as shown in reaction 68. 10^{-4} M NaBr was added into $NaNO_3$ solution in order to scavenge the hydroxyl radical and prevent the reaction between hydroxyl radical with molecular hydrogen. The full reaction mechanism of the radiolysis of $NaNO_3$ aqueous solution is shown below. Reference for these reactions, *a* (YAKABUSKIE et al., 2011), *b* (ROTH and LAVERNE, 2011)

Table 5 Reactions added to the pure water reaction scheme to simulate the radiolysis of NO_2^-/NO_3^- aqueous solutions, at 25 ºC.

Reactions	reaction rate ($M^{-1}s^{-1}$)	Reaction number
$NO_3^- + e^-_{aq} \rightarrow NO_3^{2-}$	9.7×10^9	52[a]
$NO_3^{2-} + H_2O \rightarrow NO_2 + 2OH^-$	5.5×10^4	53[a]
$NO_2^- + e^-_{aq} \rightarrow NO_2^{2-}$	3.5×10^9	54[a]
$NO_2^{2-} + H_2O \rightarrow NO^\bullet + 2OH^-$	4.3×10^4	55[a]
$NO_2^- + {}^\bullet OH \rightarrow NO_2 + OH^-$	5.0×10^9	56[a]
$NO_3^- + O_2^- \rightarrow NO_3^{2-} + O_2$	1.0×10^6	57[a]
$2NO_2 + H_2O \rightarrow NO_3^- + NO_2^- + 2H^+$	6.5×10^7	58[a]
$NO_2 + e^-_{aq} \rightarrow NO_2^-$	1.0×10^{10}	59[a]
$NO_2^- + O_2 \rightarrow NO_2^- + O_2$	2.0×10^8	60[a]
$NO_2^- + O_2^- \rightarrow NO_2^{2-} + O_2$	5.0×10^6	61[a]
$NO + {}^\bullet OH \rightarrow HNO_2$	1.0×10^{10}	62[a]
$NO + O_2^- \rightarrow ONOO^{\bullet-}$	6.7×10^9	63[a]
$NO + e^-_{aq} \rightarrow NO^-$	2.3×10^{10}	64[a]
$NO_3^{2-} + H^+ \rightarrow HNO_3^-$	5.0×10^{10}	65[b]
$HNO_2 + H_2O \rightarrow NO_2^- + H^+$	3.0×10^7	66[b]
$NO_2^- + H^+ \rightarrow HNO_2$	5.0×10^{10}	67[b]
$NO_3^- + {}^\bullet H \rightarrow HNO_3^-$	1.0×10^7	68[b]
$HNO_3^- + H_2O \rightarrow NO_2 + OH^-$	2.0×10^5	69[b]
$NO_2 + {}^\bullet OH \rightarrow ONOOH$	4.5×10^9	70[b]
$NO_2 + {}^\bullet H \rightarrow HNO_2$	1.0×10^{10}	71[b]
$O_2NOO^- + H_2O \rightarrow NO_2^- + O_2$	1	72[b]
$NO_2^- + {}^\bullet OH \rightarrow NO_2 + OH^-$	6.0×10^{10}	73[b]
$NO_2^- + {}^\bullet H \rightarrow HNO_2^-$	7.1×10^8	74[b]
$HNO_2 + H_2O_2 \rightarrow H^+ + NO_3^- + H_2O$	4.6×10^3	75[b]
$NO_2^- + O^- \rightarrow NO_2 + OH^-$	3.1×10^8	76[b]

Figure 10.5 shows the time evolution of molecular hydrogen yield over the interval 10^{-13} to 10^{-4} s as obtained from our Monte-Carlo simulation of the radiolysis of deaerated neutral pH aqueous nitrate solution (from 10^{-5} M to 5 M) by ^{60}Co-fast electron irradiation (LET ~ 0.3 keV/μm) and tritium beta-particle (using 7.8 keV for the initial energy of beta-electron, LET ~ 5.9 keV/μm), at 25°C. The simulation shows a clear increase in the absolute value of $G(H_2)$ for ^{3}H β-electrons compared to ^{60}Co γ-rays. (e.g. molecular hydrogen yield from ^{3}H bata particle shown the decrease of 0.34 from 0.62 to 0.28 molec./100 eV. But in the case of gamma radiolysis, the amount of H_2 yield reduces from 0.52 to 0.32 molec./100 eV., decrease about 0.2 molec./100 eV). This increase of $G(H_2)$ when comparing the effects of tritium beta-radiolysis with gamma radiolysis, is consistent with differences in the initial spatial distribution of primary transient species. As mention earlier, in the short track geometry of the high LET ^{3}H beta electrons, radicals are formed locally in a much higher initial concentration than in the spur (spherical) geometry of the energetic Compton electrons of the ^{60}Co gamma rays. As a result, the short track geometry favors radical-radical reactions in the diffusing tracks, which increases the proportion of molecular products at the expense of the radical products.

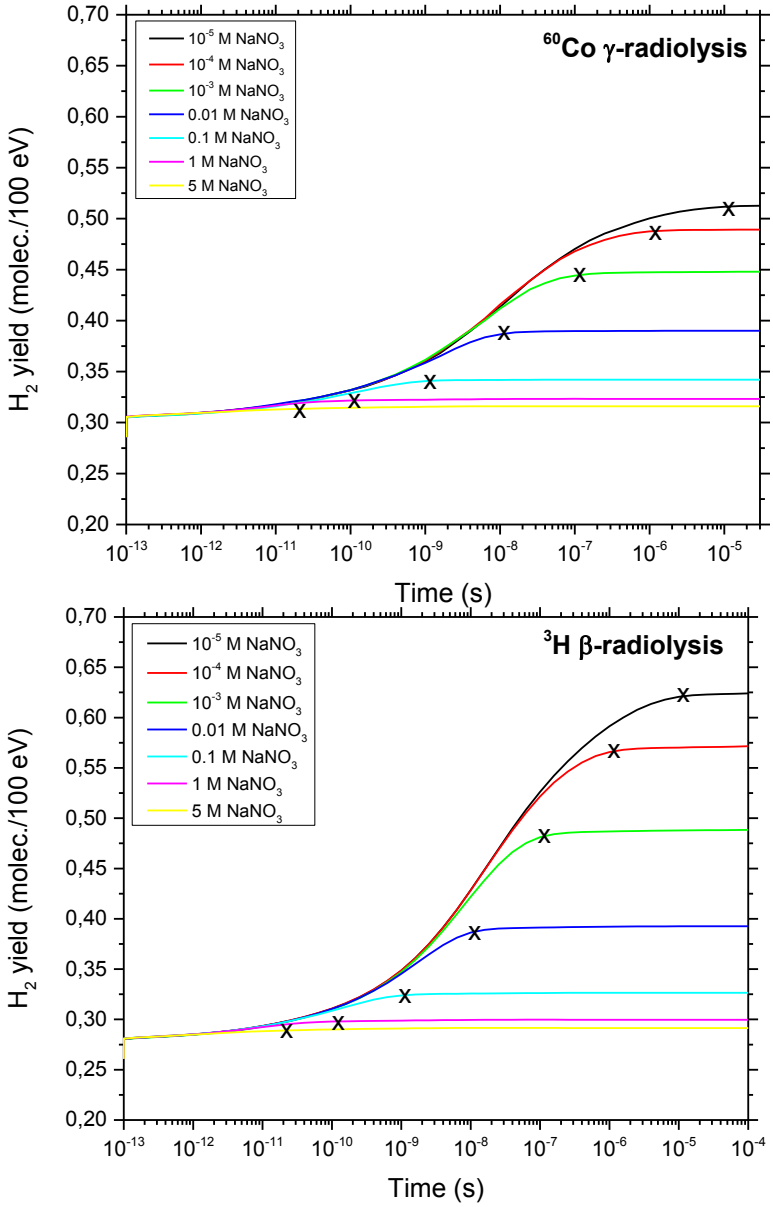

Figure 10.5 Time evolution of $G(H_2)$ (in molecule/100 eV) after 300 MeV protons irradiation (LET ~ 0.3 keV/µm) and 7.8 keV electrons (LET ~ 5.9 keV/µm) of sodium nitrate aqueous solution at 25°C, calculated from our Monte-Carlo simulations over the interval 10^{-13} to 10^{-4} s at various concentration of sodium azide (10^{-4} M to 5 M), 10^{-4}M NaBr were added into sodium nitrate solution in order to scavenge hydroxyl radical.

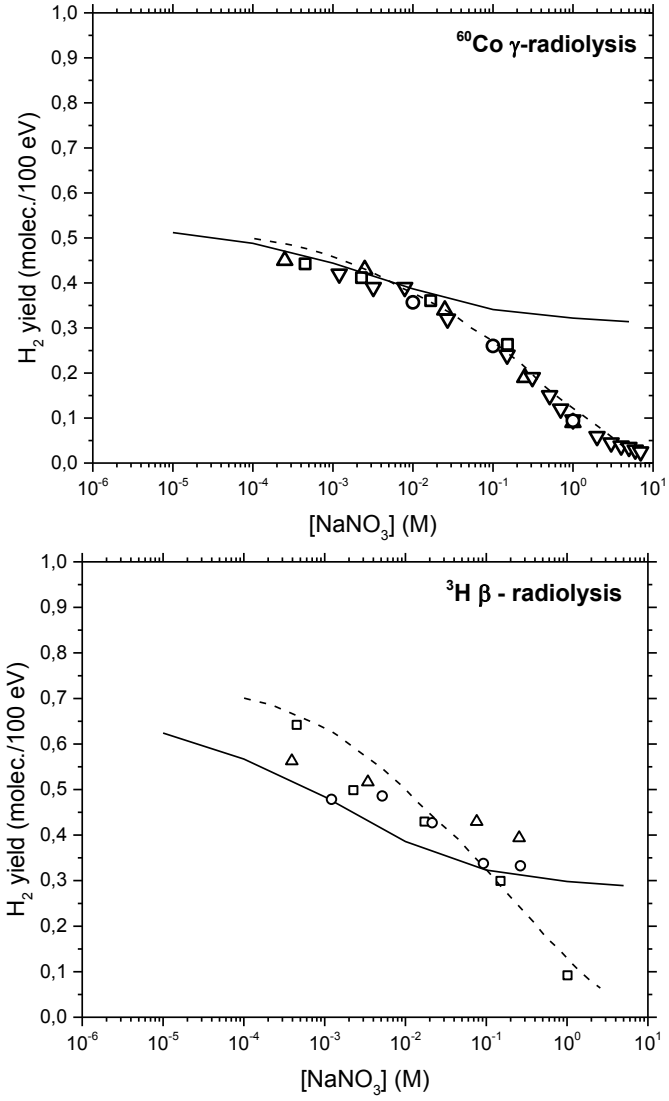

Figure 10.6 Decrease in $G(H_2)$ (in molec./100 eV) with the concentration of NO_3^- ion for 300-MeV protons (LET 0.3 keV/μm as shown in the upper panel and 7.8 keV-incident electrons (LET 6 keV/ μm) show in the lower panel for the radiolysis of neutral pH aqueous nitrate solutions at 25ºC, calculate from our Monte-Carlo simulations over the range of 10^{-5} to 5 M. 10^{-4} M of NaBr was added to scavenge hydroxyl radical. The solid lines represent our calculated $G(H_2)$ in the presence of $NaNO_3$ from 10^{-5} M to 5 M and 10^{-4} M NaBr. The dotted line is the calculated result which obtained from (HARRIS and PIMBLOTT 2002). Experimental data for ^{60}Co γ-radiolysis are denoted by: (Δ) (DRAGANIC and DRAGANIC, 1971), (∇) (MAHLMAN, 1961), (□) (FANNING, 1975), (o)(PELED and CZAPSKI, 1970). Experimental data for deaerated neutral solutions irradiated with tritium β-particle shown as: (□) (FANNING, 1975), (o)(CHRISTMAN, 1977), (Δ) (APPLEBY and GAGNON,1971).

The nitrate ion can scavenge hydrated electrons very well with the fast reaction rate constant (9.7×10^9 $M^{-1}s^{-1}$). Mahman (MAHLMAN, 1961) has used NO_3^- as a scavenger in neutral and acidic conditions to study the role of e^-_{aq} as a precursor to molecular hydrogen. His results show no pH effect on the decrease of $G(H_2)$ as a function of NO_3^- concentration. The reaction

$$e^-_{aq} + H^+_{aq} \rightarrow H, \qquad (77)$$

Occurring in acidic condition has a rate constant (2.3×10^{10} $M^{-1}s^{-1}$) and the H atom is much less reactive than e^-_{aq} toward NO_3^- ($k_{R68} = 1.0 \times 10^7$ $M^{-1}s^{-1}$) (ROTH and LAVERNE, 2011). According to this information, the decrease of H_2 as a function of NO_3^- concentration is expected to be smaller in acidic than in neutral solutions if e^-_{aq} is the main precursor of H_2.

From Figure 10.6, our simulated $G(H_2)$ can reproduce very well the experimental data at $NaNO_3$ concentration lower than 0.1 M. The calculated H_2 yield slightly decreases at concentration of NO_3^- higher than 0.1 M. In contrast with the experimental data, the H_2 yields continue to decrease significantly at high concentration of NO_3^-. With this result and the experimental result of Mahman which showing that there is no pH effect on the decrease of $G(H_2)$ as a function of NO_3^- concentration, it suggests that there is one phenomenon occur at high concentration of NO_3^-. We immediately come to the idea that high concentration of NO_3^-, NO_3^- scavenge almost all the dry electron (electron prior to its hydration). As a consequence, there is no hydrated electron to react with H^+_{aq}. This is the reason why pH plays no effect on the decrease of H_2 yield as observed by Mahman (MAHLMAN, 1961).

To improve the description of the effect of nitrate ion, it is necessary to consider the possibility that the nitrate ion scavenges the electron even prior to its hydration. Such a phenomenon has been observed with many good e^-_{aq} scavengers (ALDRICH et al., 1971; LAM and HUNT, 1975; DUPLATTRE and JONAH, 1985) and has been included in recent simulations base on the diffusion models (DOMAE et al., 1996). It is characterized experimentally by the concentration C_{37} of scavenger needed to reduce the initial e^-_{aq} yield to 37% (that is 1/e) of its value in pure water. The C_{37} value for NO_3^- ion is about 0.45 ± 0.05

mol/dm^3 (LAM and HUNT, 1975). On the contrary, the H_{aq}^+ ion, which is also a good e^-_{aq} scavenger, is known to be a poor scavenger of dry electrons (electron prior to its hydration) as evidenced by Aldrich et al. (ALDRICH et al., 1971) in their pulse radiolysis measurements on perchloric acid solutions.

10.4.3 Nitrite (NO_2^-) solutions.

The nitrite ion NO_2^- is the main intermediate product of nitrate reduction and appears in the system immediately after the beginning of irradiation. NO_3^- can initially react with reducing species (e^-_{aq}, H, O_2^-) to form NO_2^- and then the NO_2^- can react with oxidizing species (OH and H_2O_2) to re-form NO_3^-. In our Monte-Carlo simulations, we have incorporated the same reaction mechanism as used for the radiolysis of nitrate solution. The molecular hydrogen yields were calculated in the radiolysis of deaerated nitrite solution over the concentration range 10^{-5} to 5 M. 10^{-4} M of sodium bromide was used as the scavenger for hydroxyl radical for 300-MeV proton mimic irradiation with ^{60}Co ϒ-rays or fast electrons) (LET ~ 0.3 keV/µm). The same solution was used to perform the calculation for 7.8 keV electrons (mean energy of energy deposition by the β-particle) (LET ~ 5.9 keV/µm) to compare the effect of both types of radiations.

From Figure 10.7, the upper panel shows the result of molecular hydrogen yield as a function of $NaNO_2$ concentration over the concentration range 10-5 M to 5 M. for 300-MeV protons (^{60}Co ϒ-rays, LET 0.3 keV/µm). The lower panel shows the H_2 yield as a function of $NaNO_2$ concentration for ^{3}H β-particles (7.8 keV-incident electrons, LET 6 keV/ µm). There is a good agreement between our calculated G(H_2) with the experimental data for both types of radiation. The H_2 yield decreases when the concentration of $NaNO_2$ increases because the higher concentration of scavenger (NO_2^-) means the capacity to compete to take the hydrated electron, hydrogen atom, and hydroxyl radical increases, then there is less concentration of hydrated electron and H atom which is a part of the source of H_2 yields. The H_2 yield from ^{3}H β-particle is a bit higher than the H_2 yield from ^{60}Co radiolysis as we also observed from other scavengers. This is due to the difference in track structure as mentions previously.

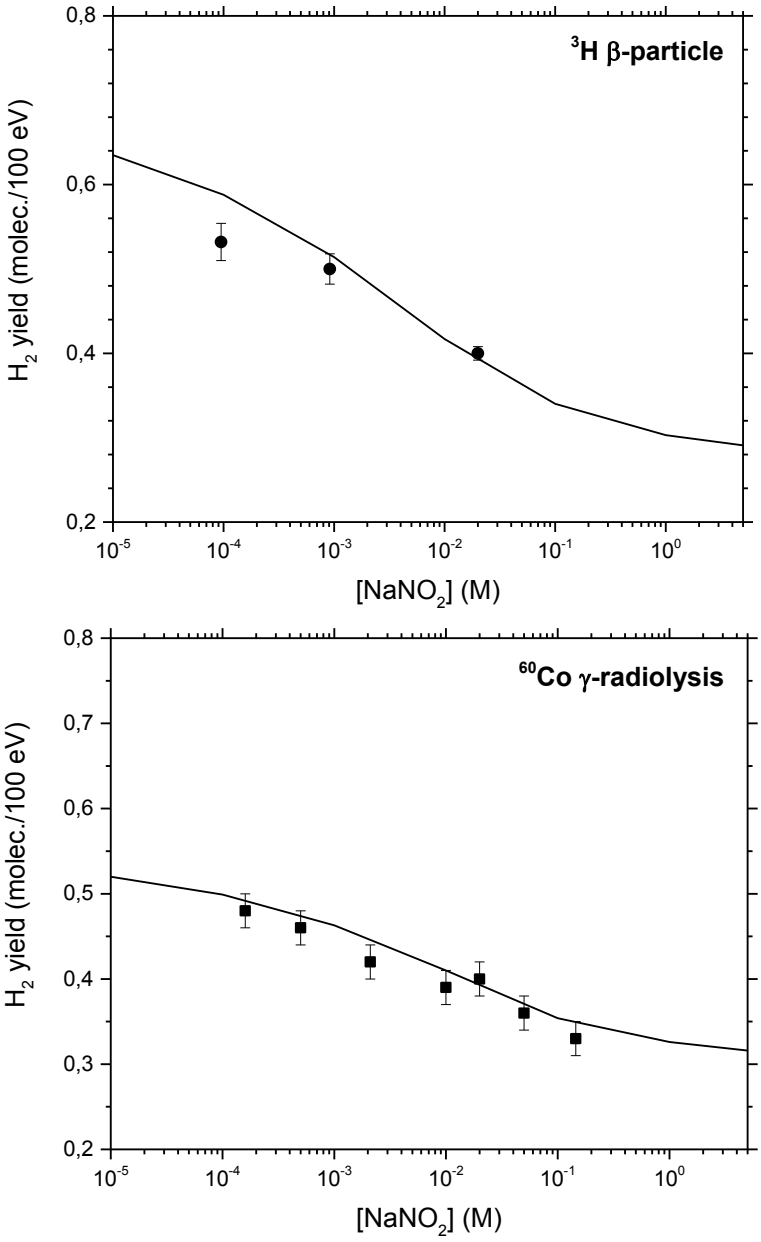

Figure 10.7 Decrease in $G(H_2)$ (in molec./100 eV) with the concentration of NO_2^- ion for 300-MeV protons (LET 0.3 keV/μm) as shown in the upper panel and 7.8 keV-incident electrons (LET 6 keV/ μm) show in the lower panel for the radiolysis of neutral pH aqueous nitrite solutions at 25ºC, calculate from our Monte-Carlo simulations over the range of 10^{-5} to 5 M, in the presence of 10^{-4} M of NaBr which used to scavenge hydroxyl radical. The solid lines represent our calculated $G(H_2)$ in the presence of $NaNO_2$ from 10^{-5} M to 5 M. Experimental data for ^{60}Co ϒ-radiolysis are denoted by: (■) (DAINTON and LOGAN, 1965), (●)(GAGNON and APPLEBY, 1971).

10.4.4 Acetone (CH_3COCH_3) solutions.

Acetone (CH_3COCH_3) is known as a good scavenger of the hydrated electron. We used it to analyze the variation of molecular hydrogen yield. Its reaction with the hydrated electron is characterized by a rate constant equal to 6.5 x 10^9 $M^{-1}s^{-1}$ and its C_{37} concentration is 1.44 mol/dm^3(DUPLATTRE and JONAH, 1985). As acetone also reacts with a hydrogen atom to give molecular hydrogen, it would be necessary to suppress the formation of hydrogen from the independent hydrogen atom yield. This would require some H atom scavenger, which does not react to give some additional H_2 to be present in sufficiently high concentration. In our calculation, we used potassium nitrite (KNO_2) to scavenge the hydrogen atoms. The concentration of KNO_2 used is about 5 times lower than the concentration of acetone. The important reactions mechanisms used in our calculations is given below.

$$CH_3COCH_3 + e^-_{aq} \rightarrow CH_3COCH_3^- \qquad (k = 6.5 \times 10^9\ M^{-1}s^{-1}) \qquad (78)$$

$$CH_3COCH_3 + H \rightarrow CH_3COCH_2 + H_2 \qquad (k = 2.6 \times 10^6\ M^{-1}s^{-1}) \qquad (79)$$

$$CH_3COCH_3 + OH \rightarrow \text{Product} \qquad (k = 1.1 \times 10^8\ M^{-1}s^{-1}) \qquad (80)$$

The simulation results are presented in Figure 10.8 and compared to the experimental data of Appleby (APPLEBY, 1967). The upper panel refer to the molecular hydrogen yield obtained from the radiolysis of ^{60}Co ϒ -rays in deaerated of 10^{-4} M to 1 M of acetone. There is a good agreement between our calculated $G(H_2)$ with the experimental data. The lower panel refers to the calculated $G(H_2)$ from the radiolysis of ^{3}H β-particle in the aqueous solution of acetone from 10^{-4} M to 1 M. Unfortunately, there is no experimental data available in the case of ^{3}H β-radiolysis in the aqueous acetone solution.

In comparison between the $G(H_2)$ from ^{60}Co ϒ-radiolysis and ^{3}H β-radiolysis in aqueous acetone solution, the $G(H_2)$ from ^{3}H β-radiolysis is still higher than the $G(H_2)$ from ^{60}Co ϒ-radiolysis. This phenomenon was observed previously with other scavenger systems. It can easily explain by the difference in radiation track structure as mention earlier. From the

studies of W.F. Gagnon and A. Appleby, they measured (G_{H2} + G_H), and found a higher amount of G_H for tritium rather than gamma rays. Since there is no reason why H-atoms should diffuse more rapidly and hence escape recombination more readily in short tracks rather than in spurs. The additional hydrogen atom yield in the bulk of the solution must be a consequence of increased hydrogen atom production by track reactions as shown below:

$$H_2O^+ + e^- \rightarrow H + OH$$

$$H_3O^+ + e^-_{aq} \rightarrow H + H_2O$$

The authors also mentioned that the reaction between H_2O^+ with e^- would probably not occur with hydrated electrons (e^-_{aq}) since the lifetime of the H_2O^+ is much shorter than the formation time of the hydrated electron (BAXENDALE and BEVAN, 1967). The reaction H_3O^+ with e^-_{aq} is an important source of the hydrogen atom in gamma radiolysis. In the presence of hydrated electrons and hydrogen ion scavengers, the hydrogen yield is observed to be lower than the value which observed in pure liquid water radiolysis.

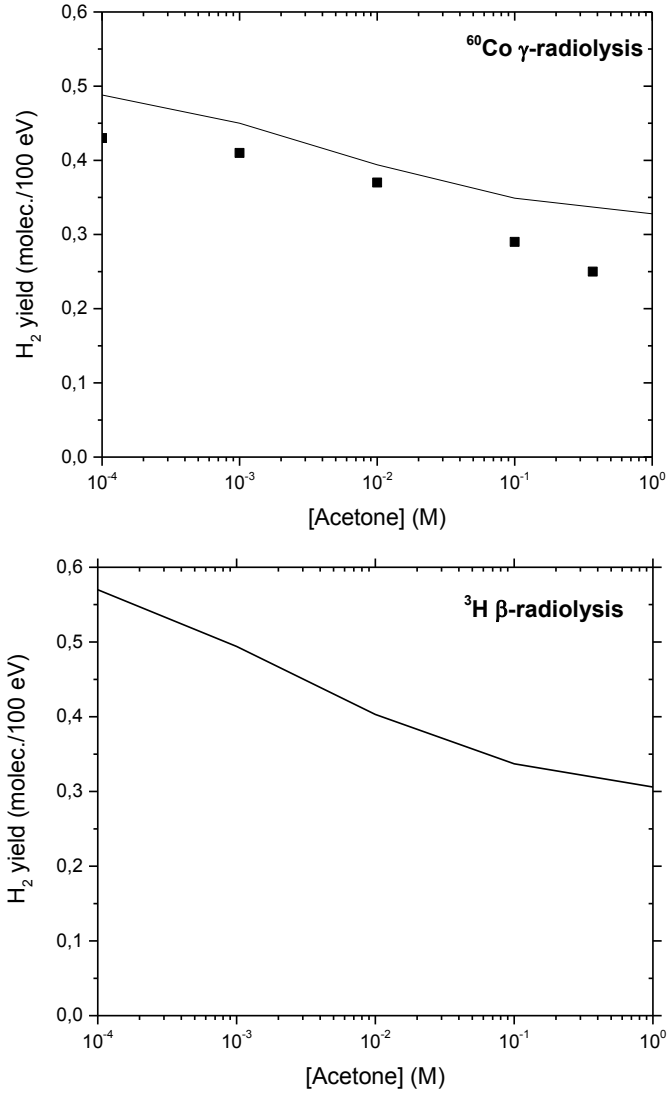

Figure 10.8 Decrease in $G(H_2)$ (in molec./100 eV) with the concentration of acetone for 300-MeV protons (LET 0.3 keV/µm as shown in the upper panel and 7.8 keV-incident electrons (LET 6 keV/ µm) show in the lower panel for the radiolysis of neutral pH aqueous acetone solutions at 25°C, calculate from our Monte-Carlo simulations over the range of 10^{-4} to 1 M. 10^{-4} M of KNO_2 was added to scavenge hydrogen atom. The solid lines represent our calculated $G(H_2)$ in the presence of $NaNO_3$ from 10^{-5} M to 5 M. Experimental data for ^{60}Co ϒ-radiolysis are shown in symbol (■) (DAINTON and LOGAN, 1965).

Monte-Carlo simulations have been employed to investigate the formation of molecular hydrogen yield in 4 scavenging systems more ($CuSO_4$, $NaNO_3$, $NaNO_2$, and CH_3COCH_3) by comparing the radiation chemistry of tritium β-rays and 300-MeV protons (which mimic irradiation with ^{60}Co γ-rays or fast electrons) at 25°C. The four scavengers which we are considered here, obviously show that the formation of H_2 from ^3H β-particle is higher than in the case of ^{60}Co γ-rays. For the same reason with the N_3^- scavenger, we can easily explain the results by the difference in the structure of the radiation track. The track structure form in the case of ^{60}Co showed as the isolated spurs. The cylinder tracks were observed in the case of tritium. The greater the linear energy transfer of tritium leads to an increased local concentration of reactants. The distance between the primary events in ^3H β-particle is much smaller than in the track of ^{60}Co γ-rays. As a consequence, we found more molecular product (in this case we consider H_2) in tritium radiolysis rather than in gamma radiolysis. Our calculations of the H_2 yields using various electron scavenger systems show a good agreement of the H_2 yield at low concentration of scavenger but fails to reproduce the experimental data at high concentration. These results also suggest the necessity, at high scavenger concentrations, to include the possibility that low-energy (or "dry") secondary electrons can be scavenged prior to hydration. Such a process was shown to reduce significantly the yields of H_2 as is observed experimentally. These results support the necessity of introducing the ultra-fast (< 1ps) capture of the dry electron as we observed for azide solution.

CONCLUSION

In this work, Monte-Carlo simulations were used to investigate the effect of the azide ion N_3^- on the yield of molecular hydrogen in an aqueous azide solution irradiated with ^{60}Co γ-rays (~1 MeV Compton electrons) and tritium β-electrons (mean electron energy of ~7.8 keV) at 25 °C. Azide was used as an effective scavenger for the hydrogen atoms and hydrated electrons. Hydrogen atom and hydrated electron are the main species that can formH_2 in the nonhomogeneous chemical stage. The formation of H_2 from ^3H β-particles is higher than in the case of ^{60}Co γ rays which can explain by the effect of LET. The track structure in the case of ^{60}Co γ irradiation is composed of well-separated (spherical) spurs, which contrasts with the short (roughly cylindrical) tracks observed in the case of higher-LET tritium β-electrons. The greater linear energy transfer of ^3H β-electrons leads to an increased local concentration of reactants. The distance between the primary events is thus much smaller than in the tracks of ^{60}Co γ rays. Consequently, we find more molecular hydrogen yield in tritium radiolysis than in γ radiolysis. Our calculations H_2 yields from γ- and ^3H β-radiolysis of NaN_3 solutions show a very good agreement with the experiment over a large range of N_3^- concentrations. For ^{60}Co γ-radiolysis, however, our H_2 yields fail to reproduce the sharp decrease that is observed experimentally at high (>1 M) azide concentrations. This decrease of H_2 yield a high concentration of azide reflected the possibility that low-energy (or "dry") secondary electrons could be scavenged by N_3^- prior to trapping and hydration in the subpicosecond physicochemical stage. Most interestingly, for ^3H β-radiolysis, the molecular hydrogen yields at high N_3^- concentration does not show a sharp decrease as for γ irradiation. In other words, there is no clear evidence that N_3^- ions scavenge the short-lived dry electrons. This is consistent with the enhanced contribution of short tracks for the higher LET ^3H β-radiolysis as compared to γ radiolysis. Indeed, the short-track geometry is competitively more favorable to the geminate recombination of e^-_{dry} with their nearby parent water cations than their scavenging by the homogeneously distributed N_3^- ions. As the continuing of this work, we have introduced this ultra-fast (<1 ps) capture of the dry electron into our simulation models. The prehydrated electron was observed to be an important species that involve in the

mechanism of DNA damage and many other biological substances. This part of our work is very interesting since it is the first time we had introduced the reactions of the dry electron with the scavenger to our Monte-Carlo simulation. The molecular hydrogen yield shows a sharp decrease when the concentration of azide ion increases which agrees well with the experimental data. This work can confirm the existence of the effect of the prehydrated electron on the formation of molecular hydrogen yields at high concentration of azide

Besides this work, I have tested the sensitivity of the density dependence of the yield of e^-_{aq} in the low linear energy transfer (LET) radiolysis of supercritical water (H_2O) at 400 °C on variations in the temperature dependence of the reaction rate constant of bimolecular self-reaction of e^-_{aq}. This reaction is important as it gives the most contribution to the H_2 yield from the nonhomogeneous chemical stage. Two different values of the e^-_{aq} self-reaction rate constant at 400 °C were used: one based on the temperature dependence of $k(e^-_{aq} + e^-_{aq})$ above 150 °C as measured in alkaline water (4.2×10^8 M^{-1} s^{-1}) and the other based on an Arrhenius extrapolation of the values below 150 °C (2.5×10^{11} M^{-1} s^{-1}). In both cases, the density dependences of our calculated e^-_{aq} yields at ~60 ps and 1 ns were found to compare fairly well with the available picosecond pulse radiolysis experimental data (for D_2O) for the entire water density range studied (~0.15-0.6 g/cm^3). Only a small effect of k on the variation of $G(e^-_{aq})$ as a function of density at 60 ps and 1 ns could be observed. Such a small effect of $k(e^-_{aq} + e^-_{aq})$ on the variation of $G(e^-_{aq})$ as a function of density prevented us to confirm the predicted sudden drop of $k(e^-_{aq} + e^-_{aq})$ at 150 °C in neutral water. Since this chemical reaction plays a role in the formation of GH_2 yield in less extent than those processes in early time. This would lead us to focus our future work to incorporate the possibility that the dry electron can get capture before its hydration to our high temperature water radiolysis program. Furthermore, we could also consider revisiting our branching ratio of the excited water molecule as another possibility to produce H_2 yields from the early time processes in the radiolysis of water. A better understanding in all details about each process in early time water radiolysis should lead a better understanding of the biological effects.

ACKNOWLEDGMENT

I would like to thank the Department of Nuclear Medicine and Radiobiology, Faculty of Medicine and Health Sciences, *Université de Sherbrooke*.

I would like to express my gratitude and appreciation to Prof. J.-P. Jay-Gerin, director of the laboratory and my supervisor, for the opportunity to pursue my study in his research group, for his pieces of advice, informative discussions, and encouragement. Thank you for being so patient and taking the time to explain everything since my first internship in 2007. It was not only the beginning of my research life but it is also the most changing point of my life. I have made a great progression since 2007.

I appreciated the help and cheerful support of Dr. J. Meesungnoen for teaching me programming, giving me advice both in research and personal life. She is the person who gave me the great opportunity to meet my supervisor. Without her, I would not be able to complete this thesis.

I would like to thank my colleagues in our laboratory for the great discussion we had together in the lab.

Special thanks to Prof. Yusa Muroya for the great opportunity to learn about the picosecond electron pulse radiolysis technique during my internship at the Institute of Scientific and Industrial Research (ISIR), Osaka University, Japan. I spent 2 months in the laboratory of Prof. Kozawa Takahiro, Oct-Dec, 2015. Thanks for the beautiful friendship from everyone in the lab of Prof. Kazawa Takahiro.

The biggest thanks to my parents, for their support and their unique unconditional great love. The more I grow up, the more I realize that I could not find this in anyone else but them. My parents take every effort to give me the best education. I have a chance to study everything that I am interested in.

Last but not least, I would like to thank my husband for supporting me and our family during these graduate years. He did the hard work of taking care of the kids while I was absent. Thanks to our most precious kids Georges, Audrey-Anne, and Naomi for teaching me to understand many things in life. Thanks for being the best source of my energy. They are the persons who make me bring out the best version of myself.

The financial support from the Natural Sciences and Engineering Research Council of Canada, and Natural Resources Canada is gratefully acknowledged.

LISTE DES RÉFÉRENCES

ALASTAIR JOHNSON, G.R., and NAZHAT, N.B., 1984. Reactions of hydrogen atoms with Cu^{2+} and Cu^{+} in aqueous solution. *J. Chem. Soc., Faraday Trans. 1*, **80**, 3455-3462.

ALCORN, C. D., BRODOVITCH, J.-Cl., PERCIVAL, P. W., SMITH, M., and GHANDI, K., 2014. Kinetics of the Reaction between $H^{\bullet}$ and Superheated Water Probed with *Muonium. Chem. Phys.*, **435**, 29-39.

ALDRICH, J.E., BRONSKILL, M.J., WOLFF, R.K., and HUNT, J.W., 1971. Picosecond pulse radiolysis. III. reaction rates and reduction in yields of hydrated electrons. *J. Chem. Phys.*, **55**, 530.

ALDRICH, J. E., LAM, K.Y., SHRAGGE, P.C., and HUNT, J. W., 1975. Fast electron reactions in concentrated solutions of amino acids and nucleotides, *Radiat. Res.* **63**, 42-52.

ALLEN, A.O., 1948. Radiation chemistry of aqueous solutions. *J. Phys. Colloid Chem.* **52**, 479-490.

ALIZADEH, E., ORLANDO, T.M., and SANCHE, L., 2015. Biomolecular damage induced by ionizing radiation: The direct and indirect effects of low-energy electrons on DNA, *Annu. Rev. Phys. Chem.* **66**, 379-398.

AMICHAI, O. and TREININ, A., 1969. Chemical reactivity of $O(^3P)$ atoms in aqueous solution. *Chem. Phys. Lett.* **3**, 611-613.

ANDERSON, D.W., 1984. *Absorption of Ionizing Radiation*. University Park Press, Baltimore, MD.

APPLEBY, A. and GAGNON, W.F., 1971. Scavenging of the molecular hydrogen yield from water irradiated with tritium β particles. *J. Phys. Chem.* **75**, 601-602.

ASSEL, M., LAENEN, R., LAUBEREAU, A., 1998. Dynamics of excited solvated electrons in aqueous solution monitored with femtosecond-time and polarization resolution, J. *Phys. Chem. A.* **102**, 2256-2262.

AUTSAVAPROMPORN, N., 2006. *The effects of pH and radiation quality (LET) on the radiolysis of liquid water and aqueous solutions: A study by using Monte-Carlo simulations*. M.Sc. Thesis, Burapha University, Bangsaen (Thailand).

AUTSAVAPROMPORN, N., MEESUNGNOEN, J., PLANTE, I., and JAY-GERIN, J.-P., 2007. Monte-Carlo simulation study of the effects of acidity and LET on the primary free-radical and molecular yields of water radiolysis – Application to the Fricke dosimeter. *Can. J. Chem.* **85**, 214-229.

AZZAM, E.I., JAY-GERIN, J.-P., and PAIN, D., 2012. Ionizing radiation-induced metabolic oxidative stress and prolonged cell injury, *Cancer Lett*. **327**, 48-60.

BALLARINI, F., BIAGGI, M., MERZAGORA, M., OTTOLENGHI, A., DINGFELDER, M., FRIEDLAND, W., JACOB, P., and PARETZKE, H.G., 2000. Stochastic aspects and uncertainties in the prechemical and chemical stages of electron tracks in liquid water: A quantitative analysis based on Monte Carlo simulations. *Radiat. Environ. Biophys.* **39**, 179-188.

BARÓ, J., SEMPAU, J., FERNÁNDEZ-VEREA, J.M., and SALVAT, F., 1995. PENELOPE: An algorithm for Monte Carlo simulation of the penetration and energy loss of electrons and positrons in matter, *Nucl. Instrum. Methods Phys. Res. B* **100**, 31-46.

BARTELS, D.M., 2009. Comment on the possible role of the reaction $H^{\bullet} + H_2O \rightarrow H_2 + {}^{\bullet}OH$ in the radiolysis of water at high temperatures. *Radiat. Phys. Chem.* **78**, 191-194.

BASS, A.D. and SANCHE, L., 2003. Dissociative electron attachment and charge transfer in condensed matter. *Radiat. Phys. Chem.* **68**, 3-13.

BAXENDALE, J.H. and BEVAN, J.L.T., 1967. Absolute rates of hydrogen atom reactions in aqueous solution. *The chemistry of Ionization and Excitation*. Johnson, G.R.A. and Scholes, G., eds., Taylor and Francis, London, p.253-257.

BECKER, D., ADHIKARY, A., and SEVILLA, M.D., 2011. Physicochemical mechanisms of radiation-induced DNA damage, in: *Charged Particle and Photon Interactions with Matter: Recent Advances, Applications, and Interfaces*, edited by Hatano, Y. Katsumura, Y., and Mozumder, A. (Taylor & Francis, Boca Raton), p. 503-541.

BELLANGER, G., 2004. Corrosion Induced by Low-Energy Radionuclides. Modeling of Tritium and its Radiolytic and Decay Products Formed in Nuclear Installations, Elsevier, Amsterdam.

BERA, P. P. and SCHAEFER, H. F., 2005. (G–H)•–C and G–(C–H)• radicals derived from the guanine*cytosine base pair cause DNA subunit lesions, *Proceedings of the National Academy of Sciences of the United States of America.* **102**, 6698-6703.

BERNAS, A., FERRADINI, C., and JAY-GERIN, J.-P., 1996. Électrons en excès dans les milieux polaires homogènes et hétérogènes. *Can. J. Chem.* **74**, 1-23.

BĚGUSOVÁ, M. and SPOTHEIM-MAURIZOT, D. Sy, MICHALIK, M., and CHARLIER, M., 2001. RADACK, a stochastic simulation of hydroxyl radical attack to DNA, *J. Biomol. Struct. Dyn.* **19**, 141-158.

BETHE, H., 1930. Zur Theorie des Durchgangs schneller Korpuskularstrahlen durch Materie. *Ann. Physik (Leipzig)* **5**, 325-400.

BETHE, H.A. and ASHKIN, J., 1953. Passage of radiations through matter. In: Segrè, E. (Ed.), *Experimental Nuclear Physics*, vol. 1. Wiley, New York, pp. 166-357.

BIEDENKAPP, D., HARTSHORN, L.G., and BAIR, E.J., 1970. The $O(^1D) + H_2O$ reaction. *Chem. Phys. Lett.* **5**, 379-380.

BJERGBAKKE, E. and HART, E.J., 1971. Oxygen formation in the γ-ray irradiation of Fe^{2+}–Cu^{2+} solutions. *Radiat. Res.* **45**, 261-273.

BOWLES, T.J. and ROBERTSON, R.G.H 1997. Tritium beta decay and the search for neutrino mass, *Los Alamos Science*, **86**, 6-11.

BUONANNO, M., DE TOLEDO, S.M., and AZZAM, E.I., 2011. Increased frequency of spontaneous neoplastic transformation in progeny of bystander cells from cultures exposed to densely ionizing radiation, *PloS One* **6**, e21540 1-6.

BURNS, W.G. and MARSH, W.R., 1981. Radiation chemistry of high-temperature (300-410 ºC) water. Part 1. Reducing products gamma radiolysis. *J. Chem. Soc., Faraday Trans. 1*, **77**, 197-215.

BUXTON, G. V., 1987. Radiation chemistry of the liquid state: (1) Water and homogeneous aqueous solutions. In: Farhataziz and Rodgers, M.A.J. (Eds.), *Radiation Chemistry. Principles and Applications*. VCH Publishers, New York, pp. 321-349.

BUXTON, G. V., GREENSTOCK, C. L., HELMAN, W. P., and ROSS, A. B., 1988. Critical-review of rate constants for reactions of hydrated electrons, hydrogen-atoms

and hydroxyl radicals ($^{\bullet}OH/^{\bullet}O^{-}$) in aqueous-solution *J. Phys. Chem. Ref. Data* **17**, 513-886.

BYAKOV, V. M., 1976. Nature of Precursors of Radiolytic Molecular-Hydrogen in Water, and Mechanism of Positronium formation in Liquids. *Int. J. Radiat. Phys. Chem.* **8**, 283– 288.

BYAKOV, V. M.; GRAFUTIN, V. I.; KOLDAEVA, O. V.; MINAICHEV, E. V.; NICHIPOROV, F. G.; OBUKHOV, Y. V.; STEPANOVA, O. P., 1977. Investigation of N-n-solvated electron reactions by means of Positron-Annihilation Method. *Chem. Phys.* **24**, 91– 95.

CHAO, T.-C., WANG, C.-C., LI, J., LI, C., and TUNG, C.-J., 2012. Cellular- and micro-dosimetry of heterogeneously distributed tritium. *Int. J. Radiat. Biol.* **88**, 151-157.

CHATTERJEE, A. and SCHAEFER, H.J., 1976. Microdosimetric structure of heavy ion tracks in tissue. *Radiat. Environ. Biophys.* **13**, 215-227.

CHATTERJEE, A. and HOLLEY, W.R., 1993. Computer simulation of initial events in the biochemical mechanisms of DNA damage. *Adv. Radiat. Biol.* **17**, 181-226.

CHRISTMAN, E. A., 1977. Molecular hydrogen yields and tritium protium isotope effects in tritium beta radiolysis. *Ph.D. thesis*, Rutgers University, New Brunswick, New Jersey.

CHRISTENSEN, H. and SEHESTED, K., 1986. The hydrated electron and its reactions at high temperatures. *J. Phys. Chem.* **90**, 186-190.

CHRISTOPHOROU, L.G., McCORKLE, D.L., and CHRISTODOULIDES, A.A., 1984. Electron attachment processes. In: Christophorou, L.G. (Ed.), *Electron-Molecule Interactions and their Applications*, vol. 1. Academic Press, Orlando, FL, pp. 477-617.

CLIFFORD, P., GREEN, N.J.B., OLDFIELD, M.J., PILLING, M.J., and PIMBLOTT, S.M., 1986. Stochastic models of multi-species kinetics in radiation-induced spurs. *J. Chem. Soc., Faraday Trans. 1*, **82**, 2673-2689.

COBUT, V., 1993. *Simulation Monte-Carlo du transport d'électrons non relativistes dans l'eau liquide pure et de l'évolution du milieu irradié: rendements des espèces créées de 10^{-15} à 10^{-7} s*. Ph.D. Thesis, Université de Sherbrooke.

COBUT, V., FRONGILLO, Y., JAY-GERIN, J.-P., and PATAU, J.P., 1994. Calculs des rendements des produits de la radiolyse de l'eau en fonction du temps par une méthode Monte-Carlo. *J. Chim. Phys.* **91**, 1018-1024.

COBUT, V., JAY-GERIN, J.-P., FRONGILLO, Y., and PATAU, J.P., 1996. On the dissociative electron attachment as a potential source of molecular hydrogen in irradiated liquid water, *Radiat. Phys. Chem.* **47**, 247-250.

COBUT, V., FRONGILLO, Y., PATAU, J.P., GOULET, T., FRASER, M.-J., and JAY-GERIN, J.-P., 1998. Monte Carlo simulation of fast electron and proton tracks in liquid water. I. Physical and physicochemical aspects. *Radiat. Phys. Chem.* **51**, 229-243.

COLLINSON, E., DAINTON, F.S. and KROH, J., 1962. The radiation chemistry of aqueous solutions. III. The isotope effect for polonium α-particles and tritium β-particles. *Proc. R. Soc. London A.* **265**, 430-435.

CZAPSKI, G. and SCHWARZ, H.A., 1962. The nature of the reducing radical in

water radiolysis. *J. Phys. Chem.* **66**, 471-474.
DAINTON, F.S. and LOGAN S.R., 1965. Radiolysis of aqueous solutions containing nitrite ions and nitrous oxide. *Trans. Faraday Soc.* **61**, 715-722.
DAVIES, C.W., 1938. The extent of dissociation of salts in water. Part VIII. An equation for the mean ionic activity coefficient of an electrolyte in water, and a revision of the dissociation constants of some sulphates. *J. Chem. Soc.* 2093-2098.
DEBYE, P., 1942. Reaction rates in ionic solutions. *Trans. Electrochem. Soc.* **82**, 265-272.
DELARA, C. M., JENNER, T. J., TOWNSEND, K. M. S., MARSDEN, S. J., O'NEILL, P., 1995. The effect of dimethyl sulfoxide on the induction of DNA double-strand breaks in V79-4 mammalian cells by alpha particles, *Radiat. Res.* **144**, 43-49.
DINGFELDER, M. and FRIEDLAND, W., 2001. Basic data for track structure simulations: Electron interaction cross-sections in liquid water. In: Kling, A., Barão, F., Nakagawa, M., Távora, L., and Vaz, P. (Eds.), *Advanced Monte Carlo for Radiation Physics, Particle Transport Simulation and Applications*. Springer-Verlag, Berlin, pp. 267-272.
DINGFELDER, M., RITCHIE, R.H., TURNER, J.E., FRIEDLAND, W., PARETZKE, H.G., and HAMM, R.N., 2008. Comparisons of calculations with PARTRAC and NOREC: Transport of electrons in liquid water. *Radiat. Res.* **169**, 584-594.
DOMAE, M., KATSUMURA, Y., ISHIGURE, K., and BYAKOV, V.M., Modeling of primary chemical processes of water radiolysis and simulation by spur diffusion model. 1996. Radiat. Phys. Chem., **48**, 485-495.
DRAGANIĆ, Z.D. and DRAGANIĆ, I.G., 1971. Formation of primary yields of hydrogen peroxide and molecular hydrogen (GH_2O_2 and GH_2) in the gamma radiolysis of neutral aqueous solutions**.** *J. Phys. Chem.* **75**, 3950-3957.
DUPLÂTRE, G.and JONAH, C. D., 1984. Reactions of electrons in high-concentration water solutions—A comparison between pulse-radiolysis and positron annihilation lifetime spectroscopy data. *Radiat. Phys. Chem.* **24**, 557– 565.
DYE, J. L., 2003. Electrons as anions, *Science*. **301**, 607-608.
ELLIOT, A.J., McCRACKEN, D.R., BUXTON, G.V., and WOOD, N.D., 1990. Estimation of rate constants for near-diffusion-controlled reactions in water at high temperatures. *J. Chem. Soc. Faraday Trans.* **86**, 1539-1547.
ELLIOT, A.J., 1994. Rate constants and *G*-values for the simulation of the radiolysis of light water over the range 0-300 ºC. Report AECL-11073. Atomic Energy of Canada Ltd., Chalk River, ON.
ELLIOT, A.J. and BARTELS, D.M., 2009. The reaction set, rate constants and *g*-values for the simulation of the radiolysis of light water over the range 20° to 350°C based on information available in 2008. Report AECL No. 153-127160-450-001. Atomic Energy of Canada Limited, Chalk River, Ontario, Canada.
EVANS, R.D., 1955. *The Atomic Nucleus*. Krieger Publ. Co., Malabar, FL.
FANO , U. and STEPHENS, J.A., 1986. Slow electrons in condensed matter, *Phys. Rev. B* **34**, 438-441.
J.E. Fanning, 1975. Evidence for spurs in aqueous radiation chemistry. *Ph.D. Thesis* University of Delaware.
FARAGGI, M. and DÉSALOS, J., 1969. Effect of positively charged ions on the "molecular" hydrogen yield in the radiolysis of aqueous solutions. *Int. J. Radiat. Phys. Chem.* **1**, 335-344.

FERRADINI, C., 1990. Aspect hétérogène des phénomènes radiolytiques. In: Tilquin, B. (Ed.), *Actions Biologique et Chimique des Radiations*, vol. 1. Éditions Ciaco, Bruxelles, pp. 52-63.

FERRADINI, C., 1979. Actions chimiques des radiations ionisantes. *J. Phys. Chim.* **76**, 636-644.

FERRADINI, C. and JAY-GERIN, J.-P., 1999. La radiolyse de l'eau et des solutions aqueuses: historique et actualité. *Can. J. Chem.* **77**, 1542-1575.

FREEMAN, G.R., 1987. Ionization and charge separation in irradiated materials. In: Freeman, G.R. (Ed.), *Kinetics of Nonhomogeneous Processes*. Wiley, New York, pp. 19-87.

FREGENE, A.O., 1967. Calibration of the ferrous sulfate dosimeter by ionometric and calorimetric methods for radiations of a wide range of energy. *Radiat. Res.* **31**, 256-272.

FRIEDLAND, W., DINGFELDER, M., KUNDRÁT, P., and JACOB, P., 2011. Track structures, DNA targets and radiation effects in the biophysical Monte Carlo simulation code PARTRAC, *Mutat. Res.* **711**, 28-40.

FRIEDLANDER, G., KENNEDY J. W., MACIAS, E. S., and MILLER, J. M., 1981. Nuclear and Radiochemistry, Wiley, New York, 3rd edn.

FRONGILLO, Y., FRASER, M.J., COBUT, V., GOULET, T., JAY-GERIN, J.-P., and PATAU, J.P., 1996. Évolution des espèces produites par le ralentissement de protons rapides dans l'eau liquid : simulation fondée sur l'approximation des temps de réaction indépendants. *J. Chim. Phys.* **93**, 93-102.

FRONGILLO, Y., GOULET, T., FRASER, M.-J., COBUT, V., PATAU, J.P., and JAY-GERIN, J.-P., 1998. Monte Carlo simulation of fast electron and proton tracks in liquid water. II. Nonhomogeneous chemistry. *Radiat. Phys. Chem.* **51**, 245-254.

GAGNON, W.F. and APPLEBY, A., 1973. In: Tritium (A. Moghissi and M.W. Carter, Eds.), Messenger Graphics, Phoenix, Arizona, p. 192.

GANGULY, A.K. and MAGEE, J.L., 1956. Theory of radiation chemistry. III. Radical reaction mechanism in the tracks of ionizing radiations. *J. Chem. Phys.* **25**, 129-134.

GAUDUEL, Y., BERROD, S., MIGUS, A., YAMADA, N., ANTONETTI, A., 1988 Femtosecond charge separation in organized assemblies: Free-radical reactions with pyridine nucleotides in micelles, Biochemistry (N. Y.). **27**, 2509-2518.

GOLDSTEIN, S. CZAPSKI, G. COHEN, H., and MEYERSTEIN, D., 1992. Deamination of β-alanine induced by hydroxyl radicals and monovalent copper ions. A pulse radiolysis study. *Inorg. Chim. Acta*, **192**, 87-93.

GOULET, T. and JAY-GERIN, J.-P., 1988. Thermalization distances and times for subexcitation electrons in solid water. *J. Phys. Chem.* **92**, 6871-6874.

GOULET, T. and JAY-GERIN, J.-P., 1989. Thermalization of subexcitation electrons in solid water. *Radiat. Res.* **118**, 46-62.

GOULET, T., PATAU, J.P., and JAY-GERIN, J.-P., 1990. Influence of the parent cation on the thermalization of subexcitation electrons in solid water. *J. Phys. Chem.* **94**, 7312-7316.

GOULET, T. and JAY-GERIN, J.-P., 1992. On the reactions of hydrated electrons with $^{\bullet}OH$ and H_3O^+. Analysis of photoionization experiments. *J. Chem. Phys.* **96**, 5076-5087.

GOULET, T., JAY-GERIN, J.-P., FRONGILLO, Y., COBUT, V., and FRASER, M.-J., 1996. Rôle des distances de thermalisation des électrons dans la radiolyse de l'eau liquide. *J. Chim. Phys.* **93**, 111-116.

GOULET, T., FRASER, M.-J., FRONGILLO, Y., and JAY-GERIN, J.-P., 1998. On the validity of the independent reaction times approximation for the description of the nonhomogeneous kinetics of liquid water radiolysis. *Radiat. Phys. Chem.* **51**, 85-91.

GREEN, N.J.B., PILLING, M.J., PIMBLOTT, S.M., and CLIFFORD, P., 1990. Stochastic modeling of fast kinetics in a radiation track. *J. Phys. Chem.* **94**, 251-258.

GREEN, N.J.B., BOLTON, C.E., and SPENCER-SMITH, R.D., 1999. The link between physics and chemistry in track modeling", *Radiat. Environ. Biophys.* **38**, 221-228.

GUGGENHEIM, E.A., 1935. The specific thermodynamic properties of aqueous solutions of strong electrolytes. *Philos. Mag.*, 7th Ser., **19**, 588-643.

GUZONAS, D., TREMAINE, P., and JAY-GERIN, J.-P., 2009. Chemistry control challenges in a supercritical water-cooled reactor. *PowerPlant Chem.* **11**, 284-291.

HALL, E.J. and GIACCIA, A.J., 2006. *Radiobiology for the Radiologist*, 6th edn (Lippincott, Williams & Wilkins, Philadelphia).

HARDWICK, T.J., 1952. The effect of the energy of the ionizing electron on the yield in irradiated aqueous systems. *Disc. Faraday Soc.* **12**, 203-2011.

HARRIS, R.E. and PIMBLOTT, S.M., 2002. On 3H β-particle and 60Co γ irradiation of aqueous systems. *Radiat. Res.* **158**, 493-504.

HART, E.J., 1954. Molecular product and free radical yields of ionizing radiations in aqueous solutions. *Radiat. Res.* **1**, 53-61.

HART, E.J., 1955. Radiation chemistry of aqueous ferrous sulfate-cupric sulfate solutions. Effect of γ-rays. *Radiat. Res.* **2**, 33-46.

HART, E. J. and BOAG, J. W., 1962. Absorption spectrum of the hydrated electron in water and in aqueous solutions*, J. Am. Chem. Soc.* **84**, 4090-4095.

HELLER, J.M., Jr., HAMM, R.N., BIRKHOFF, R.D., and PAINTER, L.R., 1974. Collective oscillation in liquid water. *J. Chem. Phys.* **60**, 3483-3486.

HERBERT, J. M., JACOBSON, L. D., 2011. Nature's most squishy ion: The important role of solvent polarization in the description of the hydrated electron, *Int. Rev. Phys. Chem.* **30**, 1-48.

HERVÉ DU PENHOAT, M.-A., GOULET, T., FRONGILLO, Y., FRASER, M.-J., BERNAT, Ph., and JAY-GERIN, J.-P., 2000. Radiolysis of liquid water at temperatures up to 300 ºC: A Monte Carlo simulation study. *J. Phys. Chem. A* **104**, 11757-11770.

HIRAYAMA, H., NAMITO, Y., BIELAJEW, A.F., WILDERMAN, S.J., and NELSON, W.R., 2005. *The EGS5 Code System*, SLAC-R-730 (US Dept. of Energy, Washington, DC).

HOCHANADEL, C.J. and GHORMLEY, J.A., 1962. Effect of temperature on the decomposition of water by gamma rays. *Radiat. Res.* **16**, 653-660.

HORNE, G. P.; PIMBLOTT, S. M.; LAVERNE, J. A. 2017., Inhibition of Radiolytic Molecular Hydrogen Formation by Quenching of Excited State Water. *J. Phys. Chem. B* **121**, 5385-5390.

IAEA-TECDOC-799, 1995. *Atomic and Molecular Data for Radiotherapy and Radiation Research*. International Atomic Energy Agency, Vienna.

ICRU REPORT 17, 1970. Radiation Dosimetry: X Rays Generated at Potentials of 5 to 150

kV, International Commission on Radiation Units and Measurements, Washington, D.C.

ICRU REPORT 31, 1979. *Average Energy Required to Produce an Ion Pair*. International Commission on Radiation Units and Measurements, Washington, DC.

INCERTI, S., BALDACCHINO, G., BERNAL, M., CAPRA, R., CHAMPION, C., FRANCIS, Z., GUÈYE, P., MANTERO, A., MASCIALINO, B., MORETTO, P., NIEMINEN, P., VILLAGRASA, C. and ZACHARATOU, C., 2010. The Geant4-DNA project, *Int. J. Model. Simul. Sci. Comput.* **1**, 157-178

ISHIGURE, K., TAKAGI, J., and SHIRAISHI, H., 1987. Hydrogen injection in BWR and related radiation chemistry. *Radiat. Phys. Chem.* **29**, 195-199.

ISHIGURE, K., KATSUMURA, Y., SUNARYO, G.R., and HIROISHI, D., 1995. Radiolysis of high temperature water. *Radiat. Phys. Chem.* **46**, 557-560.

ITO, T., BAKER, S. C., STICKLEY, C. D., PEAK, J. G., PEAK, M. J., 1993. Dependence of the yield of strand breaks induced by gamma-rays in DNA on the physical conditions of exposure: Water content and temperature, *Int. J. Radiat. Biol.* **63**, 289-296.

JANIK, D., JANIK, I., and BARTELS, D.M., 2007. Neutron and β/γ radiolysis of water up to supercritical conditions. 1. β/γ yields for H_2, $H^{\bullet}$ atom, and hydrated electron. *J. Phys. Chem. A* **111**, 7777-7786.

JAY-GERIN, J.-P., LIN, M., KATSUMURA, Y., HE, H., MUROYA, Y., and MEESUNGNOEN, J., 2008. Effect of water density on the absorption maximum of hydrated electrons in sub- and supercritical water up to 400 ºC. *J. Chem. Phys.* **129**, no. 114511.

JOACHAIN, C.J., 1975. *Quantum Collision Theory*, 3rd ed. North-Holland, Amsterdam.

JONAH, C.D., MILLER, J.R., and MATHESON, M.S., 1977. The reaction of e^-_{aq} + H_3O^+. Concentration effects of acid or salts. *J. Phys. Chem.* **81**, 931-934.

KAMBHAMPATI, P., SON, D. H., KEE, T. W., BARBARA, P. F., 2002. Solvation dynamics of the hydrated electron depends on its initial degree of electron delocalization, *J. Phys. Chem. A.* **106**, 2374-2378.

KAPLAN, I.G. and MITEREV, A.M., 1987. Interaction of charged particles with molecular medium and track effects in radiation chemistry. *Adv. Chem. Phys.* **68**, 255-386.

KARAMITROS, M., MANTERO, A., INCERTI, S., FRIEDLAND, W., BALDACCHINO, G., BARBERET, P., BERNAL, M., CAPRA, R., CHAMPION, C., EL BITAR, Z., FRANCIS, Z., GUÈYE, P., IVANCHENKO, A., IVANCHENKO, V., KURASHIGE, H., MASCIALINO, B., MORETTO, P., NIEMINEN P., SANTIN, G., SEZNEC, H., TRAN, H.N. , VILLAGRASA, C., and ZACHARATOU, C., 2011. Modeling radiation chemistry in the Geant4 toolkit, *Nucl. Sci. Technol.* **2**, 503-508.

KARA-MICHAILOVA, E. and LEA, D.E., 1940. The interpretation of ionization measurements in gases at high pressures. *Proc. Cambridge Phil. Soc.* **36**, 101-126.

KATSUMURA, Y., 2004. Application of radiation chemistry to nuclear technology. In: Mozumder, A. and Hatano, Y. (Eds.), *Charged Particle and Photon Interactions with Matter. Chemical, Physicochemical, and Biological Consequences with Applications*. Marcel Dekker, New York, pp. 697-727.

KIMMEL, G.A., ORLANDO, T.M., VÉZINA, C., and SANCHE, L., 1994. Low-

energy electron-stimulated production of molecular hydrogen from amorphous water ice. *J. Chem. Phys.* **101**, 3282-3286.

KRAFT, G. and KRÄMER, M., 1993. Linear energy transfer and track structure. *Adv. Radiat. Biol.* **17**, 1-52.

KRAUS, C. A.,1907. Solutions of metals in non-metallic solvents; i. General properties of solutions of metals in liquid ammonia, *J. Am. Chem. Soc.* **29**, 1557-1571.

KRAUS, C. A., 1908. Solution of metals in non-metallic solvents; ii.1 on the formation of compounds between metals and ammonia, *J. Am. Chem. Soc.* **30**, 653-668.

KUPPERMANN, A., 1959. Theoretical foundations of radiation chemistry. *J. Chem. Educ.* **36**, 279-285.

LAENEN, R., ROTH, T., LAUBEREAU, A., 2000. Novel precursors of solvated electrons in water: Evidence for a charge transfer process, *Phys. Rev. Lett.* **85**, 50-53.

LAM, K.Y. and HUNT, J.W., 1975. Picosecond pulse radiolysis—VI. Fast electron reactions in concentrated solutions of scavengers in water and alcohols. Radiat, Phys. Chem., **7**, 317-338.

LAVERNE, J.A. and SCHULER, R.H., 1987*a*. Radiation chemical studies with heavy ions: Oxidation of ferrous ion in the Fricke dosimeter. *J. Phys. Chem.* **91**, 5770-5776.

LAVERNE, J.A. and SCHULER, R.H., 1987*b*. Track effects in radiation chemistry: Production of $HO_2^{\bullet}$ in the radiolysis of water by high-LET ^{58}Ni ions. *J. Phys. Chem.* **91**, 6560-6563.

LAVERNE, J.A., 2000. Track effects of heavy ions in liquid water. *Radiat. Res.* **153**, 487-496.

LAVERNE, J.A., 2004. Radiation chemical effects of heavy ions. In: Mozumder, A. and Hatano, Y. (Eds.), *Charged Particle and Photon Interactions with Matter. Chemical, Physicochemical, and Biological Consequences with Applications*. Marcel Dekker, New York, pp. 403-429.

LAVERNE, J.A. and PIMBLOTT, S.M., 1995. Electron energy-loss distributions in solid, dry DNA. *Radiat. Res.* **141**, 208-215.

LAVERNE, J. A.; PIMBLOTT, S. M., 2000. New Mechanism for H_2 Formation in Water. *J. Phys. Chem. A* **104**, 9820– 9822.

LAW, J., 1969. Ferrous sulphate G-values for X-rays of 'effective' energy 48 and 25 keV. *Phys. Med. Biol.* **14**, 607-614.

LEHNERT, S., 2007. Biomolecular Action of Ionizing Radiation; Taylor & Francis, Boca Raton.

LEMAIRE, G., FERRADINI, C., PUCHEAULT, J., 1972. Radiolysis of water by tritium β rays. Scavenging of hydrogen peroxide precursors. *J. Phys. Chem.* 76 ,1542-1546.

LI, J., NIE, Z., ZHENG, Y.Y., DONG, S., and LOH, Z.-H., 2013. Elementary electron and ion dynamics in ionized liquid water, *J. Phys. Chem. Lett.* **4**, 36983703.

LIN, C.C., 1996. Radiochemistry in Nuclear Power Reactors. National Academy Press, Washington, D.C.

LINSTROM, P.J. and MALLARD, W.G. (Eds.), 2005. NIST Chemistry WebBook, NIST Standard Reference Database No. 69. National Institute of Standards and Technology, Gaithersburg, M.D. Available from http://webbook.nist.gov.

LIU, B., NIELSEN, S. B., HVELPLUND, P., ZETTERGREN, H., CEDTERQUIST, H.,

MANIL, B., HUBER, B. A., 2006. Collision-induced dissociation of hydrated adenosine monophosphate nucleotide ions: Protection of the ion in water nanoclusters, *Phys. Rev. Lett.* **97**, 133401.

LONG, F. H., LU, H., EISENTHAL, K. B., 1990. Femtosecond studies of the presolvated ELectron: An excited state of the solvated electron? *Phys. Rev. Lett.* **64**, 1469-1472.

LU, Q.-B., 2007. Molecular reaction mechanisms of combination treatments of low-dose cisplatin with radiotherapy and photodynamic therapy, *J. Med. Chem.* **50**, 2601-2604.

LU, Q.-B., 2010. Effects and applications of ultrashort-lived prehydrated electrons in radiation biology and radiotherapy of cancer, *Mutat. Res.* **704**, 190-9.

LU, Q.-B., SANCHE, L., 2001. Enhanced dissociative electron attachment to CF2Cl2 by transfer of electrons in precursors to the solvated state in water and ammonia ice, *Physical Review B*. **63**, 153403-1-152403-4.

LU, Q.-B., BASKIN, J. S., ZEWAIL, A.H., 2004. The presolvated electron in water: Can it be scavenged at long range? *J. Phys. Chem. B.* **108**, 10509-10514.

LU, Q.-B., KALANTARI, S., WANG, C.-R., 2007. Electron transfer reaction mechanism of cisplatin with DNA at the molecular level, *Molecular Pharmaceutics*. **4**, 624-628.

MA, J., SCHMIDHAMMER, U., and MOSTAFAVI, M., 2014. Picosecond pulse radiolysis of highly concentrated sulfuric acid solutions: Evidence for the oxidation reactivity of radical cation $H_2O^{\bullet+}$, *J. Phys. Chem. A* **118**, 4030-4037.

MAGEE, J.L., 1953. Radiation chemistry. *Annu. Rev. Nucl. Sci.* **3**, 171-192.

MAGEE, J.L. and CHATTERJEE, A., 1980. Radiation chemistry of heavy-particle tracks. 1. General considerations. *J. Phys. Chem.* **84**, 3529-3536.

MAGEE, J.L. and CHATTERJEE, A., 1987. In: Freeman, G.R. (Ed.), *Kinetics of Nonhomogeneous Processes*. Wiley, New York, pp. 171-214.

MAHLMAN, H.A., 1961. The OH Yield in the Co^{60} γ Radiolysis of HNO_3. *J. Chem. Phys.*, **35**, 936-939.

MALKA, V., FAURE, J., and GAUDUEL, Y.A., 2010. Ultra-short electron beams based spatio-temporal radiation biology and radiotherapy, *Mutat. Res.* **704**, 142-151.

MARIN, T.W., TAKAHASHI, K., JONAH, C.D., CHEMERISOV, S.D., and BARTELS, D.M., 2007. Recombination of the hydrated electron at high temperature and pressure in hydrogenated alkaline water. *J. Phys. Chem. A* **111**, 11540-11551.

McCRACKEN, D.R., TSANG, K.T., and LAUGHTON, P.J., 1998. Aspects of the physics and chemistry of water radiolysis by fast neutrons and fast electrons in nuclear reactors. Report AECL-11895. Atomic Energy of Canada Ltd., Chalk River, ON.

MEESUNGNOEN, J., BENRAHMOUNE, M., FILALI-MOUHIM, A., MANKHETKORN, S., and JAY-GERIN, J.-P., 2001. Monte Carlo calculation of the primary radical and molecular yields of liquid water radiolysis in the linear energy transfer range 0.3-6.5 keV/μm: Application to ^{137}Cs gamma rays. *Radiat. Res.* **155**, 269-278.

MEESUNGNOEN, J., JAY-GERIN, J.-P., FILALI-MOUHIM, A., and MANKHETKORN, S., 2002*a*. On the temperature dependence of the primary yield and the product $G\varepsilon_{max}$ of hydrated electrons in the low-LET radiolysis of liquid water. *Can. J. Chem.* **80**, 767-773.

MEESUNGNOEN, J., JAY-GERIN, J.-P., FILALI-MOUHIM, A., and MANKHETKORN, S., 2002*b*. Low-energy electron penetration range in liquid water. *Radiat. Res.* **158**, 657-660.

MEESUNGNOEN, J. and JAY-GERIN, J.-P., 2005*a*. High-LET radiolysis of liquid water with $^{1}H^{+}$, $^{4}He^{2+}$, $^{12}C^{6+}$, and $^{20}Ne^{9+}$. *J. Phys. Chem. A* **109**, 6406-6419.

MEESUNGNOEN, J. and JAY-GERIN, J.-P., 2005*b*. Effect of multiple ionization on the yield of H_2O_2 produced in the radiolysis of aqueous 0.4 *M* H_2SO_4 solutions by high-LET $^{12}C^{6+}$ and $^{20}Ne^{9+}$ ions. *Radiat. Res.* **164**, 688-694.

MEESUNGNOEN, J., 2007. *Effect of multiple ionization on the radiolysis of liquid water irradiated with heavy ions: A theoretical study using Monte-Carlo simulations*. Ph.D. Thesis, Université de Sherbrooke.

MEESUNGNOEN, J., JAY-GERIN, J.-P., 2011. Radiation chemistry of liquid water with heavy ions: Monte Carlo simulation studies, in *Charged Particle and Photon Interactions with Matter: Recent Advances, Applications, and Interfaces*, edited by Hatano, Y., Katsumura, Y., and Mozumder, A., 2011. Taylor and Francis, Boca Raton), pp. 355-400.

MEESUNGNOEN, J., SANGUANMITH, S., JAY-GERIN, J.-P., 2015. Yields of H_2 and hydrated electrons in low-LET radiolysis of water determined by Monte Carlo track chemistry simulations using phenol/N_2O aqueous solutions up to 350 °C. *RSC Adv.* **5**, 76813-76824.

MELTON, C.E., 1972. Cross sections and interpretation of dissociative attachment reactions producing OH^{-}, O^{-}, and H^{-} in H_2O. *J. Chem. Phys.* **57**, 4218-4225

MICHAUD, M., CLOUTIER, P., and SANCHE, L., 1991. Low-energy electron-energy-loss spectroscopy of amorphous ice: Electronic excitations. *Phys. Rev. A* **44**, 5624-5627.

MICHAUD, M., WEN, A., and SANCHE, L., 2003. Cross sections for low-energy (1-100 eV) electron elastic and inelastic scattering in amorphous ice. *Radiat. Res.* **159**, 3-22.

MICHAUD, M. and SANCHE, L., 1987. Absolute vibrational excitation cross section for slow-electron (1-18 eV) scattering in solid H_2O. *Phys. ReV. A* **36**, 4684-4699.

MIGUS, A., GAUDUEL, Y., MARTIN, J. L., ANTONETTI, A., 1987. Excess electrons in liquid water: First evidence of a prehydrated state with femtosecond lifetime. *Phys. Rev. Lett.* **58**, 1559-1562.

MIKKELSEN, R.B. and WARDMAN, P., 2003. Biological chemistry of reactive oxygen and nitrogen and radiation-induced signal transduction mechanisms. *Oncogene* **22**, 5734-5754.

MIRSALEH KOHAN, L., SANGUANMITH, S., MEESUNGNOEN, J., CAUSEY, P., STUART, C. R., and JAY-GERIN, J., 2013. Self-radiolysis of tritiated water. 1. A comparison of the effects of ^{60}Co γ-rays and tritium β-particles on water and aqueous solutions at room temperature. *RSC Adv.*, **3**, 19282-19299.

MOZUMDER, A. and MAGEE, J.L., 1966*a*. Model of tracks of ionizing radiations for radical reaction mechanisms. *Radiat. Res.* **28**, 203-214.

MOZUMDER, A. and MAGEE, J.L., 1966*b*. Theory of radiation chemistry. VII. Structure and reactions in low LET tracks. *J. Chem. Phys.* **45**, 3332-3341.

MOZUMDER, A., CHATTERJEE, A., and MAGEE, J.L., 1968. Theory of radiation chemistry. IX. Model and structure of heavy particle tracks in water. *Adv. Chem. Series* **81**, 27-48.

MOZUMDER, A., 1999. *Fundamentals of Radiation Chemistry*. Academic Press, San Diego, CA.

MUROYA, Y., MEESUNGNOEN, J., JAY-GERIN, J.-P., FILALI-MOUHIM, A.,

GOULET, T., KATSUMURA, Y., and MANKHETKORN, S., 2002. Radiolysis of liquid water: An attempt to reconcile Monte-Carlo calculations with new experimental hydrated electron yield data at early times. *Can. J. Chem.* **80**, 1367-1374.

MUROYA, Y., PLANTE, I., AZZAM, E.I., MEESUNGNOEN, J., KATSUMURA, Y., and JAY-GERIN, J.-P., 2006. High-LET ion radiolysis of water: Visualization of the formation and evolution of ion tracks and relevance to the radiation-induced bystander effect. *Radiat. Res.* **165**, 485-491.

MUROYA, Y., LIN, M., DE WAELE, V., HATANO, Y., KATSUMURA, Y., and MOSTAFAVI, M., 2010. First observation of picosecond kinetics of hydrated electrons in supercritical water. *J. Phys. Chem. Lett.* **1**, 331-335.

MUROYA, Y., YAMASHITA, S., LERTNAISAT, P., SANGUANMITH, S., MEESUNGNOEN, J., JAY-GERIN, J.-P. and Katsumura, Y., 2017. Rate constant for the $H^{\bullet} + H_2O \rightarrow {}^{\bullet}OH + H_2$ reaction at elevated temperatures measured by pulse radiolysis. *Physical Chemistry Chemical Physics* **19**, 30834-30841.

NIKJOO, H., UEHARA, S., EMFIETZOGLOU, D., and CUCINOTTA, F.A., 2006. Track-structure codes in radiation research. *Radiat. Meas.* **41**, 1052-1074.

NOYES, R.M., 1961. Effects of diffusion rates on chemical kinetics. In: Porter, G. and Stevens, B. (Eds.), *Progress in Reaction Kinetics*, vol. 1. Pergamon Press, Oxford, pp. 129-160.

MATATLA, N., M., LAFOND, F., JAY-GERIN, J.-P., and SOLDERA, A., 2016. Heterogeneous character of supercritical water at 400 °C and different densities unveiled by simulation. *RSC Adv.*, **6**, 30484-30487.

OGURA, H. and HAMILL, W.H., 1973. Positive hole migration in pulse-irradiated water and heavy water. *J. Phys. Chem.* **77**, 2952-2954.

O'NEILL, P. and FIELDEN, E.M., 1993. Primary free radical processes in DNA, *Adv. Radiat. Biol.* **17**, 53-120.

O'NEILL, P. and WARDMAN, P., 2009. Radiation chemistry comes before radiation biology, *Int. J. Radiat. Biol.* **85**, 9-25.

OWEN, B.B. and CURRY, R.W., 1938. The electrolytic conductivity of zinc sulfate and copper sulfate in water at 25°C. *J. Am. Chem. Soc.* **60**, 3074-3078.

PARETZKE, H.G., 1987. Radiation track structure theory. In: Freeman, G.R. (Ed.), *Kinetics of Nonhomogeneous Processes*. Wiley, New York, pp. 89-170.

PARETZKE, H.G., GOODHEAD, D.T., KAPLAN, I.G., and TERRISSOL, M., 1995. Track structure quantities. In: *Atomic and Molecular Data for Radiotherapy and Radiation Research*, IAEA-TECDOC-799. International Atomic Energy Agency, Vienna, pp. 633-721.

PASTINA, B., LAVERNE, J.A., and PIMBLOTT, S.M., 1999. Dependence of molecular hydrogen formation in water on scavengers of the precursor to the hydrated electron. *J. Phys. Chem. A* **103**, 5841-5846.

PASTINA, B. and LAVERNE, J.A., 1999a. Scavenging of the precursor to the hydrated electron by the selenate ion, *J. Phys. Chem. A* **103**, 209-212.

PASTINA, B. and LAVERNE, J.A., 1999b. Hydrogen peroxide production in the radiolysis of water with heavy ions. *J. Phys. Chem. A* **103**, 1592-1597.

PASTINA, B. and LAVERNE, J.A., 2001. Effect of molecular hydrogen on hydrogen peroxide in water radiolysis. *J. Phys. Chem. A* **105**, 9316-9322.

PELED, E. and CZAPSKI, G., 1970. Molecular hydrogen formation (GH2) in the radiation chemistry of aqueous solutions. *J. Phys. Chem.* **74**, 2903–2911.

PELED, E., MIRSKI, U., CZAPSKI, G., 1971. Radiation chemistry of aqueous solutions: On the contribution of H atoms to GH_2 in the radiation chemistry of aqueous solutions. *J. Phys. Chem*. **75**, 31-35.

PELOWITZ, D.B., (Ed.), 2013. *MCNP6 User's Manual Version 1.0*, Report LA-CP-13-00634 (Los Alamos National Laboratory, Los Alamos, NM).

PIMBLOTT, S.M., LAVERNE, J.A., MOZUMDER, A., and GREEN, N.J.B., 1990. Structure of electron tracks in water. 1. Distribution of energy deposition events. *J. Phys. Chem.* **94**, 488-495.

PIMBLOTT, S.M., LAVERNE, J.A., 1998. On the radiation chemical kinetics of the precursor to the hydrated electron, *J. Phys. Chem. A* **102**, 2967-2975.

PIMBLOTT, S.M. and MOZUMDER, A., 1991. Structure of electron tracks in water. 2. Distribution of primary ionizations and excitations in water radiolysis. *J. Phys. Chem.* **95**, 7291-7300.

PIMBLOTT, S.M., PILLING, M.J., and GREEN, N.J.B., 1991. Stochastic models of spur kinetics in water. *Radiat. Phys. Chem.* **37**, 377-388.

PIMBLOTT, S.M. and GREEN, N.J.B., 1995. Recent advances in the kinetics of radiolytic processes. In: Compton, R.G. and Hancock, G. (Eds.), *Research in Chemical Kinetics*, vol. 3. Elsevier, Amsterdam, pp. 117-174.

PIMBLOTT, S.M. and MOZUMDER, A., 2004. Modeling of physicochemical and chemical processes in the interactions of fast charged particles with matter. In: Mozumder, A. and Hatano, Y. (Eds.), *Charged Particle and Photon Interactions with Matter: Chemical, Physicochemical, and Biological Consequences with Applications*. Marcel Dekker, New York, pp. 75-103.

PIMBLOTT, S.M., LAVERNE, J.A., 2007. Production of low-energy electrons by ionizing radiation, *Radiat. Phys. Chem.* **76**, 1244-1247.

PLANTE, I.L., FILALI-MOUHIM, A., and JAY-GERIN, J.-P., 2005. SimulRad: A Java interface for a Monte-Carlo simulation code to visualize in 3D the early stages of water radiolysis. *Radiat. Phys. Chem.* **72**, 173-180.

PLANTE, I., 2009. Développement de codes de simulation Monte-Carlo de la radiolyse de l'eau et de solutions aqueuses par des électrons, ions lourds, photons et neutrons : Application à divers sujets d'intérêt expérimental. Ph.D. Thesis, Université de Sherbrooke.

PLATZMAN, R.L., 1955. Subexcitation electrons. *Radiat. Res.* **2**, 1-7.

PLATZMAN, R.L., 1958. The physical and chemical basis of mechanisms in radiation biology. In: Claus, W.D. (Ed.), *Radiation Biology and Medicine. Selected Reviews in the Life Sciences*. Addison-Wesley, Reading, MA, pp. 15-72.

PLATZMAN, R.L., 1962*a*. Superexcited states of molecules. *Radiat. Res.* **17**, 419-425.

PLATZMAN, R.L., 1962*b*. Dissociative attachment of subexcitation electrons in liquid water, and the origin of radiolytic "molecular" hydrogen. In: Abstract of Papers, Second International Congress of Radiation Research, Harrogate, England, August 5-11, 1962, p. 128.

PRYOR, W.A., and SQUADRITO, S.L., 1995. The chemistry of peroxynitrite: A product from the reaction of nitric oxide with superoxide, *Am. J. Physiol. Lung Cell. Mol. Physiol.* **268**, L699-722.

PSCHENICHNIKOV, M.S., BALTUSKA, A., and WIERSMA, D.A., 2004. Hydrated-

electron population dynamics, *Chem. Phys. Lett.* **389**, 171-175.
RAY, S. G., DAUBE, S. S., NAAMAN, R., 2005. On the capturing of low-energy electrons by DNA, *Proc. Natl. Acad. Sci.* **102**, 15-19.
ROBINSON, R.A. and STOKES, R.H., 1959. *Electrolyte Solutions: The Measurement and Interpretation of Conductance, Chemical Potential and Diffusion in Solutions of Simple Electrolytes*, 2nd ed. (revised). Butterworths Publications Ltd., London, UK.
ROTH, O. and LAVERNE, J.A., 2011, Effect of pH on H_2O_2 production in the radiolysis of water. *Phys. Chem. A.*, **115**, 700-708.
ROWNTREE, P., PARENTEAU, L., and SANCHE, L., 1991. Electron stimulated desorption via dissociative attachment in amorphous H_2O. *J. Chem. Phys.* **94**, 8570-8576.
SAMUEL, A.H. and MAGEE, J.L., 1953. Theory of radiation chemistry. II. Track effects in radiolysis of water. *J. Chem. Phys.* **21**, 1080-1087.
SANCHE, L., 2002. Nanoscopic aspects of radiobiological damage: Fragmentation induced by secondary low-energy electrons. *Mass Spectrom. Rev.* **21**, 349-369.
SANGUANMITH, S., MUROYA, Y., MEESUNGNOEN, J., LIN, M., KATSUMURA, Y., MIRSALEH KOHAN, L., GUZONAS, D.A., STUART, C.R., and JAY-GERIN, J.-P., 2011*a*. Low-linear energy transfer radiolysis of liquid water at elevated temperatures up to 350°C: Monte-Carlo simulations. *Chem. Phys. Lett*. **508**, 224-230.
SANGUANMITH, S., MUROYA, Y., TIPPAYAMONTRI, T., MEESUNGNOEN, J., LIN, M., KATSUMURA, Y., and JAY-GERIN, J.-P., 2011*b*. Temperature dependence of the Fricke dosimeter and spur expansion time in the low-LET high-temperature radiolysis of water up to 350 °C: a Monte-Carlo simulation study. *Phys. Chem. Chem. Phys.* **13**, 10690-10698.
SANGUANMITH, S., MEESUNGNOEN, J., STUART, C.R., CAUSEY, P., and JAY-GERIN, J.-P., 2018. Self-radiolysis of tritiated water. 4. The scavenging effect of azide ions (N_3^-) on the molecular hydrogen yield in the radiolysis of water by ^{60}Co γ-rays and tritium β-particles at room temperature. *RSC. Ads.* **8**, 2449-2458.
SAUER, M.C., Jr., SCHMIDT, K.H., HART, E.J., NALEWAY, C.A., and JONAH, C.D., 1977. LET dependence of transient yields in the pulse radiolysis of aqueous systems with deuterons and α particles. *Radiat. Res.* **70**, 91-106.
SCHULER, R.H. and ALLEN, A.O., 1957. Radiation chemistry studies with cyclotron beams of variable energy: Yields in aerated ferrous sulfate solution. *J. Am. Chem. Soc.* **79**, 1565-1572.
SCHWARZ, H. A., 1955. The Effect of Solutes on the Molecular Yields in the Radiolysis of Aqueous Solutions. *J. Am. Chem. Soc.* **77**, 19, 4960–4964.
SCHWARZ, H. A., 1969. Applications of the Spur diffusion Model to the Radiation Chemistry of Aqueous Solutions *J. Phys. Chem.* **73**, 1928– 1937
SILVA, C., WALHOUT, P. K., YOKOYAMA, K., BARBARA, P. F., 1998. Femtosecond solvation dynamics of the hydrated electron, *Phys. Rev. Lett.* **80**, 1086.
SIMS, H.E., 2006. Yields of radiolysis products from γ-irradiated supercritical water – A re-analysis data by W.G. Burns and W.R. Marsh. *Radiat. Phys. Chem.* 75, 1047-1050.
SIMS, H.E., HENSHAW, J., and BARTELS, D., 2010. The critical hydrogen

concentration in PWR coolant. 8th International Radiolysis, Electrochemistry & Materials Performance Workshop, Québec City, Quebec, Canada, October 8, 2010.

SOLOMON, T., 2001. The definition and unit of ionic strength. *J. Chem. Educ.* **78**, 1691-1692.

SPINKS, J.W.T. and WOODS, R.J., 1990. *An Introduction to Radiation Chemistry*, 3rd ed. Wiley, New York.

SPITZ, D.R., AZZAM, E.I., LI, J.J., and GIUS, D., 2004. Metabolic oxidation/reduction reactions and cellular responses to ionizing radiation: A unifying concept in stress response biology, *Cancer Metastasis Rev.* **23**, 311-322.

STERNICZUK, M.; BARTELS, D. M., 2016. Source of Molecular Hydrogen in High-Temperature Water Radiolysis. *J. Phys. Chem. A* **120**, 200– 209.

STRAUME, T. and CARSTEN, A. L., 1993. Tritium Radiobiology and Relative Biological Effectiveness. *Health Phys.*, 65, 657-672.

SUNARYO, G.R., KATSUMURA, Y., HIROISHI, D., and ISHIGURE, K., 1995*b*. Radiolysis of water at elevated temperatures–II. Irradiation with γ-rays and fast neutrons up to 250°C. *Radiat. Phys. Chem.* **45**, 131-139.

SWIATLA-WOJCIK, D. and BUXTON, G.V., 1995. Modeling of radiation spur processes in water at temperatures up to 300 ºC. *J. Phys. Chem.* **99**, 11464-11471.

SWIATLA-WOJCIK, D. and BUXTON, G.V., 2005. On the possible role of the reaction $H^{\bullet} + H_2O \rightarrow H_2 + {}^{\bullet}OH$ in the radiolysis of water at high temperatures. *Radiat. Phys. Chem.* **74**, 210-219.

SWIATLA-WOJCIK, D. and BUXTON, G.V., 2010. Reply to comment on the possible role of the reaction $H^{\bullet} + H_2O \rightarrow H_2 + {}^{\bullet}OH$ in the radiolysis of water at high temperatures. *Radiat. Phys. Chem.* **79**, 52-56.

TIPPAYAMONTRI, T., SANGUANMITH, S., MEESUNGNOEN, J., SUNARYO, G.R., and JAY-GERIN, J.-P., 2009. Fast neutron radiolysis of the ferrous sulfate (Fricke) dosimeter: Monte-Carlo simulations. *Recent Res. Devel. Physical Chem.* **10**, 143-211.

TAUBE, H., 1957. Photochemical reactions of ozone in solution. *Trans. Faraday Soc.* **53**, 656-665.

TOBUREN, L.H., 2004. Ionization and secondary electron production by fast charged particles. In: Mozumder, A. and Hatano, Y. (Eds.), *Charged Particle and Photon Interactions with Matter: Chemical, Physicochemical, and Biological Consequences with Applications*. Marcel Dekker, New York, pp. 31-74.

TUBIANA, M., 2009. Can we reduce the incidence of second primary malignancies occurring after radiotherapy? A critical review, *Radiother. Oncol.* **91**, 4-15.

TURI, L., BORGIS, D., 2002. Analytical investigations of an electron-water molecule pseudopotential. II. development of a new pair potential and molecular dynamics simulations, *J. Chem. Phys.* **117**, 6186-6195.

TURNER, J.E., MAGEE, J.L., HAMM, R.N., CHATTERJEE, A., WRIGHT, H.A., and RITCHIE, R.H., 1981. Early events in irradiated water. In: Booz, J., Ebert, H.G., and Hartfiel, H.D. (Eds.), *Seventh Symposium on Microdosimetry*, Oxford, U.K., Sept. 8-12, 1980. Harwood Academic Publ., London, pp. 507-520.

TURNER, J.E., MAGEE, J.L., WRIGHT, H.A., CHATTERJEE, A., HAMM, R.N., and RITCHIE, 1983. Physical and chemical development of electron tracks in liquid water. *Radiat. Res.* **96**, 437-449.

TURNER, J.E., HAMM, R.N., WRIGHT, H.A., RITCHIE, R.H., MAGEE, J.L., CHATTERJEE, A., and BOLCH, W.E., 1988. Studies to link the basic radiation physics and chemistry of liquid water. *Radiat. Phys. Chem.* **32**, 503-510.

UEHARA, S. and NIKJOO, H., 2006. Monte Carlo simulation of water radiolysis for low-energy charged particles. *J. Radiat. Res.* **47**, 69-81.

WANG, C.-R., HU, A., LU, Q.-B., 2006. Direct observation of the transition state of ultrafast electron transfer reaction of a radiosensitizing drug bromodeoxyuridine, *J. Chem. Phys.* **124**, 241102-4.

WANG, C.-R.and LU, Q.-B., 2007. Real-time observation of a molecular reaction mechanism of aqueous 5- halo-2'-deoxyuridines under UV/Ionizing radiation, *Angew. Chem. Int. Ed.* **46**, 6316-6320.

WANG, C.-R., LUO, T., and LU, Q.-B., 2008. On the lifetimes and physical nature of incompletely relaxed electrons in liquid water, *Phys. Chem. Chem. Phys.* **10**, 4463-4470.

WANG, C.-R., NGUYEN, J., LU, Q.-B., 2009. Bond breaks of nucleotides by dissociative electron transfer of nonequilibrium prehydrated electrons: A new molecular mechanism for reductive DNA damage, *J. Am. Chem. Soc.* **191**, 11320-11322

WANG, C.-R. and LU, Q.-B., 2010. Molecular mechanism of the DNA sequence selectivity of 5-halo-2'- deoxyuridines as potential radiosensitizers, *J. Am. Chem. Soc.* **132**, 14710-14713.

WANG, C., 2012. *Prehydrated Electron and Its Role in Ionizing Radiation Induced DNA Damage and Molecular Mechanisms of Action of Halogenated Sensitizers for Radiotherapy of Cancer*. Ph.D. Thesis, University of Waterloo, Ontario, Canada.

WESTON, Jr., R.E. and SCHWARZ, H.A., 1972. *Chemical Kinetics*. Prentice-Hall, Englewood Cliffs, New Jersey.

WILSON, C.D., DUKES, C.A., and BARAGIOLA, R.A., 2001. Search for the plasmon in condensed water. *Phys. Rev. B* **63**, 121101-4.

YAKABUSKIE, P.A., JOSEPH, J.M., STUART, C.R., and CLARA WREN, J., 2011. Long-term γ-radiolysis kinetics of NO_3^- and NO_2^- solutions. *J.Phys.Chem.* **115**, 4270-4278.

YOKOYAMA, K., SILVA, C., SON, D. H., WALHOUT, P. K., BARBARA, P. F., 1998. Detailed investigation of the femtosecond pump-probe spectroscopy of the hydrated electron, *J. Phys. Chem. A.* **102**, 6957-6966.

ZEWAIL, A.H., 2000. Femtochemistry: Atomic-scale dynamics of the chemical bond using ultrafast lasers (Nobel Lecture), *Angew. Chem. Int. Ed.* **39**, 2586-2631.

APPENDIX 1

LISTE DES PUBLICATIONS
Sunuchakan SANGUANMITH
(2014-2021)

Ph.D. Student in « Radiation Sciences and Biomedical Imaging »
Faculty of Medicine and Health Sciences, Université de Sherbrooke

Start date: September 2nd, 2014

During her Ph.D. thesis, Sunuchakan was awarded a NSERC doctoral scholarship (3 years).

Supervisor: Jean-Paul Jay-Gerin

---

1. "LOW-LET RADIATION CHEMISTRY OF SUPERCRITICAL WATER AT 400 °C: A RE-ANALYSIS OF THE WATER DENSITY DEPENDENCE OF THE SPUR LIFETIME AND THE "ESCAPE" e^-_{aq} YIELD"
S. Sanguanmith, J. Meesungnoen, D.A. Guzonas, C.R. Stuart and J.-P. Jay-Gerin,
Recent Research Developments in Physical Chemistry **11**, 1-14 (2014).
ISBN: 978-81-7895-608-4.

2. "RADIOLYSIS OF THE CERIC-CEROUS SULFATE DOSIMETER AT ELEVATED TEMPERATURES: MONTE CARLO SIMULATIONS"
L. Mirsaleh Kohan, J. Meesungnoen, **S. Sanguanmith**, R. Meesat and J.-P. Jay-Gerin,
Recent Research Developments in Physical Chemistry **11**, 15-27 (2014).
ISBN: 978-81-7895-608-4.

3. "EFFECT OF TEMPERATURE ON THE LOW-LINEAR ENERGY TRANSFER RADIOLYSIS OF THE CERIC-CEROUS SULFATE DOSIMETER: A MONTE CARLO SIMULATION STUDY"
L. Mirsaleh Kohan, J. Meesungnoen, **S. Sanguanmith**, R. Meesat and J.-P. Jay-Gerin,
Radiation Research **181** (*5*), 495-502 (2014).
DOI: 10.1667/RR13592.1
Impact factor: 2.911

4. "CALCULATION OF THE YIELDS FOR THE PRIMARY SPECIES FORMED FROM THE RADIOLYSIS OF LIQUID WATER BY FAST NEUTRONS AT TEMPERATURES BETWEEN 25-350 °C"
S.L. Butarbutar, **S. Sanguanmith**, J. Meesungnoen, G.R. Sunaryo and J.-P. Jay-Gerin,

Radiation Research **181** (*6*), 659-665 (2014).
DOI: 10.1667/RR13638.1
Impact factor: 2.911

5. "SELF-RADIOLYSIS OF TRITIATED WATER. 2. DENSITY DEPENDENCE OF THE YIELDS OF PRIMARY SPECIES FORMED IN THE RADIOLYSIS OF SUPERCRITICAL WATER BY TRITIUM β-PARTICLES AT 400 °C"
S.L. Butarbutar, **S. Sanguanmith**, J. Meesungnoen, P. Causey, C.R. Stuart and J.-P. Jay-Gerin,
Royal Society of Chemistry Advances **4** (*44*), 22980-22988 (2014).
DOI: 10.1039/c4ra02761b
Impact factor: 3.485

6. "YIELDS OF H_2 AND HYDRATED ELECTRONS IN LOW-LET RADIOLYSIS OF WATER DETERMINED BY MONTE CARLO TRACK CHEMISTRY SIMULATIONS USING PHENOL/N_2O AQUEOUS SOLUTIONS UP TO 350 °C"
J. Meesungnoen, **S. Sanguanmith** and J.-P. Jay-Gerin,
Royal Society of Chemistry Advances **5** (*94*), 76813-76824 (2015).
DOI: 10.1039/c5ra15801j
Impact factor: 3.289

7. "RADIOLYSIS OF SUPERCRITICAL WATER AT 400 °C: A SENSITIVITY STUDY OF THE DENSITY DEPENDENCE OF THE YIELD OF HYDRATED ELECTRONS ON THE ($e^-_{aq} + e^-_{aq}$) REACTION RATE CONSTANT"
S. Sanguanmith, J. Meesungnoen, D.A. Guzonas, C.R. Stuart and J.-P. Jay-Gerin,
ASME Journal of Nuclear Engineering and Radiation Science **2** (*2*), article no. 021014 (February 29, 2016).
DOI: 10.1115/1.4031013
(*ASME*: "The American Society of Mechanical Engineers")
Impact factor: not indexed yet.

8. "MONTE CARLO TRACK CHEMISTRY SIMULATIONS OF THE RADIOLYSIS OF WATER INDUCED BY THE RECOIL IONS OF THE $^{10}B(n,\alpha)^7Li$ NUCLEAR REACTION. 1. CALCULATION OF THE YIELDS OF PRIMARY SPECIES UP TO 350 °C"
Muhammad Mainul Islam, P. Lertnaisat, J. Meesungnoen, **S. Sanguanmith**, J.-P. Jay-Gerin, Y. Katsumura, S. Mukai, R. Umehara, Y. Shimizu and M. Suzuki,
Royal Society of Chemistry Advances **7** (*18*), 10782-10790 (2017).
DOI: 10.1039/c6ra28586d
Impact factor: 3.108
("Open Access")

9. "WATER RADIOLYSIS INDUCED BY THE RECOIL IONS OF THE $^{10}B(n,\alpha)^7Li$ NUCLEAR REACTION: MONTE CARLO CALCULATION OF THE YIELDS OF CHEMICAL SPECIES UP TO 350 °C"

M.M. Islam, P. Lertnaisat, J. Meesungnoen, **S. Sanguanmith**, Y. Katsumura, S. Mukai, R. Umehara, Y. Shimizu, M. Suzuki and J.-P. Jay-Gerin,
in "***Proceedings of the 8th International Symposium on Supercritical Water-Cooled Reactors, Chengdu (China), 13-15 March 2017***", p. 138-153.

10. "GENERATION OF ULTRAFAST TRANSIENT ACID SPIKES IN HIGH-TEMPERATURE WATER IRRADIATED WITH LOW LINEAR ENERGY TRANSFER RADIATION"
V. Kanike, J. Meesungnoen, **S. Sanguanmith**, D.A. Guzonas, C.R. Stuart and J.-P. Jay-Gerin,
CNL Nuclear Review **6** (*1*), 31-40 (2017).
DOI: 10.12943/CNR.2016.00013

11. "RATE CONSTANT FOR THE $H^{\bullet} + H_2O \rightarrow {}^{\bullet}OH + H_2$ REACTION AT ELEVATED TEMPERATURES MEASURED BY PULSE RADIOLYSIS"
Y. Muroya, S. Yamashita, P. Lertnaisat, **S. Sanguanmith**, J. Meesungnoen, J.-P. Jay-Gerin and Y. Katsumura,
Physical Chemistry Chemical Physics **19** (*45*), 30834-30841 (2017)
DOI: 10.1039/c7cp06010f
Impact factor: 4.123

12. "SELF-RADIOLYSIS OF TRITIATED WATER. 4. THE SCAVENGING EFFECT OF AZIDE IONS (N_3^-) ON THE MOLECULAR HYDROGEN YIELD IN THE RADIOLYSIS OF WATER BY ^{60}Co γ-RAYS AND TRITIUM β-PARTICLES AT ROOM TEMPERATURE"
S. Sanguanmith, J. Meesungnoen, C.R. Stuart, P. Causey and J.-P. Jay-Gerin,
Royal Society of Chemistry Advances **8** (*5*), 2449-2458 (2018)
DOI: 10.1039/c7ra12397c
Impact factor: 3.108
("Open Access")

13. "EVALUATION OF THE RADIOPROTECTIVE ABILITY OF CYSTAMINE FOR 150 keV-500 MeV PROTON IRRADIATION: A MONTE CARLO TRACK CHEMISTRY SIMULATION STUDY"
Esteban Sepúlveda, **S. Sanguanmith**, J. Meesungnoen and J.-P. Jay-Gerin,
Canadian Journal of Chemistry **97** (*2*), 100-111 (2019)
DOI: 10.1139/cjc-2018-0382
Impact factor: 1.252

14. "LOW LINEAR ENERGY TRANSFER RADIOLYSIS OF SUPERCRITICAL WATER AT 400 °C: *IN SITU* GENERATION OF ULTRAFAST, TRANSIENT, DENSITY-DEPENDENT "ACID SPIKES""
Md Mohsin Patwary, V. Kanike, **S. Sanguanmith**, J. Meesungnoen, M.M. Islam and J.-P. Jay-Gerin,
Physical Chemistry Chemical Physics **21** (*13*), 7137-7146 (2019) (2019)
DOI: 10.1039/c9cp00790c

Impact factor: 3.567

15. "“ACID-SPIKE” FORMATION IN THE FAST NEUTRON RADIOLYSIS OF SUPERCRITICAL WATER AT 400 °C STUDIED BY MONTE CARLO TRACK CHEMISTRY SIMULATIONS"
Md M. Patwary, **S. Sanguanmith**, J. Meesungnoen and J.-P. Jay-Gerin,
Canadian Journal of Chemistry **97** (*5*), 366-372 (2019)
DOI: 10.1139/cjc-2018-0505
Impact factor: 1.252

16. "FORMATION OF LOCAL, TRANSIENT “ACID SPIKES” IN THE FAST NEUTRON RADIOLYSIS OF SUPERCRITICAL WATER AT 400 °C: A POTENTIAL SOURCE OF CORROSION IN SUPERCRITICAL WATER-COOLED REACTORS?"
Md M. Patwary, **S. Sanguanmith**, J. Meesungnoen and J.-P. Jay-Gerin,
ASME Journal of Nuclear Engineering and Radiation Science **6** (*3*), article no. 031101 (July 2020).
DOI: 10.1115/1.4044409
Impact factor: 0.52
(*ASME*: “The American Society of Mechanical Engineers”)

This paper was published in a Special Section of the journal, entitled: “*Selected Papers From the Ninth International Symposium on Supercritical Water-Cooled Reactors, Vancouver, British Columbia, 10-14 March 2019*”, edited by Laurence Leung, David Guzonas and Thomas Schulenberg.

17. "SCAVENGING OF “DRY” ELECTRONS PRIOR TO HYDRATION BY AZIDE IONS: EFFECT ON THE FORMATION OF H_2 IN THE RADIOLYSIS OF WATER BY ^{60}Co γ-RAYS AND TRITIUM β-ELECTRONS"
S. Sanguanmith, J. Meesungnoen, Yusa Muroya, and J.-P. Jay-Gerin,
Canadian Journal of Chemistry
Impact factor: 1.252
Submitted: December 2020

MAY 2021

APPENDIX 2 – TEMPERATURE DEPENDENCE OF THE REACTION RATE CONSTANTS THAT HAVE BEEN UPDATED IN OUR IRT PROGRAM

Temperature dependence of the reaction rate constants which intervene in the chemical stage of radiolysis of pure liquid water in 25-350 ^{o}C temperature range.

Temperature(^{o}C)	25	50	100	150	200	250	300	350
Reactions								
1) $H^{\bullet} + H^{\bullet} \rightarrow H_2$	5.20E+09	8.43E+09	1.83E+10	3.30E+10	5.25E+10	7.65E+10	1.04E+11	1.36E+11
2) $H^{\bullet} + {}^{\bullet}OH \rightarrow H_2O$	1.61E+10	2.14E+10	3.37E+10	4.77E+10	6.26E+10	7.80E+10	9.36E+10	1.09E+11
3) $H^{\bullet} + H_2O_2 \rightarrow {}^{\bullet}OH + H_2O$	3.60E+07	6.95E+07	1.99E+08	4.45E+08	8.39E+08	1.40E+09	2.14E+09	3.05E+09
4) $H^{\bullet} + e^{-}_{aq} \rightarrow H_2 + OH^{-}$	2.76E+10	4.28E+10	9.33E+10	1.69E+11	2.48E+11	2.99E+11	3.14E+11	3.17E+11
5) $H^{\bullet} + OH^{-} \rightarrow e^{-}_{aq} + H_2O$	2.44E+07	8.46E+07	4.99E+08	1.44E+09	2.86E+09	4.91E+09	8.03E+09	1.32E+10
6) $H^{\bullet} + O_2 \rightarrow HO_2^{\bullet}$	1.31E+10	1.87E+10	3.03E+10	4.08E+10	4.93E+10	5.58E+10	6.07E+10	6.42E+10
7) $H^{\bullet} + HO_2^{\bullet} \rightarrow H_2O_2$	1.12E+10	1.81E+10	3.85E+10	6.87E+10	1.09E+11	1.57E+11	2.13E+11	2.75E+11
8) $H^{\bullet} + O_2^{\bullet-} \rightarrow HO_2^{-}$	1.12E+10	1.81E+10	3.85E+10	6.87E+10	1.09E+11	1.57E+11	2.13E+11	2.75E+11
9) $H^{\bullet} + HO_2^{-} \rightarrow {}^{\bullet}OH + OH^{-}$	1.47E+09	3.26E+09	1.17E+10	3.06E+10	6.61E+10	1.26E+11	2.03E+11	2.27E+11
10) $H^{\bullet} + O(^3P) \rightarrow {}^{\bullet}OH$	2.02E+10	3.28E+10	7.14E+10	1.29E+11	2.07E+11	3.02E+11	4.13E+11	5.37E+11
11) $H^{\bullet} + O^{\bullet-} \rightarrow OH^{-}$	2.00E+10	3.39E+10	6.84E+10	1.11E+11	1.62E+11	2.26E+11	3.04E+11	3.99E+11
12) $H^{\bullet} + O_3 \rightarrow O_2 + {}^{\bullet}OH$	3.67E+10	5.40E+10	9.24E+10	1.35E+11	1.79E+11	2.24E+11	2.67E+11	3.12E+11

13) $H^{\bullet} + H_2O \rightarrow e^-_{aq} + H^+$	4.58E-05	1.01E-03	1.43E-01	6.27E+00	1.24E+02	1.38E+03	1.00E+04	5.36E+04
14) $H^{\bullet} + SO_4^{\bullet-} \rightarrow HSO_4^-$	9.96E+09	1.54E+10	3.12E+10	5.33E+10	8.10E+10	1.14E+11	1.50E+11	1.91E+11
15) $H^{\bullet} + S_2O_8^{2-} \rightarrow SO_4^{2-}$	1.40E+07	1.94E+07	3.32E+07	4.98E+07	6.83E+07	8.82E+07	1.09E+08	1.31E+08
16) $H^{\bullet} \rightarrow e^-_{aq} + H^+$	1.07E-01	9.20E-01	2.45E+01	2.13E+02	9.50E+02	2.63E+03	4.16E+03	2.78E+03
17) $^{\bullet}OH + {}^{\bullet}OH \rightarrow H_2O_2$	6.31E+09	7.56E+09	1.15E+10	1.35E+10	1.42E+10	1.39E+10	1.30E+10	1.18E+10
18) $^{\bullet}OH + H_2O_2 \rightarrow HO_2^{\bullet} + H_2O$	2.94E+07	4.52E+07	8.99E+07	1.52E+08	2.30E+08	3.22E+08	4.24E+08	5.35E+08
19) $^{\bullet}OH + H_2 \rightarrow H^{\bullet} + H_2O$	3.95E+07	7.10E+07	1.72E+08	3.62E+08	6.11E+08	7.88E+08	7.83E+08	6.19E+08
20) $^{\bullet}OH + e^-_{aq} \rightarrow OH^-$	3.55E+10	4.88E+10	8.50E+10	1.36E+11	2.01E+11	2.80E+11	3.72E+11	4.77E+11
21) $^{\bullet}OH + OH^- \rightarrow O^{\bullet-} + H_2O$	1.33E+10	2.17E+10	4.04E+10	6.06E+10	8.27E+10	1.07E+11	1.36E+11	1.68E+11
22) $^{\bullet}OH + HO_2^{\bullet} \rightarrow O_2 + H_2O$	9.00E+09	1.11E+10	1.54E+10	1.98E+10	2.41E+10	2.83E+10	3.23E+10	3.61E+10
23) $^{\bullet}OH + O_2^{\bullet-} \rightarrow O_2 + OH^-$	1.08E+10	1.52E+10	2.61E+10	3.96E+10	5.49E+10	7.16E+10	8.91E+10	1.07E+11
24) $^{\bullet}OH + HO_2^- \rightarrow HO_2^{\bullet} + OH^-$	8.32E+09	1.35E+10	2.95E+10	5.34E+10	8.53E+10	1.25E+11	1.70E+11	2.22E+11
25) $^{\bullet}OH + O(^3P) \rightarrow HO_2^{\bullet}$	2.02E+10	3.28E+10	7.14E+10	1.29E+11	2.07E+11	3.02E+11	4.13E+11	5.37E+11
Temperature(^{o}C)	25	50	100	150	200	250	300	350
Reactions								
26) $^{\bullet}OH + O^{\bullet-} \rightarrow HO_2^-$	1.00E+09	1.27E+09	1.87E+09	2.51E+09	3.16E+09	3.81E+09	4.45E+09	5.06E+09
27) $^{\bullet}OH + O_3^{\bullet-} \rightarrow O_2^{\bullet-} + HO_2^{\bullet}$	8.50E+09	1.15E+10	1.55E+10	1.78E+10	1.92E+10	2.03E+10	2.10E+10	2.15E+10
28) $^{\bullet}OH + O_3 \rightarrow HO_2^{\bullet} + O_2$	1.11E+08	1.81E+08	3.93E+08	7.13E+08	1.14E+09	1.67E+09	2.28E+09	2.96E+09
29) $^{\bullet}OH + H_2O \rightarrow O^{\bullet-} + H^+$	1.70E-03	7.94E-03	5.74E-02	1.88E-01	4.12E-01	6.56E-01	6.39E-01	2.58E-01
30) $^{\bullet}OH + HSO_4^- \rightarrow SO_4^{\bullet-}$	1.50E+05	2.48E+05	5.54E+05	1.02E+06	1.66E+06	2.46E+06	3.40E+06	4.46E+06
31) $H_2O_2 + e^-_{aq} \rightarrow {}^{\bullet}OH + OH^-$	1.10E+10	1.79E+10	3.91E+10	7.11E+10	1.14E+11	1.67E+11	2.29E+11	2.98E+11
32) $H_2O_2 + OH^- \rightarrow HO_2^- + H_2O$	1.33E+10	2.17E+10	4.04E+10	6.06E+10	8.27E+10	1.07E+11	1.36E+11	1.68E+11
33) $H_2O_2 + O(^3P) \rightarrow {}^{\bullet}OH + HO_2^{\bullet}$	1.60E+09	2.78E+09	6.73E+09	1.32E+10	2.25E+10	3.46E+10	4.93E+10	6.64E+10
34) $H_2O_2 + O^{\bullet-} \rightarrow HO_2^{\bullet} + OH^-$	5.55E+08	9.03E+08	1.97E+09	3.56E+09	5.69E+09	8.31E+09	1.14E+10	1.48E+10

35) $H_2O_2 + H_2O \rightarrow H^+ + HO_2^-$	1.70E-03	7.94E-03	5.74E-02	1.88E-01	4.12E-01	6.56E-01	6.39E-01	2.58E-01
36) $H_2O_2 + SO_4^{\bullet-} \rightarrow SO_4^{2-} + HO_2^{\bullet}$	1.19E+07	1.92E+07	3.90E+07	6.13E+07	8.42E+07	1.10E+08	1.41E+08	1.73E+08
37) $H_2 + O(^3P) \rightarrow H^{\bullet} + {}^{\bullet}OH$	4.77E+03	1.42E+04	8.07E+04	3.05E+05	8.70E+05	2.03E+06	4.09E+06	7.36E+06
38) $H_2 + O^{\bullet-} \rightarrow H^{\bullet} + OH^-$	1.28E+08	1.91E+08	3.63E+08	5.93E+08	8.74E+08	1.20E+09	1.55E+09	1.92E+09
39) $e^-_{aq} + e^-_{aq} \rightarrow H_2 + 2OH^-$	7.26E+09	1.44E+10	3.85E+10	7.52E+10	1.50E+10	4.57E+08	5.92E+06	5.53E+04
40) $e^-_{aq} + H^+ \rightarrow H^{\bullet}$	2.13E+10	2.89E+10	5.40E+10	8.91E+10	1.54E+11	3.05E+11	7.14E+11	1.93E+12
41) $e^-_{aq} + O_2 \rightarrow O_2^{\bullet-}$	2.34E+10	3.36E+10	5.99E+10	9.32E+10	1.32E+11	1.75E+11	2.21E+11	2.69E+11
42) $e^-_{aq} + HO_2^{\bullet} \rightarrow HO_2^-$	1.30E+10	1.95E+10	3.73E+10	6.11E+10	9.03E+10	1.24E+11	1.61E+11	2.00E+11
43) $e^-_{aq} + O_2^{\bullet-} \rightarrow H_2O_2 + 2OH^-$	1.30E+10	1.95E+10	3.73E+10	6.11E+10	9.03E+10	1.24E+11	1.61E+11	2.00E+11
44) e-aq + $HO_2^- \rightarrow O^{\bullet-} + OH^-$	3.51E+09	5.67E+09	1.22E+10	2.20E+10	3.49E+10	5.08E+10	6.91E+10	8.96E+10
45) $e^-_{aq} + O(^3P) \rightarrow O^{\bullet-}$	1.98E+10	3.17E+10	6.29E+10	1.04E+11	1.54E+11	2.09E+11	2.66E+11	3.26E+11
46) $e^-_{aq} + O^{\bullet-} \rightarrow OH^- + OH^-$	2.31E+10	2.96E+10	4.39E+10	5.93E+10	7.52E+10	9.11E+10	1.07E+11	1.22E+11
47) $e^-_{aq} + O_3 \rightarrow O_3^{\bullet-}$	3.57E+10	5.71E+10	1.13E+11	1.87E+11	2.77E+11	3.76E+11	4.79E+11	5.87E+11
48) $e^-_{aq} + H_2O \rightarrow H^{\bullet} + OH^-$	1.58E+01	4.71E+01	2.01E+02	4.38E+02	7.30E+02	1.18E+03	2.01E+03	3.55E+03
49) $e^-_{aq} + S_2O_8^{2-} \rightarrow SO_4^{2-} + SO_4^{\bullet-}$	7.78E+10	1.15E+11	2.16E+11	3.49E+11	5.10E+11	6.92E+11	8.91E+11	1.10E+12
50) $H^+ + OH^- \rightarrow H_2O$	1.18E+11	1.83E+11	3.22E+11	4.54E+11	6.05E+11	8.14E+11	1.13E+12	1.63E+12
51) $H^+ + O_2^{\bullet-} \rightarrow HO_2^{\bullet}$	5.02E+10	7.55E+10	1.27E+11	1.87E+11	2.71E+11	3.92E+11	5.69E+11	8.22E+11
52) $H^+ + HO_2^- \rightarrow H_2O_2$	5.02E+10	7.55E+10	1.27E+11	1.87E+11	2.71E+11	3.92E+11	5.69E+11	8.22E+11
53) $H^+ + O^{\bullet-} \rightarrow {}^{\bullet}OH$	5.02E+10	7.55E+10	1.27E+11	1.87E+11	2.71E+11	3.92E+11	5.69E+11	8.22E+11
54) $H^+ + O_3^{\bullet-} \rightarrow {}^{\bullet}OH + O_2$	9.00E+10	1.36E+11	2.36E+11	3.50E+11	4.87E+11	6.62E+11	9.03E+11	1.25E+12
55) $OH^- + HO_2^{\bullet} \rightarrow O_2^{\bullet-} + H_2O$	1.33E+10	2.17E+10	4.04E+10	6.06E+10	8.27E+10	1.07E+11	1.36E+11	1.68E+11
56) $OH^- + O(^3P) \rightarrow HO_2^-$	4.20E+08	4.22E+08	4.24E+08	4.25E+08	4.25E+08	4.25E+08	4.26E+08	4.26E+08
57) $OH^- + SO_4^{\bullet-} \rightarrow SO_4^{2-} + {}^{\bullet}OH$	2.12E+08	3.13E+08	5.87E+08	9.49E+08	1.39E+09	1.88E+09	2.42E+09	2.99E+09
58) $O_2 + O(^3P) \rightarrow O_3$	4.00E+09	4.62E+09	5.19E+09	5.45E+09	5.59E+09	5.68E+09	5.74E+09	5.78E+09

59) $O_2 + O^{\bullet-} \rightarrow O_3^{\bullet-}$	3.72E+09	5.28E+09	9.23E+09	1.41E+10	1.98E+10	2.60E+10	3.25E+10	3.93E+10
Temperature(^oC)	25	50	100	150	200	250	300	350
Reactions								
60) $HO_2^{\bullet} + HO_2^{\bullet} \rightarrow H_2O_2 + O_2$	1.94E+08	2.38E+08	3.31E+08	4.26E+08	5.19E+08	6.10E+08	6.96E+08	7.78E+08
61) $HO_2^{\bullet} + O_2^{\bullet-} \rightarrow O_2 + HO_2^-$	9.70E+07	1.27E+08	1.95E+08	2.70E+08	3.49E+08	4.30E+08	5.11E+08	5.90E+08
62) $HO_2^{\bullet} + O(^3P) \rightarrow O_2 + OH$	2.02E+10	3.28E+10	7.14E+10	1.29E+11	2.07E+11	3.02E+11	4.13E+11	5.37E+11
63) $HO_2^{\bullet} + H_2O \rightarrow O_2^{\bullet-} + H^+$	1.40E+04	2.54E+04	4.49E+04	4.54E+04	2.95E+04	1.29E+04	3.92E+03	8.78E+02
64) $O_2^{\bullet-} + O^{\bullet-} \rightarrow O_2 + 2OH^-$	6.00E+08	6.28E+08	6.55E+08	6.74E+08	6.97E+08	7.35E+08	8.10E+08	1.03E+09
65) $O_2^{\bullet-} + O_3 \rightarrow O_3^{\bullet-} + O_2$	1.50E+09	2.13E+09	3.73E+09	5.71E+09	7.99E+09	1.05E+10	1.31E+10	1.59E+10
66) $O_2^{\bullet-} + H_2O \rightarrow HO_2^{\bullet} + {}^{\bullet}OH^-$	1.55E-01	1.14E+00	2.09E+01	1.82E+02	1.20E+03	6.78E+03	2.87E+04	6.10E+04
67) $HO_2^- + O(^3P) \rightarrow {}^{\bullet}OH + O_2^{\bullet-}$	5.30E+09	6.53E+09	7.84E+09	8.48E+09	8.85E+09	9.09E+09	9.26E+09	9.38E+09
68) $HO_2^- + O^{\bullet-} \rightarrow OH^- + O_2^{\bullet-}$	8.02E+08	1.71E+09	5.75E+09	1.45E+10	3.01E+10	5.43E+10	8.85E+10	1.33E+11
69) $HO_2^- + H_2O \rightarrow H_2O_2 + OH^-$	1.27E+06	3.65E+06	1.63E+07	4.40E+07	8.56E+07	1.33E+08	1.76E+08	2.08E+08
70) $O(^3P) + O(^3P) \rightarrow O_2$	2.20E+10	3.58E+10	7.80E+10	1.41E+11	2.26E+11	3.30E+11	4.51E+11	5.86E+11
71) $O(^3P) + H_2O \rightarrow {}^{\bullet}OH + {}^{\bullet}OH$	1.90E+03	6.84E+03	5.31E+04	2.54E+05	8.74E+05	2.37E+06	5.41E+06	1.08E+07
72) $O^{\bullet-} + O^{\bullet-} \rightarrow H_2O_2 + 2OH^-$	1.00E+08	1.11E+08	1.19E+08	1.21E+08	1.21E+08	1.20E+08	1.20E+08	1.19E+08
73) $O^{\bullet-} + O_3^{\bullet-} \rightarrow 2O_2^{\bullet-}$	7.00E+08	7.39E+08	7.78E+08	8.07E+08	8.44E+08	9.05E+08	1.04E+09	1.51E+09
74) $O^{\bullet-} + H_2O \rightarrow {}^{\bullet}OH + OH^-$	1.27E+06	3.65E+06	1.63E+07	4.40E+07	8.56E+07	1.33E+08	1.76E+08	2.08E+08
75)$O_3^{\bullet-} + H_2O \rightarrow O^{\bullet-} + O_2$	4.65E+01	1.98E+02	2.05E+03	1.25E+04	5.29E+04	1.76E+05	4.99E+05	1.34E+06
76) $H_2O \rightarrow H^+ + OH^-$	2.12E-05	1.78E-04	3.14E-03	1.68E-02	4.58E-02	7.50E-02	6.53E-02	2.04E-02
77) $SO_4^{\bullet-} + SO_4^{\bullet-} \rightarrow S_2O_8^{2-}$	1.12E+09	1.66E+09	3.12E+09	5.04E+09	7.34E+09	9.97E+09	1.29E+10	1.59E+10